Regenerative and biomimetic strategies in spinal surgery

Mr Aman Sharma

St Peter's College





This dissertation is submitted for the Degree of Doctor of Philosophy

2015

Dedication

This DPhil thesis is dedicated to my lovely wife, Naomi, who has provided me with immense support and understanding during the period of this study. She has constantly acted as a friend providing support and at times helping guide my work through constructive and intellectual discussion. Her patience during this period has been highly commendable and I would like to thank her from the deepest of my heart for her continuous and unwavering support.

Also to Anoushka, our daughter, and George, our son.

Declaration

This dissertation is the result of my own work and includes nothing that is the outcome of work done in collaboration except where specifically indicated in the text. This dissertation lies within the word limit set by the Degree Committee of Medical Sciences Division, University of Oxford.

Mr Aman Sharma

14th April 2015

Acknowledgements

I express my sincere gratitude to my supervisors Prof. Christopher Lavy, Associate Prof. Cathy Ye, Dr Jan Czernuszka and Prof. Jeremy Fairbank for their guidance, support and advice and for giving me the opportunity to undertake this research. I thank Associate Prof. Ye, Dr Czernuszka and their group members for giving me work space and helping me feel welcome in their labs, especially Maryam Tammadom, who was very patient in teaching me various techniques.
I sincerely thank Associate Prof. Afsie Sabokbar for her patience, expert advice and general guidance.
I thank the Royal College of Surgeons, England for funding through the Dunhill Medical Trust.
I thank the staff at the Begbroke Science Park, especially Philip Holdway (thank you for the chats about football), Dr Susan Warren and Dr Gabriella Chapman, who taught me many techniques, particularly SEM. Without their help I would have not achieved my goals.
I thank Dr Marko Hyvonen (University of Cambridge) for allowing me to use his research laboratory for synthesising BMPs and transglutaminase and most importantly for taking time to discuss research ideas. I am very grateful for his help.
I am indebted to Dr Brand (University of Tennessee) for his invaluable support for providing highly purified atelocollagen, without this the project would have not started.
Thanks to Laura Pitman who completed her studentship with immense enthusiasm and drive. Thanks to my clinical colleagues and friends, especially Mr Jeremy Reynolds and Mr John Morley, who provided support and an alternative viewpoint through difficult times.
Finally, I thank my wife, Naomi, who has acted as a friend, post-doc and a wife and who helped me immensely - without her support I would not have finished my DPhil.

DEDICATION II
DECLARATION III
ACKNOWLEDGEMENTS IV
ABBREVIATIONS VIII
ABSTRACT 1
CHAPTER 1 INTRODUCTION 2
1.1 ANATOMY OF THE HUMAN SPINE 3
1.1.1 Cervical spine 3
1.1.2 Thoracic spine 5
1.1.3 Lumbar spine 6
1.1.4 Sacrum 6
1.1.5 Coccyx 7
1.2 PHYSIOLOGY OF BONE 9
1.2.1 Introduction 9
1.2.2 Classification 9
1.2.3 Structure of bone 9
1.2.4 Bone cells 12
1.2.5 Bone growth and remodelling 14
1.2.6 Bone composition 15
1.3 DEGENERATIVE SPINAL CONDITIONS 18
1.3.1 Introduction 18
1.3.2 Degenerative conditions of the cervical spine 19
1.3.2.1 Cervical fusion surgery 20
1.3.3 Degenerative conditions of the thoracic spine 21
1.3.4 Degenerative conditions of the lumbar spine 22
1.3.5 Adult Deformity 26
1.4 TREATMENT STRATEGIES FOR DEGENERATIVE SPINAL CONDITIONS 32
1.4.1 Introduction 32
1.4.2 Conservative approach 32
1.4.2.1 Pharmacological therapies 32
1.4.2.2 Physical exercise and manual therapy 35
1.4.2.3 Cognitive behavioural therapy 36
1.4.3 Spinal fusion surgery 37
1.4.3.1 Principles 37
1.4.3.2 Types of lumbar fusion surgery 41
1.4.3.3 Complications 44
1.4.3.4 Outcomes 46
1.4.4 Bone substitutes in lumbar fusion surgery 48
1.4.4.1 Allografts 48
1.4.4.2 Ceramics 49
1.4.4.3 Demineralised bone matrices 49
1.4.5 Alternative approaches 50
1.4.5.1 Bone morphogenetic proteins 51
1.4.5.2 Autologous platelet concentrate 71
1.4.5.3 Gene therapy 71
1.4.5.4 Human mesenchymal stem cells 72
1.5 TISSUE ENGINEERING APPROACHES 76
1.5.1 Biomimicry 76
1.5.2 Naturally occurring materials 77
1.5.2.1 Collagen 77
1.5.2.2 Fibrin 78

1.5.2.3 Silk ... *79*
1.5.2.4 Chitosan and alginate ... *79*
1.5.3 Synthetic polymers ... *80*
1.5.4 Fabrication and modification techniques ... *81*
1.5.4.1 Electrospinning ... *82*
1.5.4.2 Gas-based techniques and salt leaching ... *83*
1.5.4.3 Reactive-ion etching ... *84*
1.5.4.4 Soft photolithography/photo-mould patterning ... *84*
1.5.4.5 Click-based hydrogel patterning ... *85*
1.5.4.6 Thermally-induced phase separation ... *85*
1.5.4.7 Biological laser printing ... *86*
1.5.4.8 Woven scaffolds ... *87*
1.6 AIMS AND OBJECTIVES ... 88
1.6.1 AIMS ... 88
1.6.2 OBJECTIVES ... 88

CHAPTER 2 FABRICATION OF COLLAGEN/GAG/HA/MTG SCAFFOLDS FOR USE IN SPINAL FUSION SURGERY ... 89
2.1 INTRODUCTION ... 90
2.2 SCAFFOLD FABRICATION ... 93
2.2.1 Collagen scaffold ... *93*
2.2.2 Collagen/nano-hydroxyapatite/chondroitin sulphate scaffold ... *94*
2.2.3 Collagen/microbial-transglutaminase scaffold ... *94*
2.3 TRANSGLUTAMINASE PURIFICATION AND CHARACTERISATION ... 94
2.3.1 TRANSGLUTAMINASE PURIFICATION ... 94
2.3.2 TRANSGLUTAMINASE ACTIVITY ... 95
2.4 SCAFFOLD CHARACTERISATION ... 96
2.4.1 Scanning electron microscopy ... *96*
2.4.2 Transmission electron microscopy ... *96*
2.4.3 Differential scanning calorimetry ... *97*
2.4.4 Thermogravimetric analysis ... *98*
2.4.5 Atomic force microscopy ... *98*
2.4.6 Energy dispersive x-ray spectroscopy ... *99*
2.4.7 X-ray diffraction ... *99*
2.4.8 Mechanical testing ... *100*
2.4.9 Statistical analysis ... *100*
2.5 RESULTS ... 101
2.5.1 Imaging ... *101*
2.5.2 Chemical Composition ... *106*
2.5.3 Active microbial transglutaminase ... *110*
2.5.4 Thermal Analysis ... *110*
2.5.5 Mechanical characterisation ... *114*
2.6 DISCUSSION AND SUMMARY ... 116

CHAPTER 3 ROLE OF HUMAN MESENCHYMAL STEM CELLS AND COLLAGEN/HA/GAG SCAFFOLD IN OSTEOGENESIS ... 119
3.1 INTRODUCTION ... 120
3.2 HUMAN MESENCHYMAL STEM CELL CULTURE ... 121
3.3 CELL GROWTH AND VIABILITY ASSAYS ... 121
3.3.1 AlamarBlue® assay ... *122*
3.3.2 Multi-Photon Microscopy ... *122*
3.4 OSTEOGENIC CHARACTERISATION OF HMSCS ... 123
3.4.1 RNA extraction ... *123*
3.4.2 cDNA synthesis ... *124*
3.4.3 RT-PCR ... *124*

3.5 MicroCT 125
3.6 Statistical analysis 126
3.7 Results 127
3.8 Discussion and Conclusions 136

CHAPTER 4 BIOACTIVE BMP-2/COLLAGEN SCAFFOLDS 139
4.1 Introduction 140
4.2 BMP-2 synthesis and purification 143
4.2.1 Gene expression 143
4.2.2 Bacterial transformation 143
4.2.3 Protein Expression 145
4.2.4 Isolation and Solubilisation of Inclusion Bodies 146
4.2.5 Protein purification 147
4.3 Bioactivity of BMP-2 148
4.4 BMP-2/collagen scaffold fabrication 149
4.4.1 Integration 149
4.4.2 Adsorption 149
4.5 BMP-2 release profile 150
4.6 Characterisation 151
4.6.1 Scanning electron microscopy 151
4.6.2 Energy dispersive x-ray spectroscopy 151
4.7 Results 152
4.8 Discussion and Conclusions 161

CHAPTER 5 LAYER-BY-LAYER COLLAGEN/HA/GAG/BMP-2 SCAFFOLDS 163
5.1 Introduction 164
5.2 Fabrication of layer-by-layer scaffolds 166
5.2.1 Layer by layer system 166
5.2.2 Collagen scaffold fabrication 166
5.2.3 Fabrication of LBL collagen/CS scaffolds 168
5.2.4 Fabrication of LBL CS/BMP-2 scaffolds 169
5.3 Characterisation of layer-by-layer scaffolds 170
5.3.1 Scanning electron microscopy 170
5.3.2 Energy dispersive x-ray spectroscopy 170
5.3.3 Differential scanning calorimetry 171
5.3.4 Fourier transform infrared spectroscopy 171
5.4 Multiphoton microscopy for imaging of hMSCs 172
5.5 BMP-2 release profile 173
5.6 Results 174
5.7 Discussion and Conclusions 189

CHAPTER 6 DISCUSSION 193

CHAPTER 7 CONCLUSIONS AND FUTURE WORK 202

CHAPTER 8 REFERENCES 207

APPENDICES 241
I. Primers 242

Abbreviations

Al_2O_3	aluminium oxide
Alk	activin-like kinase
ALP	alkaline phosphatase
α-TCP	alpha-tricalcium phosphate
BAMBI	BMP and activin membrane-bound inhibitor
BCA	bicinchoninic acid
BMP	bone morphogenetic protein
BSA	bovine serum albumin
Ca^{2+}	calcium ion
CaO	calcium oxide
Ca/P	calcium/phosphorous
CHAPS	3-[(3-Cholamidopropyl)dimethylammonio]-1-propanesulfonate
CHO	Chinese hamster ovary
CPC	calcium phosphate cement
Dan	differential screening-selected gene aberrative in neuroblastoma
DiFMU	6,8-difluoro-7-hydroxy-4-methylcoumarin
DiFMUP	6,8-difluoro-4-methylumbelliferyl phosphate
DMEM	Dulbecco's modified eagle's medium
DSC	differential scanning calorimetry
EDC	1-Ethyl-3-[3-dimethylaminopropyl]carbodiimide hydrochloride
EDTA	ethylenediaminetetraacetic acid
EDX	energy dispersive x-ray
ELISA	enzyme-linked immunosorbent assay
FBS	foetal bovine serum
FDA	Food and Drug Administration
GndCl	guanidinium chloride
h	hours
HA	hydroxyapatite
HCl	hydrogen chloride
HRP	horseradish peroxidase
ICDD	International Centre for Diffraction Data
IGF	insulin-like growth factor
IPTG	isopropyl β-D-1-thiogalactopyranoside
JNK	c-Jun N-terminal kinase
kN	kilonewton
K_2O	potassium oxide
LB	Luria-Bertani
LBL	layer-by-layer
MAP	mitogen-activated protein
Min	minutes
MW	molecular weight
NaCl	sodium chloride
NHS	N-hydroxysulfosuccinimide
O^{2-}	oxygen ion
OD_{600}	optical density at 600nm
P^{5+}	phosphorous ion
PAGE	polyacrylamide gel electrophoresis

PBS	phosphate buffered saline
PCL	poly epsilon-caprolactone
PEG	polyethylene glycol
PHBV	poly(3-hydroxybutyrate-co-3-hydroxyvalerate)
pHEMA	poly (2-hydroxyethyl methacrylate)
PLA	polylactic acid
PLGA	poly(D,L-lactide-co-glycolide)
PLLA	poly (L-lactic acid)
P_2O_5	phosphorous pentoxide
PPS	3-(1-pyridinio)-1-propanesulfonate
PRDC	protein related to Dan and cerberus
PSG	penicillin, streptomycin, L-glutamine
PTFE	polytetrafluoroethylene
rh	recombinant human
rpm	revolutions per minute
RT	room temperature
RUNX2	vertebrate homologue of the *Drosophila runt* gene
s	seconds
SDS	sodium dodecyl sulphate
SEM	scanning electron microscopy
SiO_2	silicon dioxide
Ski	transforming protein of avian homolog of Sloan-kettering retrovirus
STAT	signal transducers and activators of transcription
TCEP	Tris carboxyethyl phosphine
TCP	tricalcium phosphate
TEM	transmission electron microscopy
TGA	thermogravimetric analysis
TGFβ	transforming growth factor beta
Tob	transducer of Erb B-2
Tris	tris(hydroxymethyl)aminomethane
Tsg	twisted gastrulation
USAG-1	uterine sensitization associated gene
UV	ultraviolet
VEGF	vascular endothelial growth factor
XIAP	X-linked inhibitor of apoptosis protein
XRD	x-ray diffraction
XRF	x-ray fluorescence spectroscopy
$ZnCl_2$	zinc chloride

Abstract

Degenerative conditions of the spine are a major public health problem, leading to severe back pain, reduced quality of life and chronic disablement in a proportion of sufferers. For some of these patients, spinal fusion surgery is a treatment that can alleviate back pain and restore normal function. However, limitations in the availability of graft material mean that alternative grafts are needed and tissue-engineering approaches have been employed. The aim of this study was to identify and develop a novel targeted therapy for use in degenerative spinal conditions, which could ultimately lead to superior pain relief and improved mobility of patients compared to currently available treatments. The basis of this study was a mineralised collagen scaffold with biomimetic modifications, including the incorporation of BMP-2.

Using a novel self-organising collagen scaffold combined with nano-hydroxyapatite and chondroitin sulphate and by employing the latest materials techniques, I have studied the osteogenic capability of a biomimetic graft for use in spinal fusion surgery. The mineralised collagen scaffold has compressive strength comparable to human cancellous bone and can support the proliferation of viable human mesenchymal stem cells (hMSCs). This porous scaffold can be combined with hMSCs to further promote bone growth, as evidenced by an upregulation in the levels of bone-forming genes and mineralisation of the scaffold. This scaffold can act as a carrier system for BMP-2, with wider application for other growth factors or drugs, providing sustained release when fabricated as a layer-by-layer scaffold.

In conclusion, a novel self-organising collagen-based scaffold has been fabricated and supports the proliferation and differentiation of hMSCs towards an osteogenic lineage. In combination with BMPs, this scaffold has exciting potential for use in spinal surgery.

Chapter 1 Introduction

1.1 Anatomy of the human spine

The human spine comprises of thirty-three vertebral bodies (seven cervical, twelve thoracic, five lumbar, five fused form the sacrum and four or five fused form the coccyx, **Figure 1.1a**). Its major function is to perform protection around the spinal cord (from which nerve roots exit and traverse the spine to the upper and lower limbs and the trunk) and to provide flexible mechanical support to the upper body.

The typical vertebra consists of a body and a dorsal vertebral arch (**Figure 1.1b**). The vertebral arch is attached to the body by two pedicles, which are themselves united dorsally by two laminae and the spinous process. Thus, the bony vertebral foramen is formed around the spinal cord (**Figure 1.1b**). Articulation is facilitated by the presence of facet joints between the vertebral arches.

1.1.1 Cervical spine

The seven cervical vertebrae are numbered C1 to C7. C1, C2 and C7 have individual characteristics whilst all cervical vertebrae share some common features, including uncinate processes, transverse foraminae and bifid spinous processes (**Figure 1.1c**). Since cervical bodies bear the least weight of all the vertebrae, they are small and thin relative to the vertebral arch and vertebral foramen. The lateral edges of the superior surface of each body are sharply turned upwards to form the uncinate processes. The lateral extremities of the transverse processes give rise to anterior and posterior tubercles, from which arise anterior and posterior cervical muscles, respectively.

FIGURE 1.1

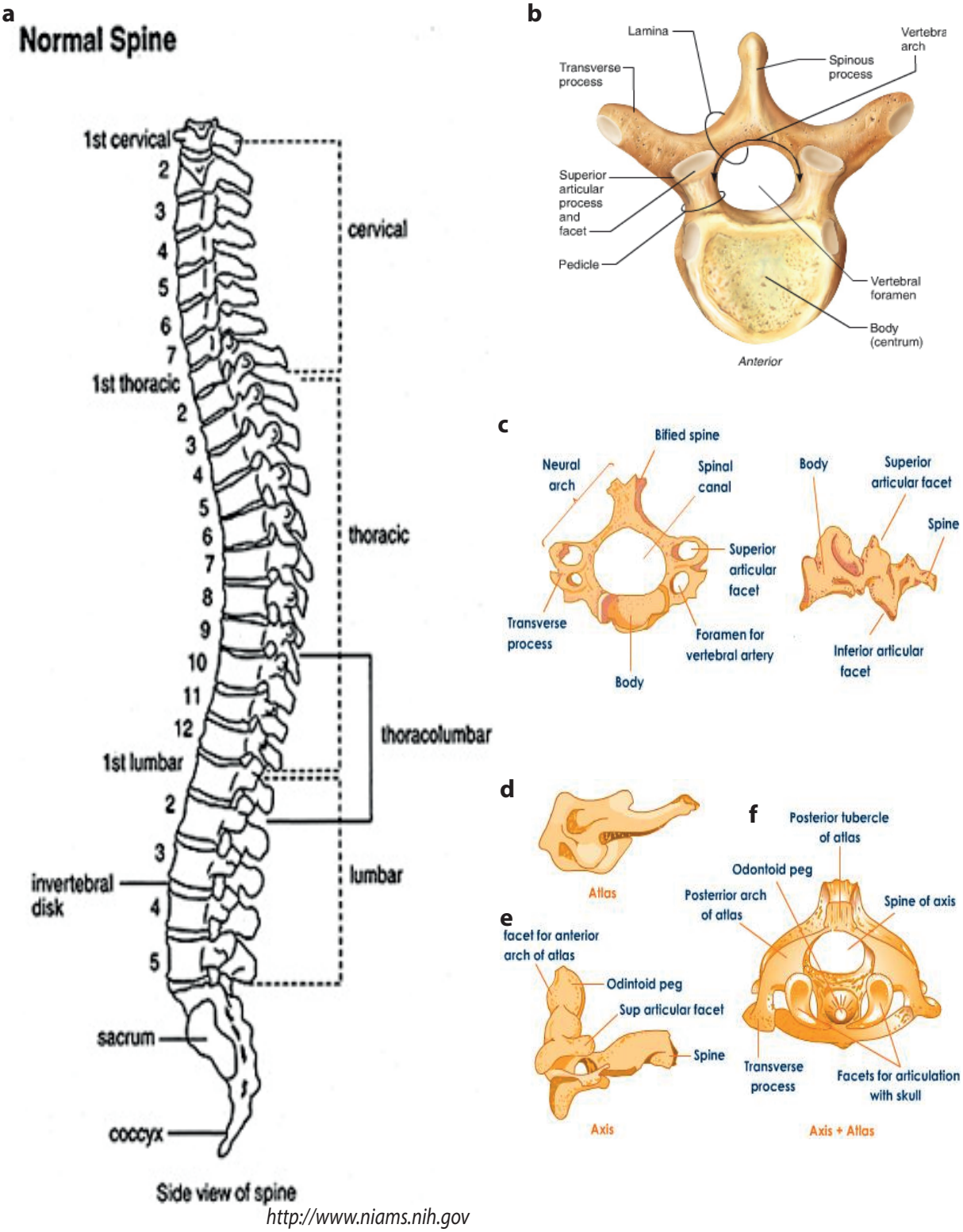


Figure 1.1 Anatomy of the spine (a) Side view of the spine, showing thirty-three vertebrae. (b) Schematic of a typical vertebra with the body attached to the vertebral arch by two pedicles. (c)Schematic of a typical cervical vertabra showing transverse foraminae and a bifid spinous process. (d) Schematic of the atlas (C1), a bony ring formed by anterior and posterior arches and lateral masses. (e) Schematic of the axis (C2), showing the odontoid peg upon which the atlas sits, as shown in (f). Images adapted from Rothman-Simeone, The Spine, 6th Ed.

The cervical spine is a tripod of flexible columns. The combination of articular processes and the intervening bone is often referred to as lateral mass in the subaxial region, a common site for screw insertion during internal fixation surgery.

The first ('atlas') and second ('axis') cervical vertebrae form a complex articular system leading to the nodding and rotational movements of the head. The atlas is a bony ring formed by anterior and posterior arches and lateral masses (**Figure 1.1d**). Its superior articular surface faces upward on the skull and its inferior articular surface faces down on the axis. The axis has a bony prominence ('odontoid peg') which projects vertically and acts as a restraint to horizontal displacements of the atlas (**Figures 1.1e-f**).

The seventh cervical vertebra is transitional, with a long spinous process ('vertebra prominens') and more steeply inclined articulating facets, similar to those of the thoracic region.

1.1.2 Thoracic spine

The 12 thoracic vertebrae are numbered from T1 to T12 and form the largest segment of the spine. The thoracic vertebrae articulate with the rib cage and form rigid protection of the spinal cord and thoracic viscera, whilst being critically important for erect bipedal support. Of note, the upper thoracic spine exhibits more axial rotation than the lower thoracic spine.

There is variation in the vertebrae from T1 through to T12. T1 is similar to the cervical vertebrae, with a vertebra prominens. T2 to T8 are 'typical' thoracic vertebrae and more uniform, consisting of a heart-shaped vertebral body, an oval

vertebral foramen and oval pedicles in cross-section (**Figure 1.2a**). T9 to T12 are considered transition vertebrae and possess a similar structure to lumbar vertebrae.

1.1.3 Lumbar spine

The main function of the lumbar spine is to bear the support of the body and provide mobility of the trunk and hips, particularly through flexion/extension and axial rotation motions. Large intervertebral discs and facet joint orientation facilitate these movements.

There are five lumbar vertebrae numbered from L1 to L5. These consist of a large weight-bearing vertebral body and a vertebral neural arch (**Figure 1.2b**). Each arch is comprised of two pedicles, two laminae and seven bony processes (one spinous, four articular and two transverse). The size of the vertebral body increases from L1 through to L5 and the absence of rib facets is a key distinguishing feature from thoracic vertebrae.

1.1.4 Sacrum

The os sacrum is a large triangular bone consisting of five fused bones. The anterior border of the upper part is the sacral promontory and the anterior aspect of this presents a central mass (**Figure 1.2c**). There is a row of four anterior sacral foramina on either side of this mass, which transmit four sacral anterior primary rami. Lateral to these rami are the lateral masses of the sacrum, the superior aspect of each forming a fan-shaped surface (the 'ala'). The spinal canal lies posteriorly, bound by short pedicles and very small spinous processes.

Inferiorly the canal terminates in the sacral hiatus, which transmits the 5th sacral nerve.

1.1.5 Coccyx

The coccyx consists of between three and five fused vertebrae that articulate with the sacrum (**Figure 1.2c**). Occasionally, the first segment remains separate.

FIGURE 1.2

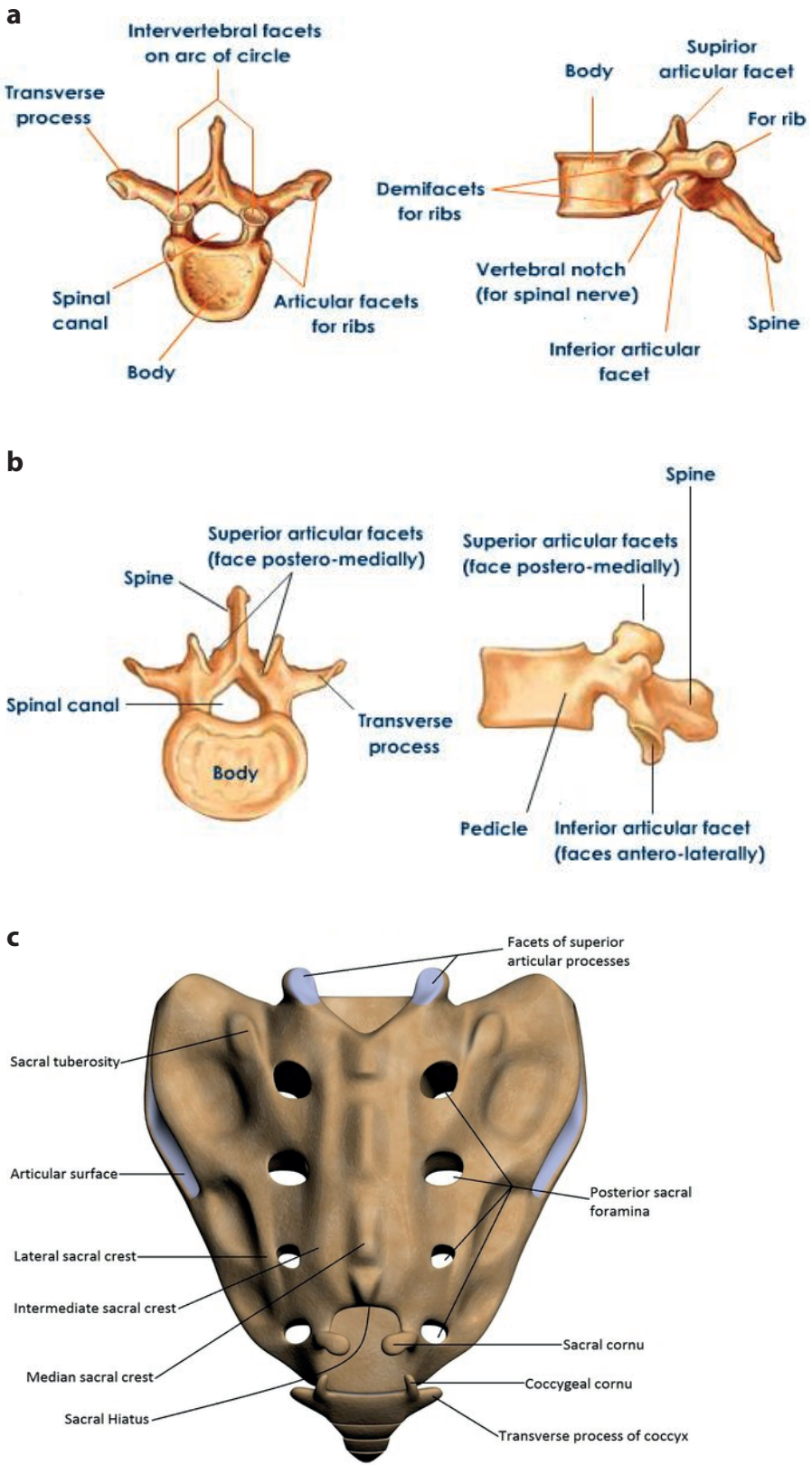


Figure 1.2 Anatomy of the throaco-lumbo-sacral spine (a) Schematic of a typical thoracic vertebra with a heart-shaped vertebral body, an oval vertebral foramen and rib facets. (b)Schematic of a typical lumbar vertabra showing the large weight-bearing vertebral body. (c) Schematic of the sacrum and coccyx. Images adapted from Rothman-Simeone, The Spine, 6th Ed.

1.2 Physiology of bone

1.2.1 Introduction

The human adult skeleton has 213 bones and is vital to the survival of the human species. Its main functions include providing mechanical stability, assisting in human motion, protecting vital organs and playing a part in mineral homeostasis. Arising from mesoderm and neural crest origins, bone is an extremely complex and dynamic structure. In this section, its classification, structure, cells, growth and composition are detailed.

1.2.2 Classification

Bones can be classified into one of four types: long (for example, clavicle, femur), short (for example, carpal and tarsal bones), flat (for example, skull, mandible), and irregular (for example, vertebrae, sacrum).

Bones are divided into three distinct morphological compartments:

a) epiphysis: the region between the articular end of the bone and the growth plate

b) metaphysis: the region immediately below the growth plate

c) diaphysis: the region between the metaphyses

1.2.3 Structure of bone

Overall, the adult human skeleton is comprised of 80% cortical bone and 20% trabecular bone. However, in the vertebrae, this ratio is 25:75 cortical to trabecular bone, and in the femoral head this ratio is 50:50.

Cortical bone has an outer periosteum and an inner endosteal surface (**Figure 1.3a**). It is dense and solid and surrounds the bone marrow. Cortical osteons (Haversian systems) are cylindrical, approximately 400 mm long and 200 mm wide and form a branching network (Tortora 2004) (**Figure 1.3b**).

Trabecular bone contains a honeycomb-like network of trabecular plates and rods interspersed in the bone marrow compartment. Trabecular osteons (packets) are semilunar, approximately 35 mm thick, and consist of concentric lamellae (**Figure 1.3c**).

FIGURE 1.3

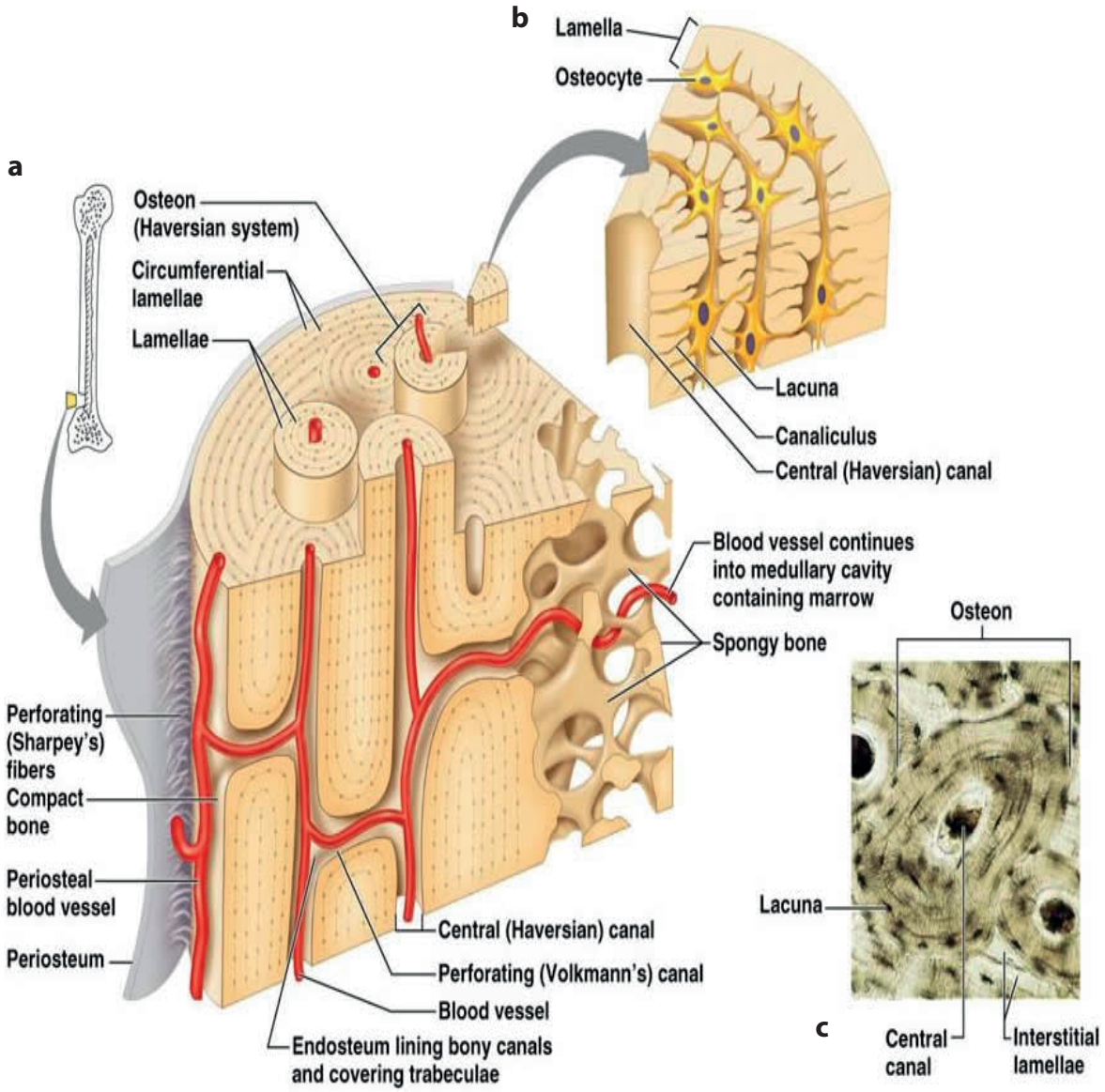


Figure 1.3 Anatomy of human bone demonstrating the Haversian system, lamellae and osteocytes. Images from Pearson Education Inc, Benjamin Cummings, 2004

1.2.4 Bone cells

There are four distinct cell types within bone:

a) osteoblasts

b) osteoclasts

c) osteocytes

d) bone-lining cells

Osteoblasts are derived from osteoprogenitor cells, which are progeny of self-renewing, pluripotent mesenchymal stem cells (MSCs) from within the bone marrow. MSCs are capable of differentiating into adipose, cartilage, bone, and connective tissue (Pittenger et al. 1999). Flattened bone-lining cells (quiescent osteoblasts) form the endosteum on trabecular and endosteal surfaces, and are found close to osteoblasts. Active osteoblasts contain large nuclei, enlarged Golgi apparatus and extensive endoplasmic reticulum. This cellular machinery synthesises and secretes Type I collagen and other bone matrix components, specific details of which depend on the skeletal site and the presence of any local bone disease.

Osteoclasts are activated multinucleated osteoclasts derived from bone marrow monocyte-macrophage precursor cells (Boyle et al. 2003). Their formation is critically dependent on two cytokines, RANKL and macrophage CSF (M-CSF), produced mainly by stromal cells of the bone marrow and by osteoblasts (Teitelbaum & Ross 2003). RANKL is a member of the TNF superfamily and a ligand for osteoprotegerin, therefore critical for osteoclast differentiation and activation. M-CSF is required for the survival of osteoclast precursors and

osteoclasts. Osteoclasts regulate bone resoprtion by the secretion of hydrogen ions (acidifying and dissolving the mineral component of bone matrix) and cathepsin K enzyme (digesting the extracellular matrix) (Boyle et al. 2003).

Osteocytes are terminally differentiated osteoblasts and lie within lacunae of mineralised bone to support bone structure and metabolism. In contrast to osteoblasts, osteocytes do not normally express alkaline phosphatase (Bonewald 1999). They do express matrix proteins which support adhesion and they also contain lysosomes so may have some phagocytic function. Gap junctions (or intracellular channels), comprised mainly of connexin43, provide a metabolic and electrical link for osteocytes and are required for their maturation and activity (Plotkin et al. 2002). Osteocytes transmit mechanical stretch of bone into biological activity via multiple signalling pathways, including prostaglandin E2, cyclo-oxygenase 2, Runx2 and nitrous oxide (Rubin & Lanyon 1987).

Bone-lining cells arise from osteoblasts after bone formation and regulate ion flux into and out of bone extracellular fluid. They retain the ability to redifferentiate into osteoblasts after parathyroid hormone stimulation or mechanical stimulation (Dobnig & Turner 1995). Before resorption, bone-lining cells within the endosteum lift off the surface of bone to form discrete bone remodelling compartments with a specific microenvironment (Hauge et al. 2001).

1.2.5 Bone growth and remodelling

During human development, longitudinal growth of bone occurs at the epiphyseal and metaphyseal regions of long bones. After this, changes in the shape of a bone occur by modelling in response to physiological challenges or mechanical forces. In such modelling, bone formation and bone resorption are not tightly coupled. However, in adults, remodelling is more common than modelling, and this process involves the resorption of old bone and replacement with new bone through four distinct phases:

1. Activation – mononuclear osteoclast precursors are recruited and activated, endosteum is lifted off the bone surface and mononuclear cells fuse to form multinucleated preosteoclasts which bind to bone matrix.
2. Resorption – osteoclast-mediated hydrogen ion acidification of mineral matrix , digestion of matrix by cathepsin K, MMP9 and gelatinase, formation of Howship's lacunae on the surface of trabecular bone and Haversian canals in cortical bone (Silver et al. 1988).
3. Reversal – transition from bone resorption to bone formation, signalling pathways include matrix-released factors TGFβ, IGF-I, IGF-II, BMPs. TGFβ released from bone matrix inhibits RANKL production by osteoblasts and therefore decreases osteoclast resorption.
4. Formation – takes 4 to 6 months to complete, new collagenous matrix synthesised by osteoblasts which themselves become osteocytes, connected to each other and bone surface lining cells by canalicular

network maintained by gap junctions (Burger et al. 2003). The osteocyte network acts as a functional syncytium. At completion of bone formation, 70% of osteoblasts undergo apoptosis and remainder become osteocytes or bone-lining cells.

A new osteon is produced after each bone remodelling cycle. Bone balance is the difference between resorbed bone and formed bone: periosteal bone balance is positive; endosteal and trabecular bones are negative. This leads to cortical and trabecular thinning with age, with endosteal resorption greater than periosteal formation. Remodelling facilitates the replacement of old damaged bone with new bone (2-3% turnover per year) and thus preserves biomechanical strength, and it also aids mineral metabolism.

1.2.6 Bone composition

Bone is composed of mineral (50-70%), organic matrix (20-40%), water (5-10%) and lipids (<3%).

The mineral content of bone is mostly hydroxyapatite, and small amounts of phosphate, magnesium and carbonate.

Bone extracellular matrix (ECM) contains predominantly Type I collagen, with smaller amounts of Types III, V and FACIT (fibril-associated collagens with interrupted triple helices) collagens (details in **Table 1.1**). Noncollagenous proteins comprise 10-15% of total bone ECM and include proteoglycans and glycosylated proteins, for example osteonectin and alkaline phosphatase.

Osteonectin affects osteoblast proliferation and bone mineralisation. Alkaline phosphatase also plays a role in bone mineralisation, although its exact mechanism of action is unknown (Whyte 1994).

Protein (Chromosome Location)	Function	Human Disease
Collagen-related proteins		
type I (17q21.23, 7q22.1)	Most abundant bone matrix protein	Osteogenesis imperfecta
type X (6q21)	Found in hypertrophic cartilage	None known
type III (2q31)	Trace amounts in bone; may regulate collagen fibril diameter	Ehlers-Danlos syndrome
type V (9q34.2-34.3; 2q24.3-31; 19q13.2)	Trace amounts in bone; may regulate collagen fibril diameter	
Serum proteins in bone matrix		
albumin (4q11-13)	Decreases hydroxyapatite crystal growth	None
α_2-HS glycoprotein (3q27)	Bovine analog is fetuin	None
Glycoaminoglycan-containing proteins and leucine-rich repeat proteins		
aggrecan (15q26.1)	Matrix organization, retention of calcium/phosphorus	None
versican (5q14.3)	Defines space destined to become bone	None
decorin (12q21.3)	Regulates collagen fibril diameter; binds TGF-β	Progeroid form of Ehlers-Danlos syndrome with decorin/ biglycan double knockout
biglycan (Xq28)	Binds collagen; binds TGF-β; genetic determinant of peak bone mass	
hyaluronan (multigene complex)	May work with versican to define space destined to become bone	None
Glycoproteins		
alkaline phosphatase (1p36.1-p34)	Hydrolyzes mineral deposition inhibitors	Hypophosphatasia
osteonectin (5q31.3-32)	Regulates collagen fibril diameter	None
SIBLING proteins		
osteopontin (4q21)	Inhibits mineralization and remodeling	None
bone sialoprotein (4q21)	Initiates mineralization	None
MEPE (4q21.1)	Regulator of phosphate metabolism	Tumor-induced osteomalacia
RGD-containing glycoproteins		
thrombospondins (15q15, 6q27, 1q21, 5q13, 19p13.1)	Cell attachment	None
fibronectin (2q34)	Binds to cells	None
vitronectin (17q11)	Cell attachment	None
fibrillin 1 and 2 (15q21.1, 5q23-31)	Regulates elastic fiber formation	Fibrillin 1: Marfan syndrome
γ-Carboxy glutamic acid–containing proteins		
matrix Gla protein (12p13.1-p12.3)	Inhibits mineralization	None
osteocalcin (1q25-q31)	Regulates osteoclasts; inhibits mineralization	None
protein S (3p11.2)	Liver product, may be made by osteoblasts	Osteopenia

[a]SIBLING proteins, Small Integrin-Binding Ligand, N-glycosylated proteins.

Table 1.1
Bone extracellular matrix proteins (Clarke 2008)

1.3 Degenerative spinal conditions

1.3.1 Introduction

Back pain is a major public health problem in the Western world, leading to suffering and distress in a large number of people; the point prevalence rates range from 12% to 35%, with around 10% of sufferers becoming chronically disabled (Tortora 2004; Maniadakis & Gray 2000). This places an enormous economic burden on society through direct medical costs, insurance, lost production and disability benefits. In the UK, overall annual costs associated with back pain have been estimated at £9.5 billion or 1-2% GDP (Maniadakis & Gray 2000).

Back pain is strongly associated with degeneration of the intervertebral disc (Luoma et al. 2000). The first findings of degeneration in the lumbar discs are seen far earlier than in other musculoskeletal tissues, in the age group 11-16 years (Boos et al. 2002). This degeneration increases sharply with age, such that 10% of 50-year olds and 60% of 70-year olds have severely degenerate discs (Miller et al. 1988). Interestingly, this age-related degeneration is more marked in males, for reasons that are not fully understood (Miller et al. 1988).

Degenerative conditions of the spine have been subdivided below into those of the cervical, thoracic and lumbar spine. However, due to the significant health burden of degenerative lumbar disease, the lumbar spine will be the focus of this section.

1.3.2 Degenerative conditions of the cervical spine

Cervical spondylosis refers to age-related degenerative changes within the cervical spinal column, particularly within the cervical spine disc.

Pathophysiology

Cervical disc degeneration results from a reduction in the content of chondroitin sulphate and an increase in keratin sulphate, leading to increased stiffness and reduced hydration of the intervertebral disc. Subsequently, the ventral portion of the disc loses height to a greater degree than the dorsal portion. This causes an increased load on the facet and uncovertebral joints, leading to motion aberration between two vertebral bodies. Formation of osteophytes at the facet and uncovertebral joints, together with posteriorly protruding disc material, leads to nerve root compression and subsequently spinal cord compression.

Axial neck pain

Axial neck pain is divided into anterior or posterior pain. Anterior pain is usually a result of sprains and strains of the sternocleidomastoid and strap muscles of the neck. Posterior pain is further divided into subaxial and suboccipital (depending on the location of symptoms) and is due to degenerative changes of the cervical spine over time. A large study of discography revealed consistent and predictable patterns of neck pain from each cervical disc (Grubb & Kelly 2000).

Axial neck pain is commonly along the posterior neck and trapezius muscles, usually (but not always) without radiation into the arms, and can be associated with headaches.

Radicular pain

Loss of intervertebral disc height leads to impingement on the nerve root origins from disc bulging, infolding of the facet joint capsule and ligamentum flavum, and osteophyte formation at the disc margins and at the uncovertebral and facet joints. This leads to foraminal stenosis and radiculopathy. In addition to direct compression of the nerve root, it is believed that there is an inflammatory response including increased vascular permeability and chronic oedema of the nerve root (Teitelbaum & Ross 2003; Pittenger et al. 1999; Cooper et al. 1995). Cervical radiculopathy refers to a sharp pain, tingling or burning sensations in the involved area (which represents a specific dermatomal distribution). Typically this is unilateral and patients can present with the head cocked to the side opposite to their arm pain.

Cervical myelopathy

Mechanical compression is the primary mechanism by which cervical myelopathy develops. However, additional factors include congenital canal stenosis, changes in intrinsic morphology of the spinal cord (thickening and shortening, due to cervical spine flexion and extension) and vascular factors. Cervical myelopathy leads to altered pain and temperature sensation, muscle weakness and abnormal reflexes, with possible disturbance of gait.

1.3.2.1 Cervical fusion surgery

Indications for cervical fusion surgery include axial neck pain, cervical radiculopathy and cervical myelopathy. Anterior cervical decompression and

fusion (ACDF) surgery was pioneered by Robinson *et al* in 1962 and has since been modified (Emery et al. 1994). ACDF is now routinely used for the treatment of axial neck pain; in a recent systematic review, an improvement in functional outcomes (32-52% from baseline) and an improvement in pain of at least 50% were reported (Riew et al. 2010). For single-level ACDF surgery, fusion rates are generally high (95-100%), but these rates fall with increasing number of levels fused, with rates of up to 35% having been reported in a recent meta-analysis (Fraser & Härtl 2007).

Autograft remains the graft of choice, with the lowest complication rate, highest fusion rates and significantly lower costs compared to allograft, cages or other graft materials (N. E. Epstein 2012).

Complications of surgery include re-operation, venous thromboembolic events, cardio-respiratory problems, sepsis and mortality, with the rate of these major complications around 3-4% in a recent retrospective study of over 2000 patients (Gruskay et al. 2014).

1.3.3 Degenerative conditions of the thoracic spine

Thoracic disc disease with a combination of degenerative facet joints encompasses the spectrum of degenerative thoracic conditions. Historically, less than 4% of all symptomatic disc protrusions are in the thoracic spine (LOVE & SCHORN 1965) and therefore symptomatic degenerative disease of the thoracic spine is an uncommon clinical problem.

Pathophysiology

Old age, excessive mechanical stress, trauma and Scheuermann's disease contribute towards degenerative thoracic facet joints and disc herniation. This can result in pain, reduced sensation, muscle weakness and disturbance of bladder and bowel function (Arce & Dohrmann 1985).

1.3.4 Degenerative conditions of the lumbar spine

1.3.4.1 Introduction

As detailed previously, lower back pain is extremely common and affects up to one in three adults each year in the UK (NICE.org.uk, 2009/031). Although most of the symptoms are short-lived (less than 6 weeks), a significant proportion of people will experience chronic pain.

Patients with chronic low back pain have reduced cortical grey matter in multiple areas of the brain, compared to pain-free controls (Apkarian et al. 2004; Schmidt-Wilcke et al. 2006; Buckalew et al. 2008) and several studies have also shown abnormal cortical function in these patients (Kobayashi et al. 2009; Tagliazucchi et al. 2010; Giesecke et al. 2004). Amongst other functions, the dorsolateral pre-frontal cortex controls pain modulation (J. Lorenz et al. 2003; Fierro et al. 2010), placebo analgesia (Wager et al. 2004; Krummenacher et al. 2010) and perceived control of pain (Pariente et al. 2005; Wiech et al. 2006).

1.3.4.2 Pathophysiology

Chronic lower back pain is known to be associated with degeneration of the spinal motion segment (Andersson 1999; Deyo & Weinstein 2001). Degeneration is believed to initiate in the intervertebral disc with subsequent degeneration occurring in the facet joints (Adams & Roughley 2006). Degenerative disc disease encompasses three distinct phases (Kirkaldy-Willis & Farfan 1982):

1. Dysfunction - the disc loses its normal function as the degenerative process begins.
2. Instability – associated with intermittent episodes of pain, instability is best demonstrated on flexion/extension radiographs
3. Stabilisation – loss of disc height and compression of disc tissue ensures the stabilisation of the spinal segment.

Degeneration of the disc can be classified into two phenotypes, endplate-driven and annulus-driven (Adams & Dolan 2012). End-plate driven degeneration is associated with endplate defects and predominantly affects the upper lumbar spine. It is more likely to be inherited and as such, often occurs before the age of 30 years. There is moderate association with pain, from the endplate or vertebral body. Annulus-driven degeneration is associated with annulus fissures are predominantly affects the lower lumbar spine. It is rare before the age of 30 years and is strongly associated with pain, which arises form the peripheral annulus and nerve root.

1.3.4.3 Clinical symptoms

Clinical presentation from internal disc disruption occurs most commonly as recurrent episodes of back pain and is often associated with a history of minor trauma, such as lifting a heavy object. The pain is frequently described as being dull and exacerbated by rotation, flexion and sideways movement of the lower back, and relieved by a lateral recumbent position. The pain can also radiate down the legs.

Pain due to degenerative disc disease is usually persistent low back pain, spread over the lumbar spine and sacro-iliac joints. It is worse with sitting and prolonged walking, but is rarely associated with radicular symptoms unless there is spinal stenosis present. Neurological examination is usually unremarkable.

Objective assessment of symptoms has been aided by the development of the Oswestry Disability Index (ODI) which remains a useful tool for the self-reported assessment of disability and quality of life for patients with low back pain (Fairbank & Pynsent 2000). The questionnaire includes details about pain, lifting, ability to care for oneself, ability to walk, sit and stand, sexual function, social life, sleep quality and ability to travel. It is also used in studies to assess the impact of an intervention, for example, spinal fusion surgery.

1.3.4.4 Diagnosis

Plain radiograph is recommended in patients with red flags signs (neurological deficit, suspicion of cancer, for example, night pain and weight loss) and, if a patient has signs of instability, flexion and extension views should be performed.

Findings are a loss of disc space, endplate sclerosis and the presence of osteophytes. Degenerative scoliosis or spondylolisthesis may also show (Rothman-Simeone).

CT is used only to aid surgical planning, if required, but it is not used as a diagnostic modality in degenerative disc disease. Occasional CT meylography must be performed in patients who cannot have an MRI due to metal clips, pacemaker, obesity or claustrophobia.

MRI is the best available imaging modality to evaluate the disc and neural pathology in back pain. Features of degenerative disc disease include loss of water, loss of disc height, disc bulges and signal irregularities within the nucleus pulposus. Three stages of MRI endplate changes associated with disc degeneration have been described (Modic et al. 1988). Stage I is associated with oedema and the endplate shows decreased signal on T1 and bright signal on T2. In Stage II, fatty degeneration in the bone adjacent to the endplate is seen, whereas in stage III, endplate sclerosis is characterized on MRI by decreased signal intensity on T1 and T2 images.

However, MRI must be used as an adjunct to accurate history taking and clinical examination, as features of advanced degenerative disease can be seen on MRI scans of up to 30% of asymptomatic individuals (Boden et al. 1990).

Finally, discography is a highly controversial modality for the evaluation of degenerative disc disease. Recent evidence has shown it might actually accelerate the degenerative process and its use is now discouraged in national guidelines (Chou et al. 2009). Additionally, it has a false-positive rate of 25% and

also a high correlation with psychosocial factors (Carragee et al. 2006), therefore it is very rarely used.

1.3.5 Adult Deformity

1.3.5.1 Adult isthmic spondylolisthesis

Adult isthmic spondylolisthesis (IS) is the forward slippage of a vertebra on the vertebra below resulting from a defect in the part interarticularis. It is common, affecting 4-6% of the general population (TAILLARD 1976). Although it is more common in males, females have higher rates of progression. L5/S1 is the most frequently affected level.

Pathophysiology

IS is classified as low or high grade and this classification is the basis of treatment decisions. According to the Meyerding classification, low grade IS refers to a slippage of less than 50% and high grade IS refers to a slippage of greater than 50% (Vaccaro et al. 2001). The Wiltse classification system contains three types: a) fatigue failure of pars resulting in a complete defect or separation of the bone; b) elongated pars, due to repeated microtrauma with subsequent bone healing as the slippage occurs gradually; or, c) acute pars fracture (Wiltse et al. 1976).

Symptoms related to spondylolisthesis include back pain, leg pain and altered sensation in the leg. Diagnosis is made with imaging in the form of plain

radiograph (standing and supine), CT and MRI. Newer modalities, such as single-photon emission CT can help to distinguish between acute and chronic IS.

Treatment options include conservative management (for example, analgesia and physiotherapy) and surgery. The aims of surgery are to stabilise the affected levels and to decompress the neural elements. Options include direct repair of the pars, decompression of the neural element with or without PLF and with or without interbody fusion.

Recent randomised controlled trials comparing instrumented with noninstrumented posterolateral fusion for IS are summarised in **Table 1.2**. Overall fusion rates ranged from 62-84%, meaning a non-union rate of 16-38% (Ekman et al. 2009; Moller & Hedlund 2000; Thomsen et al. 1997; McGuire & Amundson 1993; France et al. 1999). Such surgery is also associated with an overall complication rate of around 10%, including dural tear (2.1%), wound infection (1.9%), neurological deficit 1.1% and venous thromboembolic events (0.3%) (Sansur et al. 2010).

Study Reference	*Treatments (fusion technique)*	*Sample size*	*Levels*	*Follow-up*	*Fusion*	*Complications*
(Ekman et al. 2009)	PLF (ICBG)	40	L4-L5	2 years	72%	NR
	PLF (ICBG + CDI)	37				NR
(Moller & Hedlund 2000)	PLF (ICBG)	41	L4-S1	2 years	78%	1 blind in one eye, 2 revisions
	PLF (ICBG + CDI)	39			65%	2 revisions
(France et al. 1999)	PLF (ICBG)	11	NR	40 months	63%	NR
	PLF (ICBG + VSP plate)	16			62%	NR
(Thomsen et al. 1997)	PLF (ICBG)	19	NR	2 years	84%	NR
	PLF (ICBG + CDI)	16			73%	NR
(McGuire & Amundson 1993)	PLF (ICBG)	14	L4-S1	>2 years	72%	4 revisions
	PLF (ICBG + VSP plate)	13			78%	2 revisions

Table 1.2

Summary of randomised trials comparing non-instrumented with instrumented posterolateral fusion in isthmic spondylolisthesis PLF, posterolateral fusion; ICBG, iliac crest bone graft; CDI, Cottrel-Dubousset instrumentation; VSP, variable screw placement; NR, not recorded. Adapted from (Jacobs et al. 2006)

1.3.5.2 Adult scoliosis

Adult scoliosis is defined as a spinal deformity in a skeletally mature patient with a Cobb angle of greater than 10^0 in the coronal plane. Its prevalence ranges from 6-68% (Aebi 2005; Anasetti et al. 2010; CARTER & HAYNES 1987).
Classification is based on the Aebi system, which comprises of four groups: Type 1, primary degenerative scoliosis ("de novo scoliosis"); Type 2, idiopathic adolescent scoliosis of thoraco-lumbar spine; Type 3, secondary adult curves – a) due to leg length discrepancy, or b) due to metabolic bone disease (Aebi 2005).

Pathophysiology

Asymmetric degeneration of the disc or facet joint leads to an asymmetrical loading of the spine and subsequent deformity (scoliosis), which then leads to further asymmetrical degeneration, thus worsening the deformity. The unstable spine combined with an abnormal loading pattern creates the formation of osteophytes at facet joints and vertebral endplates, which contributes to the narrowing of the spinal canal with further stenosis occurring due to hypertrophy and calcification of the ligamentum flavum (Tribus 2003; Aebi 2005).

Common symptoms include back pain, leg pain, radicular pain, neurological deficit and curve progression (Albert et al. 1995; J. A. Epstein et al. 1979).

Treatment options include non-operative management, for which there is limited evidence (J. S. Smith et al. 2009; van Dam 1988). The main aim is to improve pain

and function, not to correct spinal the deformity (Bridwell et al. 2009). Conservative treatment strategies are discussed in detail **Chapter 1.4.2**.

The goals of operative care are to perform neural decompression, improve back pain and restore spinal alignment (Bradford et al. 1999). A recent multicentre study found that patients selected for operative care had worse health-related quality of life scores than those selected for non-operative care, and younger patients in the operative group had larger scoliosis than those in the non-operative group, therefore these factors should be taken into account when assessing patients with adult scoliosis (K.-M. G. Fu et al. 2014).

Surgical options include decompression (with or without fusion) and/or curve correction. Decompression surgery alone is not usually indicated, except in elderly patients with severe symptoms. A limited fusion would improve the stability of the spine, but long-segment disease is not always amenable to this and such surgery would be associated with a higher risk of morbidity (Yadla et al. 2010).

A recent large systematic review showed a 13% risk of psuedoarthosis in adult scoliosis treated with decompression and fusion and a 40% risk of morbidity (Yadla et al. 2010). Similarly, a further retrospective multicentre study found a 12.4% risk of pseudoarthrosis and a 39% risk of morbidity overall complications. Additionally, 26% of all patients required re-operation, with risk factors including the number of fused vertebra and fusion to the sacrum (Charosky et al. 2012). The majority of revision cases are necessitated due to the presence of pseudoarthrosis and adjacent segment disease and revision surgery is associated with a higher risk of complications (Cho et al. 2012).

Corrective surgery is mostly performed in patients with primary degenerative lumbar scoliosis and chronic back pain. Correction includes release of the posterior (facets and ligaments) and anterior (discs, posterior longitudinal ligaments) elements via a posterior approach (Aebi 2005). A systematic review of scoliosis surgery found that in cases of curve correction, the average Cobb angle correction was 26.6^0, equivalent to 40.7% of the original curve (Yadla et al. 2010).

1.4 Treatment strategies for degenerative spinal conditions

1.4.1 Introduction

Treatments for degenerative spinal conditions encompass a variety of disciplines and approaches, and can be broadly divided into conservative and surgical options. These are discussed in detail below.

1.4.2 Conservative approach

Frequently employed, conservative management comprises of many different therapies, most of which can be used in combination with varying degrees of success, as detailed below. Such therapies include pharmacological agents, physical exercise and manual therapy and cognitive behavioural therapy.

1.4.2.1 Pharmacological therapies

Drug therapy can often provide symptomatic relief for patients with back pain, even when the exact underlying pathophysiology is unknown. Neuropathic pain, specifically radicular pain, is notoriously difficult to treat. Drugs that are commonly used to relieve back pain are discussed below.

Nonsteroidal anti-inflammatories

Nonsteroidal anti-inflammatories (NSAIDs) are the most frequently prescribed medications for back pain and have anti-inflammatory and analgesic effects. They inhibit cyclo-oxygenase enzymes (COX-1, present in platelets and gastroduodenal mucosa, and COX-2, plays a role in inflammation and present in

kidney), resulting in decreased prostaglandin synthesis, and they also have a central action. Examples include aspirin, ibuprofen, diclofenac (nonselective NSAIDs) and celecoxib and meloxicam (COX-2-selective)(Rao & Knaus 2008). A systematic review of 65 randomised controlled trials showed that NSAIDs are effective for short-term symptomatic relief in acute low back pain and there is no evidence that one NSAID is more effective than another (Roelofs et al. 2008). However, NSAIDs can have severe side-effects, including gastrointestinal bleeding, renal failure, hypertension and cardiac failure (Hernández-Díaz & García-Rodríguez 2001). COX-2-selective inhibitors are associated with a reduced risk of gastrointestinal bleeding, but the same risk of renal failure and a higher risk of coronary events, compared with nonselective NSAIDs (Silverstein et al. 2000; Bresalier et al. 2005).

Muscle relaxants

Skeletal muscle relaxants exert their effect through sedation and depression of neuronal transmission (Waldman 1994) and are effective in acute low back pain. Examples include diazepam and baclofen. Adverse effects include drowsiness and dizziness, and they can lead to dependence and abuse (Beebe et al. 2005).

Antidepressants

Serotonergic-noradrenergic (for example, amitriptyline and venlafaxine) and noradrenergic antidepressants (for example, desipramine and nortriptyline) are effective in chronic low back pain and neuropathic pain (Fishbain 2000; Salerno et al. 2002). It is thought that the analgesic effect is independent of the effect on

depression (V. Chang et al. 2008). Adverse effects include drowsiness, dizziness, dry mouth, constipation, urinary retention and weight gain (Chou et al. 2007).

Opioids

Opiods are used in the treatment of moderate and severe pain and act mainly via μ receptors (G-protein-coupled receptors) in the central and peripheral nervous systems. Examples include morphine, oxycodone and fentanyl. Controlled-release preparations are recommended in chronic pain due to comparable pain reduction with a significantly lower dosage and therefore reduced averse effects (Hale et al. 1999). Side effects are common and include nausea, vomiting, constipation, urinary retention, itching, sedation and respiratory depression (Portenoy 1996). In addition, physical dependence, tolerance and addiction can occur, therefore the use of opioids for back pain must be with caution and close monitoring.

Antiepileptics

Antiepileptics are most commonly used for neuropathic pain and examples include gabapentin and pregabalin. These membrane stabilisers are alpha$_2$-delta ligands and act on calcium channels (V. Chang et al. 2008). Side effects include dizziness, weight gain, confusion and fatigue.

1.4.2.2 Physical exercise and manual therapy

Physical therapies can be used to treat back pain, including spinal manipulative therapy, stabilization and directional (McKenzie-type) exercises. These are discussed in detail below.

Spinal manipulative therapy

Spinal manipulative therapy has been practised for centuries and there is evidence supporting its use, particularly in those patients with a new exacerbation of axial pain, spinal stiffness and/or low levels of psychological distress (Chou & Huffman 2007; Flynn et al. 2002; Crombez et al. 1999).
This therapy involves the use of a high-velocity, low-amplitude thrust force to the spine, with the aim of reducing the pain to the level at which the patient can then participate in general strengthening exercises (Childs et al. 2004).

Spinal stabilisation exercises

Spinal stabilisation exercises address deficits in strength, endurance and function of the trunk muscles. It is thought that this leads to a decrease in pain and disability by improving the motor control of spinal segments during movement (Danneels et al. 2001). A systematic review found that stabilisation exercises targeting the deep trunk muscles are more effective than 'usual care' by the GP but not more effective than other physiotherapy programmes (Rackwitz et al. 2006). However, those who benefit most from this therapy include those patients under 40 years old, greater overall flexibility, lumbar segmental hypermobility and those with clinical 'instability' (Hicks et al. 2005; Fritz et al. 2005).

Directional exercises

First described by Robin McKenzie, directional exercises are repeated movements to the end range of a particular lumbar motion, for example, extension (ref: McKenzie RA, May S, The Lumbar Spine: Mechanical Diagnosis and Therapy, 2nd ed. Minneapolis, MN, Orthopaedic Physical Therapy Products, 2003). Treatments progress by increasing the amount of force and increasing the range of motion. Patients most likely to benefit from this therapy include those who are able to centralise their pain with movement and those who have signs of nerve root compression (Browder et al. 2007).

1.4.2.3 Cognitive behavioural therapy

Cognitive behavioural therapy (CBT) includes self-talk, relaxation techniques, and coping strategies. A systematic review of 4 randomised trials comparing lumbar fusion surgery to nonsurgical (either traditional nonsurgical treatment or CBT) treatment of pain associated with degenerative lumbar disc disease showed that CBT outcomes were comparable with surgical outcomes at 1 year. Both surgery and CBT were more efficacious than unstructured nonoperative care, although limitations of the trials included high rates of cross-over and loss to follow-up (Mirza & Deyo 2007). Interdisciplinary programs have shown superior outcomes, such as those including occupational therapy, psychology, medicine and vocational rehabilitation (Chou et al. 2009).

1.4.3 Spinal fusion surgery

Spinal fusion is defined as a bony union between two vertebral bodies following surgical manipulation and was first reported in 1911 for the treatment of Pott's disease, tuberculous infection of the spine (Albee 2007). Advancements in surgical approach and technique have improved the safety of this operation and, importantly, there is a better understanding of the biological principles underpinning this surgery.

This section details the principles of spinal fusion surgery, including the fusion site, the bone graft, and systemic and local factors affecting fusion, with regards to lumbar fusion surgery. This section also details specific examples of lumbar fusion surgery and their complications and outcomes.

1.4.3.1 Principles

Fusion site

As previously discussed, bone growth is dependent on the presence of viable cells. Meticulous preparation of the fusion site is therefore critically important in preserving the local population of human mesenchymal stem cells, local vasculature and inflammatory cells, and subsequently facilitating a successful arthrodesis. Local blood supply is a source of oxygen and nutrients, allows recruitment of inflammatory cells, is a source of endothelial cells and a potential source of circulating osteogenic cells (Zvaifler et al. 2000).

The inflammatory response is a critical event, allowing the removal of necrotic tissue debris and the synthesis of an early matrix rich in hyaluronic acid (D. J. Simmons 1985). Local paracrine signalling via cytokines, kinins and

prostaglandins leads to proliferation, migration and differentiation of a variety of cells.

The host bone surface itself acts as a reservoir of osteogenic cells and provides an osteoinductive surface for graft incorporation. The larger the surface area of cancellous bone exposed during surgery, the greater the fusion rate (Lim et al. 2001).

Bone graft

Bone grafting is performed to promote and enhance bone regeneration. Grafts have osteogenic (from viable stem and osteoprogenitor cells), osteoinductive (capacity to activate immature cells and commit them to bone cells) and osteoconductive (capacity to enhance proliferation of osteoprogenitor cells) properties. Osteoinduction is dependent on the activity of BMPs (particularly 2, 4, 6, 7, and 9), TGF-β, IGF-I, IGF-II and bFGF. Osteoconduction is dependent on the size of the pores of the graft material, its surface chemistry and its degradation rate (Muschler & Midura 2002).

Grafts can be divided into autograft, allograft or synthetic graft.

Autograft can be either local or nonlocal, which is usually from the posterior or anterior iliac crest. This usually yields sufficient quantity of bone for fusion and the iliac tubercle, 5 cm posterolateral to the anterior superior iliac spine, yields the most cancellous bone. Due to it providing osteogenic bone and marrow cells, an osteoconductive matrix of collagen, mineral and proteins, and a range of osteoinductive proteins, autologous cancellous bone is considered the gold

standard graft material (Heiple et al. 1963; OIKARINEN & KORHONEN 1979), although it is of limited availability.

Additionally, bone graft harvest is associated with significant complications. Donor site pain is common and, in up to 15% of patients, persists for more than 3 months post-operatively (Boyle et al. 2003; Dawson et al. 1981; KURZ et al. 1989). Other complications include arterial injury (particularly the superior gluteal, fourth lumbar, iliolumbar and deep circumflex iliac arteries), nerve injury (particularly the ilioinguinal, iliohypogastric and lateral femoral cutaneous nerves) and haematoma formation (1-10%, depending on the use of a wound drain (SACKS 1965; Stauffer & Coventry 1972)).

Allograft is cadaveric bone and therefore has several advantages over autograft, including the lack of morbidity associated with harvesting autologous bone, unlimited availability, mechanical strength (as they can be selected from any bone), and the ability to be pre-processed into a customised shape and size. However, the preparation of these grafts leads to a loss in osteogenic and a reduction in osteoinductive properties, thereby limiting their use usually to operations in which significant mechanical strength is required, for example as a ring allograft in anterior lumbar interbody fusion (Cohen et al. 2000; Janssen et al. 2000).

Synthetic bone grafts are a growing area of development and interest, particularly due to the increased understanding of bone healing. Of note, BMPs, collagen and ceramics are now in clinical use and are discussed later in this chapter (**1.4.4**). **Table 1.3** summarises the osteogenic, osteoinductive and osteoconductive properties of clinical and experimental graft materials currently available (ref: Rothman-Simeone vol 2 p 1137).

Material	Osteogenic	Osteoinductive	Osteoconductive
Autogenous cancellous bone	+	+	+
Autogenous cortical bone	+	+	+
Vascularised autograft	+	+	+
Allograft		±	+
Deproteinated xenograft			+
Bone marrow	+	±	+
Demineralised bone matrix		+	+
Collagen			+
Ceramics			+
Bone morphogenetic protein		++	+

Table 1.3
Properties of graft materials (Rothman-Simeone, The Spine, 6th Edition)

Systemic factors influencing bone healing

Many systemic factors affect bone healing and these should be controlled and optimised as much as possible, particularly in the critical period of the first 7 days of healing. Factors associated with promoting bone healing include insulin, IGF, testosterone, oestrogen, growth hormone, thyroxine, parathyroid hormone and vitamins A, D and C. Factors negatively associated with bone healing include corticosteroids, anaemia, rheumatoid arthritis, NSAIDs, tobacco (nicotine) and sepsis (Bonewald 1999; Andersen et al. 2001; Glassman et al. 2000; Glassman et al. 1998).

Local factors influencing bone healing

Whilst some local factors associated with poor bone healing are unavoidable (for example, osteoporosis, tumour), others can be avoided or minimised, such as radiation and mechanical motion. Factors associated with improved bone healing include osteoinductive factors (for example, BMPs), angiogenic factors (for example, VEGF, VGF) and local stem cells from the bone marrow and periosteum.

1.4.3.2 Types of lumbar fusion surgery

Lumbar fusion surgery should be undertaken only after thorough discussion between by the surgeon and the patient, and usually after a multi-disciplinary team meeting including spinal surgeons, physiotherapists and radiologists. Usually conservative options have been attempted and failed.

A variety of fusion procedures can be undertaken and these are outlined below.

Posterolateral fusion

Posterolateral fusion surgery (PLF) is performed through a midline approach, with exposure of the posterior spinal elements, disruption of the facets and decortication of the transverse processes. Allo- or autograft is placed over these surfaces to stimulate bone growth. PLF can be augmented with pedicle screws to provide further stability and hence improve fusion rates, although this might be at the expense of a higher complication rate in instrumented PLF (M. Lorenz et al. 1991; Schwab et al. 1995; Wood et al. 1995). Overall, PLF is considered a good option for a single level lumbar fusion.

Lumbar Interbody Fusion

Lumbar interbody fusion (LIF) techniques have been used for years to treat a number of pathologies of the lower back including spinal stenosis, spinal deformity, and radiculopathy secondary to degenerative disc disease. Recently many variants of lumbar interbody spinal fusion have been popularised. The common principle of these techniques is to remove the intervertebral disc, which is presumed to be the main cause of the back pain, and place an implant with or without graft material. By restoring the height of the spinal motion segment a return to normal biomechanics is achieved. Also, additional load on the posterior spinal elements is removed. Furthermore, for the purpose of achieving spinal fusion, interbody fusion surgery offers a larger surface area than the posterolateral method.

Interbody fusion surgery is classified according to the approach used, as outlined below.

Anterior Lumbar Interbody Fusion (ALIF)

ALIF is performed via a retroperitoneal approach, which allows complete exposure of the ventral surface of the spine, centred on the disc space with lateral extension as required. Indications for this procedure include axial back pain due to degenerative disc disease with degeneration of the spine. Relative contraindications include obesity, severe atherosclerotic disease of the major vessels and extensive previous abdominal surgery (such patients might require a transperitoneal approach). Specific complications include injuries to adjacent structures, particularly the ureters and segmental vessels, and in men,

retrograde ejaculation. ALIF is associated with the highest reported fusion rates (80-89% (Loguidice et al. 1988; Newman & Grinstead 1992)), however, it is technically more demanding and associated with higher complication rates than other fusion techniques therefore it is employed less frequently.

Posterior and Transforaminal Lumbar Interbody Fusion

Posterior lumbar interbody fusion (PLIF) is performed via a posterior approach to the disc space, yet provides good anterior column support. In PLIF the disc is approached through laminectomy, partial facetectomy and retraction of the dura and its contents.

Transforaminal lumbar interbody fusion (TLIF) can also be performed through a posterior approach however, a wiltse approach is considered more appropriate. A complete facetectomy is performed, through which the disc is removed. A thorough preparation of the endplate is undertaken and a structural graft or a cage is placed to restore the disc height. The placement of pedicle screws is mandatory and these are connected through rods to provide further stability to the spinal segment. Benefits of this method of interbody fusion includes decompression of the neural foramen and improved sagittal alignment.

1.4.3.3 Complications

Advances in surgical technique have improved the safety of spinal fusion surgery, although complications remain a significant cause of morbidity. These can be broadly divided into neural injury, dural injury, vascular injury and instrumentation complications (biological: infection, osteoporosis, pseudathrosis; biomechanical failure; error in application) and infection.

A recent retrospective analysis of interbody fusion surgery performed in the United States reported the complications following ALIF, P/TLIF (posterior/transforaminal lumbar interbody fusion) and LIF with a combined anterior-posterior interbody fusion (APF) (Goz et al. 2013). The vast majority of these procedures were performed for degenerative disorders (94.7%, 97.6% and 97.8%, respectively), with the remainder performed for trauma or cancer. Additionally, the authors performed multivariate analysis for primary outcomes, adjusting for overall comorbidity burden, race, gender, age, and length of fusion. A summary of the complications is shown in **Table 1.4**.

A meta-analysis of randomized controlled trials showed that, compared with instrumented PLF, circumferential fusion is associated with a higher complication rate and a higher blood loss (Han et al. 2009).

Revision surgery is associated with a higher risk of complications than primary fusion surgery, specifically dural tears (odds ratio 1.1; 95% CI 1.19 to 1.67, $p<0.001$) and surgical site infection (odds ratio 3.4; 95% CI 2.44 to 4.74; $p<0.001$) (Rajaee et al. 2014).

Complication	*ALIF (%)*	*P/TLIF (%)*	*APF (%)*	*p value*	*Multivariate logistic regression analysis, compared to ALIF*			
					APF		*P/TLIF*	
					OR	*95% CI*	*OR*	*95% CI*
Dysphagia	0.17	0.13	0.11	0.0017	0.48	0.17-1.33	**0.37**	**0.21-0.65**
Device-related	5.43	2.44	3.89	<0.0001	**0.57**	**0.47-0.69**	**0.39**	**0.34-0.44**
Central nervous system	0.37	0.96	0.55	<0.0001	0.88	0.46-1.68	**2.09**	**1.37-3.20**
Cardiac	0.90	0.87	1.23	<0.0001	1.39	0.96-2.00	**0.68**	**0.51-0.90**
Peripheral vascular	0.22	0.08	0.28	<0.0001	0.81	0.37-1.80	**0.19**	**0.10-0.36**
Respiratory	1.65	1.25	2.20	<0.0001	1.27	0.96-1.69	**0.63**	**0.51-0.78**
Gastrointestinal	4.83	2.02	5.56	<0.0001	1.05	0.87-1.26	**0.40**	**0.35-0.46**
Genitourinary	0.84	1.02	1.11	<0.0001	1.08	0.70-1.68	0.92	0.68-1.26
Postoperative shock	0.08	0.08	0.13	0.0002	0.85	0.25-2.95	0.60	0.26-1.40
Haematoma/seroma	0.63	0.62	0.82	<0.0001	0.93	0.60-1.45	**0.68**	**0.50-0.92**
Intraoperative injury of nerve/vessel	3.41	3.43	4.20	<0.0001	1.03	0.82-1.29	0.91	0.78-1.07
Wound dehiscence	0.27	0.15	0.37	<0.0001	1.52	0.71-3.25	**0.53**	**0.29-0.99**
Postoperative infection	0.74	0.43	0.74	<0.0001	**0.45**	**0.26-0.80**	**0.45**	**0.32-0.62**
Anaemia due to bleeding	7.39	11.42	11.60	<0.0001	**1.23**	**1.07-1.40**	1.03	0.93-1.13
Acute respiratory distress syndrome	1.36	0.75	1.36	<0.0001	0.79	0.58-1.09	**0.40**	**0.32-0.50**
Venous thromboembolic events	0.62	0.41	0.73	<0.0001	1.06	0.68-1.63	**0.46**	**0.33-0.63**

Table 1.4

Summary of complications in lumbar interbody fusion surgery, multivariate analysis compared to ALIF. OR, odds ratio; CI, confidence interval; APF, anterior-posterior interbody fusion; ALIF, anterior lumbar interbody fusion; PLIF, posterior/transforaminal lumbar interbody fusion. Adapted from (Goz et al. 2013)

1.4.3.4 Outcomes

There is some high-quality evidence from six prospective, randomised controlled trials showing a superior effect of spinal fusion surgery with regards to improving quality of life (as assessed by the ODI) and reducing back pain, compared to conservative management (Fritzell et al. 2001; Brox et al. 2010; Brox et al. 2006; Brox et al. 2003; Ohtori et al. 2011; Fairbank et al. 2005). Patients in the trials summarised in **Table 1.5** who received surgical treatment underwent 1-2 level fusion. Overall, there was a weighted average improvement in back pain of 35% in the surgical group, compared with 20% in the non-operative group (Phillips et al. 2013). ODI improved by 29% in the surgical group and 17.5% in the non-operative group. Average fusion rates in the surgical groups were 84%, with a reoperation rate of 7%.

Reference	*Groups (n)*	*Follow-up (months)*	*Mean age (years)*	*Change in back pain (%)*	*Change in ODI (%)*	*Fusion rate (%)*	*Re-operation rate (%)*
(Fritzell et al. 2001)	PLIF, Instr. PLF, ALIF/PLIF (222)	24	43	33	25	83	7.6
	Physiotherapy (72)		44	7	6	NA	NA
(Brox et al. 2003)	Instr. PLF (37)	12	44.1	37	37	84	NR
	Cognitive intervention & exercise (27)		42.4	24	31	NA	NA
(Brox et al. 2006)	Instr. PLF (29)	12	42	22	19	85	NR
	Cognitive intervention & exercise (31)		43	23	28	NA	NA
(Fairbank et al. 2005)	Lumbar fusion (176)	24	NR	NR	27	NR	6
	Intensive rehab (173)		NR	NR	19	NA	NA
(Brox et al. 2010)	Instr. PLF (62)	48	42.7	36	34	NR	NR
	Cognitive intervention & exercise (49)		43.9	27	6	NA	NA
(Ohtori et al. 2011)	ALIF, PLF (21)	24	35.6	77	79	100	NR
	Exercise (20)		33	39	38	NA	NA
Surgery	**TOTAL**	**547**	**41.5**	**35.3**	**29.0**	**84.5**	**7.0**
Nonoperative	**TOTAL**	**372**	**41.3**	**20.0**	**17.5**	**NA**	**NA**

Table 1.5

Summary of outcomes of spinal fusion surgery compared to conservative management, with total weighted averages displayed. Instr. PLF, instrumented posterolateral fusion; PLIF, posterior lumbar interbody fusion; ALIF, anterior lumbar interbody fusion; ODI, Oswestry Disability Index. Adapted from (Phillips et al. 2013)

1.4.4 Bone substitutes in lumbar fusion surgery

As previously discussed, spinal fusion surgery is associated with significant rates of nonunion (or pseudoarthrosis), leading to pain, reduced mobility and overall poor quality of life. In order to improve fusion rates, and avoid the morbidity associated with bone graft harvest, substitutes for autologous bone grafts have been sought. The 'diamond concept' has been proposed to describe the necessary components of proper bone healing and consists of growth factors, scaffolds, mesenchymal stem cells and the mechanical environment (Giannoudis et al. 2007), therefore the optimal substitute would contain all these components.

1.4.4.1 Allografts

As detailed in Chapter **1.4.3.1**, allografts are readily available and widely-used substitutes for autologous bone graft. Whilst they possess no osteogenic capability, they do provide mechanical support and have been used as ring allografts in anterior lumbar fusion surgery (Kozak et al. 1994; Silcox 1998). In fact, one study of revision surgery showed that outcomes with allograft were comparable to those with autograft (Buttermann et al. 1997).

However, there is a large body of evidence showing that the use of allografts is associated with lower fusion rates than autografts in posterior spinal fusion surgery and therefore allografts should not be used for this indication (Jorgenson et al. 1994; An et al. 1995).

1.4.4.2 Ceramics

Ceramics provide an osteoconductive matrix which is biodegradable, nontoxic, nonimmunogenic, easy to sterilise and readily available. In spinal fusion, the most commonly used are calcium phosphates such as hydroxyapatite and tricalcium phosphate.

However, ceramics have poor biomechanical strength and must therefore be used in conjunction with internal fixation, often in combination with local autograft (as 'bone graft extenders') (W. J. Chen et al. 2005; N. E. Epstein 2006). Coralline hydroxyapatite together with internal fixation has shown good outcomes in anterior lumbar interbody fusion, but it is not alone sufficient to promote bone fusion (Plotkin et al. 2002; Thalgott, Klezl, et al. 2002b; Thalgott, Giuffre, et al. 2002a).

When combined with osteogenic and osteoinductive materials, such as autograft or bone marrow, ceramics can support angiogenesis and promote new bone formation (Silverstein et al. 2000; Ohgushi et al. 1989; Bresalier et al. 2005). Ceramics can also function as effective carriers for the delivery of osteoinductive growth factors. Hydroxyapatite is retained in vivo for prolonged periods of time and is a relatively inert substance, making it a good scaffold material (Waldman 1994; Jarcho 1981).

1.4.4.3 Demineralised bone matrices

Demineralised bone matrices (DBMs) are produced by removing the mineralised component from allograft bone. Decalcified bone was first noted to cause

heterotopic bone in rodents, primarily due to the presence of osteoinductive BMPs (Beebe et al. 2005; Urist 1965).

In animal studies, DBM have been used with efficacy in posterolateral spinal fusion models alone or with autograft, bone marrow or ceramics (Fishbain 2000; Choi et al. 2007; Salerno et al. 2002; Louis-Ugbo et al. 2004; Yee et al. 2003). Clinically, DBMs have been used successfully as bone graft extenders for posterolateral spinal fusion (V. Chang et al. 2008; Sassard et al. 2000; Girardi & Cammisa 2003). There is also weaker evidence to support the use of DBM composites (DBM with titanium mesh cage and coralline hydroxyapatite) as part of a rigidly instrumented circumferential fusion in anterior lumbar interbody fusion surgery (Thalgott et al. 1999). The physical state of the DBM can influence its osteoinductive ability, with putty and flexible sheets having a greater capacity to form bone than DBM gel (Martin et al. 1999). As they contain no viable cells, DBMs require the concomitant use or presence of osteoprogenitor cells and some supporting vasculature to achieve the best osteoinductive effect.

1.4.5 Alternative approaches

In order to obtain the best possible fusion rates in spinal surgery, attempts have been made to identify superior products which can be used as adjuvant therapies. These include osteoinductive growth factors (predominantly BMPs), autologous platelet concentrate, gene therapy and mesenchymal stem cells. These will be discussed in this section in detail.

1.4.5.1 Bone morphogenetic proteins

In 1965, Marshall Urist discovered that extracts from demineralised bone matrix could give rise to functional bone tissue (Chou et al. 2007; Urist 1965). He named this activity 'bone by auto-induction' and named the active compounds responsible for bone formation Bone Morphogenetic Proteins (BMPs). BMPs initiate the events which lead to differentiation of progenitor cells to osteoblasts (Sampath & Reddi 1981). The BMPs are the largest subgroup in the TGF-β superfamily of genes and to date 20 members of the BMP sub-family have been identified (Xiao et al. 2007; Wozney et al. 1988).

Structure

All 45 members of the TGF-β superfamily possess an N-terminal signal sequence, a prodomain and a mature domain (containing a highly conserved 7-cysteine motif) at the carboxy-terminus. BMPs are grouped together on the basis of amino acid sequence homology of the mature domain. BMP-2 and BMP-4 share 80% amino acid sequence homology, BMP-5, 6, 7, 8 share 78% amino acid sequence homology and other groups have approximately 50% amino acid sequence homology (Giannoudis et al. 2007; Ozkaynak et al. 1992; Bessa, Casal, et al. 2008a).

Like other TGF-β family members, BMP-2 protomer is produced as a precursor protein consisting of an N-terminal signal sequence, a prodomain, and a mature domain at the carboxy-terminus. Intra-subunit disulphide bond formation generates the unique 6-cystine knot motif and subsequent folding leads to disulphide bond linking of 2 subunits into a stable dimeric protein (Scheufler et al. 1999). The prodomain region is then cleaved by a furin-like protease to

release the mature bioactive dimeric protein of most of the members of the BMPs (Urist 1965; Aono et al. 1995; Y. Cui et al. 1998). However, in the case of BMP-8 and BMP-9, the prodomain remains associated with the ligand, inhibiting their binding to the receptors (Sampath & Reddi 1981; Brown et al. 2005). The elucidation of the crystal structure of BMP-2, BMP-7 and BMP-9 (Xiao et al. 2007; Scheufler et al. 1999; Wozney et al. 1988; Griffith et al. 1996; Brown et al. 2005) provided further evidence of the structural similarity between BMPs and TGF-β.

Functions

The biologically active proteins consist of homodimers or their heteromeric forms (Ozkaynak et al. 1992; Israel et al. 1996; Bessa, Casal, et al. 2008a). Physiological roles of BMPs include cell proliferation, differentiation, apoptosis and morphogenesis (**Table 1.5**).

BMPs-2, -4, -6, -7, and -9 are inducers of bone formation, with BMP-9 having the highest capacity (Scheufler et al. 1999; Massie et al. 2007). Various studies have shown BMPs to be responsible for dorsal-ventral patterning in embryogenesis and recently it has been shown that heteromeric forms of BMPs are responsible for the initiation and development of dorsoventral patterns in embryogenesis (Aono et al. 1995; Little & Mullins 2009; Y. Cui et al. 1998).

BMP	***Nomenclature***	***Gene locus***	***Main physiological roles***
BMP-2	BMP-2a	20pl2	Cartilage and bone morphogenesis/heart development
BMP-3	Osteogenin	14p22	Negative regulator of osteogenesis
BMP-3b	GDF-10		Negative regulator of osteogenesis
BMP-4	BMP-2b	14q22-q23	Osteogenesis, chondrogenesis, kidney, lung, eye morphogenesis
BMP-5		6p12.1	Osteogenesis and chondrogenesis
BMP-6	Vrg1, Dvr6	6p12.1	Cartilage hypertrophy, osteogenesis,
BMP-7	OP-1	20q13	Osteogenesis, kidney morphogenesis, eye development
BMP-8	OP-2	1p35-p32	Osteogenesis, spermatogenesis
BMP-9	GDF-2	11q11.22	Hepatogenesis, osteogenesis, development of cholinergic neurons, glucose metabolism
BMP-11	GDF-11, myostatin	12q13.13	Axial skeleton patterning, eye development, pancreas development, kidney formation
BMP-12	CDMP-3, GDF-7	2p24-2p23	Tendon and ligament development
BMP-13	CDMP-2, GDF-6	8q22.1	Cartilage development
BMP-14	CDMP-1, GDF-5	20q11.2	Chondrogenesis and angiogenesis
BMP-15		Xp11.2	Modifies follicle stimulating hormone activity

Table 1.5

Details of BMP nomenclature, gene locus and main physiological roles (Brown et al. 2005; Bessa, Casal, et al. 2008a; Xiao et al. 2007)

Signalling Pathways

The BMP ligands bind to extracellular receptors that translate the signal from outside of the cell into the cytoplasm, where various intracellular signal transducer molecules induce gene activation through activation of transcription

factors. Two types of transmembrane serine/threonine kinase receptors (type I & type II) are activated by BMP ligands. The structure of both receptors consists of an extracellular ligand binding domain, a transmembrane domain and an intracellular serine/threonine kinase domain.

The type I receptor is different from the type II receptor, possessing two distinct motifs: a glycine/serine (GS box) located at the juxtamembrane region and a L45 loop in the kinase domain. BMP ligands are known to bind to at least three type I receptors: activin receptor Ia (ActR-I or Alk2), BmprIa (Alk3) and BmprIb (Alk6).

Binding of BMP to the type II receptor (BmprII) leads to the activation of the GS box and the L45 loop in the type I receptor (Scheufler et al. 1999; Y. G. Chen et al. 1998; Griffith et al. 1996; Shimasaki et al. 2004; Brown et al. 2005). BMPs bind to two isomeric forms (short and long) of type II receptors (Israel et al. 1996; Bessa, Casal, et al. 2008a). Other receptors that have been implicated in the signalling pathway include activin type II receptor, activin type IIB receptor and recently type III TGF-β receptors (Massie et al. 2007; Kirkbride et al. 2008).

Binding of BMP to its receptors can activate either a Smad-dependent signalling pathway or a Smad-independent signalling pathway.

Smad-dependent signalling pathway

This pathway functions through the binding of BMP to a pre-formed heteromeric receptor complex (Little & Mullins 2009; Nohe et al. 2002). Upon BMP-2 binding to BmprII, the BmprI GS box is phosphorylated which allows the recruitment of BMP Smad1, 5 and 8 (R-Smads) to BmprI and leads to their subsequent phosphorylation by BmprI kinase. R-Smads dissociates itself from the receptor

complex, forms oligomers with Smad4 and translocates into the nucleus where it regulates the transcription of BMP target genes, such as the transcription factor RUNX2, which regulates the differentiation of mesenchymal progenitor cells into osteoblasts (Bessa, Casal, et al. 2008a; Lee et al. 2000; Xiao et al. 2007). Smad6 and 7 can negatively regulate this pathway.

Smad-independent signalling pathway

In contrast to the Smad-dependent pathway, it has been shown that the Smad-independent signalling pathway is activated by the formation of heteromeric receptor complexes induced by BMP-2 (Y. G. Chen et al. 1998; Nohe et al. 2002; Shimasaki et al. 2004). Upon binding of BMP to the high-affinity BmprI, there is recruitment of BmprII into the signalling complex and, via XIAP, activation of the MAP kinase-signalling pathway. This results in activation of JNK and p38, and subsequent target gene expression. Of particular importance is the phosphorylation of p38, which induces the expression of specific BMP target genes, including type I collagen, fibronectin, osteopontin, osteocalcin and ALP (Bessa, Casal, et al. 2008a; K. K. Nakamura et al. 1999; Lai & Cheng 2002).

In addition to the Smad-dependent and Smad-independent pathways, there are multiple interactions and cross-talk with other pathways, including the Wnt, Notch, EGF, STAT/LIF, MAPK and IGF pathways. Wnt signalling leads to an increase in the expression of RUNX2, thus promoting osteogenesis (Kirkbride et al. 2008; Gaur et al. 2005). Conversely, inhibition of Wnt signalling leads to an inhibition of BMP-2-induced ALP activity (Nohe et al. 2002; Rawadi et al. 2003).

BMP antagonists

Whilst there is some autoregulation of BMP expression in osteoblasts (Lee et al. 2000; Pereira et al. 2000), there are many other inhibitors of BMP signalling. These can be broadly divided into extracellular and intracellular antagonists.

Extracellular antagonists

All the extracellular BMP antagonists are characterised by a cysteine-rich domain that allows the formation of cystine knot strctures, which facilitate protein-protein interactions. These antagonists can therefore be classified on the basis of the spacing of the cysteine residues in the cystine rings into noggin, chordin, Tsg and Dan family (Nohe et al. 2002; Gazzerro & Canalis 2006). Noggin is a glycosylated homdimer of 64kDa and binds to BMP-2, -4, -5, -6 and -7, thus preventing them from binding to their receptors (K. K. Nakamura et al. 1999; Zimmerman et al. 1996; Lai & Cheng 2002). Its expression is increased by the presence of BMPs and it plays an important negative regulatory role in osteogenesis and chondrogenesis (Gaur et al. 2005; Gazzerro et al. 1998; Pathi et al. 1999).

Chordin is a glycosylated protein of 120kDa and binds specifically to BMP-2, -4 and -7 (Rawadi et al. 2003; Piccolo et al. 1996). Although it has not been reported to have a role in osteoblastic function, it is expressed by chondrocytes and its expression is increased in osteoarthritic joint cartilage (Pereira et al. 2000; D. Zhang et al. 2002).

Tsg is a secreted glycoprotein of 24kDa which can act as either a promoter or inhibitor of BMP signalling, depending on its concentration in osteoblasts (Gazzerro & Canalis 2006; Gazzerro, Deregowski, et al. 2005a; C. Chang et al. 2001; Scott et al. 2001). Tsg binds to BMP-2 or -4 (or directly to a BMP-chordin complex) and forms a complex with chordin, inhibiting BMP signalling.

The Dan family comprises of 9 members (Dan, gremlin, USAG-1, Cerberus, caronte, coco, dante, PRDC, sclerostin), but only a few of these have a role in skeletogenesis. The expression of gremlin is induced by BMPs and prevents the differentiation and function of osteoblasts, resulting in osteopenia and bone fractures (Zimmerman et al. 1996; Pereira et al. 2000; Gazzerro, Pereira, et al. 2005b). Sclerostin is expressed in osteoblasts, osteocytes and hypertrophic chondrocytes. Its expression is upregulated by BMP-2, -4 and -6 and it has high homology to USAG-1. Both USAG-1 and sclerostin can act as Wnt antagonists (Gazzerro et al. 1998; Yanagita 2005; Pathi et al. 1999).

Intracellular Inhibition

BAMBI is a transmembrane glycoprotein with a similar extracellular domain to BmprI, but without an intracellular kinase domain. It associates with and inhibits activated type I and type II receptors, but does itself not require the binding of BMPs (Piccolo et al. 1996; Onichtchouk et al. 1999).

Smad6 and 7 are inhibitory Smads which bind to type I receptors, interfering with the phosphorylation of Smad1, 5 and 8, and prevents their heterodimerisation with Smad4 (D. Zhang et al. 2002; Miyazono 1999).

Ski interferes with the formation of Smad complexes by interacting with signalling Smads (1, 4, 5, and 8), but not with inhibitory Smads (Gazzerro, Deregowski, et al. 2005a; W. W. Wang et al. 2000; C. Chang et al. 2001; Scott et al. 2001). Tob also interferes with the formation of Smad complexes and also inhibits BMP signalling by interacting with type I receptors (Pereira et al. 2000; Yoshida et al. 2000; Gazzerro, Pereira, et al. 2005b).

Smurf1 and 2 are Smad-specific E3 ubiquitin ligases that specifically interact with Smad1 and 5 (but also the inhibitory Smads6 and 7), triggering their inactivation via ubiquitination and proteasomal degradation (Yanagita 2005; H. Zhu et al. 1999; Y. Zhang et al. 2001).

Synthesis of Recombinant BMPs

Since the discovery of BMPs and the subsequent demonstrations of their critical importance in osteogenesis, considerable efforts have been put into the production of recombinant BMPs, particularly BMP-2 and BMP-7, which are free of impurities and therefore do not illicit a host response (in contrast to purified extracts).

Soon after the initial discovery of BMPs, attempts were made to isolate BMPs from the bone of different species, including rabbit (Onichtchouk et al. 1999; Urist et al. 1979), human (Miyazono 1999; Bauer & Urist 1981), cow (W. W. Wang et al. 2000; Mizutani & Urist 1982), pig (Yoshida et al. 2000; L. Ko et al. 1990), dog (H. Zhu et al. 1999; Boyan et al. 1992; Y. Zhang et al. 2001) and baboon (Urist et al. 1979; Ripamonti 1992). However, these attempts were

limited by very low yields of approximately 1-2μg BMPs/kg of bone (Bauer & Urist 1981; Bessa, Casal, et al. 2008a). Although yield was low, extraction of BMPs in such a way allowed the amino acid sequences to be determined and subsequent cloning of these sequences into expression vectors (Mizutani & Urist 1982; Wozney et al. 1988; Rosen et al. 1989; Celeste et al. 1990).

The first published evidence of recombinant human (rh) BMP-2 production used Chinese hamster ovary (CHO) cells (L. Ko et al. 1990; E. A. Wang et al. 1990). Subsequent studies have used either mammalian expression systems (Boyan et al. 1992; Sampath et al. 1992; Israel et al. 1996) or bacterial expression systems (Ripamonti 1992; Ruppert & Hoffmann 1996; Vallejo et al. 2002; Long et al. 2006; Bessa, Pedro, et al. 2008b). The mammalian expression system has the advantage of producing glycosylated, active BMPs, but is relatively low-yield. The bacterial expression system has the advantage of producing large amounts of BMPs, but this requires time-consuming and complicated isolation from inclusion bodies, solubilisation and refolding, which is therefore costly. Furthermore, no BMPs produced in *E. coli* expression systems have yet received FDA approval for clinical use, although other recombinant proteins from such systems are in regular clinical use (for example, human insulin (Humulin®, Lilly), human growth hormone (Nutropin®, Genentech) and human interferon (Bayer)).

The production of recombinant BMPs so far described has resulted in the production of homodimeric BMPs. However, it was considered that heterodimeric forms of BMPs might exist and possess enhanced bioactivity, therefore recombinant xenopus BMP-2/7 and BMP-4/7 heterodimers were synthesised using a baculovirus/insect expression system (Bessa, Casal, et al. 2008a; Hazama et al. 1995). BMP-4/7 heterodimers showed increased in-vivo

bone formation by up to approximately 20-fold compared to homodimers. Similarly, rhBMP-2/6 and rhBMP-2/7 heterodimers produced using CHO cells showed approximately 20-fold higher in-vitro bioactivity (ALP assay) and approximately 10-fold higher in-vivo bone formation, compared to homodimers (Wozney et al. 1988; Israel et al. 1996; Rosen et al. 1989; Celeste et al. 1990). Such enhanced osteogenic potential could be explained by the finding that BMP heterodimers induce lower levels of the BMP antagonist Noggin (E. A. Wang et al. 1990; W. Zhu et al. 2006).

Delivery of rhBMP in clinical applications

As recombinant BMPs possess significant osteogenic potential, there is considerable interest in the use of BMPs in tissue engineering, particularly for bone and cartilage. BMPs have a short half-life (approximately 6 mins in non-human primates) and their rapid clearance from the site of application continues to drive the need to find an optimal delivery system or carrier matrix (Sampath et al. 1992; Poynton & Lane 2002; Israel et al. 1996). The delivery system should deliver BMPs in adequate concentrations to the anatomical site of interest and facilitate the retention of BMPs at the site of injury (Ruppert & Hoffmann 1996; Mont et al. 2004; Vallejo et al. 2002; Long et al. 2006; Bessa, Pedro, et al. 2008b).

The 'ideal' delivery system would be predictably biodegradable, whilst protecting the BMPs from degradation. It should stimulate a minimal inflammatory response but allow vascularisation and ingress of cells. As with other delivery systems for in-vivo use, it should lack toxicity and carcinogenicity, be easily sterilised, stable and cost-effective (Hazama et al. 1995; Haidar, Hamdy & Tabrizian 2009a; Geiger et al. 2003).

Release of growth factors such as BMPs can be diffusion-controlled, chemical reaction-controlled, solvent-controlled, or a combination of these mechanisms (Israel et al. 1996; Luginbuehl et al. 2004). BMP release from within the pores of porous scaffolds is diffusion-controlled, whereas BMP that is physically immobilised in a carrier matrix and released by its degradation is a chemical reaction-controlled system. The rate of release also depends on the molecular weight of the BMP, its conformation and its solubility (W. Zhu et al. 2006; Kirker-Head 2000). The release kinetics of BMP from its delivery system is of great importance, as it has been shown for BMP-2 that extremes of release (i.e. bolus injection or prolonged low-level release) are not beneficial to osteogenesis (Poynton & Lane 2002; Geiger et al. 2003). Although the optimal release pattern will be specific both to the material and BMP used, and the nature and size of the defect, the ideal delivery system would provide a sustained release (to achieve a threshold concentration of BMP) for a period of time sufficient for bone growth.

The optimal concentration of BMP at the defect site has not yet been determined, although it depends on the size of the defect, its vascularisation and the delivery system being used (Mont et al. 2004; Haidar, Hamdy & Tabrizian 2009b). BMPs are capable of osteoinduction in non-bony sites, leading to ectopic bone formation, therefore the lower the dose which can be used to enhance osteogenesis, the lower the risk of such side-effects (Haidar, Hamdy & Tabrizian 2009a; Okubo et al. 2000; Geiger et al. 2003).

Systems for BMP delivery

The methods currently used to fabricate BMP delivery systems can be divided into attachment on the surface of the scaffold and entrapment within the pores

or within the matrix of a scaffold during its fabrication (Luginbuehl et al. 2004; Sokolsky-Papkov et al. 2007). Attachment methods include adsorption of BMP and chemical attachment of BMP onto the scaffold. Entrapment methods include entrapment within hydrogels, porous solid scaffolds (fabricated by solvent casting/particulate leaching or by supercritical fluid), electrospun scaffolds and within nano-/microsphere-based scaffolds. Other methods include double emulsion; wet spinning and fused deposited modelling.

Depending on the method employed, different release patterns of BMPs will be achieved based on a biphasic release profile (initial burst release followed by a period of slower sustained release). However, the method of entrapment using supercritical CO_2 foaming to fabricate a porous solid scaffold has shown a more sustained release profile, with only a minimal initial burst release (Kirker-Head 2000; Schliephake et al. 2007).

Natural-origin polymers as BMP delivery systems

Natural-origin polymers possess excellent properties such as being biodegradable, bioresorbable, versatile and having good availability. The most widely used of these is collagen, which is discussed in detail and other natural-origin polymers are also briefly mentioned.

Collagen is a naturally occurring polymer and is the largest non-mineral component of bone. There are over 29 types of collagen but over 90% of the collagen in the body is type I, II, III and IV, with the most abundant being type I. It is degraded and absorbed in-vivo and there are a large number of preparations available which make it a very versatile delivery system. Indeed, type I collagen is considered to be the 'gold standard' delivery system and two such products

have been approved by the FDA. INFUSE® Bone Graft (Medtronic) consists of an absorbable collagen sponge (ACS) carrier with rhBMP-2 at a concentration of 1.5mg/ml and has been approved for use in interbody spinal fusions, fresh tibial fractures and some oral-maxillofacial procedures. OP-1 Implant/Putty (Stryker) contains an ACS carrier with rhBMP-7 at a concentration of 1mg/ml. Advances in the incorporation of rhBMP into collagen carriers are ongoing, and His-tagged rhBMP-2 and His-antibody-containing collagen carriers have been used together to increase the retention of BMP by the carrier (Geiger et al. 2003; Zhao et al. 2010).

Despite its versatility, the binding of BMP to collagen carriers has been shown to be highly dependent on pH, protein concentration and protein isoelectric point; the retention of BMP by collagen carriers has been show to vary by up to 100-fold depending on the isoelectric point of the BMP used (Haidar, Hamdy & Tabrizian 2009b; Uludag et al. 1999). Additionally, collagen carriers are produced from animal tissues and therefore pose a potential risk of infection transmission and immunogenicity.

Alginate is a polysaccharide from seaweed, which has been combined with rhBMP-2, TGF-β3 and bone marrow cells (Okubo et al. 2000; C. A. Simmons et al. 2004) to successfully promote bone formation. Alginate has also been combined with a 73-92 peptide from the knuckle epitope of BMP-2, in an attempt to reduce the production costs, and this has been shown to promote bone formation (Sokolsky-Papkov et al. 2007; A. Saito et al. 2003).

Chitosan is a copolymer of N-acetyl-D-glucosamine and glucosamine and has been used to deliver rhBMP-2 by itself (Schliephake et al. 2007; Prabaharan & Mano 2005), with alginate (Zhao et al. 2010; D.-J. Park et al. 2005), and with gelatine (Uludag et al. 1999; Liang et al. 2005).

Hyaluronic acid is an anionic glycosaminoglycan, which can therefore form ionic bonds with cationic BMPs, and it has been shown to be superior in bone formation when compared with collagen as a carrier of rhBMP-2 (C. A. Simmons et al. 2004; Arosarena & Collins 2005).

Synthetic ceramics as BMP delivery systems

Synthetic ceramics possess the ability to form a bone-like mineral surface layer, which leads to an increased interface between the material and the bone, thus promoting bone growth.

Synthetic hydroxyapatite (HA) has been used extensively as a bone substitute material since the 1980s (A. Saito et al. 2003; Frame et al. 1981), as it provides a stable interface between itself and bone, the 'apatite layer'. A Langmuir-type adsorption mechanism has been shown for BMP-2 attachment on nano-crystalline-coated HA/tricalcium phosphate (TCP) and apatite-coated ceramics display better BMP-2 release than uncoated ceramics (Prabaharan & Mano 2005; Autefage et al. 2009).

HA has been shown to induce bone formation when used in combination with mesenchymal stem cells as a carrier for rhBMP-2 (D.-J. Park et al. 2005; Noshi et al. 2001) and when used in combination with ACS as a carrier for rhBMP-2

(Liang et al. 2005; Kraiwattanapong et al. 2005). A greater proportion of BMP is released from HA compared to from TCP, supporting the use of HA as a delivery system *in vivo* (Arosarena & Collins 2005; Tazaki et al. 2009).

More recently, HA has been combined with natural and synthetic polymers, such as collagen and PLGA, for the delivery of BMPs and this combination has been shown to increase bone formation more than hydroxyapatite or rhBMPs alone (Frame et al. 1981; C.-K. Wang et al. 2009; S. Itoh et al. 2004). However, the inherent inability of HA to completely degrade limits its clinical use as a carrier system.

Calcium phosphates have excellent osteoconductivity and, due to this, high doses of rhBMPs are not required for bone induction (Autefage et al. 2009; Yuan et al. 2001). Lyophilised BMPs can be used in low-temperature cements and solutions of BMPs can be adsorbed onto the surface of high-temperature cements. Calcium phosphate coatings have been shown to be capable of delivering BMPs when coated onto titanium, and much less BMP is needed than that used in collagen matrices (Noshi et al. 2001; Yuelian Liu et al. 2004; Y Liu et al. 2005). However, one of the significant limitations of calcium phosphates is a lack of mechanical tensile and shear strength.

Synthetic biodegradable polymers as BMP delivery systems

Polylactic acid (PLA) and poly(D,L-lactide-co-glycolide) (PLGA) are synthetic polymers that degrade via hydrolysis.

PLGA has been used successfully as a delivery system for BMP-2 (Kraiwattanapong et al. 2005; Kenley et al. 1994; Sigurdsson et al. 1995; Mayer

et al. 1996; T. T. Itoh et al. 1998). PLA has also been shown to be capable of being a delivery system for BMP-2, both alone and in combination with other polymers (Tazaki et al. 2009; Clarke 2008; Rubin & Lanyon 1987; N. Saito et al. 1999; N. Saito et al. 2001; Whyte 1994; Sandhu et al. 1995). PLA and PLGA have been used in combination as drug delivery systems, and, since PLGA degrades much faster than PLA, biodegradation can be controlled by altering the proportions of PLGA and PLA (C.-K. Wang et al. 2009; Zellin & Linde 1997; S. Itoh et al. 2004). PLA and PLGA can be fabricated into scaffolds of varying porosity, fibres, sheets, blocks or microspheres, which increase their versatility, but a major limitation is that of their acidic breakdown products, which can increase the inflammatory response and might alter the function of the BMPs (Yuan et al. 2001; Winet & Hollinger 1993).

Other delivery systems include the encapsulation of BMPs within PLGA nanospheres (Yuelian Liu et al. 2004; Wei et al. 2007; Y Liu et al. 2005), poly(propylene fumarate-co-ethylene glycol) hydrogels (Kenley et al. 1994; Fisher et al. 2004; Sigurdsson et al. 1995; Mayer et al. 1996; T. T. Itoh et al. 1998) and the synthesis of PLA porous scaffolds using a supercritical CO_2 gas-foaming technique which lead to a constant release profile of rhBMP-2 (Schliephake et al. 2007).

As the individual materials discussed above have their own advantages and disadvantages, combinations of different material classes have been used in order to maximise the benefits and overcome the limitations. A summary of the published pre-clinical studies using such composites with BMPs is shown in **Table 1.6**.

Recently there has been much interest in nano- and microparticles as delivery systems for the controlled release of BMPs, particularly since these would mimic the nanostructure of bone itself. Various materials such as synthetic and natural polymers and ceramics have been used to synthesise nano- and micro-devices, and there is evidence to suggest that nanodevices are better than microdevices and even conventional bone grafts (Kikuchi et al. 2001; Nair & Laurencin 2007). In addition, nanoparticles have a much greater surface area and more active free sites than microparticles, which can lead to enhanced BMP release from a smaller loading dose (Liu and Webster, 2009).

Composite material	*BMP (conc^n)*	*Method of fabrication*	*In-vivo or in-vitro testing*	*Release profile*	*Ref.*
PLGA microspheres/ CPC	rhBMP-2 (1.6mg/ml)	Double emulsion solvent extraction	in-vitro (ALP assay)	Initial burst (24hrs) then linear sustained release to 28days (ELISA)	(Fei et al. 2008)
PEI/albumin nanoparticles	rhBMP-2 (-)	double emulsion	in-vitro (ALP assay)	Initial burst release (24hrs) then sustained release to 7days (radiolabelling)	(Zellin & Linde 1997; S. Zhang et al. 2009)
PLGA nanocapsules/PHBV nanocapsules/ chitosan	rhBMP-2/rhBMP-7 (-)	double emulsion solvent evaporation/ wet spinning	in-vitro (cell proliferation and ALP assay)	Initial burst release (3ydas) then sustained release to 25days (Coomassie spectrophotometry)	(Winet & Hollinger 1993; Yilgor et al. 2009)
PLGA microsphere/ PPF/ VEGF/ gelatine	rhBMP-2 (2mg/g PLGA)	double emulsion solvent extraction	in-vitro and in-vivo (rat femur)	Initial burst (3days) then slow sustained release to 56days(radiolabelling)	(Wei et al. 2007; Kempen et al. 2009)
nano-HA/collagen/ PLLA/chitosan microspheres	BMP-2 derived synthetic peptide (50-90mg/g composite)	double emulsion and cross-linking	in-vitro (ALP assay)	Initial burst release (4wks), sustained release to 13wks, burst to 20wks(HPLC & ELISA)	(Fisher et al. 2004; Niu et al. 2009)
PLGA/HA nanoparticles	rhBMP-2 (1.7µg/g of PLGA)	electrospinning	in-vitro (cell attachment and viability & ALP assay)	Initial burst (24hrs) then linear sustained release to 60days (ELISA)	(Schliephake et al. 2007; Nie & C.-H. Wang 2007)
PLGA/HA microspheres	rhBMP-2 (-)	double emulsion	in-vitro and in-vivo (mouse necrotic tibia)	Sustained release for 1wk (ELISA)	(Kikuchi et al. 2001; C.-K. Wang et al. 2009; Nair & Laurencin 2007)
interconnected-porous calcium HA/ PLA-PEG	rhBMP-2 (-)	solvent evaporation	in-vivo (rabbit radius)	-	(Fei et al. 2008; Kaito et al. 2005)
PLGA/HA and fibrin gel	rhBMP-2 (0.1mg/g PLGA/HA)	gas foaming and particulate leaching	in-vitro (ALP assay) and in-vivo (rat parietal bone)	Initial burst release (24 hrs) then sustained release to 60days (ELISA)	(S. Zhang et al. 2009; S.-S. Kim et al. 2008)
heparin-conjugated PLGA	rhBMP-2 (-)	solvent casting	in-vitro (ALP assay) and in-vivo (rat intramuscular)	Initial burst (24hrs) then sustained release to 30days (ELISA)	(Yilgor et al. 2009; Jeon et al. 2007)
pHEMA hydrogel/ HA/TCP	rhBMP-2/7 heterodimer (0.4-1.6mg/g composite)	solvent casting	in-vitro (ALP assay)	Initial burst (10hrs) then sustained release to 6days (ELISA)	(Kempen et al. 2009; Xu et al. 2009)
PCL-TCP/collagen	rhBMP-2 (-)	fused deposited modelling	in-vitro (ALP assay) and in-vivo (rat parietal bone)	Initial burst release (8hrs) then sustained release to 50hrs (ELISA)	(Niu et al. 2009; Sawyer et al. 2009)
dextran/gelatin/PEG	rhBMP-2 (-)	double emulsion	in-vitro (cell proliferation)	Initial burst release (24hrs) then sustained release to 28days (ELISA)	(Nie & C.-H. Wang 2007; F.-M. Chen et al. 2009)
PLA-DX-PEG/ porous β-TCP	rhBMP-2 (200µg/g PLA-DX-PEG)	solvent evaporation	in-vivo (rabbit femur)	-	(C.-K. Wang et al. 2009; Yoneda et al. 2005)

Table 1.6

Summary of published composite delivery systems for BMPs

Use of BMPs in spinal surgery

To date there have been many randomised controlled trials (RCT) of the use of rhBMP-2 in spinal fusion surgery. A recent meta-analysis of these showed that rhBMP-2 was superior to iliac crest bone graft in achieving fusion (Z. Chen et al. 2012). However, substantial limitations exist with the published RCTs, including underestimation of adverse events and relatively short follow-up. Concerns have recently been raised about the possible link between the use of rhBMP-2 in spinal surgery and the subsequent risk of cancer, although reporting studies have been poorly designed to collect this data and no substantial conclusions can yet be reached (R. Fu et al. 2013).

A summary of recent RCTs is shown in Table **1.7**, including rates of nonunion, adverse events and details of osteoconductive materials used (Boden et al. 2000; Burkus et al. 2002; Burkus et al. 2005; Boden et al. 2002; Dawson et al. 2009; Dimar et al. 2009; Dimar et al. 2006; Glassman et al. 2008; Haid et al. 2004).

Reference	*Study details*	*Dose rhBMP-2 (conc[n]) and osteoconductive agent*	*Fusion device*	*Nonunion at 24 months, rhBMP2 vs ICBG RR (95% CI)*	*ODI, mean change at 24 months*			*Adverse events (%)*	
					rhBMP-2	*ICBG*	p value	*rhBMP-2*	*ICBG*
ANTERIOR									
(Boden et al. 2000)	n=14 (11 vs 3) ALIF, single level	1.95-3.9 mg (1.5 mg/ml) + ACS	NOVUS LT tapered interbody fusion cage	0.11 (0.01, 2.22)	-25	-15	0.12	3 (27.3)	2 (66.7)
(Burkus et al. 2002)	n=279 (143 vs 136) ALIF, single level	4.2-8.4 mg (1.5 mg/ml) + ACS	NOVUS LT tapered interbody fusion cage	0.49 (0.20, 1.18)	-29	-29.5	>0.05	6 (4.19)	14 (10.3)
(Burkus et al. 2005)	n=131 (79 vs 52) ALIF, single level	8.4-12 mg (1.5 mg/ml) + ACS	threaded cortical bone dowels	0.05 (0.01, 0.41)	-33.4	-27.0	0.119	-	-
				0.25 (0.12, 0.52)					
POSTEROLATERAL									
(Boden et al. 2002)	n=16 (11 vs 5) IPLF, single level	40 mg (2 mg/ml) + 60% HA/40% TCP granules	Texas Scottish Rite Hospital pedicle screw	0.10 (0.01, 1.77)	-	-	-	2 (18.2)	0
(Dawson et al. 2009)	n=46 (25 vs 21) IPLF, single level	12 mg (1.5 mg/ml) + 15% HA/85% TCP granules	CD Horizon pedicle screw	0.15 (0.02, 1.13)	-28.2	-23.0	0.953	2 (8.0)	3 (14.3)
(Dimar et al. 2009)	n=463 (239 vs 224) IPLF, single level	40 mg (2 mg/ml) + 15% HA/85% βTCP CRM	CD Horizon pedicle screw	0.39 (0.17, 0.87)	-	-	>0.05	20 (8.4)	20 (8.9)
(Dimar et al. 2006)	n=150 IPLF, single level	40 mg (2 mg/ml) +HA-TCP CRM	CD Horizon pedicle screw	0.35 (0.13, 0.93)	-24.5	-21.4	0.445	41	41
(Glassman et al. 2008)	n=102 (50 vs 52) IPLF, single or multilevel	NR	pedicle instrumentation, NR	0.42 (0.18, 0.99)	-	-	-	7 (14.0)	19 (36.5)
(Haid et al. 2004)	n=67 (34 vs 33) PLIF, single level	4-8 mg (1.5 mg/ml)	Cylindrical threaded titanium fusion cages	0.30 (0.07, 1.35)	-29.6	-24.9	-	16 (47.0)	21 (63.6)
				0.34 (0.22, 0.53)					

Table 1.7

Summary of published studies to date of rhBMP-2 vs iliac crest bone graft use in spinal surgery; ICBG iliac crest bone graft; CRM compression resistant matrix; ALIF anterior lumbar interbody fusion; PLIF posterolateral interbody fusion; IPLF instrumented posterolateral fusion; TCP tricalcium phosphate; HA hydroxyapatite; ACS absorbable collagen sponge; ODI Oswestry Disability Index (Z. Chen et al. 2012)

1.4.5.2 Autologous platelet concentrate

Platelet degranulation forms part of the normal bone healing process, with release of growth factors (for example, PDGF and TGF-β) that promote the proliferation of mesenchymal stem cells and osteoblasts (Alanay et al. 2008). Autologous growth factor concentrate (AGF), when used with autograft, has been shown to possibly enhance bone formation in lumbar fusion surgery (Lowery et al. 1999). More recently, fibrinogen preparations (derived from platelet-rich plasma) have been combined with thrombin to form a fibrin clot, which can be used as part of a composite bone graft with an osteoconductive scaffold. However, studies to date have failed to demonstrate any increase in fusion rates, although AGF might promote a faster rate of fusion (Hee et al. 2003; Carreon et al. 2005).

1.4.5.3 Gene therapy

Gene therapy is the transfer of a DNA sequence of a specific protein into target cells that subsequently express the protein of interest. Therefore, gene therapy may be used to express osteoinductive growth factors in target cells, in a sustained release, at the required fusion site.

DNA can be transferred into target cells using either viral or nonviral vectors. Nonviral vectors (for example, liposomes) are easier to produce and theoretically safer than viral vectors. Viral vectors, however, offer better transfer efficiency, despite short (around 3 weeks) protein production by the target cells due to adenoviral DNA being unable to integrate into the host DNA. Nell-1, an osteoinductive factor, has been used for gene therapy in a rat model of spinal

fusion and showed potent osteoinduction (Lu et al. 2007). Bone marrow cells transfected with the gene for LIM mineralisation protein (LMP-1), which stimulates the expression of multiple osteoinductive factors, have shown bone formation in a rat model of thoraco-lumbar posterior fusion (Boden et al. 1998). Clearly, many more detailed studies with long-term safety data are required before gene therapy could be even considered for clinical use.

1.4.5.4 Human mesenchymal stem cells

Human mesenchymal stem cells (hMSCs) are present in adult bone marrow, possess self-renewal capabilities and are considered to be multipotent as they have the potential to differentiate into adipocytic, chondrocytic, or osteocytic lineages (Jaeger AA 2013; Pittenger et al. 1999). hMSCs can be further defined by the expression of cell surface markers, including CD29, CD31, CD34, CD44, CD71, CD73 CD90, CD106 and CD124, although no consensus has yet been reached on exactly which markers need to be present in order for a cell to be called an MSC (Occhetta P 2013; Pittenger et al. 1999; Dominici et al. 2006).

The main functions of MSCs which are of critical importance in bone healing are their secretory function (including immunomodulatory, anti-inflammatory, anti-apoptotic, pro-angiogenic and pro-proliferative factors) and their stimulation of cellular differentiation for bone formation (Caplan 2005; Petrie Aronin & Tuan 2010; Kolf et al. 2007). The harvesting of MSCs from bone marrow is a complex process requiring the cells to undergo *ex vivo* selection, processing and maintenance, whilst the success of therapy depends on high quality MSCs (with respect to cellular integrity, age, senescence, poliferative and differentiative

capacity and intact paracrine function) (Steinert et al. 2007; Lepperdinger 2011). Therefore, in order to maximise the available MSCs from patient samples, several methods are available including immediate injection of autologous blood or bone marrow, or single-step processing in theatre (for example, centrifugation of sample or recovery form cell filters (Cox et al. 2011)). In addition, MSCs are often implanted together with an osteoconductive scaffold or osteoinductive factors in order to further enhance the bone forming capabilities.

Animal studies have demonstrated successful fusion achieved in spinal surgery using MSCs alone or in combination with various grafts (summary in **Table 1.8**). In addition, there are several clinical studies demonstrating the results of MSCs used in regenerative orthopaedic surgery (summarised in **Table 1.9**). Two of these studies were performed in patients undergoing spinal fusion surgery and these results show similar efficacy of MSCs to the use of autograft (Neen et al. 2006; P. Zhang et al. 2008), supporting further research in this area.

Reference	*Animal*	*Type of fusion*	*Graft material*	*Final evaluation*	*Fusion rate*
(Nakajima et al. 2007)	Rabbit	posterolateral lumbar spine	differentiated MSCs vs MSCs vs ICBG	6 weeks	fusion in differentiated MSCs 4/5, 80%; MSCs 2/6, 33%; ICBG 4/6, 67%
(Minamide et al. 2005)	Rabbit	posterolateral lumbar spine	collagen gel + HA + differentiated bone marrow cells (100 million vs 1 million) vs ICBG	6 weeks	100 million cells resulted in fusion in 5/7, 71%; 1 million cells, no fusion; ICBG 4/7, 57%
(Kai et al. 2003)	Rabbit	interbody lumbar spine	calcium phosphate + bone marrow stromal-derived osteoblasts vs ICBG	3 months	fusion in experimental group 6/6, 100%; ICBG 4/6, 67%
(T. Wang et al. 2005)	Rhesus monkey	interbody lumbar spine	calcium phosphate + differentiated MSCs vs ICBG	3 months	fusion in experimental group 4/6, 67%; ICBG 5/6, 83%
(Gupta et al. 2007)	Sheep	posterolateral lumbar spine	TCP + osteoprogenitor cells (SCR) vs ICBG	6 months	fusion in experimental group 33%; ICBG 25%
(Shamsul et al. 2014)	Sheep	posterolateral lumbar spine	HA+ differentiated bone marrow cells vs TCP/HA + differentiated bone marrow cells vs ICBG	3 months	fusion in HA construct 1/6, 17%; TCP/HA construct 5/6, 83%; ICBG 6/6, 100%
(Q. Cui et al. 2001)	Athymic rat	posterolateral lumbar spine	collagen gel + cloned osteoprogenitor cells from mouse marrow vs mixed marrow cells	6 and 9 weeks	fusion in cloned cells group 8/8, 100%; mixed marrow cells group, 4/8, 50%
(Schubert et al. 2013)	Pig	interbody lumbar spine	polyetheretherketone cage +/- allograft, autograft or differentiated MSCs	3 months	Bone growth in cage-only, and + MSC groups was significantly higher than in + autograft group; bone resorption in allograft group,

Table 1.8

Summary of published animal studies to date of cell-based therapies for spinal fusion. Adapted from (Gottfried & Dailey 2008)

Reference	*Number of patients*	*Adjuvant treatment*	*Indication*	*Summary*
(Connolly 1998)	20	-	non-union of tibia	Case series, injection of unprocessed bone marrow. Healing occurred in 18 of 20 cases after a mean of 6–8 months (±1.25)
(Warnke et al. 2004)	1	titanium mesh scaffold, BMP-7, collagen I, bone mineral block	mandibular defect	Heterotopic bone induction to form a mandible replacement inside latissimus dorsi muscle after injection of unprocessed bone marrow
(Dallari et al. 2007)	33	allograft	high-tibial osteotomy	Significantly increased osteoid areas in bones treated with platelet gel or platelet gel + bone marrow stromal cells, compared to allograft
(Schmid et al. 2007)	125	allograft	bone defects of lower limb, primary + revision THA and fractures	Bone grafting with bone marrow cells + allografts is a good alternative to conventional bone grafting
(Ochs et al. 2008)	78	allograft	acetabular defects in revision THA	No difference in functional outcome between allograft or allograft + bone marrow
(Hendrich et al. 2009)	101	calcium phosphate	bone defects due to AVN or pseudoarthrosis	Safety study, no control group, use of bone marrow aspirate concentrate alone or + scaffold, safe at 2-24 months follow-up
(Jäger et al. 2011)	39	collagen scaffold (12), HA (27)	bone defects	Bone marrow aspirate + collagen matrix or hydroxyapatite, latter group had better outcomes
(Quarto et al. 2001)	3	HA	non-union of long bones	Ex vivo expansion of bone marrow cells on hydroxyapatite scaffolds, abundant callus formation at 2 months follow-up
(Kitoh et al. 2007)	46	-	distraction osteogenesis of long bones	Ex vivo expansion of bone marrow cells, + platelet-rich plasma, higher healing index and less complications than control group (no cell-based therapy)
(Neen et al. 2006)	50	Type I collagen + HA	lumbar spine fusion	No differences in clinical and radiological outcome between type 1 collagen/hydroxyapatite matrix combined with BMA and conventional autologous bone grafting, but no donor site morbidity
(P. Zhang et al. 2008)	56	β–TCP	posterior lumbar spine fusion	Enriched bone-marrow-derived mesenchymal stem cells + B-TCP showed successful spinal fusion in 95.6%, similar to ICBG

Table 1.9

Summary of published clinical studies to date of cell-based therapies for bone regeneration; TCP tricalcium phosphate; HA hydroxyapatite; ICBG iliac crest bone graft. Adapted from (Steinert et al. 2012)

1.5 Tissue engineering approaches

1.5.1 Biomimicry

The three-dimensional cellular environment, and hence cell behaviour, is influenced by the properties of the scaffold materials in three key aspects: their chemical composition; the dimensions and spatial arrangement of the structure, and their physical characteristics such as substrate stiffness. For example, only scaffolds with a nano-fibrous morphology were able to force stem cells down an osteogenic lineage, showing the importance of scaffold structure on stem cell fate (Kaito et al. 2005; Kumar et al. 2011). Similarly, the degree of bone formation by stem cells grown in scaffolds was dependent on the scaffold architecture and composition (S.-S. Kim et al. 2008; Declercq HA 2013).

Within the past 10 years, there has been a vast increase in knowledge of the way in which topographical features of a scaffold influence cell properties such as adhesion, morphology, viability, motility and apoptosis, and features compatible with cellular scale (1–100 μm) can have an effect on cell function. Three-dimensional scaffolds must have a highly porous structure to allow the cells to infiltrate the structure and to guide their growth, as well as to facilitate diffusion of gases and waste products, but must be able to maintain shape and integrity. Patterned scaffolds can mimic the structure of native tissues. A fibrillar structure has long been known to be important for cell attachment, proliferation, differentiation and function (Jeon et al. 2007; Elsdale 1972). Pore size and distribution governs the cell migration and penetration within the scaffold, as well as affecting the diffusion of nutrients and gases (Xu et al. 2009; Colom A

2013).

The decision regarding use of natural or artificial materials is a complex one, and many studies have tested a wide range of different materials and combinations with different cell types. Single-component scaffolds are simpler to produce, but multi-component scaffolds better reproduce the properties of the natural ECM. Development of scaffolds for use in surgical applications requires properties such as biodegradability, integration with native tissues, and similar mechanical characteristics to the natural tissue they are intended to replace.

1.5.2 Naturally occurring materials

Natural materials include collagen, fibrin, matrigel, silk, chitosan and alginate, and these are discussed in detail below.

1.5.2.1 Collagen

Collagen is the most abundant protein in the ECM of human tissues and has, therefore, been well-studied as the principal component of 3-D models (Sawyer et al. 2009; Ulrich et al. 2010).

Whilst it has low mechanical strength, it has excellent cell adhesion properties, and collagen I has been used as a substrate for cell cultures for decades (F.-M. Chen et al. 2009; Elsdale 1972). However, the density of collagen gels can present problems; a low-density gel has insufficient strength and structural integrity, but a high-density gel may inhibit cell ingrowth, resulting in cells penetrating only the outside edges of the scaffold, as well as exhibiting poor

diffusion of gases and nutrients and inhibiting removal of waste (Yoneda et al. 2005; Colom A 2013). These problems can be overcome by creating internal channels within the collagen scaffold (Kumar et al. 2011; Yahyouche et al. 2013). Collagen can be combined with other substances to improve scaffold characteristics, for example hydroxyapatite or hyaluronic acid (Declercq HA 2013; Campbell et al. 2011), and can be formed into scaffolds in various ways, including simple gelation, freeze-drying or printing and critical-point drying (Elsdale 1972; Sachlos E 2008) or electrospinning (Colom A 2013; Hartman et al. 2009), while cross-linking improves stability as well as controlling porosity, pore size and distribution, and network interconnectivity (Ulrich et al. 2010; Hartman et al. 2009; Liu CZ 2008).

1.5.2.2 Fibrin

Fibrin can be formed into a gel by exploiting the clot-forming process involving cleavage of fibrinogen molecules by thrombin and assembly into a 3-D network. Optimising this process can produce a biodegradable fibrin scaffold that has been used for cell delivery and combined with platelet-rich exudates to support the growth of human primary chondrocytes and a chondrosarcoma cell line (Elsdale 1972; Chien CS 2012). Fibrin clots are largely used in tissue engineering for clinical use, such as in combination with stem cells to treat bony non-union (Colom A 2013; Giannotti S 2013).

1.5.2.3 Silk

Silk consists of a glue-like coating of sericin proteins surrounding fibroin, a filament core protein. Silk is most frequently harvested from the larvae of either Bombyx mori or Antheraea mylitta and has been used for centuries as a biomedical suture material. Silk fibroin is first isolated by degumming to remove the sericins, which abolishes the antigenic effect of silk and improves biocampatibility. Degumming can be carried out by chemical degumming using boiling alkaline solutions, or by the use of proteolytic enzymes, specifically alkaline proteases. Fibroins are filaments composed of bundles of nanofibrils which are strongly bound together, contributing to the strength and toughness of silk (Yahyouche et al. 2013; Miller LD 1999). The degumming process weakens the fibroin fibres and makes it difficult to braid or knit the fibres into a scaffold; however, coating the fibres with an alternative material such as gelatin restores many of their physical properties. Tests of a non-woven fibroin net showed good compatibility with a range of cell types (Campbell et al. 2011; Unger et al. 2004).

1.5.2.4 Chitosan and alginate

Chitosan (poly 1,4-D-glucosamine) is a partially deacetylated derivative of chitin, a natural polymer forming the exoskeleton of arthropods. Chitosan hydrogels have been widely used as tissue engineering scaffolds as well as for drug-delivery systems and have a number of advantages including low cytotoxicity, biocompatibility and biodegradability, while the ability to dissolve the hydrogel in cell-compatible solutions allows release of cultured cells for analysis (Sachlos E 2008; Boos et al. 2002; Jayakumar R 2010; Luoma et al. 2000; Bhattarai N

2010). Chitosan has a structure similar to glycosaminoglycans (GAGs), major components of bone ECM, and as the second most abundant natural polysaccharide, it is cheaper and more widely available than native human GAGs. It has been extensively used in the study of bone biology (particularly in respect to tissue engineering), due to its mechanical properties and ability to stimulate osteoblastic activity (Hartman et al. 2009; Arya et al. 2012; Kai H 2009). Incorporating other components into the scaffold can augment these useful properties. A composite material formed from chondroitin- sulphate and nano-SiO_2 showed good biocompatibility and supported proliferation of an osteosarcoma cell line, while the initial cell attachment was improved by coating the scaffold with fibrin (Hartman et al. 2009; Kavya KC 2012; Liu CZ 2008).

Sodium alginate forms a biodegradable gel when cross- linked with calcium ions and can be used to encapsulate cells for tissue engineering applications (Chien CS 2012; Wang L 2003). Alginate has excellent biological properties and limited immunogenicity so is widely used in biomedical applications. Like chitosan, its structure resembles that of GAGs (Giannotti S 2013; Bhattarai 2006).

1.5.3 Synthetic polymers

A range of synthetic polymers have been tested for use as cell scaffolds, and many have produced promising results. Much of the work on these polymers has focused on their application in tissue engineering and specifically as bone grafts. As with the natural polymers, synthetic compounds can also be fabricated into scaffolds in a variety of ways and modified by the incorporation of ECM

components or other proteins to improve cell adhesion and growth and promote natural behaviour.

Poly(e-caprolactone) (PCL) can be surface modified to improve cell–scaffold interactions (Miller LD 1999; Choong et al. 2012) and has been used successfully as a scaffold for bone marrow fibroblasts and endothelial cells (Unger et al. 2004; Choong CS 2006). It can be formulated in a variety of ways to produce scaffolds with different structures (Kumar et al. 2011).

Other polymers frequently used to form scaffolds include polymethylmethacrylate (PMMA), polydimethylsiloxane (PDMS), polyglycolic acid (PGL), poly(L-lactic acid) (PLLA), polyurethane (PU) and poly(lactic-co-glycolic acid) (PLGA). PLGA microfiber scaffolds formed by microfluidic chip-based fabrication have also shown promise when used to culture fibroblasts or neural progenitor cells (Hwang CM 2008).

1.5.4 Fabrication and modification techniques

Many different processes have been utilized in the manufacture of biocompatible scaffolds and novel methods are continuously being developed. Additionally, several types of scaffold can be formed from the same substrate by the use of different physical processes, including electrospinning, weaving, salt leaching, gas foaming (with or without phase separation), spin coating and freeform fabrication, while surface topography can be ordered or unordered and can be created by photolithography or electron beam lithography for the former, or polymer demixing, phase separation, chemical etching or colloidal lithography

for the latter (Norman & Desai 2006). In each process, the ultimate characteristics of the scaffold can be varied by altering the fabrication conditions or subsequently modifying the fabricated material. When manufacturing a scaffold, its features and properties need to be taken into account from the macro- to the nanoscale, considering its overall shape and size as well as cellular and subcellular scale structure (Arya et al. 2012; Stevens MM 2005; Kai H 2009).

1.5.4.1 Electrospinning

The use of electrospinning to produce fibrous membranes for use in tissue engineering is popular, because such substrates are thought to mimic the scale and structure of the ECM. Electrospinning is frequently used to produce scaffolds of synthetic materials such as poly(e-caprolac-tone) (PCL) but can also be used with natural materials such as chitin and chitosan (Kavya KC 2012; Jayakumar R 2010) or collagen (Wang L 2003; Hartman et al. 2009). Electrospinning generally creates a non-woven fibre mat consisting of one continuous filament, which can be tailored to individual requirements by altering the diameter, which can range from tens of nanometres to micrometres (Bhattarai 2006; Grubb & Kelly 2000; Miller et al. 1988; Kumar et al. 2011; J. Xie et al. 2008), or even the cross-sectional shape of the fibres (Choong et al. 2012; S. J. Park et al. 2013). Alternatively, electrospun fibres can be aligned into uniaxial arrays then stacked to form multi-layered structures (Choong CS 2006; J. Xie et al. 2008). Electrospun materials can be modified to tailor the com- position and architecture to suit different cell types, with fibres of different diameters, and can be used to form membranes or multi-layered 3-D meshes (Kumar et al. 2011). They can be

engineered to contain pores, with varying porosity, by inducing phase separation between two polymers, or between a single polymer and a solvent during the electrospinning process (Hwang CM 2008; J. Xie et al. 2008). They can incorporate different materials to alter their characteristics and improve tissue compatibility, for example the incorporation of hydroxyapatite into a collagen/PLGA membrane for bone tissue engineering (Norman & Desai 2006; Mouthuy et al. 2010).

1.5.4.2 Gas-based techniques and salt leaching

Several physical processes, including salt leaching, gas foaming (with or without phase separation), spin coating and freeform fabrication can be used to produce non-woven scaffolds (Stevens MM 2005; Kumar et al. 2011). Salt leaching involves mixing the scaffold material with sodium chloride to form a homogenous paste, pressing the mixture into a mould and allowing it to air dry. The salt is then leached out in deionized water over several days, after which the scaffolds are air-dried.

Gas foaming is similar to salt leaching in that the scaffold material is mixed to a paste with a salt, this time NH_4HCO_3, and pressed into moulds. However, in this procedure, the dried scaffolds are incubated in warm deionized water until no further gas is produced, then washed in deionized water and air-dried as before (Jayakumar R 2010; Kumar et al. 2011).

Gas-foamed phase-separated scaffolds are fabricated by combining the techniques of thermally induced phase separation with gas foaming.

1.5.4.3 Reactive-ion etching

Changes in scaffold surface structure influence cell attachment and behaviour, and consequently various methods have been used to modify the surface of engineered scaffolds. Etching can be used to modify a surface by creating patterns in the surface material, and can thus be used to create a surface that mimics the topography of the ECM. One such method is reactive-ion etching, which is a dry method as it uses gas plasma such as oxygen, carbon dioxide or argon (Hartman et al. 2009; Riekerink et al. 2003). The process is performed using a chamber with two electrodes that create an electric field, which is intended to accelerate ions towards the sample surface. Gas is pumped into the chamber and forms ionized plasma; the accelerated ions then collide with the sample surface, where they combine with the material before dispersing. Masking protects areas that are not to be etched. This is a process that is often used in the manufacture of sensitive electronic devices, but it has also been applied to scaffolds for mesenchymal stem cell growth (Y. Xie et al. 2002).

1.5.4.4 Soft photolithography/photo-mould patterning

This is an innovative method of scaffold fabrication that has been used to create pre-defined polydimethylsiloxane (PDMS) scaffolds with precise microarchitecture and surface microtexture (Mata A 2009). The process involves laying down a mould as a series of spin-coated layers of defined thickness onto a silicon wafer, pouring in PDMS and curing in an oven. The patterned PDMS layers are then aligned and stacked, bonded with uncured PDMS and cured as before. In a recent study, soft lithography techniques have been used to create silicone

hydrogel synthetic membranes for culture of ovarian cancer cells in a bioreactor (Jaeger AA 2013).

A newly developed method described as 'photo-mould patterning' combined hydrogel micromoulding of PDMS and photopolymerization and was shown to be compatible with culture of GFP-labelled human umbilical vein endothelial cells (HUVECs) and primary bone marrow stromal cells (BMSCs) (S. J. Park et al. 2013; Occhetta P 2013).

1.5.4.5 Click-based hydrogel patterning

To increase the ability to customize a scaffold and enable reversible presentation of biological cues, as well as complex defined biomolecular gradients, click-based patterning has been applied to the creation of polymer hydrogels (J. Xie et al. 2008; DeForest & Anseth 2012; Polizzotti et al. 2008). Modular 'click' coupling reactions allow the synthesis of a wide variety of novel nanoscopic structures. This technique adapts traditional photolithography to allow the use of UV light of different durations and intensities to independently add or cleave biologically active peptides.

1.5.4.6 Thermally-induced phase separation

Thermally induced phase separation (TIPS) has been used as a way of engineering a well-connected porous scaffold (Kumar et al. 2011; Martel-Estrada et al. 2010; Olivas-Armendariz et al. 2009). The technique uses thermal energy to induce the separation of a mixed homogenous polymer solution into a multi-

phase system domain. Phase separation results in a polymer-rich phase and a solvent-rich phase; the solvent is then extracted leaving a polymer scaffold with different morphologies and characteristics depending on the system and phase separation conditions (J. Xie et al. 2008; Martínez-Pérez & Olivas-Armendariz 2011). TIPS can be used to produce scaffolds with a variety of structures such as closed or open pores, spheres, powders or bead-like morphology. The process produces an intricately connected porous scaffold in one simple process that is fast and controllable and is thus convenient and scalable.

Clickable poly(ethylene glycol) (PEG) derivatives have also been combined with sequential phase separations to produce microsphere-based cell encapsulation systems (Mouthuy et al. 2010; Nguyen PK 2013), while a nano-fibrous poly(L-lactic acid) scaffold reinforced by surface modified chitosan microfibres has been created by thermally induced phase separation to produce a scaffold which mimics the fibrillar structure of the natural ECM (Kumar et al. 2011; Lou et al. 2013).

1.5.4.7 Biological laser printing

This is another novel method of incorporating cells into scaffolds, and has been used to overcome the problems associated with viability and penetration of cells into scaffolds more than 300 μm thick (Kumar et al. 2011; Pirlo RK 2012). This technique has been successfully used to bioprint HUVEC cells onto PLGL 'biopapers' which could then be stacked to produce thicker scaffold structures. HUVEC cells are frequently used to recreate the endothelial component of vessel walls (Riekerink et al. 2003; Ma & X.-F. Wang 2008). Pores in the 'biopapers' can

be created by salt leaching.

1.5.4.8 Woven scaffolds

As well as generating non-woven matrices, electrospun fibres can also be used to generate woven fabrics, for example from polycaprolactone (Y. Xie et al. 2002; Khil et al. 2005).

Composite hydrogel scaffolds for cartilage regeneration have been created using a microscale 3-D weaving technique (Mata A 2009; Moutos et al. 2007).

1.6 Aims and objectives

1.6.1 Aims

The aim of this study is to identify and develop a novel targeted therapy for use in degenerative spinal conditions, which could ultimately lead to superior pain relief and improved mobility of patients compared to currently available treatments. The basis of this study is a collagen scaffold with biomimetic modifications.

1.6.2 Objectives

1. To fabricate and characterise a mineralised collagen scaffold containing glycosaminoglycans

2. To test the ability of the mineralised scaffold to promote bone growth *in vitro*

3. To fabricate a fibrillar collagen scaffold containing the growth factor BMP-2 and study its release profile

Chapter 2 Fabrication of collagen/GAG/HA/mTG scaffolds for use in spinal fusion surgery

2.1 Introduction

Spinal fusion surgery is one of the most commonly performed procedures for the treatment of chronic back pain and other degenerative spinal conditions. Furthermore, there has been a rapid increase in the number of procedures performed in the last two decades; Rajaee *et al* showed a 2.4 fold increase in the annual number of spinal fusion procedures in the United States from 174,223 to 413,171 (Rajaee et al. 2012). A major determinant of successful fusion is the bone graft, which is commonly iliac crest bone graft, allograft or synthetic graft. The limited availability and increased morbidity associated with autologous graft harvesting has led to the development of alternative grafts. However, many existing synthetic grafts have failed to achieve fusion rates superior to or even comparable to autologous graft, and continuing efforts are needed to identify better grafts.

Collagen is the most abundant protein in the extracellular matrix (ECM) of the human body and has therefore been studied extensively as a graft material in orthopaedic surgery. Collagen is non-toxic, biodegradable and has excellent osteoconductive properties. Its biodegradability depends on its resistance to collagenase, which is in turn dependent on intermolecular crosslinking, with crosslinking increasing the biodegradation time of collagen (Vater et al. 1979). A limitation of the use of collagen *in vivo* is its immunogenicity. An immune response against collagen mainly targets epitopes in the telopeptide region of the tropocollagen molecule (Schmitt et al. n.d.; Davison et al. 1967), although

atellocollagen does not contain telopeptides due to the digestion of peptides by pepsin during its extraction process (RUBIN et al. 1963).

To date, 29 different types of collagen have been identified (Parenteau-Bareil et al. 2010). Types I, II, III, V and XI are known to form collagen fibres and bone ECM contains predominantly (at least 90%) Type I collagen.

As outlined in **Figure 2.1a**, the primary structure of Type I collagen contains three polypeptide chains: two α1 chains and one α2 chain. Each α-chain consists of a repeating triplet amino acid sequence of residues glycine-X-Y, where X and Y are most commonly proline and hydroxyproline, although can be any residue. Collagen synthesis occurs in the cell to form α-chains about 1400 amino acids long, which then each twist to form the secondary structure, a tightly-packed left-handed helix. The three α-chain helices then supercoil around each other to form the tertiary structure, a right-handed triple helix 'procollagen' (Rich & Crick 1955). Procollagen is secreted out of the cell and then the C- an N-terminal propeptide ends are cleaved to form a tropocollagen molecule. Tropocollagen is stabilised by interchain hydrogen bonds within the triple helix and amino acid side chains interact with adjacent collagen molecules to form the quaternary structure of collagen (Miles & Ghelashvili 1999)(figure of all). As observed with transmission electron microscopy (BEAR 1952), the collagen molecules are aligned unidirectionally in a head-to-tail manner with a 47 nm gap between each molecule in the same row and a 20 nm sequential offset between each row, leading to the characteristic 'd-spacing' of 67 nm in five-stranded microfibrils (J. W. Smith 1968) (**Figure 2.1a**). Microfibrils become associated to form collagen

fibrils, which in turn bundle together in a tightly-packed collagen fibre (approximately 300 nm diameter). This fibrillar structure has electrostatic and hydrophobic interactions giving it stability, but as the particular tissue matures, covalent intramolecular and intermolecular crosslinks are formed, to increase its stability (Ottani et al. 2002).

Collagen is frequently used as a scaffold to which osteoinductive or other components are added, for use as a bone graft in orthopaedics. For example, it can be combined with the ceramic tricalcium phosphate, or BMPs. In this chapter, a biomimetic approach has utilised collagen as the main component of a novel scaffold for use as a bone graft in spinal fusion surgery.

2.2 Scaffold Fabrication

2.2.1 Collagen scaffold

Bovine atelocollagen Type I was generously provided by Dr David Brand (Divison of Rheumatology and Connective Tissue Disorders, Veterans Affairs Medical Centre, Memphis, Tennessee, US). Collagen solution (0.5 g collagen in 50 ml of de-ionised H_2O) was adjusted to pH 3.2 and blended thoroughly with a hand-blender (Braun, MR400) for 10 min. The blending was carried out in an ice bath to prevent denaturation of the proteins that might be caused by the heat generated during this process. After the suspension was made, it was subjected to a vacuum of 10 Pa for 30 min at room temperature to remove the entrapped air bubbles and then stored at 4°C.

For collagen fibrillogenesis, equal amounts of collagen solution and sodium phosphate buffer (50 mM sodium dihydrogen phosphate, 10 mM potassium dihydrogen phosphate) were mixed and the solution was adjusted to pH 7.4, transferred into a 10 cm diameter mould and incubated at 37°C overnight (DeForest & Anseth 2012; Douglas et al. 2006; Polizzotti et al. 2008).

Both afibrillar and fibrillar collagen scaffolds were then frozen at -20°C (EU7120C, Electrolux, UK) for 24 h and then placed in a Christ I-5 freeze-dryer (Martin Christ Gefriertrocknungsanlagen GmbH, Germany) for 24 h in a vacuum of 5 Pa, removing the ice crystals by sublimation and leaving the porous solid scaffolds.

2.2.2 Collagen/nano-hydroxyapatite/chondroitin sulphate scaffold

Collagen/nano-hydroxyapatite[HA]/chondroitin sulphate[CS] were prepared as for the collagen scaffolds (**2.2.1**), with the addition of nanoHA (Sigma-Aldrich) and CS (Sigma-Aldrich) to the collagen solution *at the time of blending*: 30 wt% (0.238 g), 50 wt% (0.555 g), 75 wt% (1.65 g) for HA, and 1 wt% (0.055 g) for CS, respectively. The collagen/nanoHA/CS scaffolds were then prepared as for the collagen scaffolds (**2.2.1**).

2.2.3 Collagen/microbial-transglutaminase scaffold

Collagen/microbial-transglutaminase[mTG] scaffolds were fabricated as for collagen scaffolds (**2.2.1**) with the addition of 300 U mTG per gram of collagen *during fibrillogenesis* and adjustment of pH to 7.4. The scaffolds were then fabricated as in **2.2.1**.

2.3 Transglutaminase purification and characterisation

Microbial transglutaminase (mTG) was purified from a complex of mTG with maltodextrin and the enzymatic activity of mTG was quantitatively assessed using a commercial kit, as described below.

2.3.1 Transglutaminase purification

This was performed under the supervision of Dr Marko Hyvönen, Department of Biochemistry, University of Cambridge. mTG (combined with a carrier molecule, maltodextrin) was received as a kind gift from Ajinomoto®. The mTG was further

purified using ÄKTA purification system (GE Healthcare) and a method adapted from that previously published (Kuwahara et al. 2011).

Briefly, 0.7 g of maltodextrin/mTG was dissolved in 14 ml of phosphate buffer (20mM phosphate, pH 6.0), centrifuged and loaded onto a HiTrap Sepharose cation exchange column (GE Healthcare). mTG was eluted with phosphate buffer with 1 M NaCl and protein concentration was evaluated using a spectrophotometer (NanoDrop, Thermo Scientific).

2.3.2 Transglutaminase activity

Enzymatic activity was calculated using a commercial assay (Zedira®) utilising Z-Gln-Gly as the amine acceptor substrate and hydroxylamine as the amine donor. Briefly, 50 μl purified mTG (as described in **Chapter 2.3.1**) were added to 500 μl TRIS pH 6.0 (containing Z-Gln-Gly, hydroxylamine and reduced glutathione) and incubated at 37^0C for 10 min. 500 μl of stop solution (Fe^{3+}/H^+) were added, developing a coloured complex, and the solution centrifuged for 5 min at 10,000 g at RT. The supernatant was transferred to a multi-well plate and absorbance was measured at 525 nm (POLARStar Omega plate reader, BMG LABTECH). Results were obtained by comparison with those from kit-supplied known standards.

2.4 Scaffold characterisation

A range of techniques, as described below, was used to characterise the scaffolds.

2.4.1 Scanning electron microscopy

High resolution scanning electron microscopy (SEM) was used to perform morphological analysis of the scaffolds, using a JEOL scanning microscope JSM840F (JEOL Ltd, Japan) with a working distance of 10-30 mm, electron voltage of 3-5 kV and 50-25,000X magnification. Cylindrical scaffold samples, 10 mm in diameter, were horizontally bisected to analyse the inner pore structure. Before imaging, the samples were mounted onto aluminium stubs with adhesive carbon tabs. As all the scaffolds were non-conductive, samples were coated with 3 nm thick platinum using a 280HR sputter coater (Cressington Scientific Instruments Ltd, UK). SEM images were analysed with ImageJ software to calculate pore size, taking the average result from 3 individual areas per scaffold (Martel-Estrada et al. 2010; Schneider et al. 2012; Olivas-Armendariz et al. 2009).

2.4.2 Transmission electron microscopy

Transmission electron microscopy (TEM) was used to visualise the D-banding pattern of collagen and any changes in the ultrastructure of the collagen scaffolds after fabrication.

A 2000FX TEM (JEOL Ltd, Japan) was used to confirm the presence of D-banding pattern and therefore that fibrillogenesis had occurred in the fabrication process. Collagen samples were re-suspended in distilled water, placed on copper TEM

grids (Agar Scientific, UK) and then air-dried overnight. The solution was then examined using bright field imaging mode at an accelerating voltage of 200 kV.

2.4.3 Differential scanning calorimetry

Differential scanning calorimetry (DSC) is a method used to measure the energy required to heat or cool a specimen at a constant, controlled rate. Upon heating, collagen undergoes a conformational change to a denatured state, resulting in an endothermic peak. The area under this transition peak is directly proportional to the enthalpy change (Martínez-Pérez & Olivas-Armendariz 2011; Flandin et al. 1984). The temperature at the peak of the transition curve (denaturation temperature, Td) is a measure of the thermal stability of the collagen scaffold and therefore its potential suitability for *in vivo* application. A higher Td would reflect an increased stability of the molecules, while a broad shape of the peak and/or the presence of 'shoulders' would correspond to an increased dispersion in terms of stability of the fibres.

Using a Perkin Elmer Hyper Differential Scanning Calorimeter, 5-10 mg of each scaffold were placed in a 40 μl aluminium pan (Perkin Elmer) and heated to 180^0C at 50^0C min^{-1}. The raw data was compiled and analysed using Pyris Data Analysis Software and the denaturation temperature for each sample was recorded.

2.4.4 Thermogravimetric analysis

Thermogravimetric analysis (TGA) is a method used to analyse the chemical composition of a material through analysis of characteristic decomposition patterns. TGA was utilised to identify the actual weight percent of HA in each of the scaffolds. Each sample (5-10 mg) was placed in an open ceramic pan and heated from 37^0C to 900^0C at a rate of 10^0C min^{-1} in a nitrogen atmosphere purged at 100 mls min^{-1} (Diamond TGDTA).

2.4.5 Atomic force microscopy

Atomic force microscopy (AFM) was used to obtain high-resolution nano-scale topography from the samples as it is widely used to characterise the structure of collagen (Nguyen PK 2013; Gale et al. 1995). The principle of AFM imaging is based upon the vertical deflection of an extremely sharp-tipped cantilever when it is scanned across the surface of a material. The deflection is measured using a laser spot reflected from the cantilever's top surface into an array of photodiodes.

1 cm^2 samples were cut from the scaffolds and mounted on a Park Instruments AutoProbe Atomic Force Microscope. Samples were scanned in non-contact mode using Ultrasharp NSC12 diving-board levers with spring constants in the range 4-14 N m^{-1} and with resonant frequencies in the range 150-310 kHz. The images obtained were 256 x 256 pixels in all cases.

2.4.6 Energy dispersive x-ray spectroscopy

Energy-dispersive x-ray is based on the principle of each element having a unique atomic structure, which correlates to a unique set of peaks on its x-ray spectrum. The number and energy of emitted x-rays are measured with an energy-dispersive spectrometer.

EDX analyses the characteristic X-rays produced by the interaction between the primary electron beam and the sample. The technique identifies all elements present with atomic numbers of 5 and greater (boron) with a detection limit of approximately 0.1 weight %. The measurements are semi-quantitative.

The homogeneity of the mineralised collagen scaffold was analysed using JEOL 6480 LV SEM with EDX. The surface and cut sections were mapped with respect to Ca^{2+}, P^{5+} and O^{2-} ions. Three regions per sample were investigated using voltage 15 kV and pressure 40 Pa with backscattered contrast and magnification of 100 X.

2.4.7 X-ray diffraction

X-ray diffraction (XRD) is a technique with which chemical composition of a material can be analysed. Phase identification using XRD is achieved by comparing the diffraction pattern obtained from the unknown to a standard database that is compiled by the International Centre for Diffraction Data (ICDD). If and when a positive identification is made, the constituent is indicated by a stick pattern that is superimposed on the XRD diffractogram.

XRD analysis was carried out using a fully automated Bruker D5000 powder diffractometer employing copper kα radiation (λ=0.15406nm) and a secondary monochromator. The sample, which was supported on a single crystal of silicon, was continuously spun during data collection and scanned using a step size of 0.05°2θ between the range of 10°-70°2θ and a count time of 15 seconds $step^{-1}$.

2.4.8 Mechanical testing

Young's modulus of the mineralised collagen scaffold was evaluated by uni-directional compression testing (Perkin Elmer Dynamic Mechanical Analyzer 7e, and for 50 and 75 wt%, with an analyser from Denison Mayes Group Ltd, Leeds UK). The samples were fabricated using a custom mold with diameter 12.5 mm and height 13.5 – 15 mm (n=3). Young's modulus was calculated by defining the gradient of the linear elastic part of the stress/strain curve (Gibson 2000).

2.4.9 Statistical analysis

All data were reported as means with standard deviations. One-way analysis of variance (ANOVA) followed by Tukey's test was used to compare groups of data, with a probability value of 95% ($p<0.05$) to determine statistical significance.

2.5 Results

2.5.1 Imaging

A representative photograph of a typical fibrillar collagen scaffold is shown in **Figure 2.1b**. Scanning electron microscopy (SEM) was used to determine the surface and cross-section morphology of the scaffolds. The cut surfaces of afibrillar and fibrillar collagen contained pores, which were uniformly distributed (**Figures 2.1c-d**). A homogeneous pore microstructure with interconnected polyhedral pores was observed throughout the scaffolds (**Figures 2.1a-b** and **2.2**). The cut surfaces of fibrillar collagen/CS/HA scaffolds containing increasing wt% HA showed maintained interconnecting pore structures (**Figures 2.2a-c**).

In the same scaffolds at higher magnification (25,000X and 3 kV), self-assembling fibres with characteristic D-banding spacing distribution of fibrillar collagen were observed (**Figures 2.3a-c**). Nanoparticles of HA with agglomeration were seen interwoven throughout the collagen fibrils (**Figures 2.3b-c**).

Analysis of the SEM images was performed with ImageJ software. The mean pore diameter and area within all the scaffolds were calculated to be within the ranges 130 – 186 μm and 200 – 600 μm^2, respectively, apart from collagen/CS/50 wt% HA which had larger pores (**Figures 2.4a-b**).

FIGURE 2.1

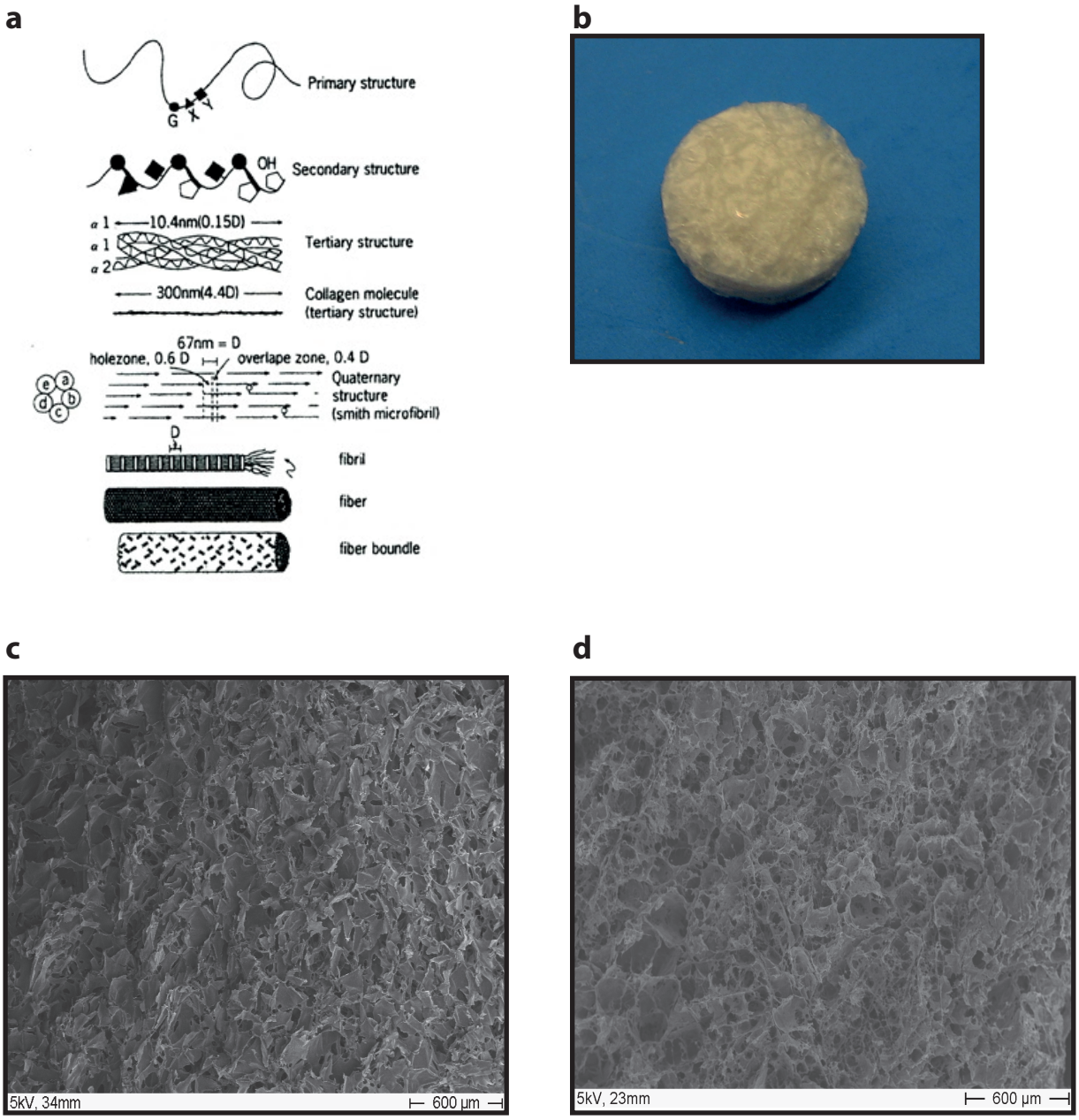


FIGURE 2.1 Collagen (a) Schematic representation of hierarchial structure of collagen, from amino acid chains to fibre bundles (Smith, 1968). (b) Photograph of fibrillar collagen scaffold as fabricated in this study. Scanning electron microscopy images show porous structure of cut surface of collagen scaffolds, (c) afibrillar collagen, and (d) fibrillar collagen. All images were obtained using a JEOL scanning microscope 840F with a working distance of 10-30 mm, electron voltage of 5 kV and 50-10,000X magnification.

FIGURE 2.2

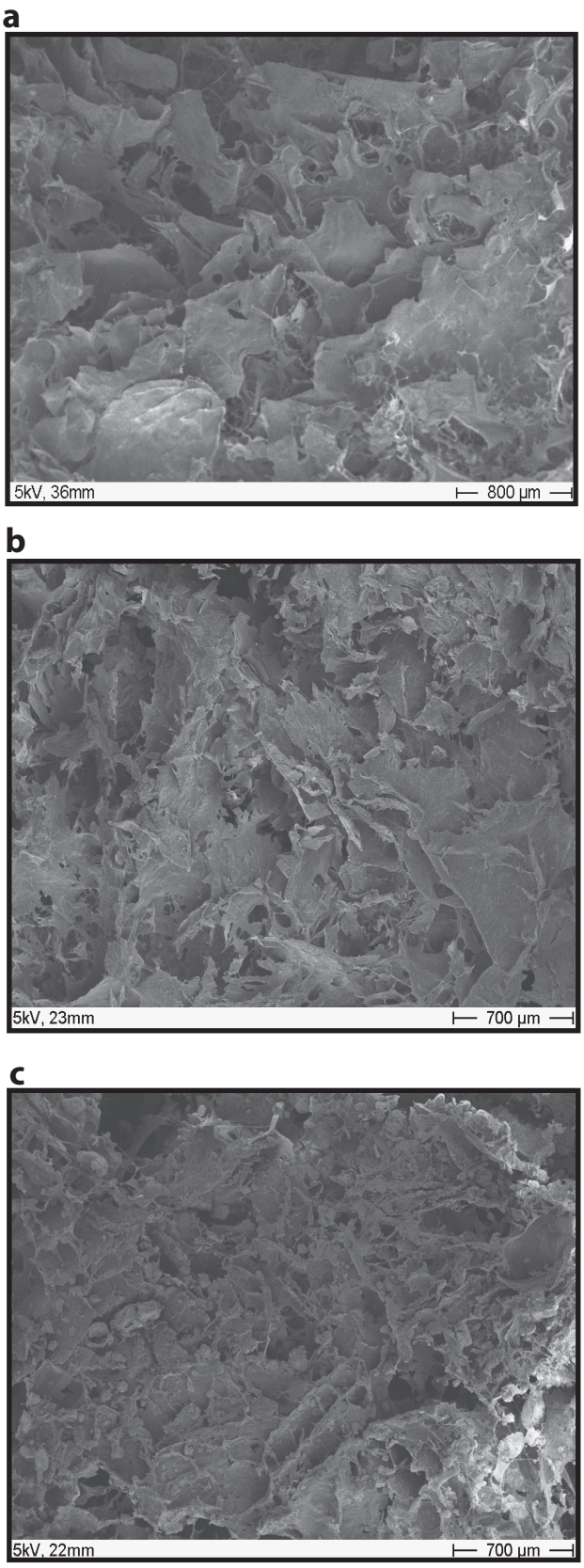


Figure 2.2 Scanning electron microscopy images show porous structure of cut surface of collagen/CS/HA scaffolds (a) Collagen/CS 1wt%/HA 30wt%. (b) Collagen/CS 1wt%/HA 50wt%. (c) Collagen/CS 1wt%/HA 75wt%. All images were obtained using a JEOL scanning microscope 840F with a working distance of 10-30 mm, electron voltage of 5 kV and 50-10,000X magnification. CS, chondroitin sulphate; HA, hydroxyapatite

FIGURE 2.3

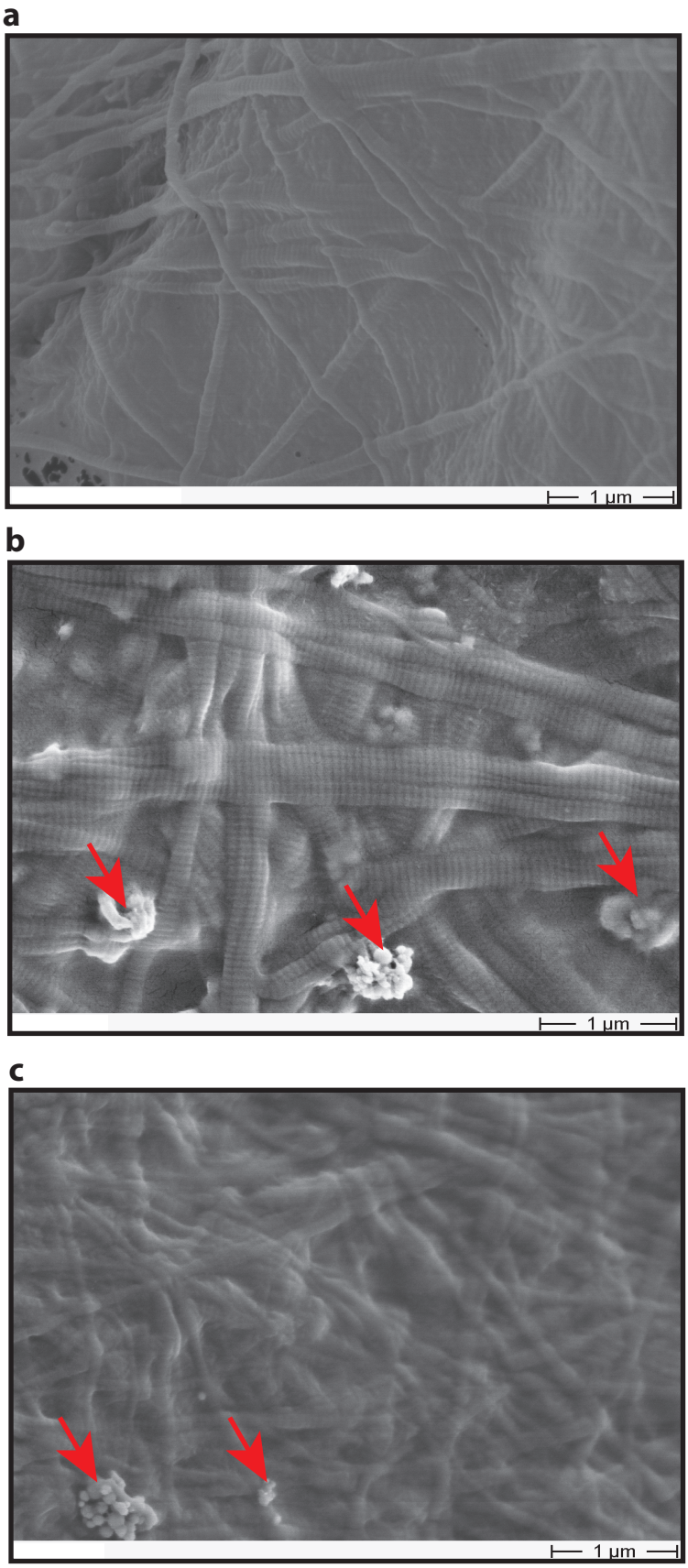


FIGURE 2.3 SEM images show D-banding spacing of collagen, with agglomerates of nanoHA interwoven throughout the fibrils (a) Fibrillar collagen. (b) Collagen/CS 1wt%/HA 50wt%. (c) Collagen/CS 1wt%/HA 75wt%. All images were obtained using a JEOL scanning microscope 840F with a working distance of 10-30 mm, electron voltage of 3-5 kV and 25,000X magnification. CS, chondroitin sulphate; HA, hydroxyapatite. Arrowhead, nanoHA.

FIGURE 2.4

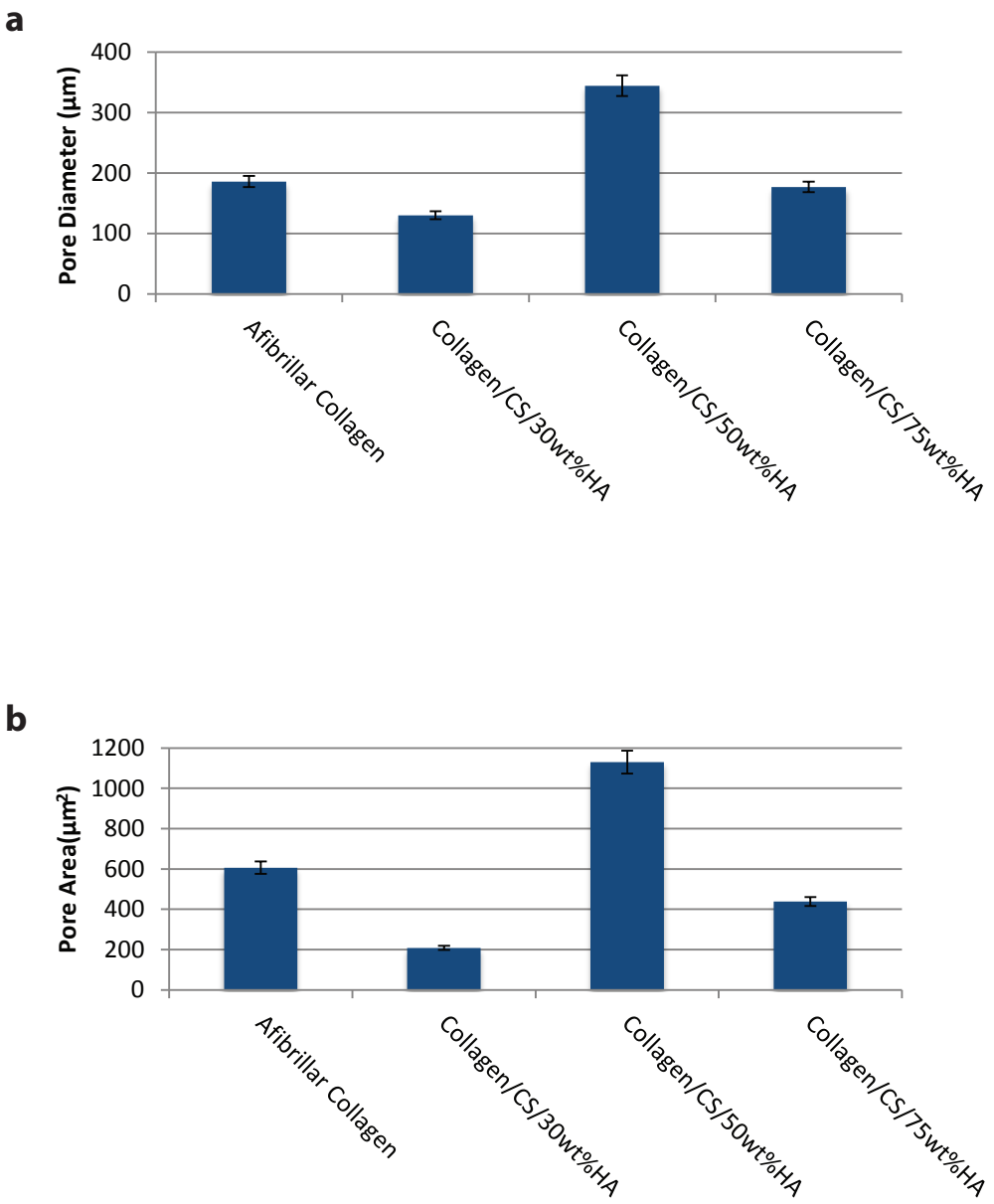


Figure 2.4 Pore size analysis of collagen scaffolds ImageJ software was used to calculate pore size of collagen scaffolds from SEM images. Graphs represent average pore diameter (a) and area (b) of afibrillar and HA/CS collagen scaffolds. Experiments performed in triplicate, error bars show standard deviation. SEM, scanning electron microscopy; CS, chondroitin sulphate; HA, hydroxyapatite.

Transmission electron microscopy (TEM) supported the findings of SEM, with characteristic D-banding patterns of fibrillar collagen observed in collagen/CS/HA scaffolds, compared to afibrillar collagen (**Figures 2.5a-c**). Collagen scaffolds were scanned using atomic force microscopy (AFM) and non-contact mode images confirmed the ultrastructured D-banding pattern within the collagen fibrils (**Figure 2.5d**).

2.5.2 Chemical Composition

Thermogravimetric analysis (TGA), energy-dispersive x-ray (EDX) and x-ray diffraction (XRD) were undertaken to analyse the chemical composition of the scaffolds.

TGA showed differences between the expected and actual weight percent of HA within the scaffolds (**Figure 2.6a**). Overall, TGA confirmed increasing wt% of HA as fabricated within collagen/CS/HA scaffolds (as expected). The thermograms for each of these scaffolds showed the same pattern for all (**Figures 2.6b-d**): up to 200^0C the absorbed water was evaporated; subsequent loss in weight of collagen molecules was observed from 200 - 500^0C; a slight loss was observed from 500 – 700^0C due to further combustion of residual collagen/CS components.

EDX analysis of collagen scaffolds with increasing wt% HA showed homogenous distribution of HA throughout the scaffolds (**Figure 2.7**).

FIGURE 2.5

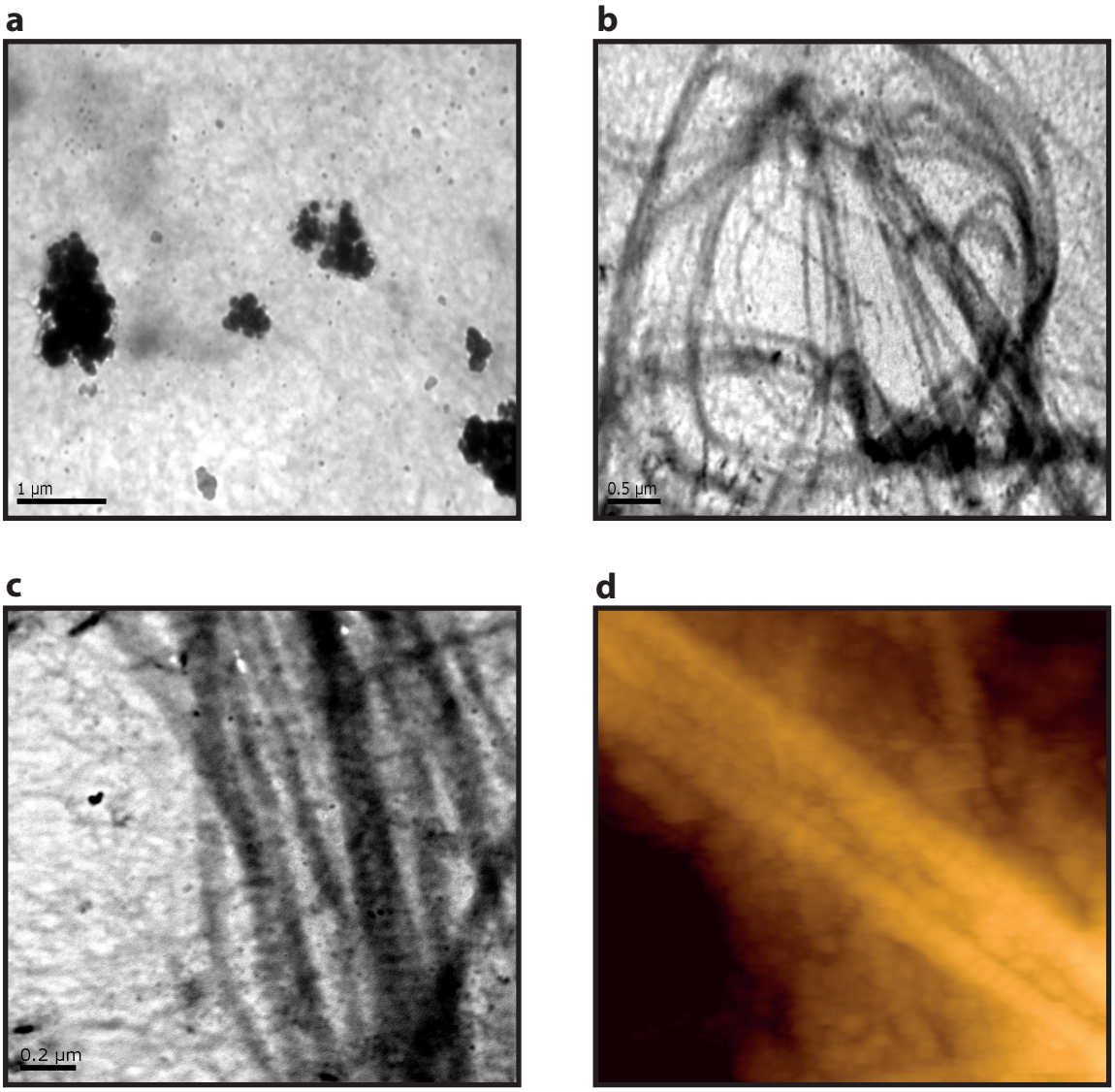


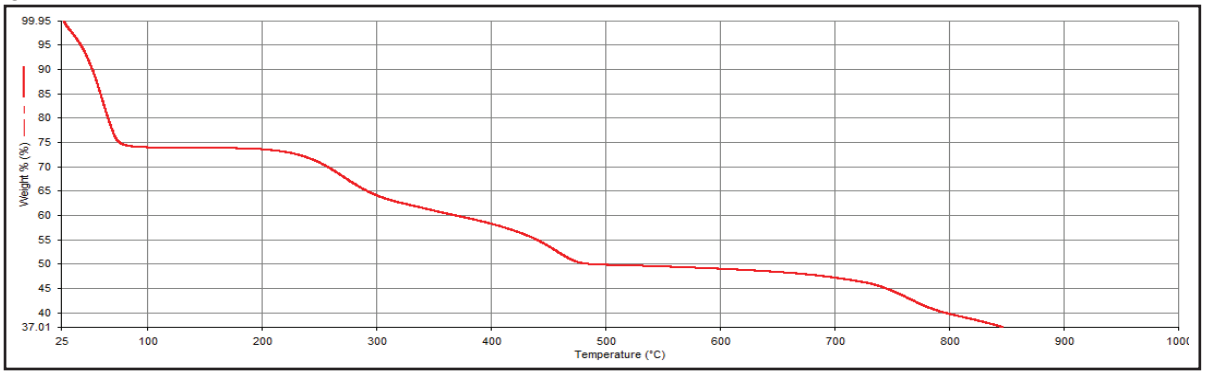
FIGURE 2.5 Transmission electron microscopy (TEM) and atomic force microscopy (AFM) images show D-banding spacing of collagen, with agglomerates of nanoHA interwoven throughout the fibrils. TEM images of (a) afibrillar collagen, (b) and (c) fibrillar collagen/CS 1wt%/HA 50wt%, scale as shown. (d) AFM image of fibrillar collagen scaffold. CS, chondroitin sulphate; HA, hydroxyapatite.

FIGURE 2.6

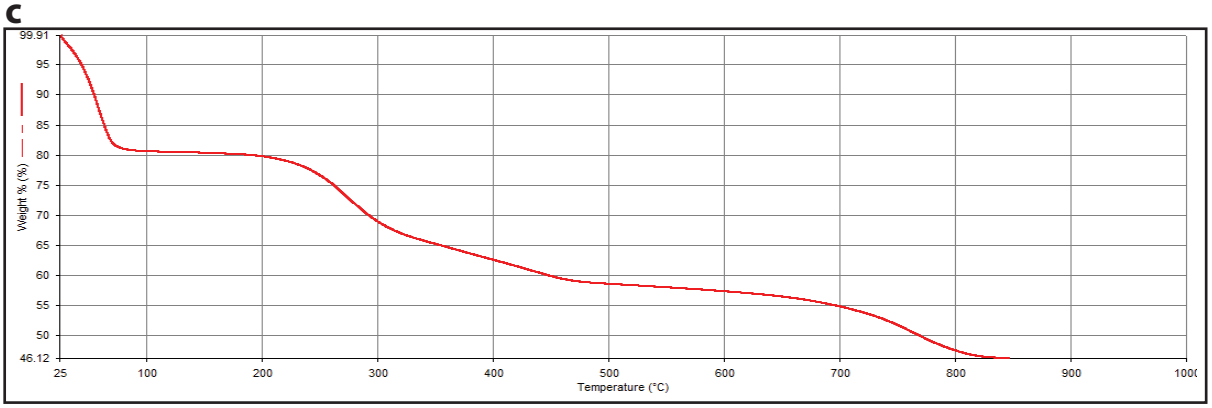
a

	TGA-derived actual hydroxyapatite wt % in scaffold			
Expected HA wt% in scaffold as fabricated	Triplicate Set #1	Triplicate Set #2	Triplicate Set #3	Mean (+/- SD)
30 %	37.01	37.89	36.90	37.27 (+/- 0.54)
50 %	46.12	48.05	46.90	47.02 (+/- 0.97)
75 %	72.92	76.63	75.63	75.06 (+/- 1.92)

b



c



d

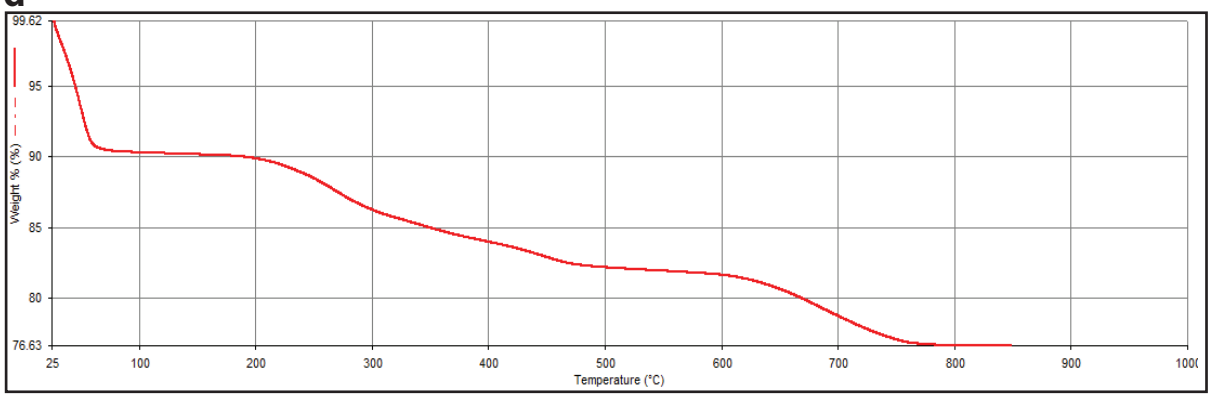


FIGURE 2.6 Thermogravimetric analysis (TGA) confirms composition of scaffolds. (a) Summary table of TGA-derived wt% values of HA in collagen/CS/HA scaffolds. Data are shown for each sample in triplicate with mean values +/- SD. TGA data for scaffolds as prepared with 30-75 wt% HA and heated from 25 °C to 1000 °C at a rate of 10 °Cmin^{-1} in nitrogen. Graphs show representative data for each scaffold prepared with desired weight percentage of HA (b) 30 (c) 50 and (d) 75. CS, chondroitin sulphate; HA, hydroxyapatite.

FIGURE 2.7

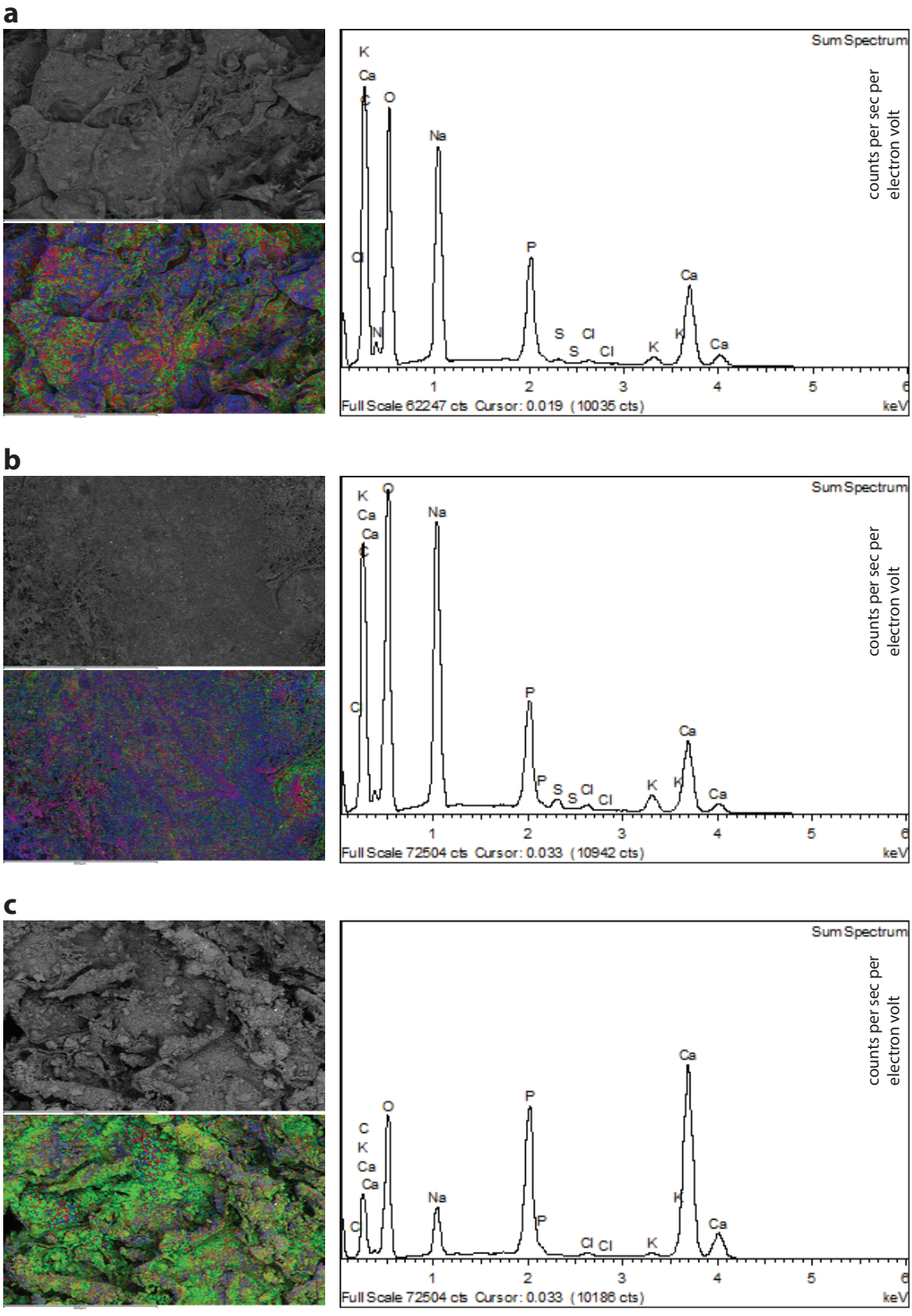


FIGURE 2.7 Energy dispersive x-ray (EDX) analysis of collagen scaffold with increasing wt% of hydroxyapatite (HA)**.** Collagen scaffold containing (a) 30 wt% (b) 50 wt% and (c) 75 wt% HA were analysed by EDX. For each sample, SEM images are shown for the cross-sectional cut surface with and without EDX overlay, demonstrating the homogeneity of HA throughout the scaffold. Red, phosphorous; Green, calcium; Blue, oxygen. For each sample, graphs of elemental mapping are shown on the right. HA, hydroxyapatite; SEM, scanning electron microscopy.

XRD patterns were analysed using the International Centre for Diffraction Data (ICDD) standard diffraction pattern for HA (#09-432, **Figure 2.8a**). XRD diffraction patterns were obtained for collagen/CS/HA scaffolds containing 30, 50 and 75wt% HA (**Figures 2.8b-d**) and the samples were found to be exact matches for HA, confirming the phase purity of the HA and its homogeneous distribution throughout the scaffolds.

2.5.3 Active microbial transglutaminase

Microbial transglutaminase (mTG) was purified from its carrier molecule, maltodexrin, using a cation exchange sepahrose-containing column (**Figure 2.9a**). The purified protein was analysed with SDS-PAGE and the product was shown to have the expected molecular weight of TG, 37.8 kDa (**Figure 2.9b**). Using a commercially-available assay, this TG was shown to possess enzymatic activity and had a concentration of 19.58 U/ml (**Figure 2.9c**).

2.5.4 Thermal Analysis

Differential scanning calorimetry (DSC) was used to assess the thermal stability, and thus suitability for *in vivo* use, of the scaffolds. Denaturation temperatures were similar for all samples tested (average 65.1^0C, range 63.7 – 66.2^0C), apart from mTG-crosslinked collagen, which had a significantly higher Td of 74.1^0C ($p<0.02$, **Figure 2.10**).

FIGURE 2.8

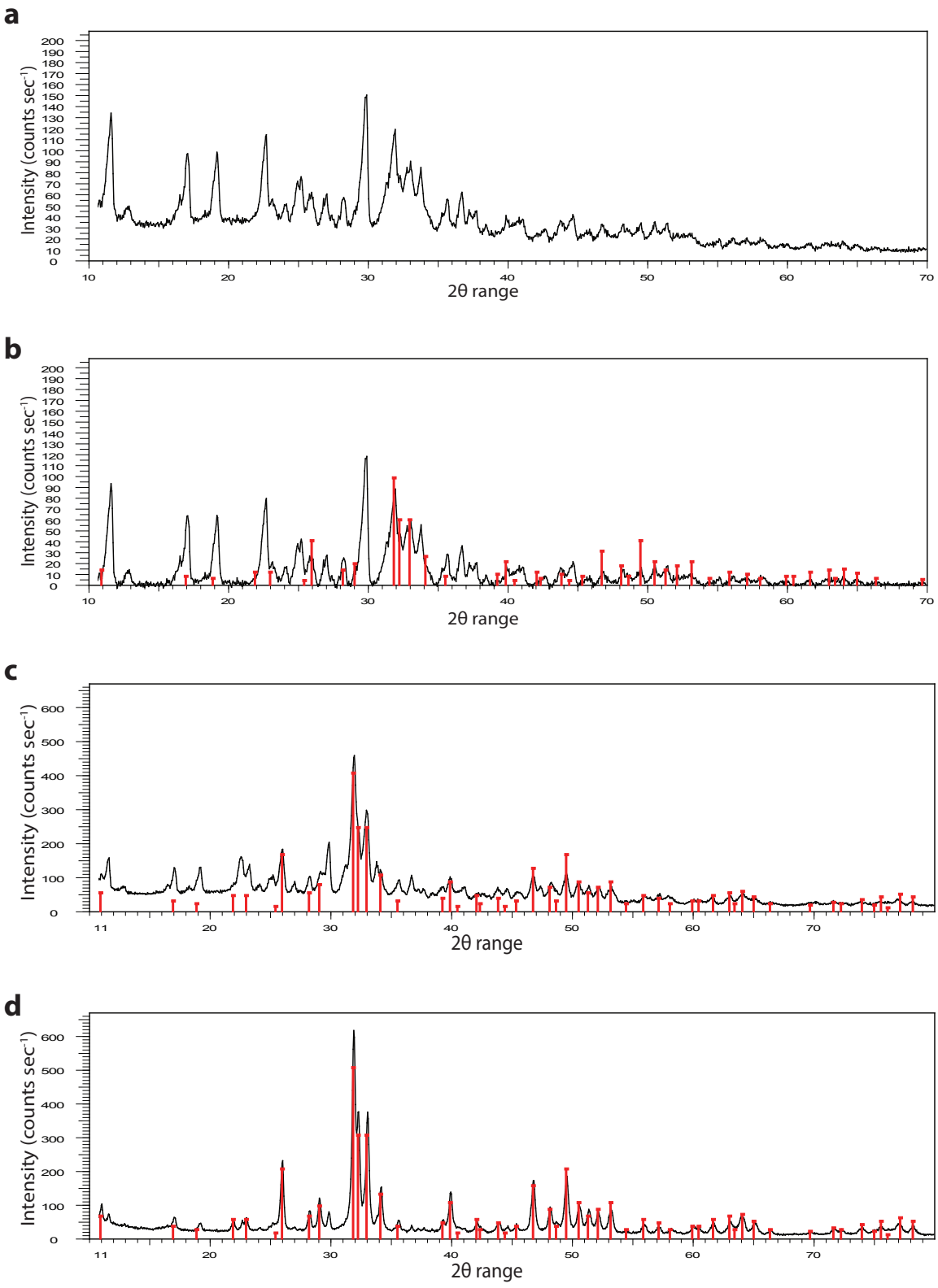


Figure 2.8 X-ray diffraction (XRD) analysis of collagen scaffolds XRD was performed over a 2θ range of 10-80^0 with a step size of 0.05, dwell time of 12 s at RT and divergent slit of 0.5. Bruker analysis software was used to analyse the data. (a) ICDD standard diffraction pattern for HA (#09-432). XRD plots for collagen/CS scaffolds containing (b) 30 wt%, (c) 50 wt% and (d) 75 wt% HA. RT, room temperature; XRD, X-ray diffreaction; ICDD, International Centre for Diffraction Data; CS, chondroitin sulphate; HA, hydroxyapatite.

FIGURE 2.9

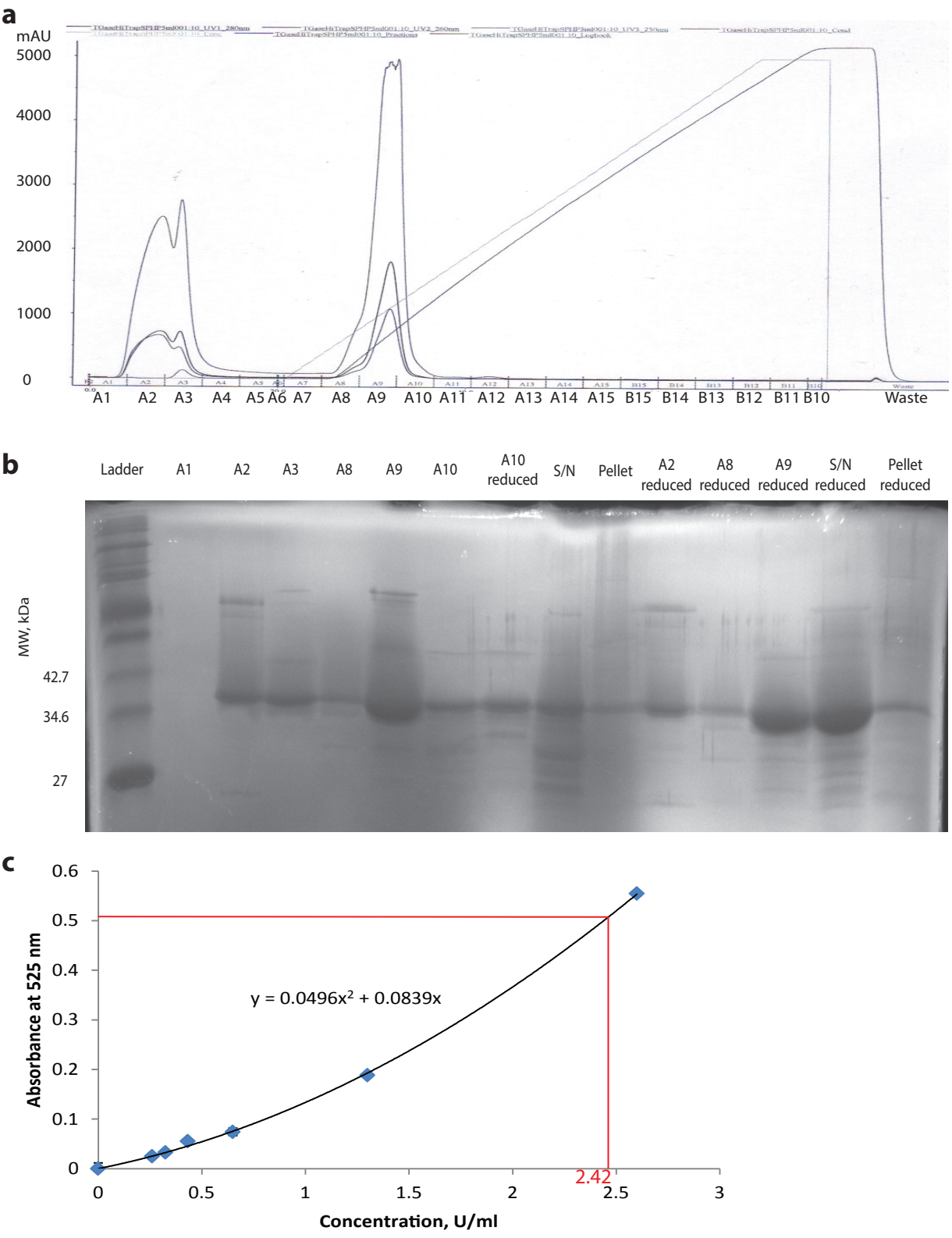


Figure 2.9 Purified transglutaminase (TG) possesses biological activity (a) Chromatogram showing products of purification of mTG/maltodextran compounds using HiTrap sepharose column. (b) SDS-PAGE gel showing molecular weight of purified fractions of mTG. (c) Graph showing absorbance results of purified mTG in commercially-available activity assay (Zedira). Red line shows absorbance of test mTG diluted 1:7 to be 2.42 U/ml. mTG, microbial transglutaminase.

FIGURE 2.10

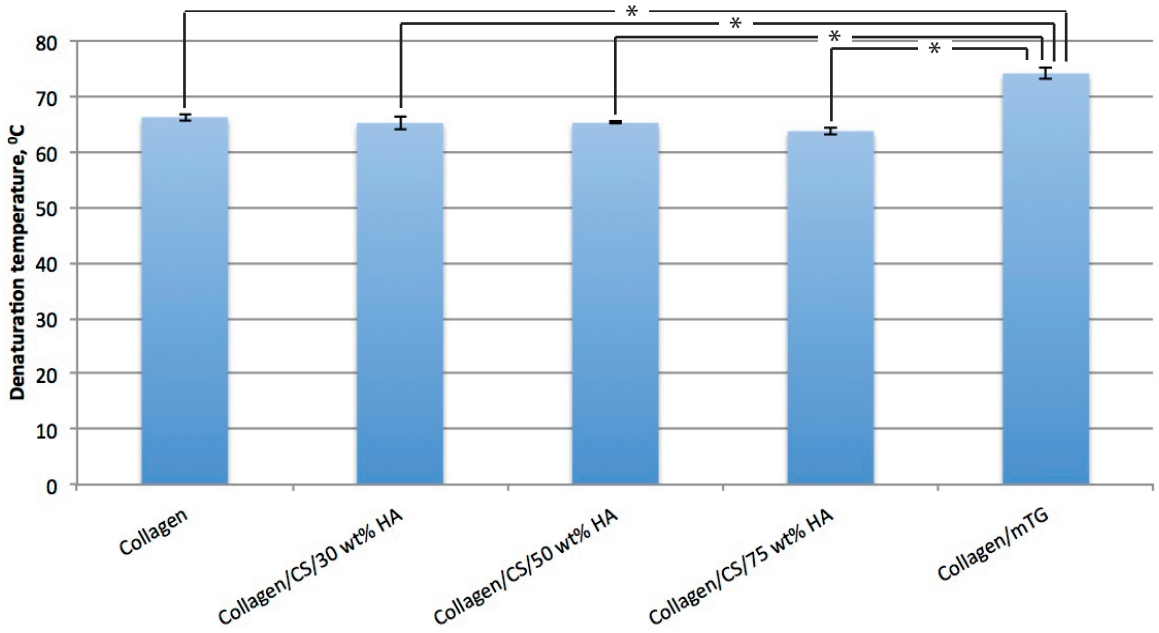


FIGURE 2.10 Dynamic scanning calorimetry (DSC) shows thermal stability of scaffolds at body temperature Graph of mean denaturation temperatures for each scaffold type, calculated from DSC data of peak temperature. Error bars, standard deviation. CS, chondroitin sulphate; HA, hydroxyapatite.

2.5.5 Mechanical characterisation

Mechanical testing was performed to establish the compressive modulus for the scaffolds. Only compressive strength was evaluated, as the scaffold will be applied to spinal surgery models, where the principal force is compression. Representative stress/strain curves for each sample tested are shown (**Figures 2.11a-e**).

From such curves, Young's modulus was calculated as shown in the schematic representation in **Figure 2.11f** (Gibson 2000), using a curve with three distinct parts: linear elastic, collapse plateau, densification. The average values of triplicate samples for each scaffold are shown (**Figure 2.11g**). Afibrillar collagen had the lowest Young's modulus of all samples tested (0.004 MPa, **Figure 2.11g**), which was significantly lower than fibrillar collagen (0.079 MPa, $p<0.0002$, student's t-test). The addition of 30 wt% HA did not significantly change the compressive modulus (0.079 MPa). However, at higher HA wt % (50 and 75), there was a significant and large increase in compressive modulus (13.7 and 33.6 MPa, respectively, $p<0.0002$).

FIGURE 2.11

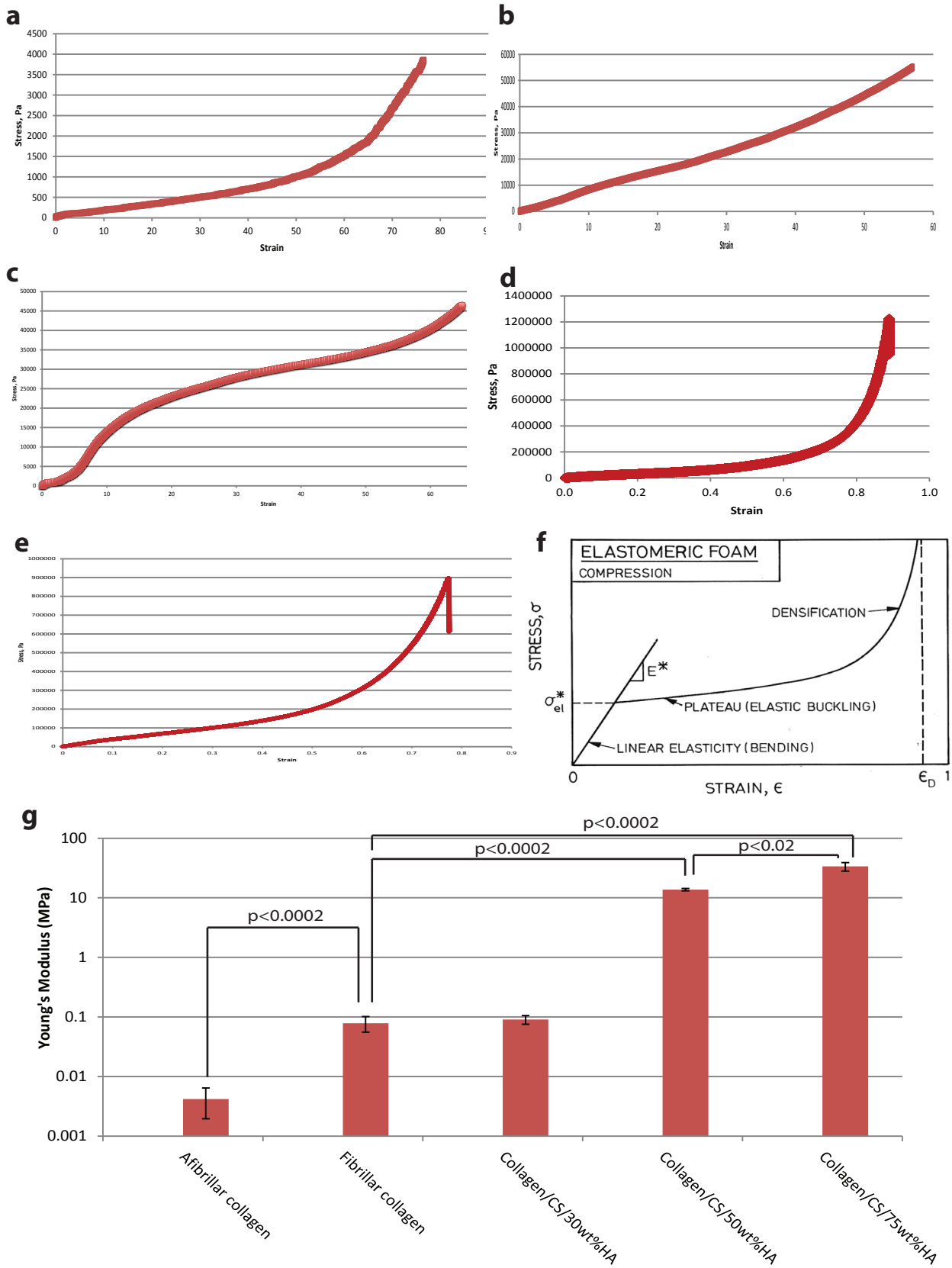


FIGURE 2.11 Mechanical testing of collagen scaffolds Compression testing was performed. Graphs showing stress/strain curves for (a) afibrillar collagen, (b) fibrillar collagen and scaffolds containing collagen/CS with (c) 30, (d) 50 and (e) 75 wt% HA. (f) Schematic representation of calculation of Young' modulus from stress/strain surves, Gibson, 2000. (g) Graph of Young's moduli calculated using LINEST function in Microsoft Excel; log-scale, average of triplicate samples. CS, chondroitin sulphate; HA, hydroxyapatite.

2.6 Discussion and Summary

We have successfully fabricated a novel collagen-based scaffold and characterised it with a range of imaging, chemical composition and thermal analysis techniques. Self-organising atellocollagen was combined with nano-hydroxyapatite and chondroitin sulphate, and the effect of cross-linking was studied using microbial transglutaminase. Hydroxyapatite has been widely used as a bone substitute material since the 1980s (Frame et al. 1981). Recently, interest has grown in nanoparticles due to their greater surface area and more active free sites than microparticles, leading to improved bone healing (Kikuchi et al. 2001; Nair & Laurencin 2007). Chondroitin sulphate, the most abundant glycosaminoglycan in the human body, was added to the scaffold as it is present in bone and has been shown to minimise the inflammatory-mediated catabolism of cartilage and bone (Pecchi et al. 2012).

The ultrastructure of collagen is critical to its biological roles, including cell adhesion. Using a range of imaging techniques, such as SEM and TEM, we have shown that the self-organising collagen did form fibrils, as demonstrated by the presence of typical d-banding pattern. The pH and ionic concentration of the fibrillogenesis buffer has a significant effect on the formation of classical d-banded fibrils. Detailed studies have shown the optimal conditions of fibrillogenesis buffer to be near-physiological, with pH 7.4 and low ionic strength (below 150 mM) {Douglas:2006dc}(Harris et al. 2013). In our fibrillogenesis process, we used a buffer of pH 7.4 and ionic strength 60 mM, which is similar to those in the previous studies.

We have shown the presence of single collagen fibrils in the scaffold, interspersed with HA, as found in human bone. The presence and homogeneous distribution of HA was confirmed using XRD and EDX. The porous structure of scaffolds after freeze-drying arises from the deposition of ice crystals in the collagen solution, which is then evaporated under vacuum conditions. The pore size of scaffolds in tissue engineering is critical for cell growth and function and is cell-type specific (Hollister 2005). As osteoblasts are 20-25 μm in diameter, it has been identified that for bone tissue engineering, the minimum pore diameter is approximately 100 μm (Karageorgiou & Kaplan 2005). Moreover, pore sizes greater than 300 μm diameter have been shown to enhance cell migration, osteogenesis and capillary formation (Chvapil 1977).

DSC showed thermal stability of all samples at physiological body temperature, 37^0C. Interestingly, the presence of mTG led to a significant increase in thermal stability, with a denaturation temperature of $74.^0$C. Although a small amount of cross-linking normally occurs during fibrillogenesis, mTG was added to the collagen solution scaffolds to promote cross-linking of collagen fibrils. Such increased thermal stability suggests a slower degradation profile of collagen/mTG scaffolds and therefore the potential for a longer-lasting scaffold *in vivo*. Similar results have been obtained for Type II collagen scaffolds, with mTG decreasing rate of degradation (Halloran et al. 2006). Such a degradation profile would enable the scaffold to promote bone growth over a longer period of time, which could in turn promote fusion rates.

Transglutaminase catalyses the formation of covalent bonds between a free amine group from a protein (for example, collagen) or peptide-bound lysine and the γ-carboxamide group of a protein (for example, collagen) or peptide-bound glutamine (L. S. M. Teixeira et al. 2012). Other cross-linking agents have previously been studied in scaffolds for bone regeneration, including glutaraldehyde, EDC/NHS and UV radiation, due to the improvement in mechanical and physicochemical properties observed with their use. However, disadvantages of these techniques include toxicity and altered structural properties of the material. mTG, an enzymatic cross-linking agent, has gained recent interest for *in vivo* use due to its lower toxicity than chemical cross-linking agents, and it was therefore chosen for this work with potential clinical application.

Mechanical testing of the scaffolds fabricated showed distinct linear elastic, collapse plateau and densification regions and the Young's modulus of mineralised collagen (50 wt% and 75 wt% HA, 13.7 and 33.6 MPa, respectively) was well above that of developing osteoid tissue (25 – 100 kPa, (García & Reyes 2005)) and close to that of cancellous bone (90 – 400 MPa, (Rohl et al. 1991)), therefore it should provide an appropriate stiffness for the adhesion, growth and differentiation of MSCs (Yeung et al. 2005).

Chapter 3 Role of human mesenchymal stem cells and collagen/HA/GAG scaffold in osteogenesis

3.1 Introduction

The current 'gold standard' graft material in spinal fusion surgery is autologous bone graft (commonly iliac crest bone graft, ICBG), as detailed in **Chapter 1.4.3.1**. Autologous bone graft contains critical components: a bony scaffold; growth factors in the bone extracellular matrix; and osteoprogenitor cells within the bone marrow. However, the harvesting of such graft is associated with significant complications and the graft itself is of limited availability. Therefore, alternative therapies that include some or all of these critical graft components are being studied in regenerative orthopaedic surgery.

The combination of hMSCs with an osteoconductive scaffold and/or osteoinductive factors has been shown to increase their osteoblastic differentiation and hence promote bone formation.

Vertebral marrow aspirates contain significantly higher concentrations of osteoprogenitor cells than iliac crest aspirates, suggesting that vertebral bodies might be a good source of MSCs for spinal fusion. Furthermore, there is some evidence to suggest that there is an age-related decline in cellularity in iliac crest aspirate, but not in vertebral body aspirate, supporting the use of vertebral body aspirates in fusion surgery in the older population (McLain et al. 2005).

To date, two studies have used hMSCs in spinal fusion surgery. One study used enriched bone-marrow-derived MSCs in combination with a β-TCP ceramic scaffold and found similar rates of spinal fusion (95.6%) to ICBG (P. Zhang et al. 2008). Another study compared ICBG with cross-linked Type I collagen/HA scaffold/bone marrow aspirate and also found similar rates of fusion (94% vs 84%, respectively) (Neen et al. 2006), supporting the potential use of MSCs in spinal fusion surgery.

Therefore, the work in this chapter was undertaken to assess the potential enhancement of bone formation by the scaffold with the combination of hMSCs, and hence possibly identify a material with superior clinical applicability. In this chapter, the study of hMSCs seeded on collagen-based scaffolds is described, including the growth of MSCs in the scaffold, as assessed by growth rates and live-cell imaging, and their osteogenic capability as measured by the induction of key osteogenic genes.

3.2 Human mesenchymal stem cell culture

Human mesenchymal stem cells (hMSC) (Lonza) were grown in MSCGM™ (Mesenchymal Stem Cell Growth Medium) (Lonza) supplemented with BulletKit™ (Lonza). Cells were grown on Matrigel™-coated plates (Matrigel™, BD #354262) in a humidified incubator with 5% CO_2 at 37^0C. Passage was performed at 70% confluence using 0.05% Trypsin EDTA (Invitrogen).

3.3 Cell growth and viability assays

All experiments were performed with biological and technical triplicates. Cell growth was assessed using AlamarBlue® assay and live cell imaging using multi-photon microscopy was performed to visualise viable cells within the scaffolds. The principle of AlamarBlue® assay (containing resazurin) is that viable cells take up blue non-fluorescent resazurin and reduce it to a red highly fluorescent

resorufin, which is detected using a plate-reader (Nakayama et al. 1997). This quantitative assay can then provide a surrogate marker of cell number.

3.3.1 AlamarBlue® assay

Quantitative assessment of viable cell number over time, and hence proliferation rate, was performed using an AlamarBlue® assay. In order to harvest all the cells and obtain an accurate result, digestion of the scaffold was performed with collagenase Type I (Sigma #CO130) at 100 collagenase digestion units per scaffold and 1 h incubation at 37^0C. After a brief vortex, AlamarBlue® (Life Technologies #DAL1025) was added to cells as 10% of total volume. After 2 h incubation at 37^0C and a brief vortex, fluorescence of the media/AlamarBlue was read using 570 nm excitation and 585 emission wavelengths (POLARstar Omega, BMG Labtech).

3.3.2 Multi-Photon Microscopy

In collaboration with Mr Shaoyong, three-dimensional fluorescent live cell imaging of MSCs within the collagen-based scaffolds was performed using a modified BioRad Radiance 2100 MP Multiphoton Microscope (Zeiss; Jena, Germany). Near infrared (NIR) laser beams (wavelength 800 nm) were obtained from a tunable 76 MHz femtosecond pulsed Ti:sapphire laser (Mira 900-F, Coherent, Ely, UK) pumped by a 10 W multiline argon ion laser (Verdi; Coherent). A Nikon S Fluor 20X objective with a numerical aperture of 0.75 was

used for all images. The emission filters selected were: 495 nm for blue, 525 nm for green and 595 nm for red. Scanning speed was 166 lines per second and the Z-step was 2.55um. Imaris 7.6.1 was used for imaging processing works.

3.4 Osteogenic characterisation of hMSCs

To evaluate the osteogenic capabilities of the MSCs within the scaffold, the expression of critical osteogenic genes was quantitatively analysed using RT-PCR. Osterix (Sp7), osteocalcin (BGLAP), ALP, BMP-2, TGFβ1 and RUNX2 were selected for analysis based on their previous identification as markers of osteogenesis.

Osterix is expressed in developing bone (Nakashima et al. 2002), osteocalcin is a marker of osteogenic differentiation of MSCs (A. Nakamura et al. 2009) and ALP is a marker of osteoblast activity (Pagani et al. 2005). RUNX2 is a marker of proliferation and differentiation of pre-osteoblasts (Pratap et al. 2003; Ducy et al. 1997). TGFβ1 and BMP-2 are produced by osteoblasts and are markers of bone formation (Teitelbaum & Ross 2003; Urist 1965).

3.4.1 RNA extraction

Three days after seeding, cells were harvested from the scaffolds with collagenase digestion performed at 37^0C for 1 h and centrifugation at 3000 rpm for 3 min at RT. For all cells, RNA was extracted using TRI® Reagent (Sigma) according to the Sanger Institute Protocol

(http://www.sanger.ac.uk/Projects/Microarrays/arraylab/protocol1.pdf) and quantified using a NanoDrop 2000 Spectrophotometer (Thermo Scientific). RNA samples were stored at -80^{0}C.

3.4.2 cDNA synthesis

cDNA was synthesised using High Capacity RNA-to-cDNA MasterMix (AppliedBiosystems™ #4390779) according to the manufacturer's protocol, with 2 µg RNA in a 20 µl reaction. cDNA was stored at -20^{0}C.

3.4.3 RT-PCR

Reactions were performed using 5 µl SYBR® Green PCR Master Mix (AppliedBiosystems™ #4385618), 400 nM of forward and reverse primers, and 1 µl of cDNA in a total volume of 10 µl (with RNAase-free water), using technical and biological triplicates. The cycling conditions used were 2 min at 50^{0}C, 10 min at 95^{0}C, and 40 cycles of 15 sec at 95^{0}C followed by 1 min at 60^{0}C, 15 sec at 95^{0}C, 15 sec at 60^{0}C and a final 15 sec at 95^{0}C. All reactions were performed on an AppliedBiosystems™ 7500 Fast Real-Time PCR System and data was normalised to a panel of housekeeping genes (β-actin, UBC, TBP and GAPDH) using the comparative Ct method, where 'reference gene' denotes the average Ct value across the panel of housekeeping genes (Lou et al. 2013; Schmittgen & Livak 2008):

$$\Delta Ct1 = Ct(Gene\ of\ interest, test\ sample) - Ct(Reference\ gene, test\ sample)$$

$$\Delta Ct2 = Ct(Gene\ of\ interest, ctrl\ sample) - Ct(Reference\ gene, ctrl\ sample)$$

$$\Delta\Delta Ct = \Delta Ct1(test) - \Delta Ct2(control)$$

$$Normalised\ gene\ expression = 2^{\Delta\Delta Ct}$$

Test genes included osterix, osteocalcin, TGFβ-1, RUNX2, alkaline phosphatase (ALP) and BMP-2. All primers were designed using PrimerQuest (http://eu.idtdna.com/PrimerQuest) and sequences are shown in **Appendix i**.

3.5 MicroCT

Dr Andrew Freidin, Kennedy Institute, University of Oxford, performed micro CT and the data were analysed to calculate the bone mineral density (BMD) of scaffolds with and without hMSCs (after 5 days of culture on the scaffold).
Each collagen scaffold sample was scanned using Skyscan 1174 (Bruker, Belgium) compact micro CT scanner, at 50 kV, 800 µA, Image Pixel Size 8.30 µm, 0.7^0 rotation step. The micro CT scans were reconstructed using NRecon software from Skyscan. A volume of interest (VOI) of equal size (3 x 3 x 1 mm) was selected from the centre of each sample. This VOI selection was saved and analysed using Skyscan CT Analyzer software version 1.9.3.0.
The calibration of BMD against greyscale density measurements had been standardised for the scan settings using materials of known density (air, water and hydroxyapatite phantoms of 0.25 and 0.75 g/cm^3). BMD measurements

were obtained by summing of density measurements for each voxel of the sample.

3.6 Statistical analysis

For comparisons of gene expression and cell number between two samples, an unpaired t-test with Welch's correction was used, with a p value less than 0.05 considered significant. All analyses were performed in GraphPadPrism v6 software.

3.7 Results

Using multiphoton microscopy (MPM) after 3 days of cell growth, viable human mesenchymal stem cells (hMSCs) were observed in a homogenous distribution throughout each of the collagen-based scaffolds (representative images shown in **Figures 3.1*i-iii***). Although such imaging does not permit quantitative assessment, the images showed a greater number of viable cells in the collagen/CS/HA50wt% and collagen/CS/mTG scaffolds than in the collagen-only and collagen/CS/HA30wt% scaffolds (**Figures 3.1*ii*b**, **3.1*iii*b** and **3.1*i*a**, **3.1*ii*a**, respectively).

Compared to hMSCs seeded in 2-D culture on Matrigel™-coated plastic culture plates, there were significantly more cells in the 3-D collagen scaffolds at 24 hours, relative to the seeding density as measured by AlamarBlue® assay ($p<0.02$, **Figure 3.2b**). This shows that the cells grew faster in the collagen scaffolds than on 2-D culture. Over time, although the cells continued to grow in the scaffolds, there was a relative reduction in the rate of increase in cell number, compared to cells on 2-D culture (**Figures 3.2a-b**); at 72 hours, there was no significant further increase in cell number for hMSCs grown in HA-containing collagen scaffolds, whilst hMSCs grown in 2-D culture, and in collagen/CS/mTG and collagen scaffolds did continue to proliferate. By 14 days, the cells grown in 2-D culture had increased in number significantly more than the cells grown in any of the collagen scaffolds (**Figure 3.2b**).

FIGURE 3.1*i*

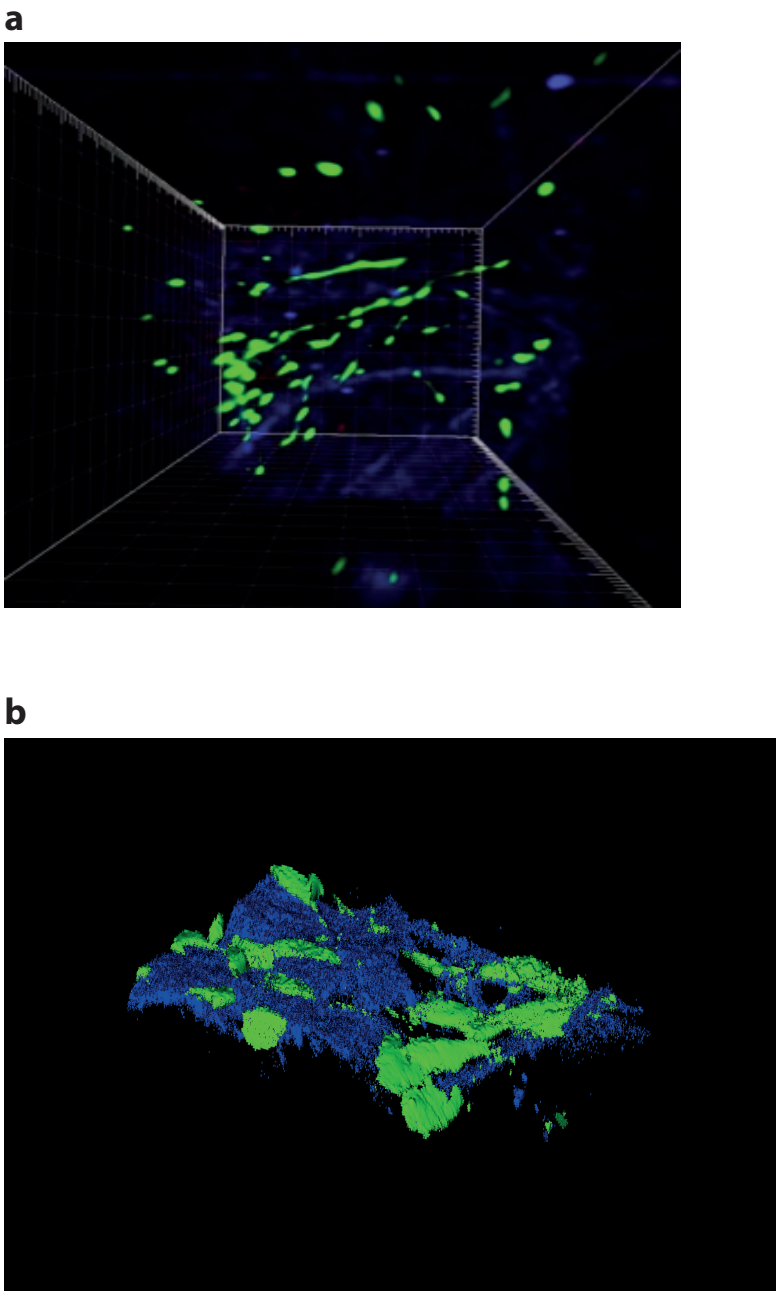


FIGURE 3.1*i* Viable human mesenchymal stem cells grow throughout 3-dimensional collagen-based scaffolds. (a) Representative multiphoton microscopy image of live hMSCs in collagen scaffold. (b) 3-D reconstruction of hMSCs in collagen scaffold. 100,000 hMSCs seeded per scaffold, all images obtained after 3 days of culture using a BioRad Radiance 2100 MP Multiphoton Microscope. Blue, collagen; Green, live cells; Red, dead cells.

FIGURE 3.1*ii*

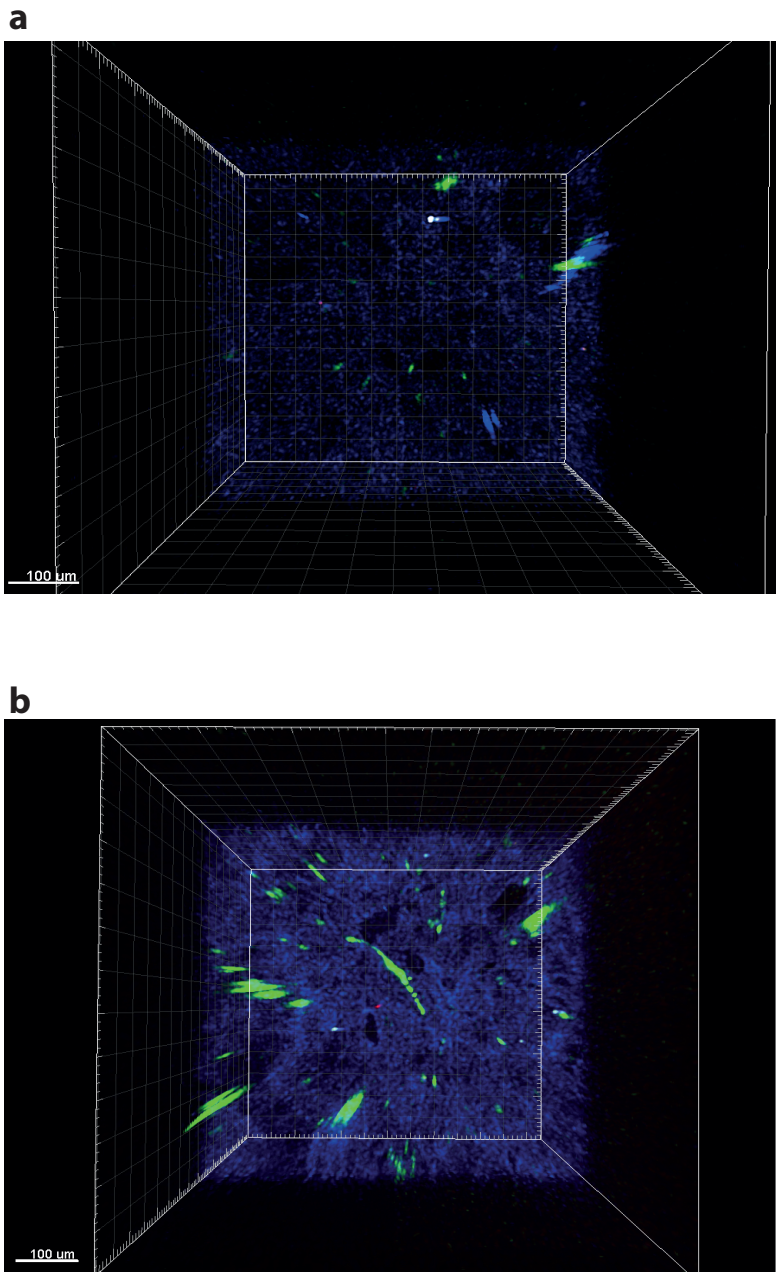


FIGURE 3.1*ii* Representative multiphoton microscopy images of live human mesenchymal stem cells in (a) collagen/CS/HA30wt% and (b) collagen/CS/HA50wt% scaffolds. Blue, collagen; Green, live cells; Red, dead cells. CS, chondroitin sulphate; HA, hydroxyapatite.

FIGURE 3.1*iii*

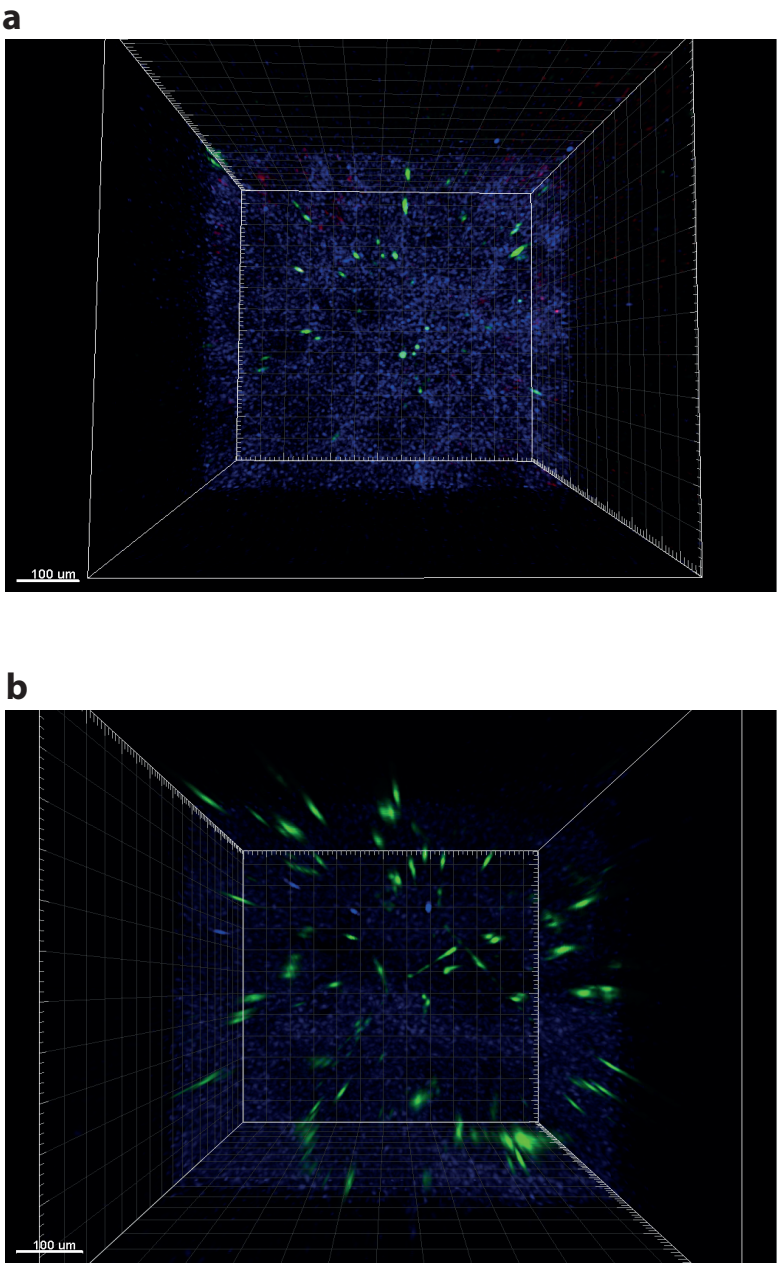
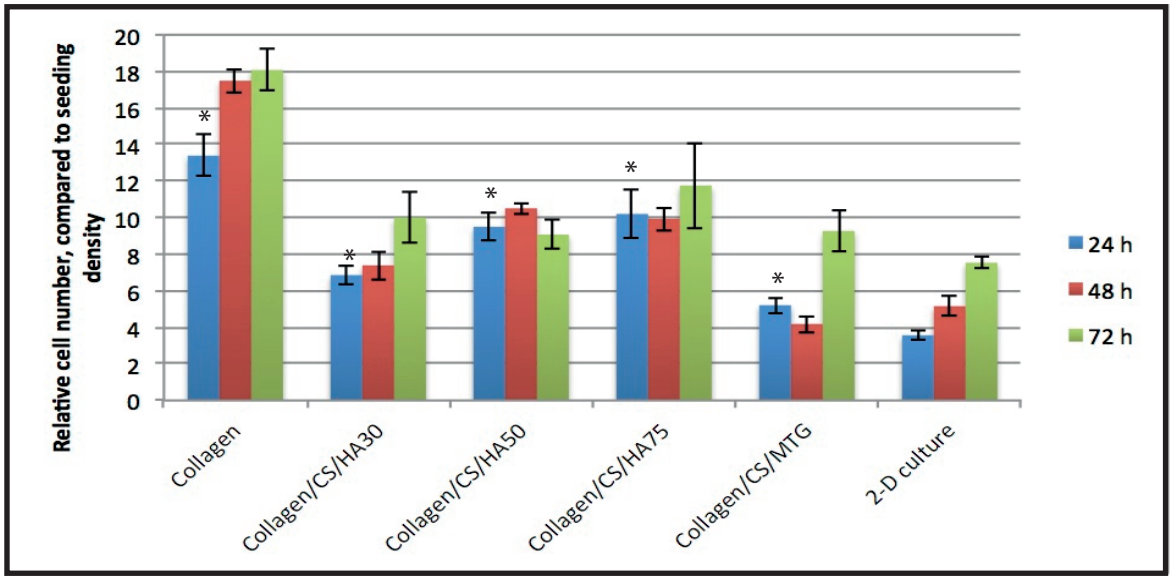


FIGURE 3.1*iii* Representative multiphoton microscopy images of live human mesenchymal stem cells in (a) collagen/CS/HA75wt% and (b) collagen/mTG scaffolds. Blue, collagen; Green, live cells; Red, dead cells. CS, chondroitin sulphate; HA, hydroxyapatite; mTG, microbial transglutaminase.

FIGURE 3.2

a



b

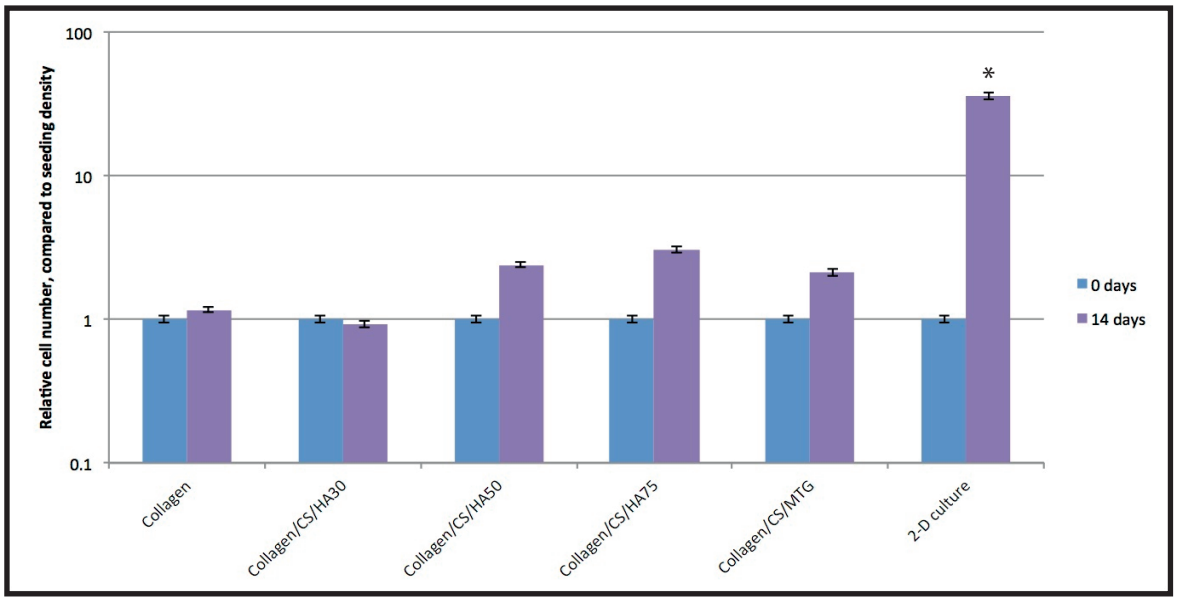


FIGURE 3.2 Collagen-based scaffolds support the growth and differentiation of human mesenchymal stem cells. (a) Graph showing relative number of hMSCs grown on collagen, collagen/CS/HA30wt%, collagen/CS/HA50wt%, collagen/CS/HA75wt%, collagen/CS/MTG or 2-D culture, compared to seeding density, using alamar blue assay. Values at 24, 48 and 72 hours. (b) Graph showing relative number (shown as log scale) of hMSCs grown on collagen, collagen/CS/HA30wt%, collagen/CS/HA50wt%, collagen/CS/HA75wt%, collagen/CS/MTG or 2-D culture, compared to seeding density, using alamar blue assay. Values at 0 and 14 days. Mean values, error bars represent standard deviation. * $p<0.05$, unpaired t-test with Welch's correction

Quantitative gene expression showed a significant increase in the mRNA levels of osterix in hMSCs grown in collagen/CS/HA scaffolds compared to cells in 2-D culture and collagen-only scaffolds, with the greatest increases seen in collagen/CS/HA 50wt% and collagen/CS/HA 75wt% scaffolds of 7.5 and 20.6 fold change, respectively, relative to 2-D culture and normalised to housekeeping genes ($p<0.05$, **Figure 3.3a**). Expression levels of osteocalcin, TGFβ-1 and RUNX2 were significantly higher in cells grown in collagen-based scaffolds than in 2-D culture with the greatest increase observed in collagen/CS/HA 50wt% scaffolds (fold change of 13.9, 32.7 and 22.2, respectively, $p<0.05$, **Figures 3.3b-d**). A significantly higher expression level of ALP was observed in cells grown in collagen scaffolds than cells grown in 2-D culture, with the highest levels seen in collagen/CS/HA 75wt% scaffolds (fold change of 4.2, $p<0.05$, **Figure 3.3e**). Expression levels of BMP-2 were significantly higher in cells from all scaffolds apart from collagen/CS/mTG, compared to cells from 2-D culture, with the greatest levels observed in cells from collagen/CS/HA 30wt% and collagen/CS/HA 50wt% scaffolds (fold change of 1025.2 and 994.0, $p<0.05$, **Figure 3.3f**).

Micro CT demonstrated a significant increase in BMD with the addition of HA to the collagen scaffolds ($p<0.02$, **Figure 3.4a**). The culture of hMSCs on collagen/30wt% HA scaffolds resulted in a significant increase in BMD ($p<0.02$, **Figure 3.4a**) compared to collagen-only scaffolds. Representative images obtained from micro CT analysis are displayed in **Figures 3.4b-c** and **Figures 3.5a-d**.

FIGURE 3.3

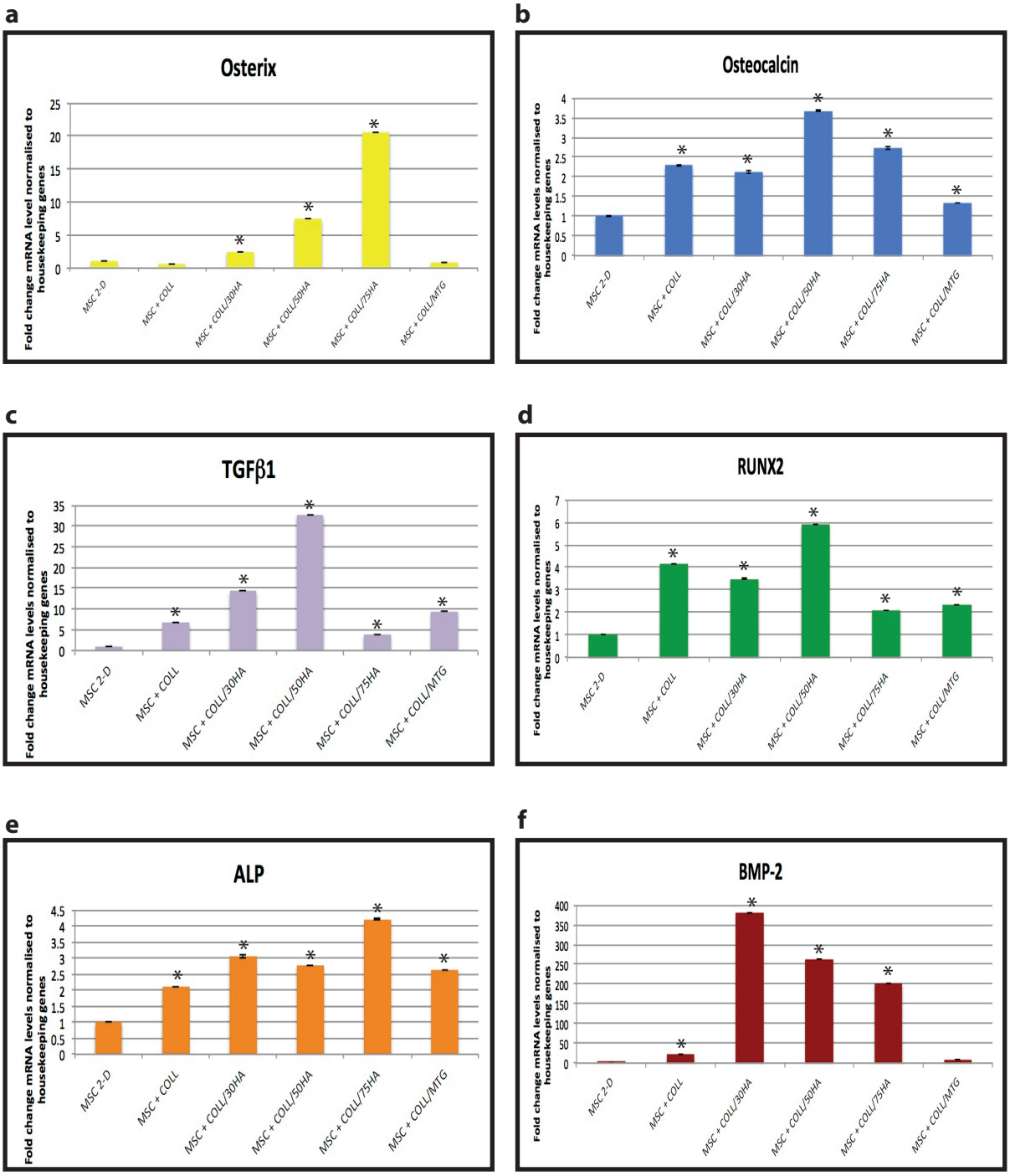


Figure 3.3 Osteogenic gene expression is enhanced by the presence of collagen-based scaffolds. Quantitative gene expression in hMSCs harvested from either 2-D culture on Matrigel-coated dishes or 3-D collagen-based scaffolds (collagen, collagen/CS/30 wt% HA, collagen/CS/50 wt% HA, collagen/CS/75 wt% HA, collagen/mTG) using RT-PCR. Values shown for fold change in expression level of mRNA normalised to a panel of housekeeping genes (TBP, β-ACTIN), error bars represent standard deviation. Genes tested were (a) osterix, (b) osteocalcin, (c) TGF-β1, (d) RUNX2, (e) alkaline phosphatase, (f) BMP-2. * $p<0.05$, unpaired t-test using Welch's correction.

FIGURE 3.4

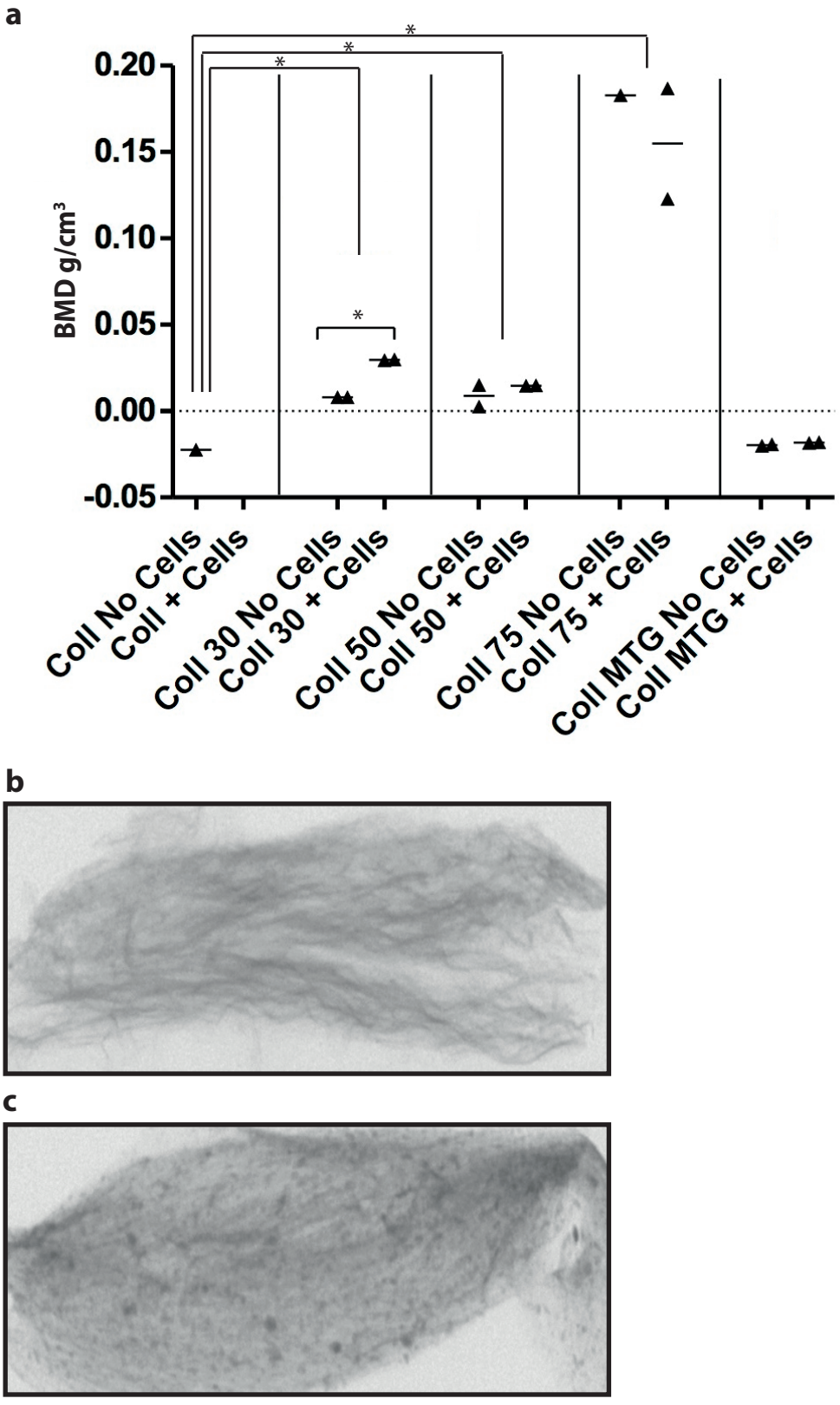


FIGURE 3.4 Bone mineral density of collagen scaffolds is increased with presence of HA (a) Graph showing mean BMD of collagen scaffolds with and without hMSCs, after 7 days of culture. Error bars, standard deviation. *, $p<0.02$. Representative micro CT images of (b) collagen and (c) collagen/50wt% HA scaffolds, obtained using Skyscan 1174 (Bruker, Belgium) compact micro CT scanner, at 50 kV, 800 μA.

FIGURE 3.5

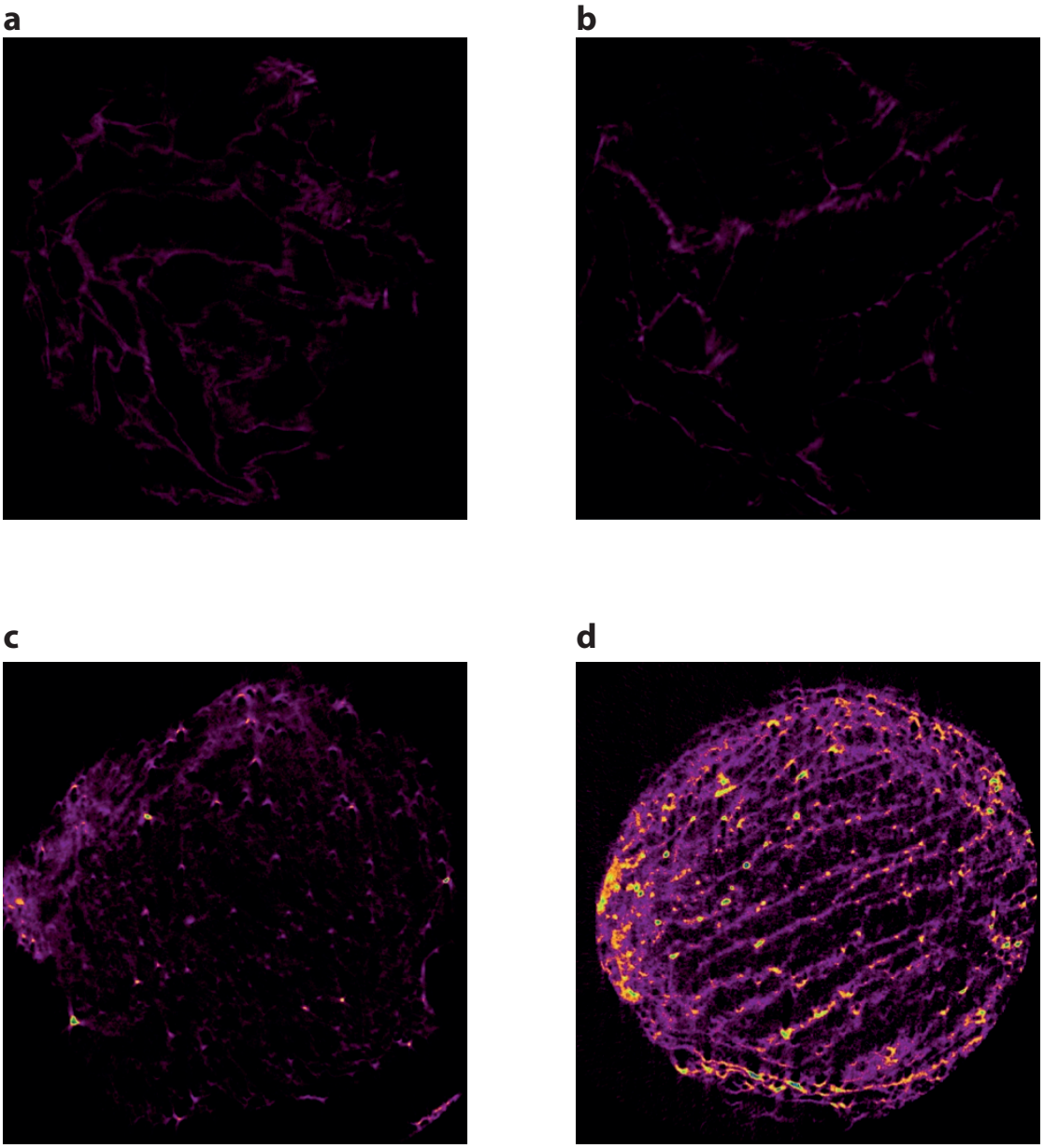


FIGURE 3.5 Representative images of scaffolds using micro CT (a) Collagen scaffold (b) Collagen/mTG scaffold (c) Collagen/50wt% HA scaffold (d) Collagen/75wt% HA scaffold. All images obtained using Skyscan 1174 (Bruker, Belgium) compact micro CT scanner, at 50 kV, 800 µA.

3.8 Discussion and Conclusions

Multiphoton microscopy is a reproducible method for imaging live cells growing in 3-D culture systems (McFadden et al. 2013). Here, MPM has been used to show the viability of hMSCs growing in the scaffolds and the presence of cells throughout the entire scaffold. Other groups have previously reported the use of perfusion bioreactor systems in order to support the growth of hMSCs in scaffold-based culture systems and maintain a homogenous distribution (Wendt et al. 2003; Braccini et al. 2005). However, although these systems attempt to recreate the circulatory system and microenvironment of the human body, they are very costly and do not take into account all the complex factors of the *in vivo* situation to be sufficiently representative of the clinical setting. Therefore, they were not used in this work.

The AlamarBlue® assay was chosen to study cell number because of its reproducibility and ability to provide quantitative assessment of cell viability (Nakayama et al. 1997). AlamarBlue® was added directly to the scaffolds after collagenase digestion, thus avoiding the need to harvest the cells from the scaffold for methods such as fluorescence-activated cell sorting or cell counting. It has been shown that high-density cultures or long incubation times can lead to a secondary reduction of the AlamarBlue® product to a non-fluorescent product, thus confounding the results (C. F. Jones & Grainger 2009). In order to avoid this problem, a range of cell seeding densities were tested on the scaffolds and 100,000 cells was found to be the optimal seeding density, and at which the hMSCs proliferated within the scaffolds over the two-week time period.

Over the first 24 hours of culture, hMSCs grew significantly faster in 3-D collagen scaffolds than in 2-D plates, but this rate of growth slowed over time as shown by the AlamarBlue® assay. By two weeks, hMSCs in 2-D culture had a significantly higher rate of growth than those cells in collagen scaffolds. This could be explained by an initial increase in proliferation rates for cells grown in scaffolds and subsequent differentiation into osteoblasts, at which point the rate of cell growth slows down, as previously shown by other studies (Birmingham et al. 2012). This is supported by the finding of an upregulation in the expression of genes associated with osteogenesis in cells grown in scaffolds compared to cells grown in 2-D culture. Furthermore, the differences for both cell number and osteogenic genes were more marked in cells grown in HA-containing scaffolds, suggesting that HA enhances the osteogenic capabilities of the MSCs grown in collagen scaffolds.

Whilst all of the osteogenic genes showed higher expression levels in cells grown in collagen/HA scaffolds than in 2-D culture, the levels of BMP-2, and to a lesser extent osterix and TGFβ-1, showed the most marked differences. These three genes are associated with osteoblasts and bone formation, suggesting that hydroxyapatite induces the hMSCs to differentiate into osteoblasts and form new bone. Indeed, the fate of hMSCs is known to be determined by the composition and mechanical properties of collagen scaffolds, with stiffer scaffolds (such as those containing HA in this work, **Chapter 2.5**) and those containing chondroitin sulphate directing hMSCs towards an osteogenic lineage (Murphy et al. 2012). Another study has shown that hMSCs grown in nanoHA scaffolds are directed towards an osteogenic lineage with increased expression of osteocalcin, osteopontin and collagen I (YuKan Liu et al. 2009). Further confirmation of bone

formation was provided by micro CT analysis, in the case of collagen/30 wt% HA scaffolds seeded with hMSCs. Larger numbers of scaffolds would need to be analysed to see if this is reproducible for other scaffold types (for example, collagen/50 wt% HA).

In conclusion, hMSCs proliferate and differentiate when grown in collagen/CS/HA scaffolds and this osteogenic induction is most marked in collagen/CS/HA 50 wt% scaffolds. The collagen/CS/HA 50wt% scaffold therefore represents the most interesting material both to take forward for further work and as a potential clinical therapy.

Chapter 4 Bioactive BMP-2/collagen scaffolds

4.1 Introduction

Bone morphogenetic proteins (BMPs) are growth and differentiation factors which are members of the TGF-β superfamily (**Figure 4.1a**). BMPs are soluble, low molecular weight transmembrane glycoproteins that exist as dimers linked by a disulphide bond within normal bone, as shown in **Figure 4.1b** (Scheufler et al. 1999).

Dr Marshall Urist discovered BMPs in 1965 while observing the capacity for new bone formation of devitalized bone when implanted into an animal model (Urist 1965). Subsequent studies have shown BMP-2, -4, -6, -7 and -9 to have the highest osteoinductive properties (Kang et al. 2004) (**Figure 4.1c**) and therefore these molecules have been the subject of intense research within orthopaedics, where it is hypothesized that they could promote bone healing at fracture sites.

RhBMP-2 and its role in bone formation have been extensively studied, with numerous reports of its pharmacokinetics in animal models. The uptake of rhBMP-2 is generally rapid, but retention at any particular site is short, with rapid elimination from the systemic circulation following intravenous administration (McKay et al. 2007). Hence, the carrier system for BMP-2 delivery is important in facilitating the retention of BMP-2 at a critical threshold concentration at the required site. The exact concentration of BMP-2 released by the body during normal healing remains unspecified and therefore the optimal dose of rhBMP-2 at the application site is also unknown.

FIGURE 4.1

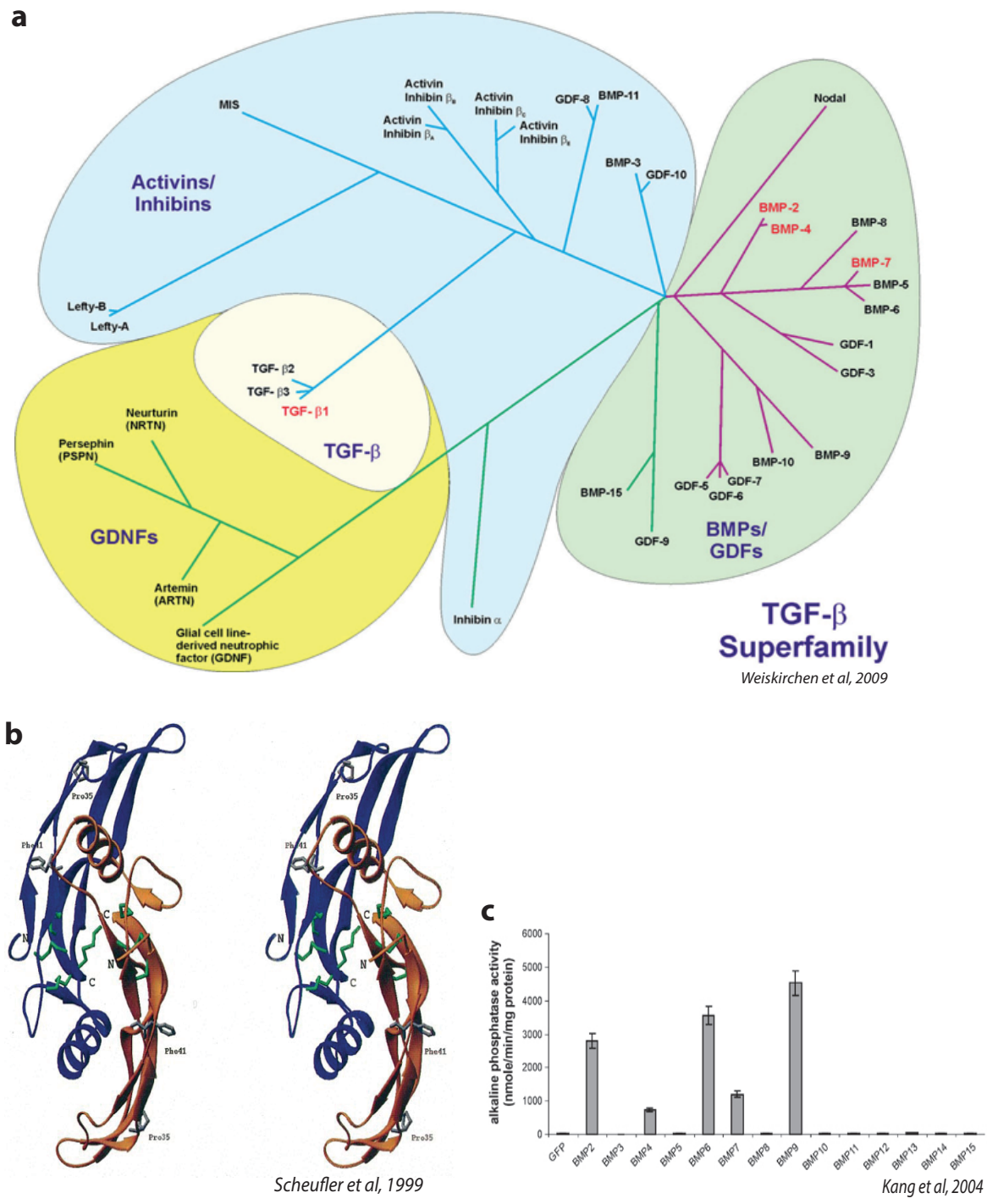


FIGURE 4.1 Overview of bone morphogenetic proteins (BMPs). (a) Schematic representation of the TGF-β superfamily and its sub-families, including BMPs, activins/inhibins and GDNFs, grouped according to their amino acid sequence homology (Weiskirchen et al, 2009). (b) Folding topology of native BMP-2 dimer (Scheufler et al, 1999). (c) Results of bone induction assessed by alkaline phosphatase activity of all BMPs in C2C12 cells (Kang et al, 2004).

Since there is only a minimal quantity of active BMP-2 protein/kg bone (1–2 g/kg cortical bone), extraction of adequate amounts would require a large quantity of bone, making this process both very difficult and expensive. Through advances in biotechnology, rhBMPs are now available for clinical use.

BMP-2 and BMP-7 are the only recombinant BMP molecules to have been granted licence for use in Orthopaedics. These interesting molecules have been the subjects of intense research, although an optimal delivery mechanism is still being sought for their release. A variety of composite delivery systems have been tested, including collagen, chitosan and PLGA-based carriers, as previously summarised in **Table 1.6**. Many randomised clinical trials have now studied the outcomes of BMP-2 use in spinal surgery, and these suggest that rhBMP-2 is superior to iliac crest bone graft in achieving spinal fusion (Z. Chen et al. 2012), as previously summarised in **Table 1.7**. Despite this benefit, there has not been widespread uptake in routine clinical practice and this is probably due in part to the complications associated with such treatment, including vertebral osteolysis (up to 44%), graft subsidence (22%), graft migration (31%), and ectopic/heterotopic ossification (7%) (Cahill et al. 2009). These complications could be attributable to the carrier system, with none of these systems supporting an optimal sustained release profile of BMPs.

The work in this chapter was undertaken with the aim of fabricating an improved collagen/BMP-2 scaffold for potential clinical use in spinal fusion surgery.

4.2 BMP-2 synthesis and purification

In collaboration with the Department of Biochemistry, University of Cambridge (Dr Marko Hyvönen), rhBMP-2 was synthesised and purified for use in combination with the collagen-based scaffolds. This method was undertaken due to the prohibitive costs of commercially-available rhBMP-2.

4.2.1 Gene expression

Subcloning of BMP-2 into the pET-30a vector (Novagen, vector map shown in **Figure 4.2**) was performed by GenScript. The sequence of BMP-2 used for cloning is shown below:

MQAKHKQRKRLKSSCKRHPLYVDFSDVGWNDWIVAPPGYHAFYCHGECPFPLADHLNS
TNHAIVQTLVNSVNSKIPKACCVPTELSAISMLYLDENEKVVLKNYQDMVVEGCGCR

4.2.2 Bacterial transformation

Escherichia coli BL21D3 cells were transformed with the recombinant plasmid pET30a-hBMP-2. Cells were thawed on ice and DNA was added to 100 μl of cells and gently mixed. Cells were incubated for 30 min on ice and then heat shocked for 90 s at 37°C. Cells were placed on ice for 2 min before they were mixed with 900 μl of LB broth and incubated with shaking at 37°C for 1 h. Cells were then plated onto agar plates containing kanamycin (as were cells transformed with plasmid without insert as a negative control) and grown overnight at 37°C. Single colonies were inoculated into 2 ml of LB broth with 30 ng/ml of kanamycin. These were grown at 37°C with shaking (220 rpm) until the OD_{600} reached 0.6.

FIGURE 4.2

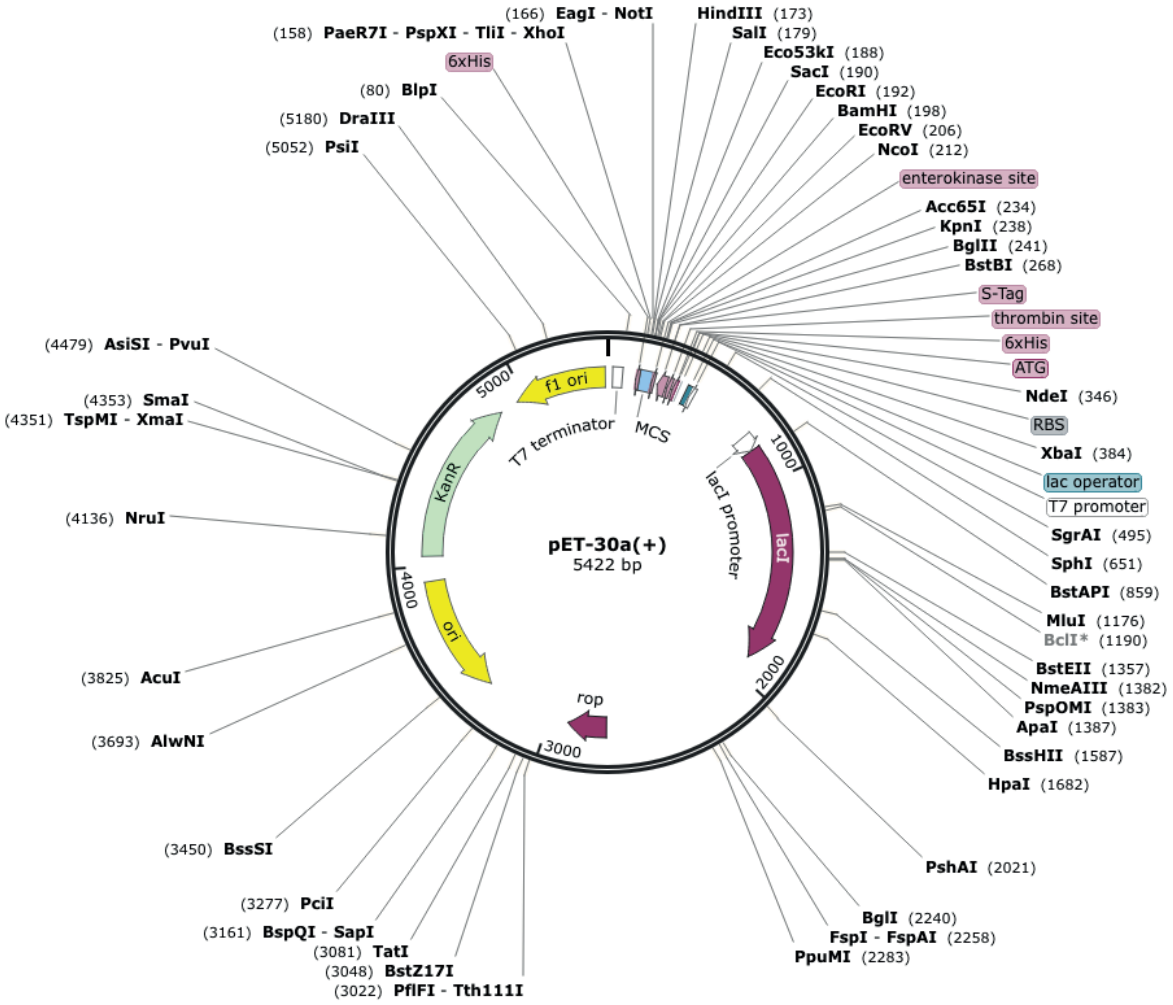


FIGURE 4.2 Vector map for pET-30a as supplied by Novagen, showing 5.422 kb structure with restriction sites. This vector was used for the cloning of BMP-2, performed by GenScript.

4.2.3 Protein Expression

Expression of BMP-2 was induced by addition of IPTG to a final concentration of 400 μM when the OD_{600} reached 0.6-0.8 and expression was continued at 37^0C for a further 4 h. Cells were pelleted by centrifugation at 4200 rpm for 20 min, suspended in 20 ml of de-ionised water per 1 l of culture medium, and stored at –20^0C.

2 ml of this cell suspension was used for a small-scale protein expression test: cells were pelleted from this suspension by centrifugation at 4200 rpm for 1 min and resuspended in 1 ml of BugBuster (Novagen) and 4 μl of Lysonase. This solution was incubated at room temperature for 15 min and centrifuged at 14000 rpm for 3 min. The supernatant (soluble cell fraction) was collected and the pellet was again resuspended in BugBuster (pellet fraction). These fractions were analysed by SDS-PAGE.

4.2.3.1 SDS-PAGE

Samples were loaded with 1x sample buffer and run on a 15% acrylamide gel at 150 mV for 60 min. Gels were rinsed in deionised water and incubated with 0.2 M imidazole for 10 min with shaking at RT. Imidazole was removed and gels were incubated with 0.3 M zinc chloride for 30 s. Zinc chloride was removed and protein bands (transparent against a white background) were viewed with white light.

4.2.4 Isolation and Solubilisation of Inclusion Bodies

After protein expression, the previously frozen cell suspensions were thawed to room temperature and Tris pH 8.0, EDTA pH 8.0 and DTT were added to final concentrations of 50 mM, 2 mM and 10 mM, respectively. Cells were lysed using an Emulsiflex homogeniser. After first passage through the homogeniser, Ralufon DM detergent was added to a final concentration of 1% and lysates were passed three more times through the homogeniser.

200 µl of 2 mg/ml DNase and MgCl (4 mM final concentration) were added to each 20 ml of lysate and lysates were incubated at room temperature for 30 min. Inclusion bodies were pelleted by centrifugation at 15000 g for 20 min at 4^0C. Supernatants were discarded and pellets were resuspended in lysis buffer with 0.5% Ralufon DM using a handheld homogeniser (Ultra Turrax T5). Inclusion bodies were again pelleted, resuspended in lysis buffer and 2 M NaCl and then, after centrifugation at 15000 g, in lysis buffer alone. After a final centrifugation, clear inclusion body pellets were resuspended in 5 ml of 100 mM TCEP pH 7.0 and 15 ml of 8 M GndCl (solubilisation buffer) were added to each sample. Solutions were incubated with shaking at room temperature for 30 min and centrifuged at 15000 g for 20 min at 4^0C. Supernatant containing BMP-2 protomers were removed carefully. GndCl was exchanged with 6 M Urea and 20 mM HCl through a buffer exchange column (XK26/20 column, GE Healthcare) and samples were stored at -20^0C for refolding.

4.2.5 Protein purification

The solution containing BMP-2 protomers was added to PPS-NaCl refolding buffer in order to produce bioactive dimers. Purification was then performed using reverse-phase, cation-exchange and final reverse-phase chromatography.

4.2.5.1 Reverse-phase purification

BMP-2 refolded in PPS buffer was applied to an AKTA purifier and 15 ml Source reverse-phase column (GE Healthcare) to remove PPS from the solution. The column was washed with Buffer A (10% acetonitrile, 90% deionised water and 0.1% trifluoroacetic acid) and BMP-2 was eluted with a gradient of Buffer B (90% acetonitrile, 10% deionised water and 0.1% trifluoroacetic acid) at RT. All elutes were analysed using unreduced SDS-PAGE gels.

4.2.5.2 Cation-exchange purification

BMP-2-containing elutes were applied to an AKTA purifier and Resource S columns (GE Healthcare Sr No: 936487) for further purification. The columns were washed with Buffer A (6 M Urea and 20 mM HCL) and protein eluted with a gradient of Buffer B (6 M urea, 20 mM HCL and 1 M NaCl).

4.2.5.3 Final reverse-phase purification

Finally, BMP-2-containing elutes were applied to an AKTA purifier and HI-Chrom C8 reverse phase columns to achieve 95% purity. The columns were washed with Buffer A (10% acetonitrile, 90% deionised water and 0.1% trifluoroacetic

acid) and proteins were eluted separately with a gradient of Buffer B (90% acetonitrile, 10% deionised water and 0.1% trifluoroacetic acid) at RT.

4.3 Bioactivity of BMP-2

C2C12 cells (mouse myoblasts) and an established alkaline phosphatase assay (BESSEY et al. 1946) were used to test the bioactivity of BMP-2. A 48-well plate was seeded with 5 x 10^4 C2C12 cells in 500 µl media (DMEM supplemented with 4.5 g/l glucose, 10% FBS and 1% PSG (Invitrogen)) per well and the cells were incubated at 37^0C. The medium was changed after 24 h with 500 µl media enriched with varying concentrations of BMP-2 (0-6 µg/µl, negative control was media without BMP).

After 4 days incubation, the cells were washed with PBS and 300 µl of 1x CyQuant buffer (Invitrogen) were added to each well. The plate was then incubated at RT for 5 min with shaking, and then centrifuged at 1400 rpm for 5 min. 50 µl of supernatant were transferred to a clean 96-well plate. Standards of DiFMU 0-100 µM were prepared in 1x CyQuant buffer/2x ALP assay buffer (200 mM glycine, 2 mM $MgCl_2$, 2 mM $ZnCl_2$) and also placed in the 96-well plate. DiFMUP was then added to the 2x ALP assay buffer and 50 µl of this were added to each well and the plate was incubated for 15 min at RT. The fluorescence was measured using 455 nm wavelength.

Total protein was calculated using a BCA method (Pierce). 25 µl of each sample were placed in a 96-well plate (in duplicate). 50 parts of Solution A were mixed

with 1 part of Solution B, and 200 μl were added to each well. The plate was incubated at 37^0C for 30 min and then read at 562 nm.

ALP activity of BMP-2 was then calculated as a value per μg of total protein.

4.4 BMP-2/collagen scaffold fabrication

Collagen/BMP-2 scaffolds were fabricated with either integration or adsorption methods.

4.4.1 Integration

Collagen scaffolds were prepared as in **2.2.1** and after fibrillogenesis and pH adjustment to 7.4, 250 μg of BMP-2 in 250 μl PBS were added. The scaffolds were then fabricated as in **2.2.1**.

4.4.2 Adsorption

Collagen scaffolds were prepared as in **2.2.1**. After freeze-drying, the 10 cm-diameter disc was placed in a plastic dish containing 250 μg BMP-2 in 9 ml PBS and incubated with gentle shaking at RT for 45 min. Scaffolds were then freeze-dried again for 24 h.

4.5 BMP-2 release profile

Triplicate scaffold samples (discs 8 mm diameter, 3 mm thick) were placed in a 24-well plate with 500μl 0.1% BSA/PBS and incubated at RT with gentle shaking. The BSA/PBS solution was replaced at every timepoint (0, 2, 4, 6, 8, 12, 24, 48, 60, 72, 84, 96, 108, 120 h) and the amount of BMP-2 in the solutions was quantified using a BMP-2 enzyme-linked immunosorbent assay (ELISA) kit (Sigma-Aldrich®, #RAB0028). All incubations were performed at RT with gentle shaking. Briefly, 100 μl of sample (or supplied BMP-2 standard) were added to each well and incubated for 3 h. After washing four times with wash buffer, 100 μl of biotinylated anti-human BMP-2 antibody were added and incubated for 1 h. After washing four times, 100 μl of HRP-conjugated streptavidin were added and incubated for 45 min. After washing four times, 100 μl of a tetra-methylbenzidine substrate solution were added and incubated for 30 min in the dark. 50 μl of 0.2 M sulphuric acid were added and the absorbance of each well was measured at 450 nm (POLARstar Omega, BMG Labtech).
Concentrations of BMP-2 in each sample were calculated based on the standard curve derived from the ELISA.

4.6 Characterisation

BMP-2/collagen scaffolds were characterised using SEM and EDX, as detailed below.

4.6.1 Scanning electron microscopy

Scanning electron microscopy (SEM) images were captured using a Hitachi TM3000 table-top SEM system equipped with a Bruker Quantax70 x-ray analysis software system. Images were taken on both an exterior and a cut surface (after horizontal bisection) of each sample at 50-25,000 X magnification.

4.6.2 Energy dispersive x-ray spectroscopy

Energy dispersive x-ray (EDX) spectroscopy was used to analyse the scaffolds. A Hitachi TM3000 table-top SEM system equipped with a Bruker Quantax70 x-ray analysis software system was used.

Each sample was placed on an aluminium stub on a carbon tab, and this was placed in the SEM chamber with a working voltage of 15 kV. Both the external surface and an internal surface of each scaffold were studied using EDX.

4.7 Results

BMP-2 was identified within inclusion bodies, as shown by its expression in bacterial cell pellets and not in the soluble fraction (**Figure 4.3a**). Using reverse-phase purification, BMP-2 was eluted at a gradient of 34% of Buffer B (**Figure 4.3b**). Elution fractions A10 and A11 contained the most BMP-2, as confirmed by SDS-PAGE analysis (**Figure 4.3c**). Cation-exchange purification was then used and BMP-2 was eluted at a gradient of 77% of Buffer B (**Figure 4.4a**). Elution fractions B15 and B14 contained the most BMP-2, as confirmed by SDS-PAGE analysis (**Figure 4.4b**).

A final reverse-phase purification of BMP-2 showed that BMP-2 was eluted at a gradient of 37% of Buffer B (**Figure 4.5a**). Elution fractions E8 and E9 contained the most BMP-2, as confirmed on SDS-PAGE analysis (**Figure 4.5b**). The SDS-PAGE analysis also showed the purity of BMP-2 (fractions E8 and E9) to be approximately 95%. Fractions E10-E12 were pooled together and reapplied to an AKTA purifier and HI-Chrom C8 reverse-phase columns in order to maximise the yield of protein.

The bioactivity of BMP-2 was confirmed in C2C12 cells, where ALP activity was directly proportional to the BMP-2 concentration, up to 2 μg/ml, after which further increases in BMP-2 concentration did not increase ALP activity (**Figure 4.6**).

FIGURE 4.3

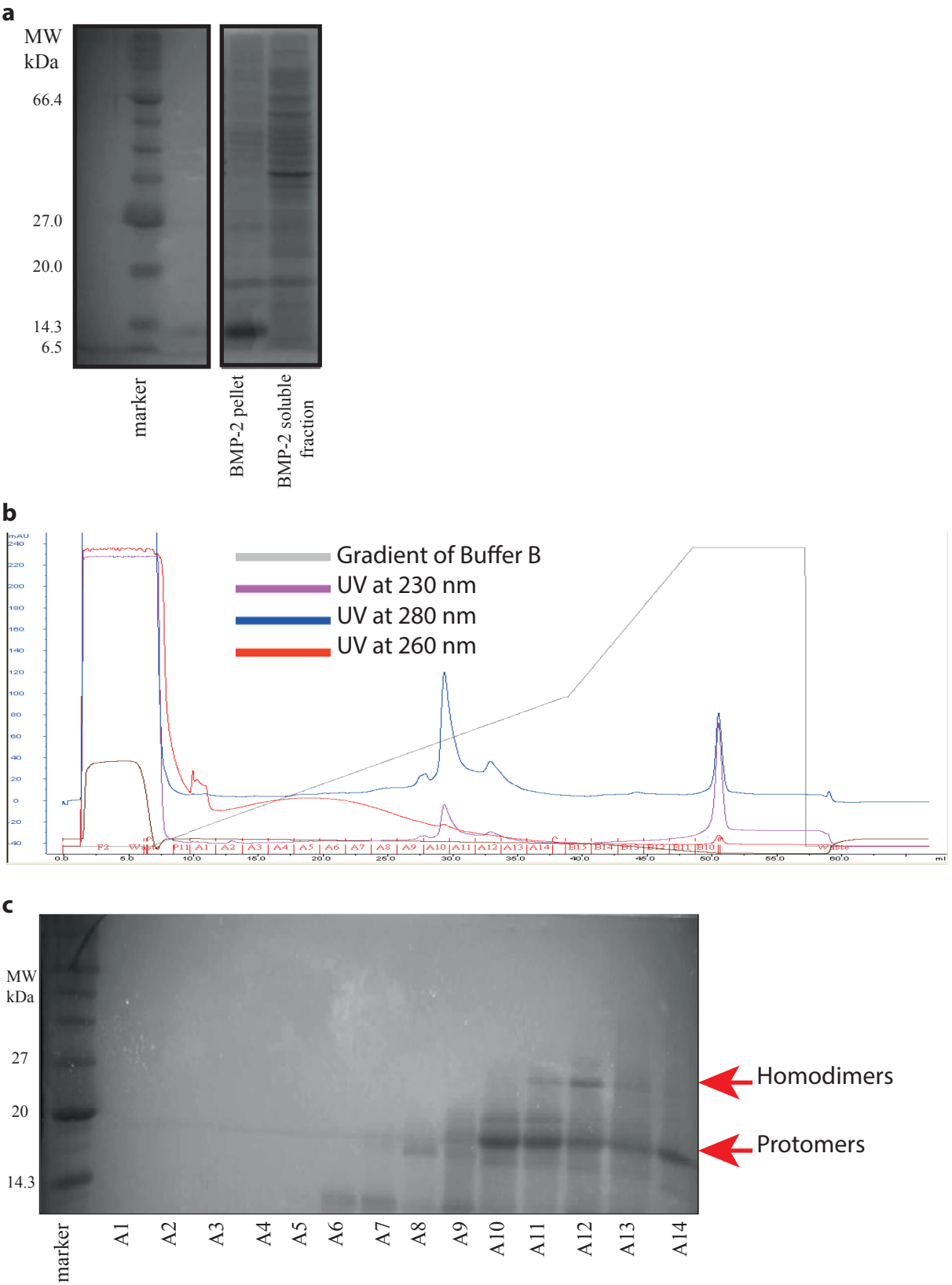


FIGURE 4.3 Reverse-phase purification of BMP-2 from *E. coli* expression system (a) SDS-PAGE gel analysis of protein expression: BMP-2 is present within the cell pellet but not the soluble fraction, showing its presence within inclusion bodies. (b) Chromatogram of BMP-2 reverse-phase purification. (c) SDS-PAGE gel analysis of elutes containing BMP-2 after reverse-phase purification, protomers and homodimers highlighted.

FIGURE 4.4

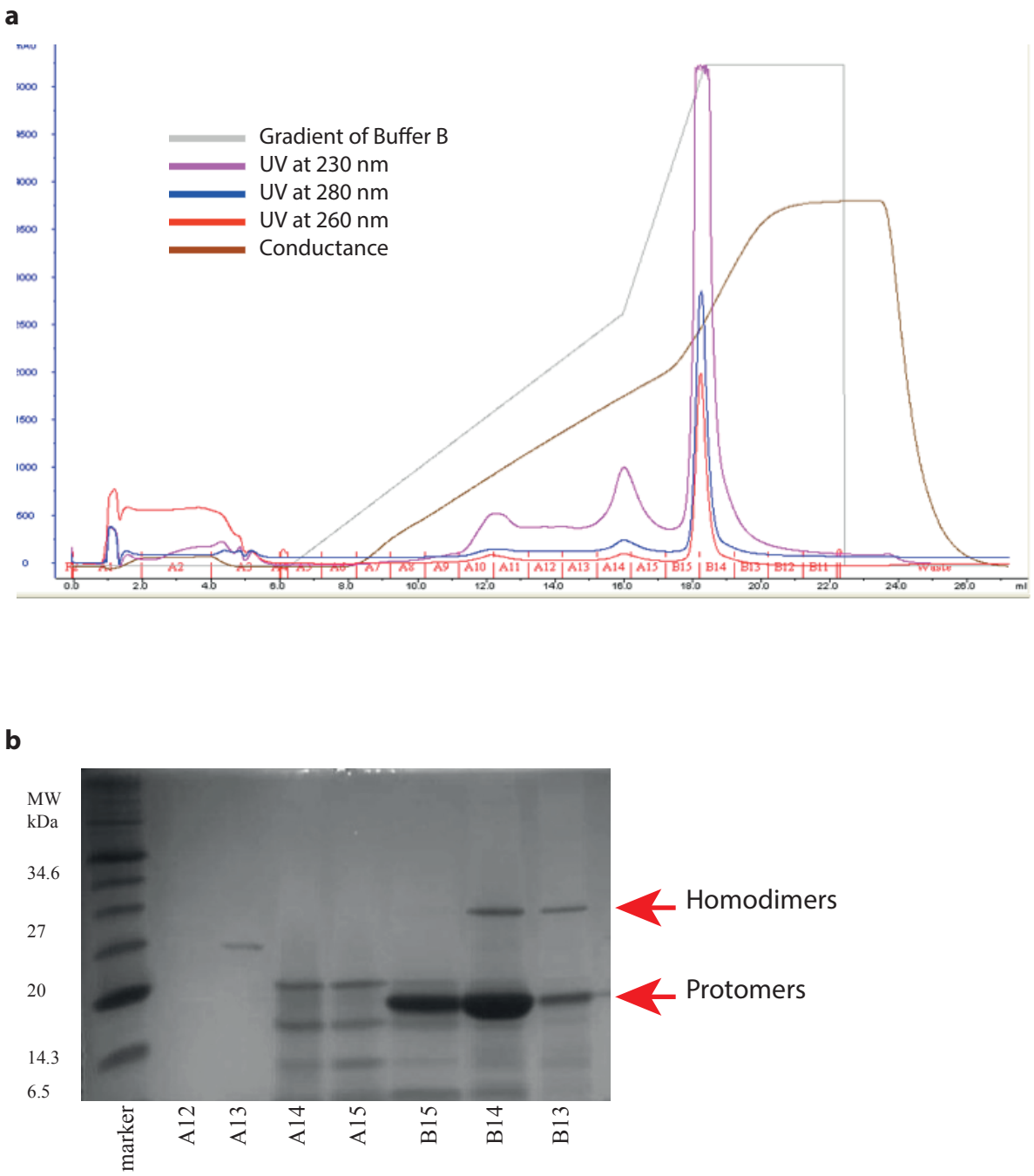
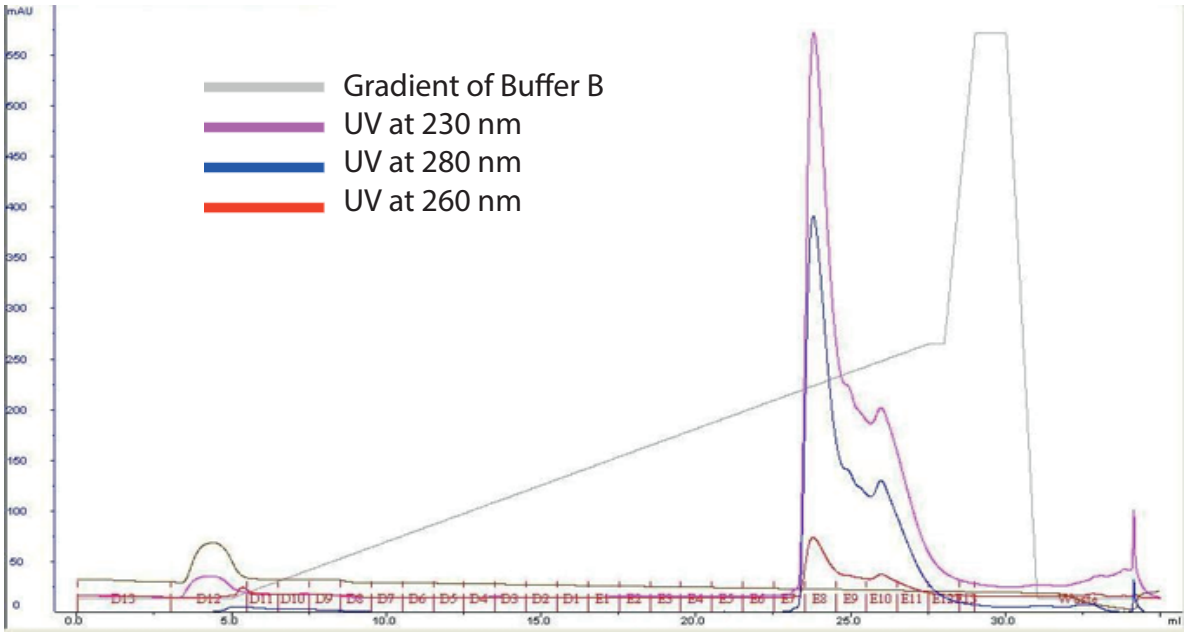


FIGURE 4.4 Cation-exchange purification of BMP-2 from *E. coli* expression system (a) Chromatogram of BMP-2 cation-exchange purification. (b) SDS-PAGE gel analysis of elutes containing BMP-2 after cation-exchange purification, protomers and homodimers highlighted.

FIGURE 4.5

a



b

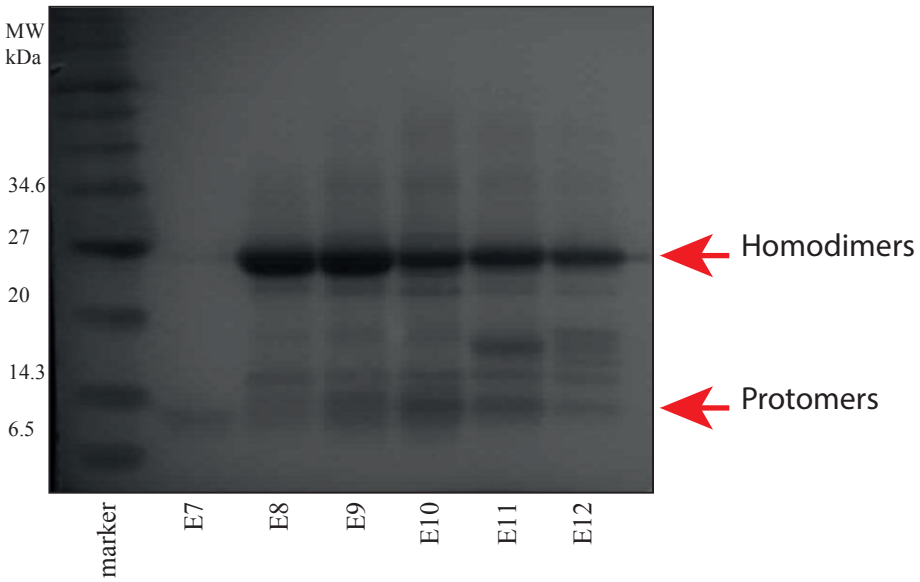


FIGURE 4.5 Final reverse-phase purification of BMP-2 (a) Chromatogram of BMP-2 final reverse-phase purification. (b) SDS-PAGE gel analysis of elutes containing BMP-2 after final reverse-phase purification, protomers and homodimers highlighted.

FIGURE 4.6

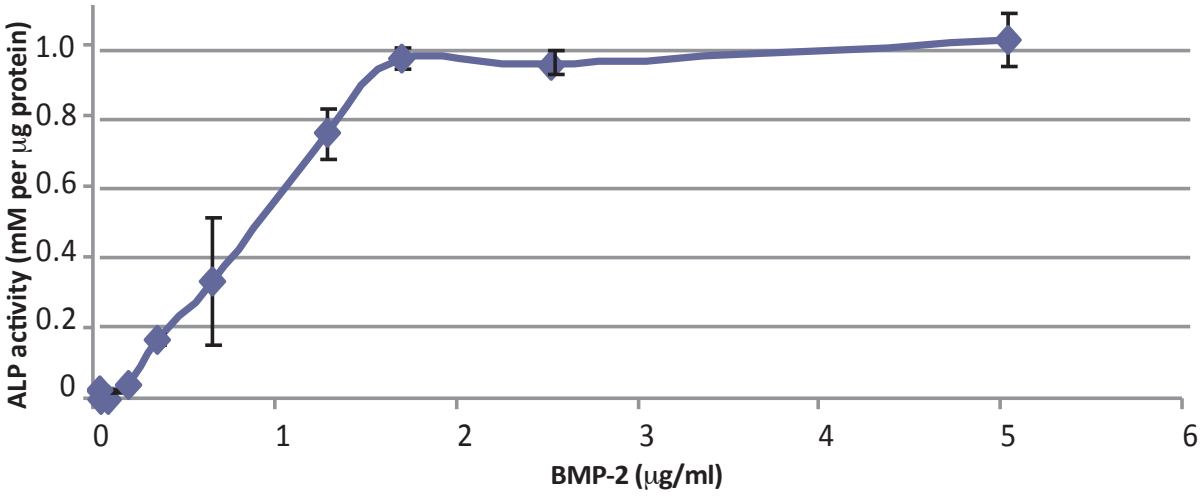


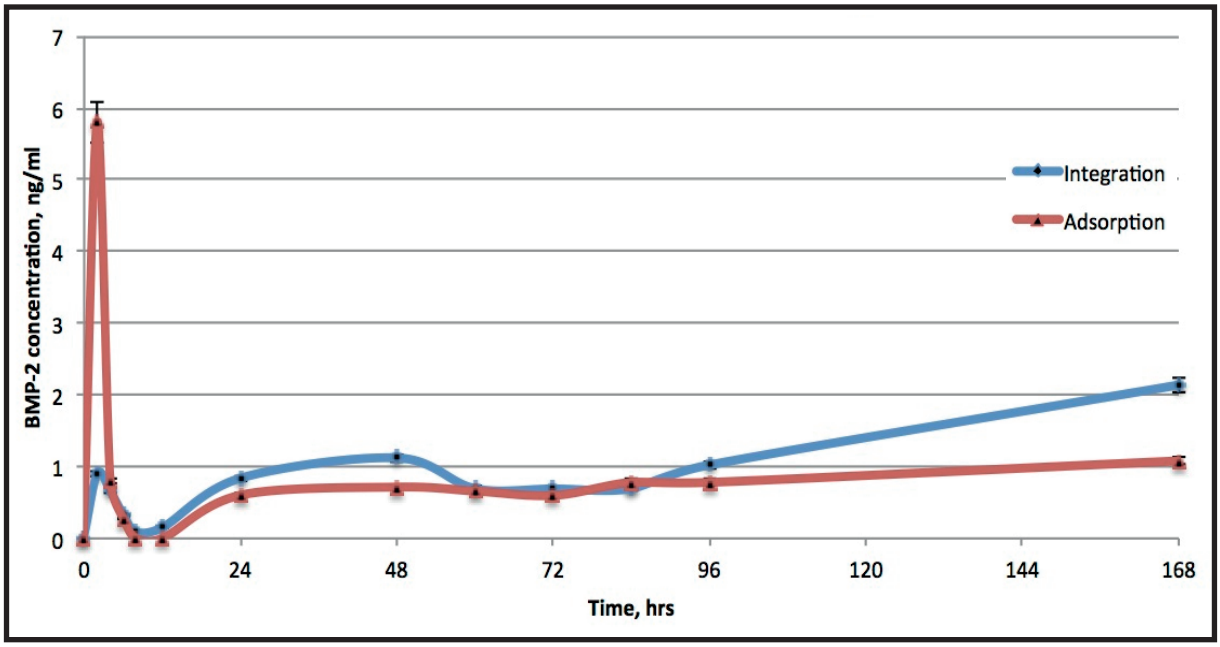
FIGURE 4.6 Bioactivity of BMP-2 Graph showing alkaline phosphatase (ALP) activity of BMP-2 refolded in PPS and NaCl-containing refolding buffer, performed using C2C12 cells and an assay described by Bessey et al, 1946.

Detectable levels of BMP-2 (up to 12 ng/ml) were released from collagen scaffolds over time (**Figure 4.7a**), with cumulative levels of BMP-2 continuing to rise at 7 days for scaffolds fabricated with both integration and adsorption (**Figure 4.7b**). Although cumulative release was significantly higher for adsorption than integration ($p<0.02$, **Figure 4.7b**), the non-cumulative release profiles showed a sustained pattern of BMP-2 release from the integrated BMP-2/collagen scaffolds, compared to a burst-release from the adsorbed BMP-2/collagen scaffolds (**Figure 4.7a**).

SEM images show the porous structure of the collagen scaffolds was maintained with the addition of BMP-2 (**Figures 4.8a-c**). EDX analysis shows a high purity of the collagen/BMP-2 scaffolds, with only carbon, oxygen, sodium, phosphorous and no other elements present (**Figures 4.9a-c**).

FIGURE 4.7

a



b

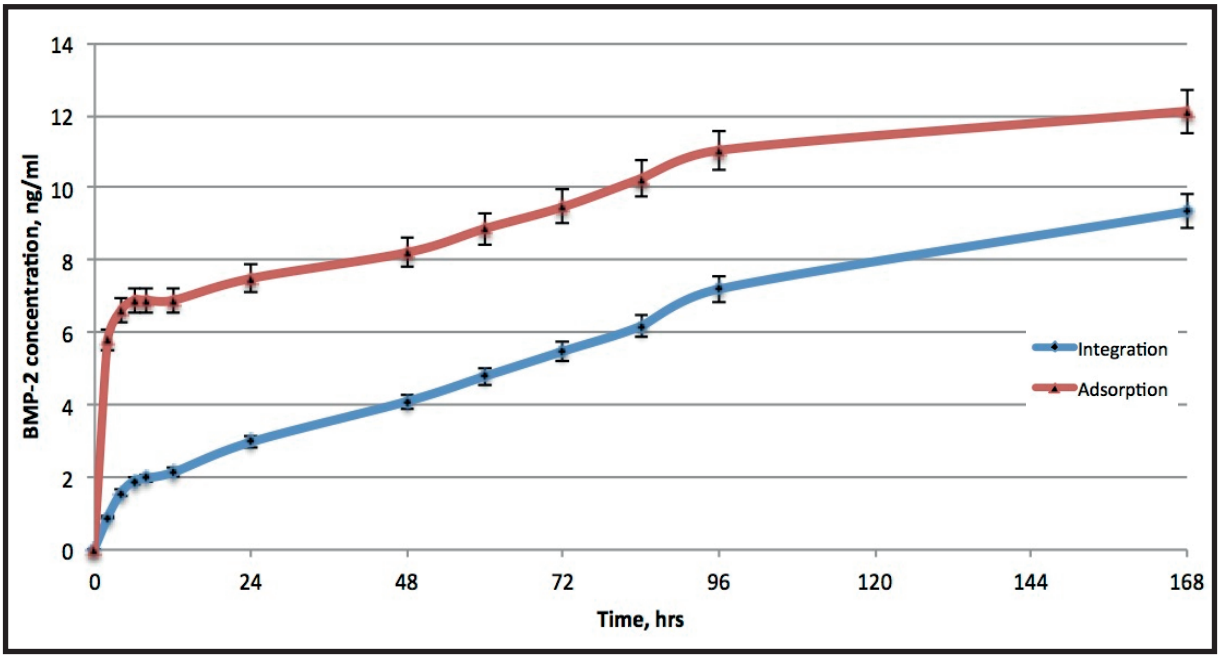


FIGURE 4.7 Release of BMP-2 from collagen scaffolds (a) Graph showing BMP-2 release from collagen scaffolds fabricated with integration and adsorption methods, over 7 days. (b) Graph showing cumulative BMP-2 release from collagen scaffolds fabricated with integration and adsorption methods, over 7 days.

FIGURE 4.8

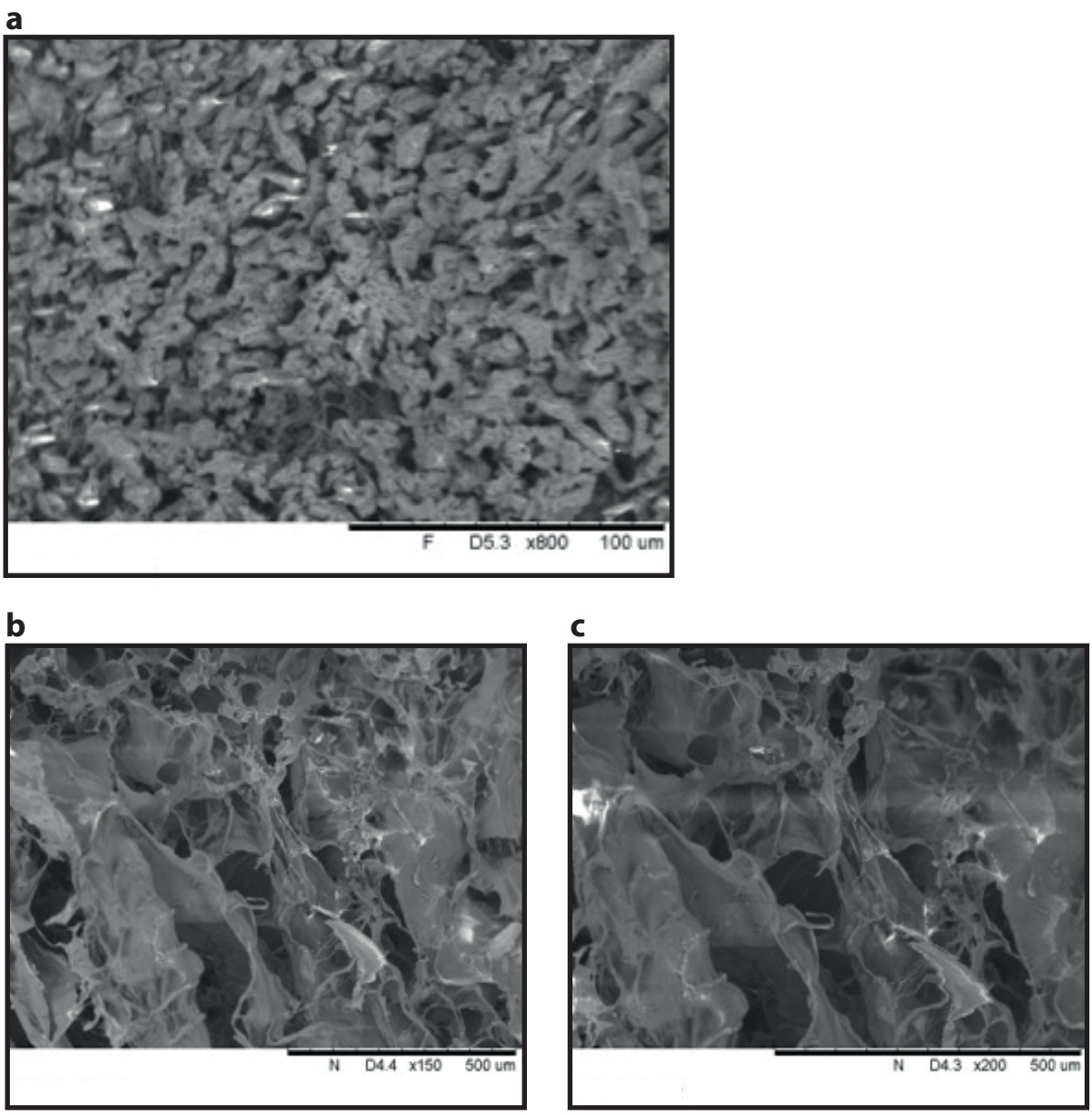


FIGURE 4.8 Scanning electron microscopy shows porous structure of collagen scaffolds maintained after BMP-2 addition (a) Representative image of external surface of integrated collagen/BMP-2 scaffold. (b) Representative image of cut surface of integrated collagen/BMP-2 scaffold. (c) Representative image of cut surface of adsorbed collagen/BMP-2 scaffold. SEM images were obtained using Hitachi TM3000 tabletop SEM system, 100-300X magnification.

FIGURE 4.9

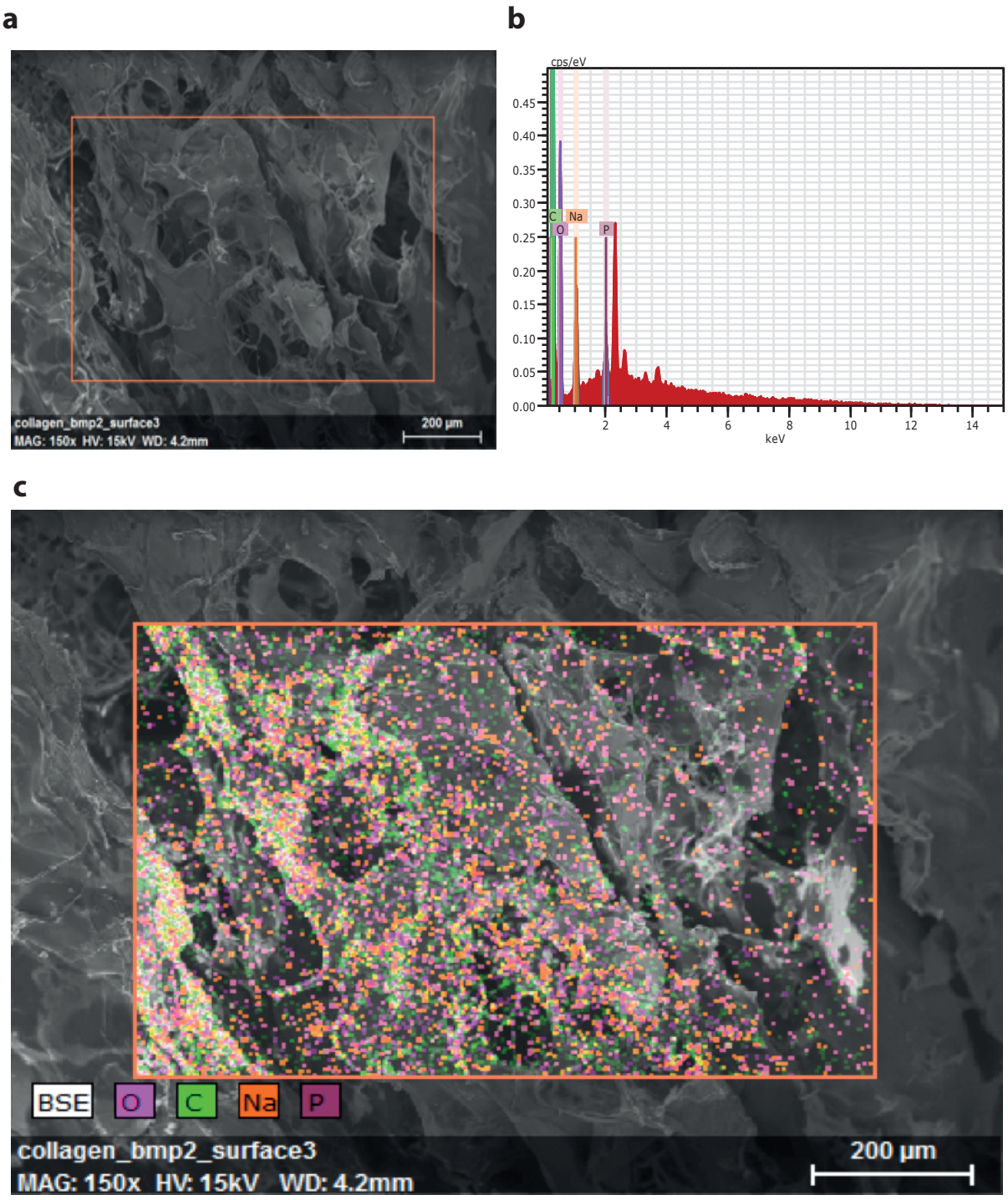


FIGURE 4.9 Energy-dispersive x-ray spectroscopy shows high purity of collagen/BMP-2 scaffolds (a) Representative SEM image of cut surface of collagen/BMP-2 scaffold. (b) Representative elemental map of collagen/BMP-2 scaffold. (c) Representative SEM image with EDX overlay for collagen/BMP-2 scaffold. EDX analysis was undertaken using Hitachi TM3000 tabletop SEM system, 100-300X magnification.

4.8 Discussion and Conclusions

Using recombinant technology, purified bioactive BMP-2 has been produced from an *E. coli* expression system. The maximum bioactivity of BMP-2 was approximately 0.42 μM/μg total protein at BMP concentration of 1 μg/ml), which is in concordance with the results shown by Kang *et al* (2004).

As yet, no BMPs produced in *E. coli* expression systems have received FDA approval for clinical use, although other recombinant proteins from such systems are in regular clinical use (human insulin, Humulin®, Lilly, human growth hormone, Nutropin®, Genentech, and human interferon, Bayer). Recently, BMP-2 derived from an *E. coli* expression system has been used in humans in combination with biphasic tricalcium phosphate for maxillary sinus floor augmentation, and clinical outcomes were compared to current standard practice using deproteinized bovine bone (M.-S. Kim et al. 2014). Although this particular study did not demonstrate any significant benefit with the use of rhBMP-2, it is the first published use of *E. coli* derived BMP-2 in humans and therefore suggests that it is a technically viable option.

Collagen is the principal structural protein in the human body and therefore any artificial scaffold derived from this should closely resemble the natural ECM of bone. Bovine collagen was chosen as a carrier system due to its high biocompatibility and the unique fabrication methodology employed in this study. Fibrillar collagen, which represents the native state of collagen, possesses less antigenic activity than afibrillar collagen, and it was therefore selected as the carrier system for BMP-2 in this study. Material characterisation analysis

demonstrated no significant change in material properties after combination with BMP-2.

Most published studies to date, regardless of the carrier material used, have reported an initial burst release then a sustained release profile of BMP-2 (as summarised in **Table 1.6**), although their data are presented as cumulative values and therefore must be interpreted with caution. Ideally, a sustained release of BMP-2 would be desirable, as this would achieve high levels of BMP-2 at the site of healing for the duration of the healing process. In this study, such a sustained release profile was observed for the integrated BMP-2/collagen scaffolds, but less so for the adsorption scaffolds. This could be explained by the fact that as the scaffold degrades, more BMP-2 is exposed on its surface and therefore the release of BMP is dependent on the degradation properties of the collagen scaffold rather than the weak electro-chemical forces between collagen and BMP-2.

In conclusion, purified bioactive rhBMP-2 has been combined with a fibrillar collagen scaffold and this biocomposite displays a sustained BMP-2 release profile *in vitro*.

Chapter 5 Layer-by-layer collagen/HA/GAG/BMP-2 scaffolds

5.1 Introduction

The layer-by-layer (LBL) technique is used to alter the surface characteristics of a material and has evolved over the last twenty years to be used for enhanced cell adhesion, mineralisation and improved and controlled drug delivery. The biomedical engineering community has also adopted it in an attempt to improve the implants' integration into the human body (Costa & Mano 2014).

The initial description of the LBL technique by Langmuir in 1941 (US patent #2232539) was of a monolayer system. Further groups have successfully synthesised multi-layer systems containing alternative layers of positive and negative charged materials, such as silica and alumina on glass (Iler n.d.). The effective deposition of each layer has been shown to depend on factors such as thorough rinsing of the free reagent, the concentration of the solutions used and, critically, the pH of the solutions (Iler n.d.).

The first evidence of multilayer assemblies, with alternating adsorption of anionic and cationic colloids, which were ultra-thin and completely independent of substrate size and topology was described in 1991 (Decher & Hong 1991).

In addition, multi-layered films can act as drug reservoirs, preserving drug bioactivity until delivery is achieved (Costa & Mano 2014).

Although the most common fabrication strategy for LBL films is electrostatic interactions, they can also rely on weaker interactions such as van der Walls forces and hydrogen bonding (Clark & Hammond 2000).

The fundamental drawback of LBL fabrication is the time-consuming nature of this technique. To assemble a single layer usually takes a few minutes, although this varies with the constituents, and the process has to be repeated many times

to produce a multi-layered film. Automated systems can overcome this problem, to a degree, but the cost of fabrication remains high.

As LBL technology allows the modification of the surface characteristics of a material, there is rapidly growing interest in its application within orthopaedics for the fabrication of implants with biomimetic coatings (which facilitate enhanced osseointegration). As yet, no such materials have been tested in humans. However, pre-clinical *in vivo* studies have shown the potential benefits of such a technique, for example, dual-release of antibiotics (gentamicin) and growth factors (BMP-2) from a chitosan-clay material in a rabbit model of bone infective defect (Min, Braatz & Hammond 2014a). Furthermore, the same group have demonstrated that dual-release of growth factors VEGF and BMP-2 from chitosan/hydroxyapatite-based scaffolds leads to successful osteogenesis in a rat model of tibial defects (Shah et al. 2013).

No previous study has reported the use of collagen scaffolds in LBL fabrication. A porous scaffold, which facilitates cell growth throughout the entire scaffold (and not only on its surface), could be utilised as a base for LBL technology with growth factors and stem cells and subsequently create a superior material for osseointegration.

Therefore, I proceeded to study the effect of LBL fabrication on the physical properties of the collagen/CS/HA scaffold and the effects of LBL fabrication on the release profile of BMP-2.

The work in this chapter was carried out by myself, with assistance from a student of the taught MsC in Biomedical Engineering (Laura Pittman).

5.2 Fabrication of layer-by-layer scaffolds

Layer-by-layer scaffolds were fabricated using a 3-D printer system with dip coating, as detailed below.

5.2.1 Layer by layer system

Dip coating was performed using a custom-made 3-D printer controlled by fit-for-purpose G-Code programs (designed by Dr Julian George, **Figure 5.1a**). To improve scaffold-building efficiency, a custom-made three-pronged holding apparatus attachment was designed and subsequently fabricated by the Old Road Campus Research Building (ORCRB) Machine Workshop using Delrin® (an acetal resin, DuPont™). This attachment allowed three samples to be dip coated simultaneously (**Figure 5.1a**).

Finally, a 16-well mould was designed and subsequently fabricated by the ORCRB Machine Workshop Delrin® (**Figure 5.1b**). The mould allowed the samples to be frozen in a solution with the base in place then, by removing the base, the mould could be transferred into the freeze dryer whilst ensuring that the maximum surface area of the sample was exposed so that proper freeze drying was possible.

5.2.2 Collagen scaffold fabrication

Collagen scaffolds were fabricated as described in **Chapter 2.2.1**. Briefly, collagen Type I solution was blended, de-gassed and added to fibrillogenesis buffer, with the pH adjusted to 7.4.

FIGURE 5.1

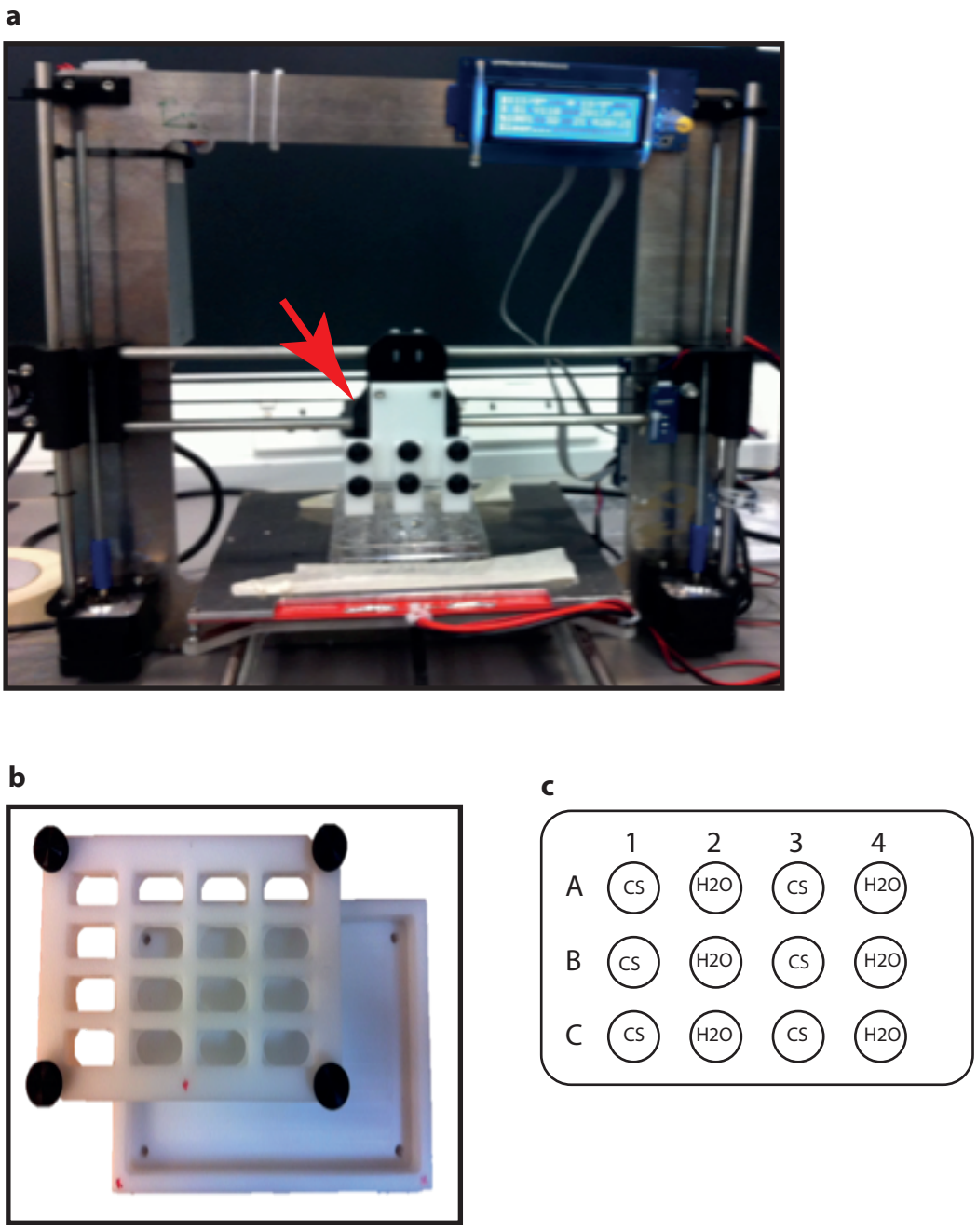


Figure 5.1 A custom-made dip coating system for fabrication of layer-by-layer scaffolds. (a) Photograph of the 3-D printer system used for dip coating, including the 3-pronged holding apparatus (as marked by arrowhead). Custom-made in the Institute of Biomedical Engineering, University of Oxford by Dr Julian George. (b) Photograph of the custom-made 16-well mould for sample preparation. (c) Schematic of plate layout for coating solutions. Plate was used at 90^0 clockwise rotation to align with the holding apparatus.

This solution was transferred into a 10 cm diameter mould and incubated at 37°C overnight (DeForest & Anseth 2012; Douglas et al. 2006; Polizzotti et al. 2008). The scaffolds were then frozen at -20°C for 24 h and then placed in a freeze-dryer for 24 h in a vacuum of 5 Pa.

Four types of scaffold were prepared for this experiment: 1) collagen-only; 2) collagen with 30 wt% HA; 3) collagen with 50 wt% HA; 4) collagen with 75 wt% HA. The appropriate amount of HA (Sigma-Aldrich) was added to the collagen solution at the time of blending and the scaffolds were then prepared as for the collagen-only scaffolds.

The scaffolds used as non-LBL comparisons for the DSC experiment were made in a similar fashion, with the addition of CS 1 wt% (with or without HA) to the collagen solution at the time of blending.

5.2.3 Fabrication of LBL collagen/CS scaffolds

CS salt from bovine trachea (Sigma-Aldrich) was mixed with dH_2O to create a 5 mg/mL negatively-charged solution. The solution was slightly acidic, with a pH of approximately 6.5, so 1 M sodium hydroxide (NaOH) was used to increase the pH to between 7.35 - 7.45.

In preparation for the dipping sequence, 6 ml CS solution were transferred into each well in the first and third rows of a 12-well plate and 6 ml dH_2O were placed in the wells in rows two and four (schematic shown in **Figure 5.1c**). Three collagen scaffold discs (5 mm height, 15 mm diameter) were connected to the holding apparatus. Using G-code, a dipping program was setup on the 3-D printer so that scaffolds were dipped in CS solution for 2 min, followed by a rinse in

dH_2O for 1 min. This sequence continued for the next rows of CS and dH_2O and the entire process was repeated for at least 150 cycles. After the dipping sequence was complete, the scaffolds were placed in dH_2O in the custom-made mould for 24 h at -20°C before being transferred to a FTS Systems Lyostar freeze dryer (shelf -20°C, condenser -150°C and vacuum 100 mT) where they were freeze dried for 24 h. The same procedure was followed for HA-containing collagen scaffolds.

5.2.4 Fabrication of LBL CS/BMP-2 scaffolds

A positively-charged 100 μg/mL BMP-2 solution was created using rhBMP-2 (synthesised as described in **Chapter 4.2**), PBS and filtration through a 0.45 μm Millex HA filter unit (Merck Millipore). A negatively-charged 5 mg/mL CS solution was prepared as described in **Chapter 5.2.3**. Collagen-only scaffolds (5 mm height, 15 mm diameter) were loaded onto the 3-D printer and dipped in negatively-charged CS for 2 min, followed by a 1 min in dH_2O and finally dipped for 2 min in positively-charged BMP-2 solution. The sequence was repeated for at least 200 cycles and then the scaffolds were frozen in BMP-2 solution at -20°C for 24 h. The scaffolds were then transferred to the freeze dryer at -20°C for 24 h and stored at 4°C until use.

5.3 Characterisation of layer-by-layer scaffolds

Scanning electron microscopy, energy dispersive x-ray spectroscopy, differential scanning calorimetry and Fourier transform infrared spectroscopy were used to characterise the scaffolds. These are detailed below.

5.3.1 Scanning electron microscopy

Scanning electron microscopy (SEM) images were captured using a Zeiss EVO LS15 machine at 10 kV. Scaffold samples were coated with a gold-palladium mixture using a Quorum SC7620 Sputter Coater. Images were taken on both an exterior and a cut surface (after horizontal bisection) of each sample at 50-25,000 X magnification. SEM images were analysed with ImageJ software to calculate pore size, taking the average result from 27 individual areas per scaffold (Martel-Estrada et al. 2010; Schneider et al. 2012; Olivas-Armendariz et al. 2009).

5.3.2 Energy dispersive x-ray spectroscopy

Energy dispersive x-ray (EDX) spectroscopy was used to confirm the presence of CS throughout the collagen scaffolds and to determine the effect of pH on CS absorption. A Hitachi TM3000 table-top SEM system equipped with a Bruker Quantax70 x-ray analysis software system was used.

Each sample was placed on an aluminium stub on a carbon tab, and this was placed in the SEM chamber with a working voltage of 15 kV.

Collagen/CS scaffolds were prepared as described in **Chapter 5.2.3**, with a range of CS solution pH (6.0, 7.4, 10.0, 11.0). Both the external surface and an internal surface of each scaffold were studied using EDX.

5.3.3 Differential scanning calorimetry

DSC was performed using a PerkinElmer Hyper Differential Scanning Calorimeter to assess the thermal stability of the LBL collagen/CS scaffolds, using collagen/CS 1 wt% scaffolds as a control. 5-6 mg of each scaffold were placed in a 40 μl aluminium pan (Perkin Elmer) and heated to 200^0C at 50^0C min^{-1}. The raw data was compiled and analysed using Pyris Data Analysis Software and the denaturation temperature for each sample was recorded.

5.3.4 Fourier transform infrared spectroscopy

FTIR was performed using a Bruker Tensor 37 system containing a Pike Technologies MIRacle Single Reflection Attenuated Total Reflection (ATR) attachment with a 2.5 mm aperture, to investigate the bonding between the collagen scaffold and CS.

Spectra of absorbance were measured in the range from 400 to 4000 cm^{-1} with a resolution of 4 cm^{-1}, and were recorded as averages of 32 scans per sample. Numerical analysis was conducted on the spectra with EssentialFTIR (Operant, LLC. FL) and PeakFit (SeaSolve Software, Inc. MA).

5.4 Multiphoton microscopy for imaging of hMSCs

Human mesenchymal stem cells (hMSC) (Lonza) were grown in MSCGM™ (Mesenchymal Stem Cell Growth Medium) (Lonza) supplemented with BulletKit™ (Lonza). Cells were grown on Matrigel™-coated plates (Matrigel™, BD #354262) in a humidified incubator with 5% CO_2 at 37^0C. Passage was performed at 70% confluence using 0.05% Trypsin EDTA (Invitrogen) and 100,000 cells were seeded onto each scaffold.

After 3 days of incubation, three-dimensional fluorescent live cell imaging of MSCs within the collagen-based scaffolds was performed using a modified BioRad Radiance 2100 MP Multiphoton Microscope (Zeiss; Jena, Germany).

To prepare the cells for imaging a solution of two dyes was created. Calcein AM was added to identify live cells by staining the membrane green and ethidium homodimer was added to identify dead cells by staining the nucleus red (Live/Dead Viability/Cytotoxicity Kit, Molecular Probes Invitrogen Detection Technologies, USA). The dyes were combined and mixed with 5 mL of filtered PBS. Media was removed from each well and the scaffolds were rinsed once with PBS, then 1 mL of the dye solution was added to each scaffold and the plate was incubated at RT in the dark for 1 h.

Near infrared (NIR) laser beams (wavelength 800 nm) were then obtained from a tunable 76 MHz femtosecond pulsed Ti:sapphire laser (Mira 900-F, Coherent, Ely, UK) pumped by a 10 W multiline argon ion laser (Verdi; Coherent). A Nikon S Fluor 20X objective with a numerical aperture of 0.75 was used for all images. The emission filters selected were: 495 nm for blue, 525 nm for green and 595 nm for red. Scanning speed was 166 lines per second and the Z-step was 2.55um.

Imaris 7.6.1 was used for imaging processing works and deconvolution was achieved using a standard adaptive blind point spread function (PSF).

5.5 BMP-2 release profile

The release of BMP-2 from the LBL collagen/CS/BMP-2 scaffolds was tested as previously described in **Chapter 4.5**, using an ELISA kit (Sigma-Aldrich®, #RAB0028). Briefly, triplicate scaffold samples were incubated with 500μl 0.1% BSA/PBS at RT with gentle shaking. The BSA/PBS solution was replaced at every timepoint (0, 2, 4, 6, 8, 12, 14, 48, 60, 72, 84, 96, 168 h) and the amount of BMP-2 in the solutions was quantified as described previously, using the instructions and reagents supplied with the kit. Absorbance of the samples was measured at 450 nm (POLARstar Omega, BMG Labtech) and concentrations of BMP-2 were calculated based on the standard curve derived from the ELISA.

5.6 Results

EDX spectroscopy confirmed the presence of CS on the LBL collagen/CS scaffolds (**Figures 5.2a-b**) and further showed that CS was present not only on the external surface, but also on the cut surface, showing that CS was present throughout the scaffolds (**Figures 5.3a**). The difference in mean percent weight of CS between the external and cut surfaces was not statistically significant ($p>0.02$, Student's t-test).

The percent weight of CS within the LBL collagen/CS scaffolds was dependent on pH, with the highest values observed in scaffolds fabricated using a CS solution of pH 7.4 and pH 10.0. Using a pH of 6.0 or 11.0 resulted in a statistically significant reduction in the percent weight of CS of approximately 38% ($p<0.02$, **Figure 5.3b**).

Successful incorporation of CS into the LBL collagen/CS and collagen/HA/CS scaffolds was further confirmed by the use of FTIR (average data for each scaffold type displayed in **Figure 5.4**). Absorbance peaks representing S=O stretch and C-O-S stretch (as identified from the published literature (Tamaddon et al. 2013; Tian et al. 2012; Amrutkar & Gattani 2009) are consistent with the presence of CS (**Figure 5.4**).

SEM demonstrated that a highly connected, porous structure of the scaffold was maintained after the LBL fabrication process (**Figures 5.5-5.6**).

FIGURE 5.2

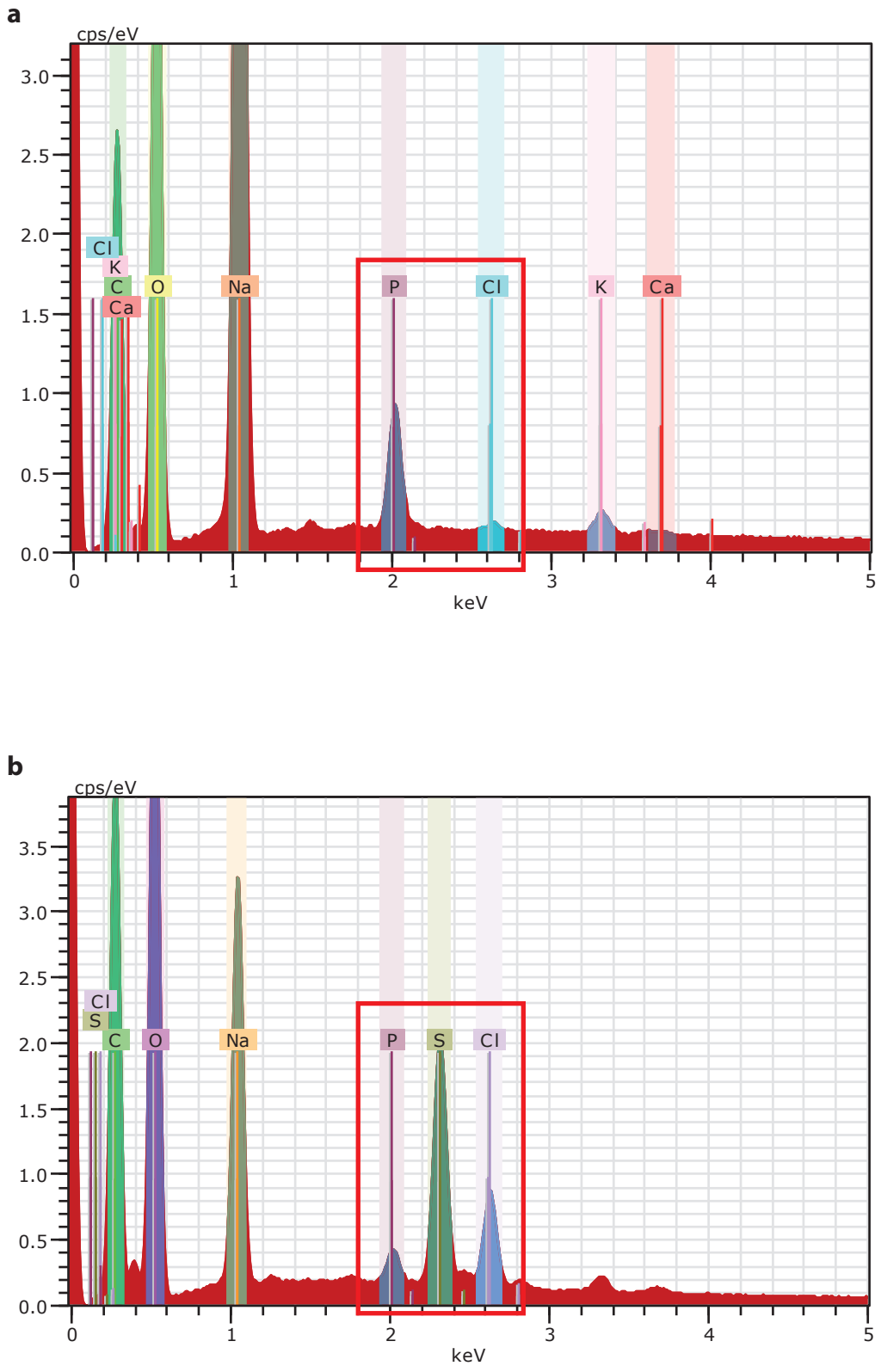


Figure 5.2 Energy-dispersive x-ray (EDX) spectroscopy confirmed the presence of chondroitin sulphate on the LBL collagen/CS scaffolds (a) Representative EDX spectra obtained from analysis of collagen scaffold, prior to dip coating. (b) Representative EDX spectra obtained from analysis of LBL collagen/CS after LBL fabrication process. Rectangle highlights change in spectra with peak for sulphur component in LBL collagen/CS scaffold. LBL, layer-by-layer; CS, chondroitin sulphate.

FIGURE 5.3

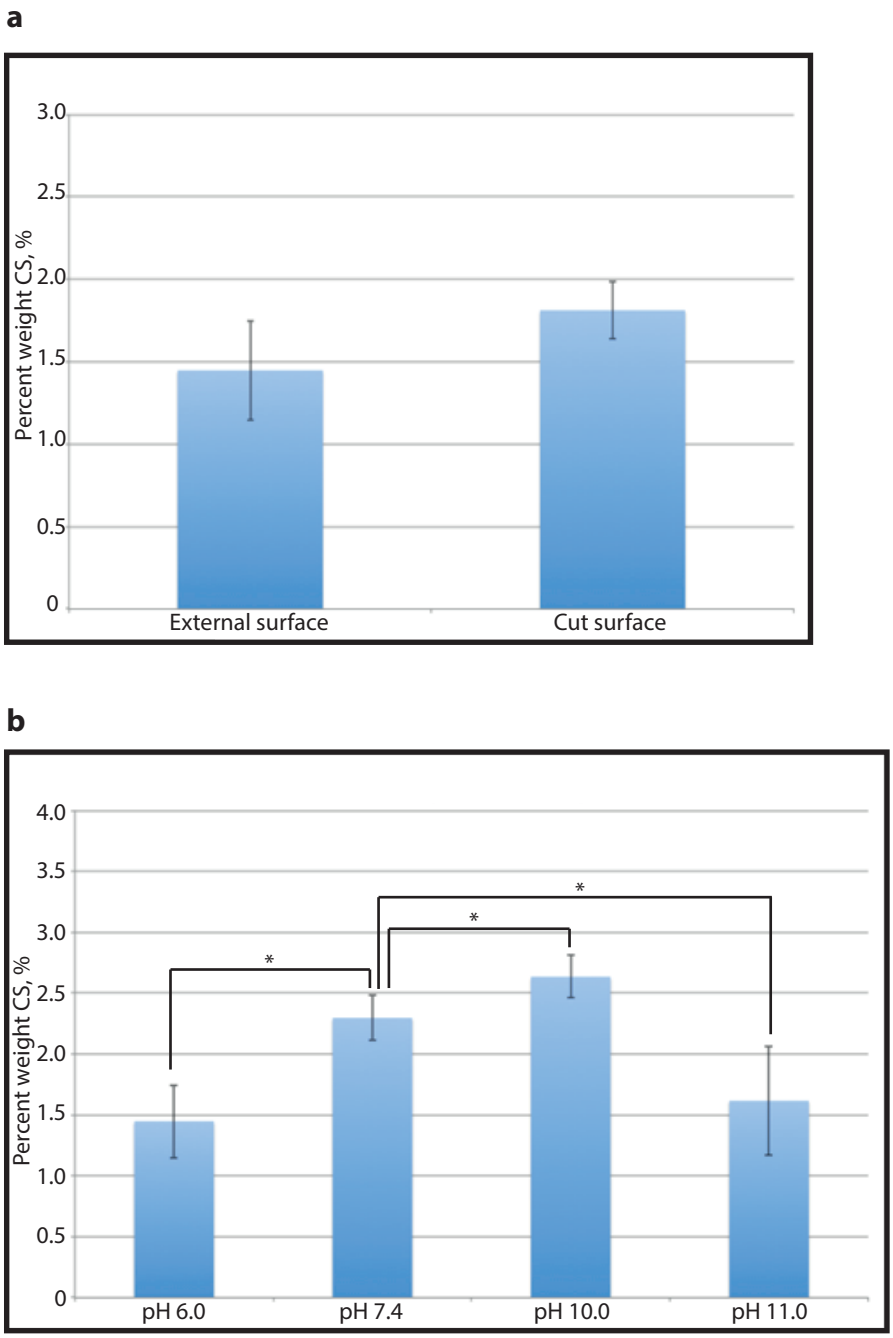


Figure 5.3 Energy-dispersive x-ray spectroscopy confirmed the presence of chondroitin sulphate throughout the LBL collagen/CS scaffolds which was pH-dependent (a) Graph showing mean values of percent weight CS of external and cut surfaces of LBL collagen/CS scaffolds. (b) Graph showing mean values of percent weight CS of scaffolds fabricated at a range of pH values (6, 7.4, 10, 11). Error bars, standard deviation; * $p<0.02$, t-test comparison versus pH 7.4.

Figure 5.4

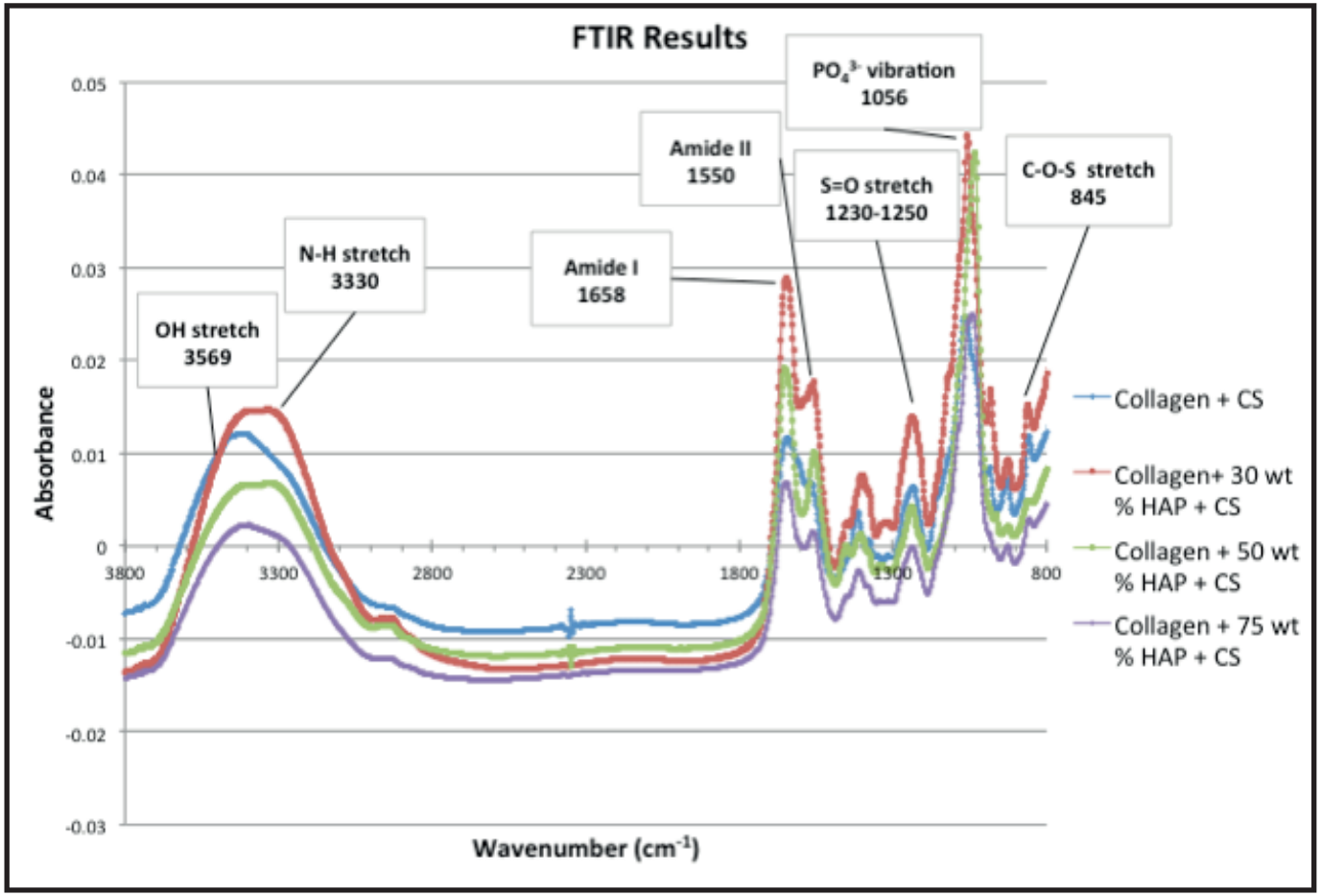


Figure 5.4 Fourier transform infrared spectroscopy (FTIR) confirms the presence of CS within the LBL scaffolds. Absorbance results for LBL collagen/CS and collagen/HA/CS scaffolds shown, absorbance peaks are labelled based on values found in the literature (Tamaddon et al, 2013, Tian et al, 2012, Amrutkar et al, 2009.

FIGURE 5.5

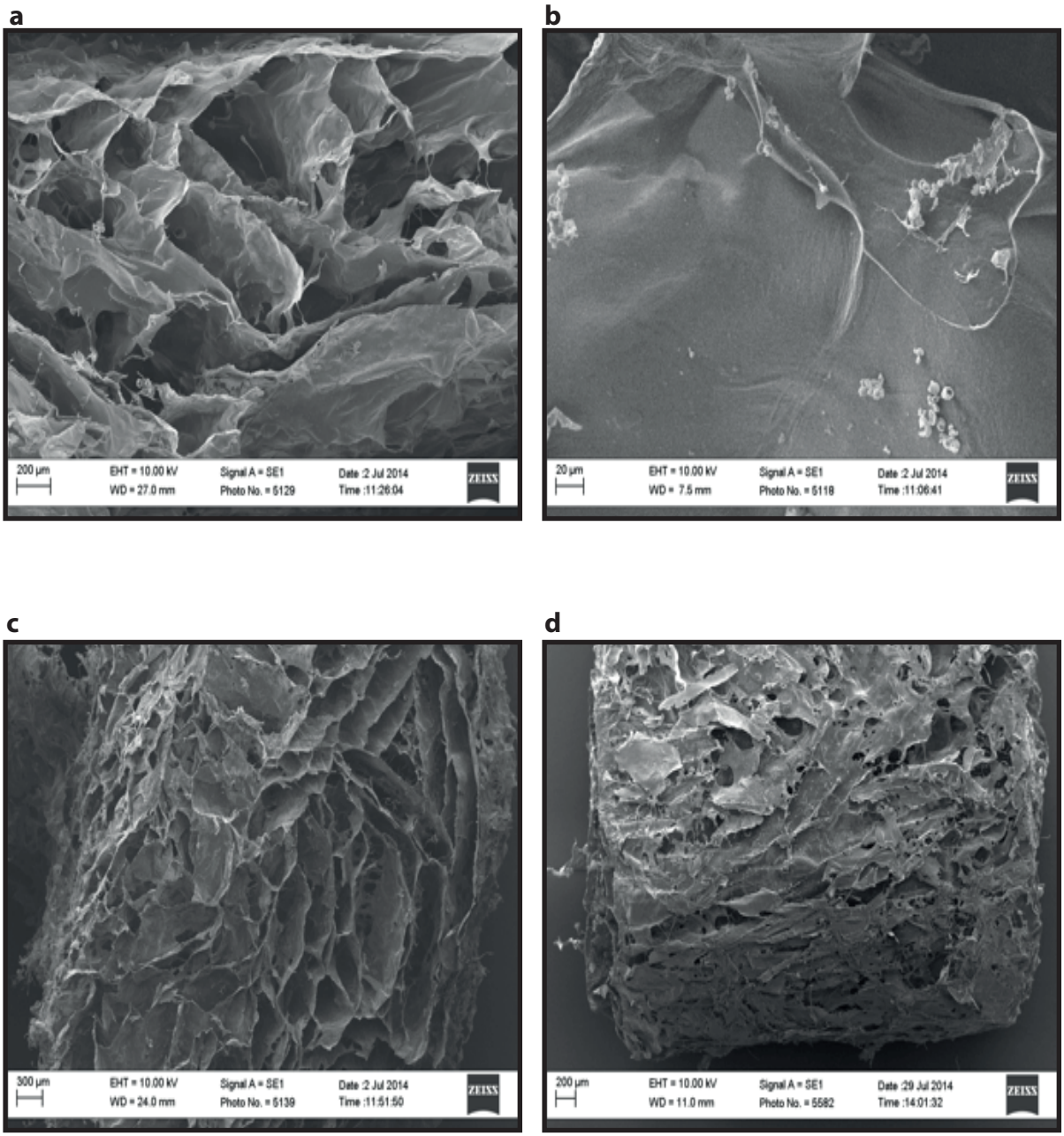


Figure 5.5 Scanning electron microscopy (SEM) images show the interconnected porous structure of the LBL scaffolds (a) Collagen/CS scaffold, cut surface, 100X magnification. (b) Collagen/CS scaffold, external surface, 500X magnification. (c) Collagen/CS/HA 30 wt% scaffold, cut surface, 50X magnification. (d) Collagen/CS/HA 30 wt%, external surface, 10X magnification. Representative images are displayed, all obtained using a Zeiss EVO LS15 microscope at 10 kV.

FIGURE 5.6

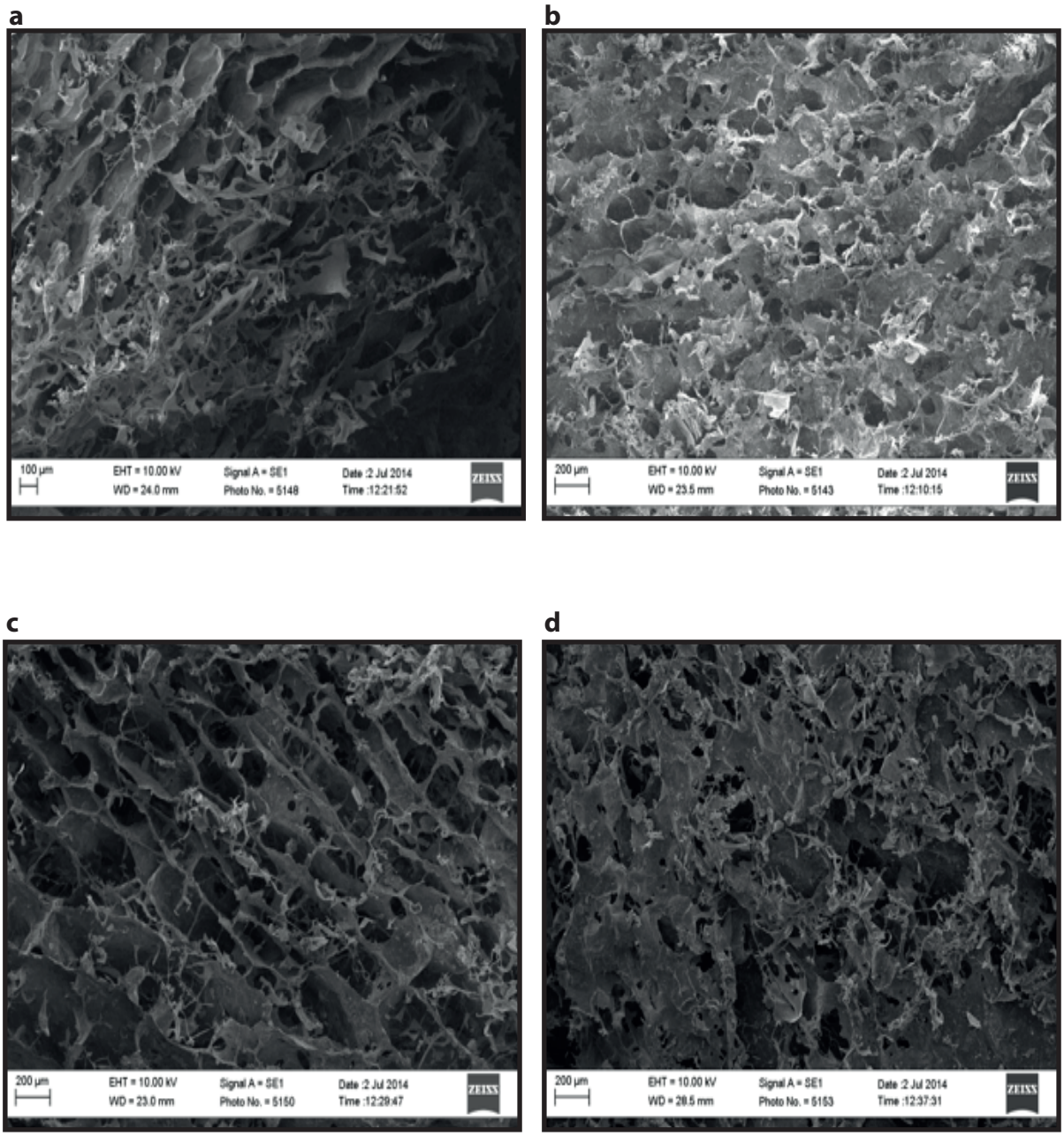


Figure 5.6 Scanning electron microscopy (SEM) images show the interconnected porous structure of the LBL collagen/CS/HA scaffolds (a) Collagen/CS/HA 50 wt% scaffold, cut surface, 100X magnification. (b) Collagen/CS/HA 50wt% scaffold, external surface, 100X magnification. (c) Collagen/CS/HA 75 wt% scaffold, external surface, 100X magnification. (d) Collagen/CS/HA 75 wt%, cut surface, 100X magnification. Representative images are displayed, all obtained using a Zeiss EVO LS15 microscope at 10 kV.

Using SEM images obtained from the cut surface of each scaffold and ImageJ software, all LBL scaffolds contained pores with an average diameter of greater than 170 μm (**Figure 5.7a**). The LBL collagen/CS/HA 50 wt% and collagen/CS/HA 75 wt% scaffolds had significantly smaller pores than the LBL collagen/CS scaffolds ($p<0.02$, **Figure 5.7b**).

DSC was used to determine the thermal stability of the scaffolds. Compared to integrated collagen scaffolds, the LBL collagen/CS+/-HA scaffolds showed a significantly higher Td (range 88 - 123^0C, compared to 62^0C, $p<0.02$, **Figure 5.8a**). Representative DSC plots for the scaffolds show a narrow peak for the integrated scaffolds and a broader peak for the LBL scaffolds (**Figures 5.9-5.12**).

MPM images demonstrate the presence of viable hMSCs throughout the LBL collagen scaffolds (**Figures 5.13a-d**).

The BMP-2 release profile for LBL scaffolds shows an initial burst release within the first 12 h followed by a phasic and sustained release over the following six days (**Figures 5.14a-b**). The cumulative release profiles show a much higher amount of BMP-2 is released from LBL scaffolds, compared to integration and adsorption methods of scaffold fabrication (**Figure 5.14b**).

FIGURE 5.7

a

Scaffold type	Mean +/- standard deviation (μm)
Collagen/CS	266.356 ± 103.867
Collagen/CS/HA 30wt%	255.404 ± 78.224
Collagen/CS/HA 50wt%	217.680 ± 67.282
Collagen/CS/HA 75wt%	177.835 ± 54.459

b

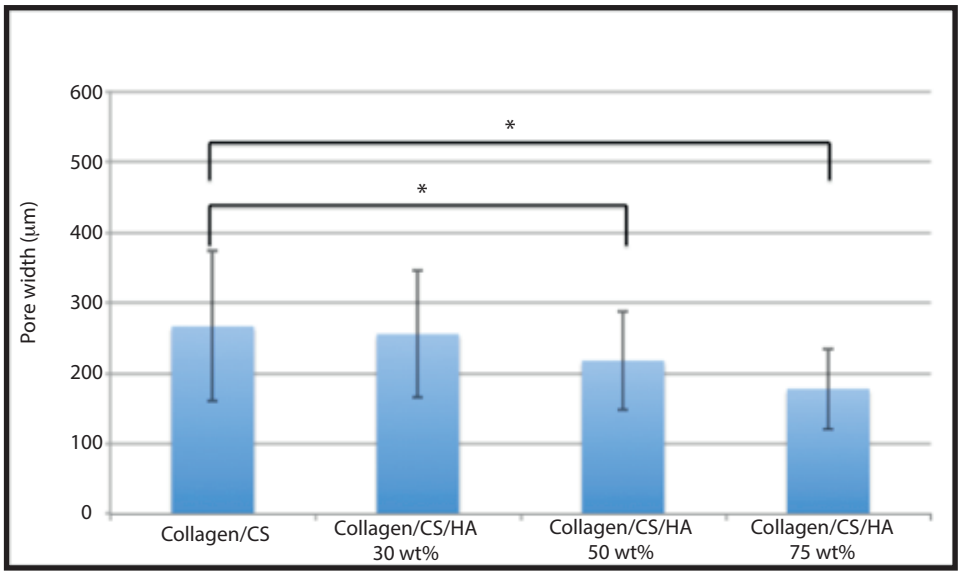


Figure 5.7 Layer-by-layer scaffolds have pore sizes sufficient to support cell growth (a) Table showing mean pore size of LBL scaffolds as calculated using SEM images and open source ImageJ software. (b) Graph displaying pore size of LBL scaffolds, * $p<0.02$. All SEM images obtained using a Zeiss EVO LS15 microscope at 10 kV.

FIGURE 5.8

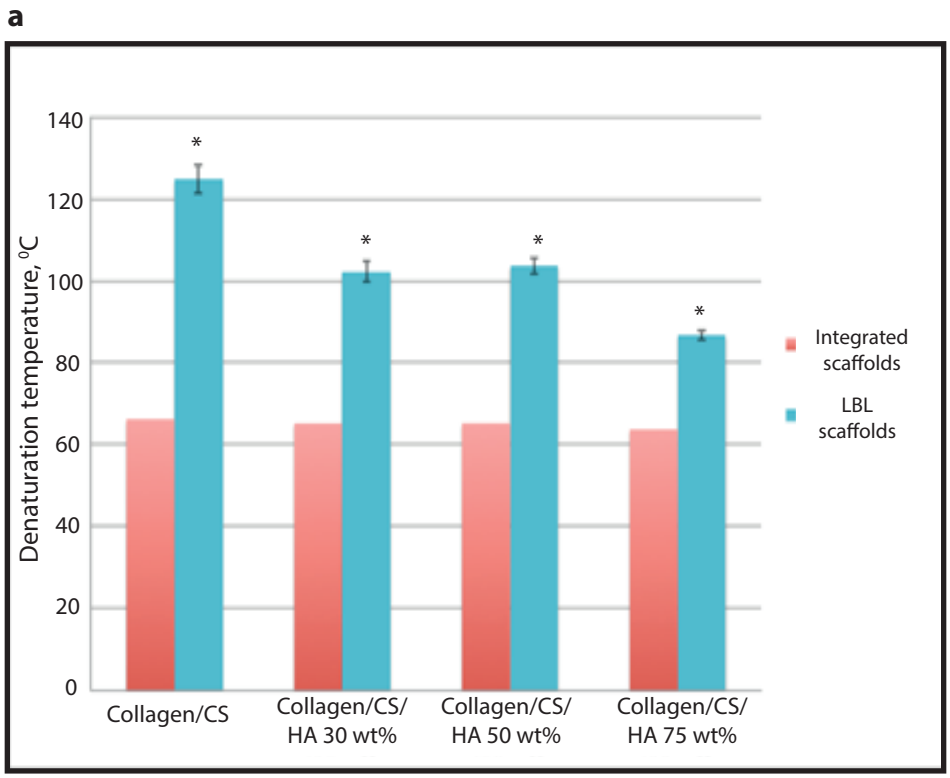


Figure 5.8 Dynamic scanning calorimetry shows higher denaturation temperatures of layer-by-layer scaffolds (a) Graph showing mean denaturation temperatures of integrated and LBL scaffolds. Error bars, standard deviation; * $p<0.02$.

FIGURE 5.9

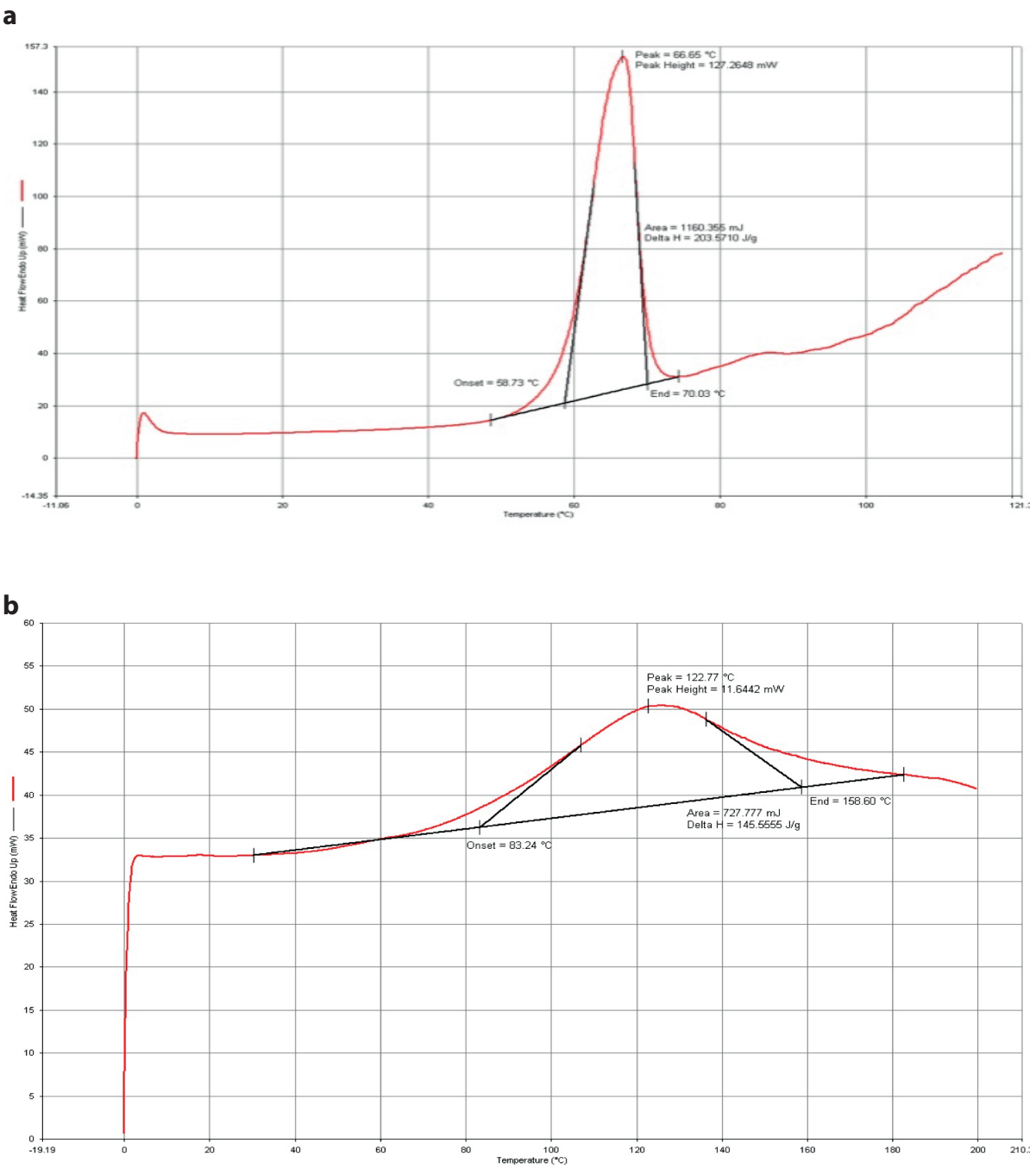
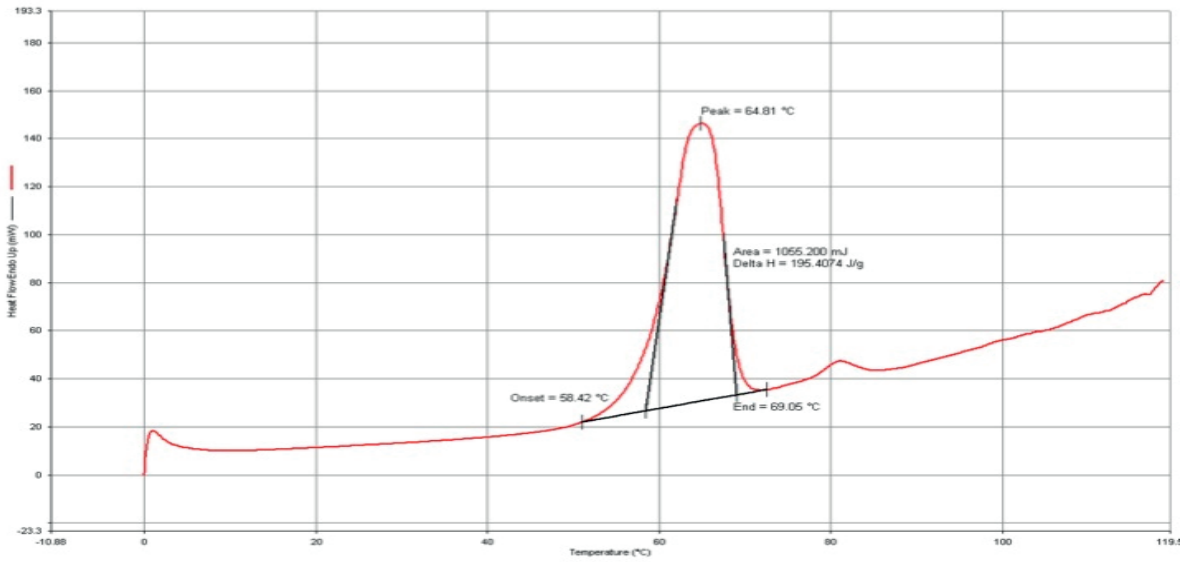


Figure 5.9 Dynamic scanning calorimetry shows higher denaturation temperatures of layer-by-layer scaffolds Representative DSC plots from (a) collagen/CS integrated and (b) LBL collagen/CS scaffolds. DSC, dynamic scanning calorimetry; LBL, layer-by-layer; CS, chondroitin sulphate.

FIGURE 5.10

a



b

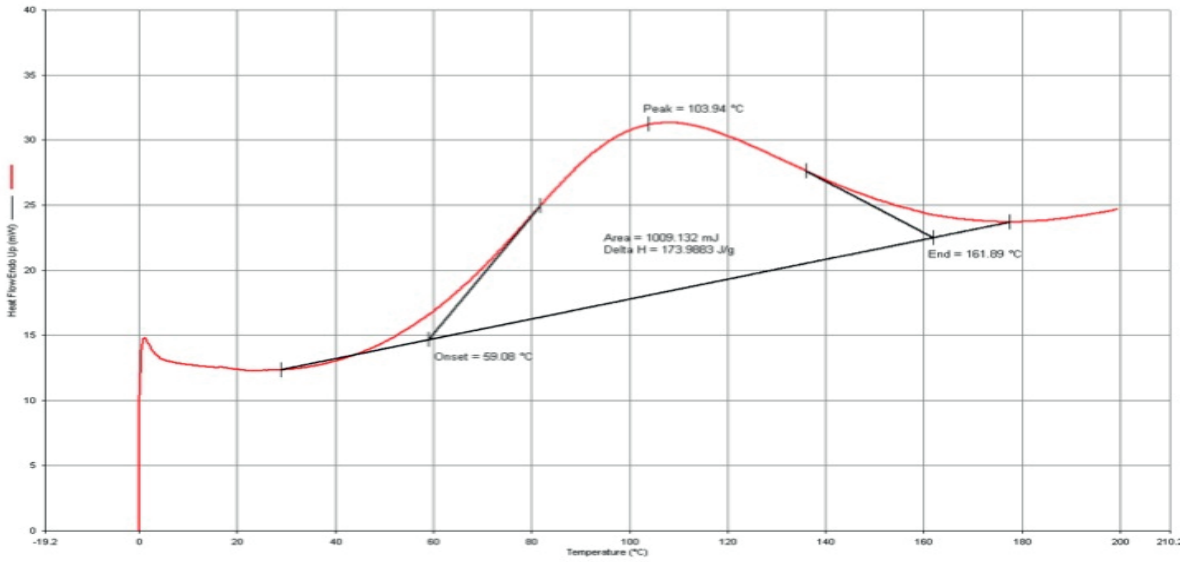
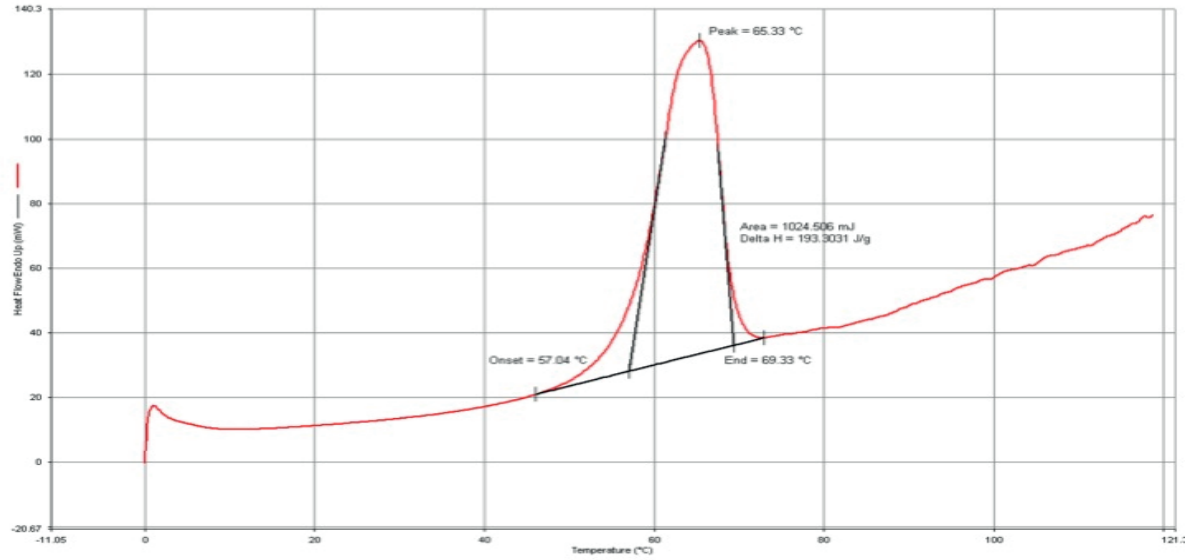


Figure 5.10 Dynamic scanning calorimetry shows higher denaturation temperatures of layer-by-layer scaffolds Representative DSC plots from (a) collagen/CS/HA 30wt% integrated and (b) LBL collagen/CS/HA 30 wt% scaffolds. DSC, dynamic scanning calorimetry; LBL, layer-by-layer; CS, chondroitin sulphate.

FIGURE 5.11

a



b

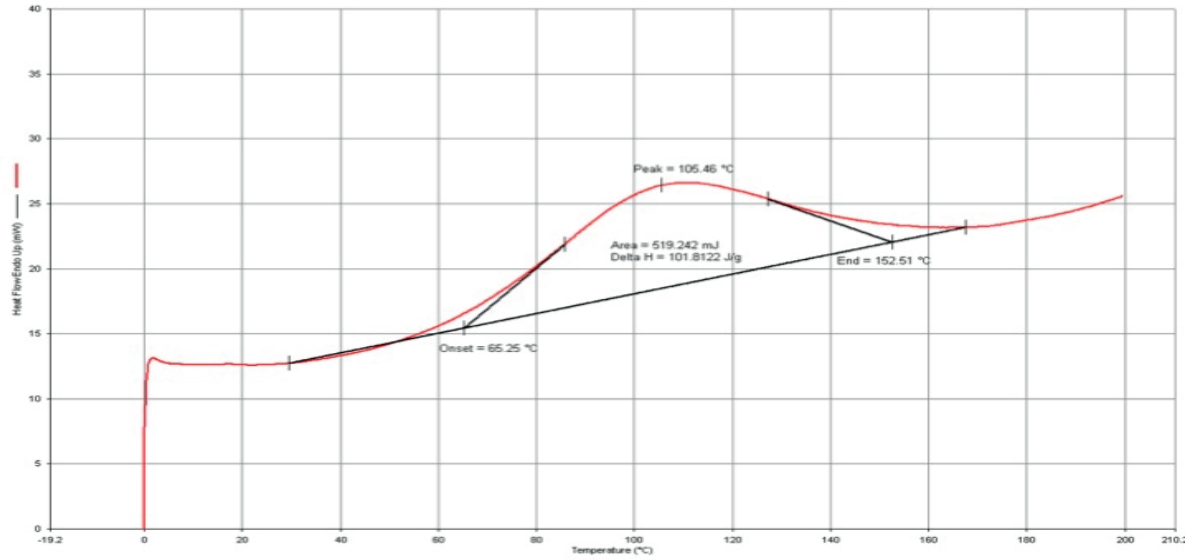
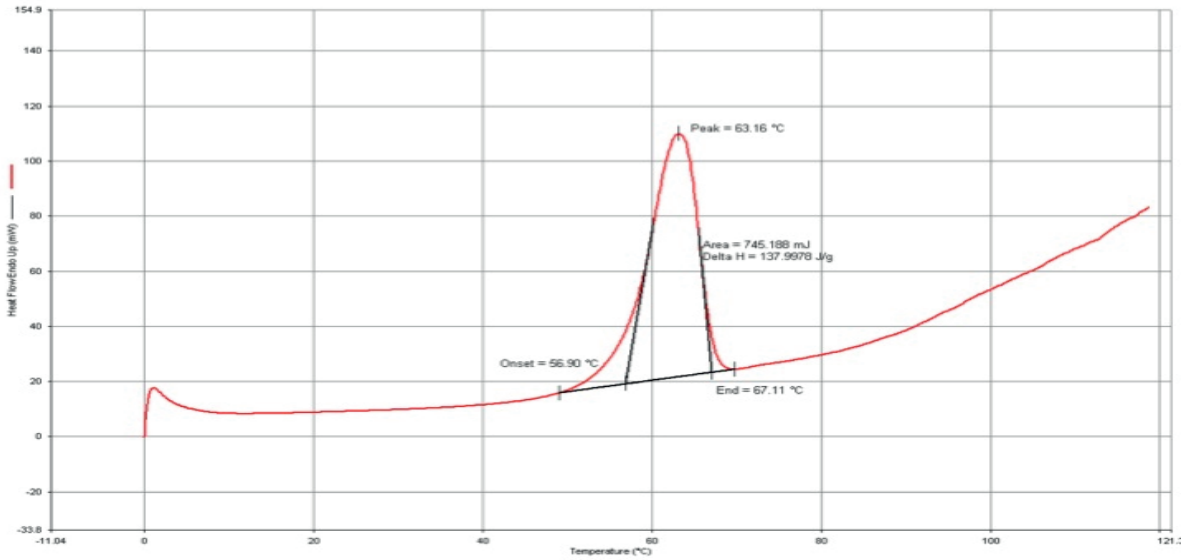


Figure 5.11 Dynamic scanning calorimetry shows higher denaturation temperatures of layer-by-layer scaffolds Representative DSC plots from (a) collagen/CS/HA 50wt% integrated and (b) LBL collagen/CS/HA 50 wt% scaffolds. DSC, dynamic scanning calorimetry; LBL, layer-by-layer; CS, chondroitin sulphate; HA, hydroxyapatite.

FIGURE 5.12

a



b

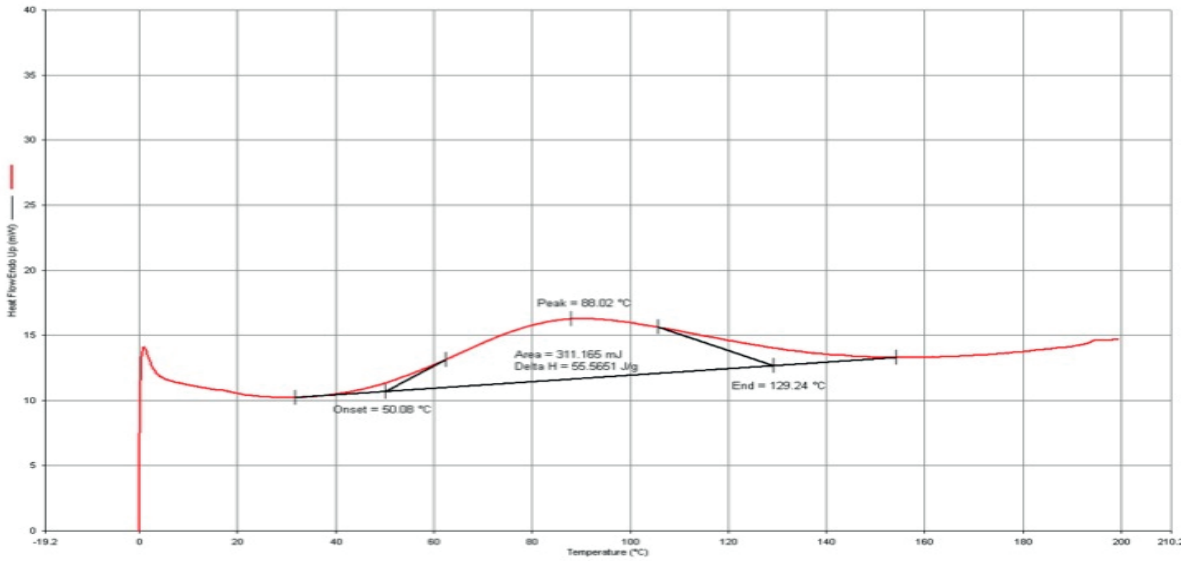


Figure 5.12 Dynamic scanning calorimetry shows higher denaturation temperatures of layer-by-layer scaffolds Representative DSC plots from (a) collagen/CS/HA 75wt% integrated and (b) LBL collagen/CS/HA 75 wt% scaffolds. DSC, dynamic scanning calorimetry; LBL, layer-by-layer; CS, chondroitin sulphate; HA, hydroxyapatite.

FIGURE 5.13

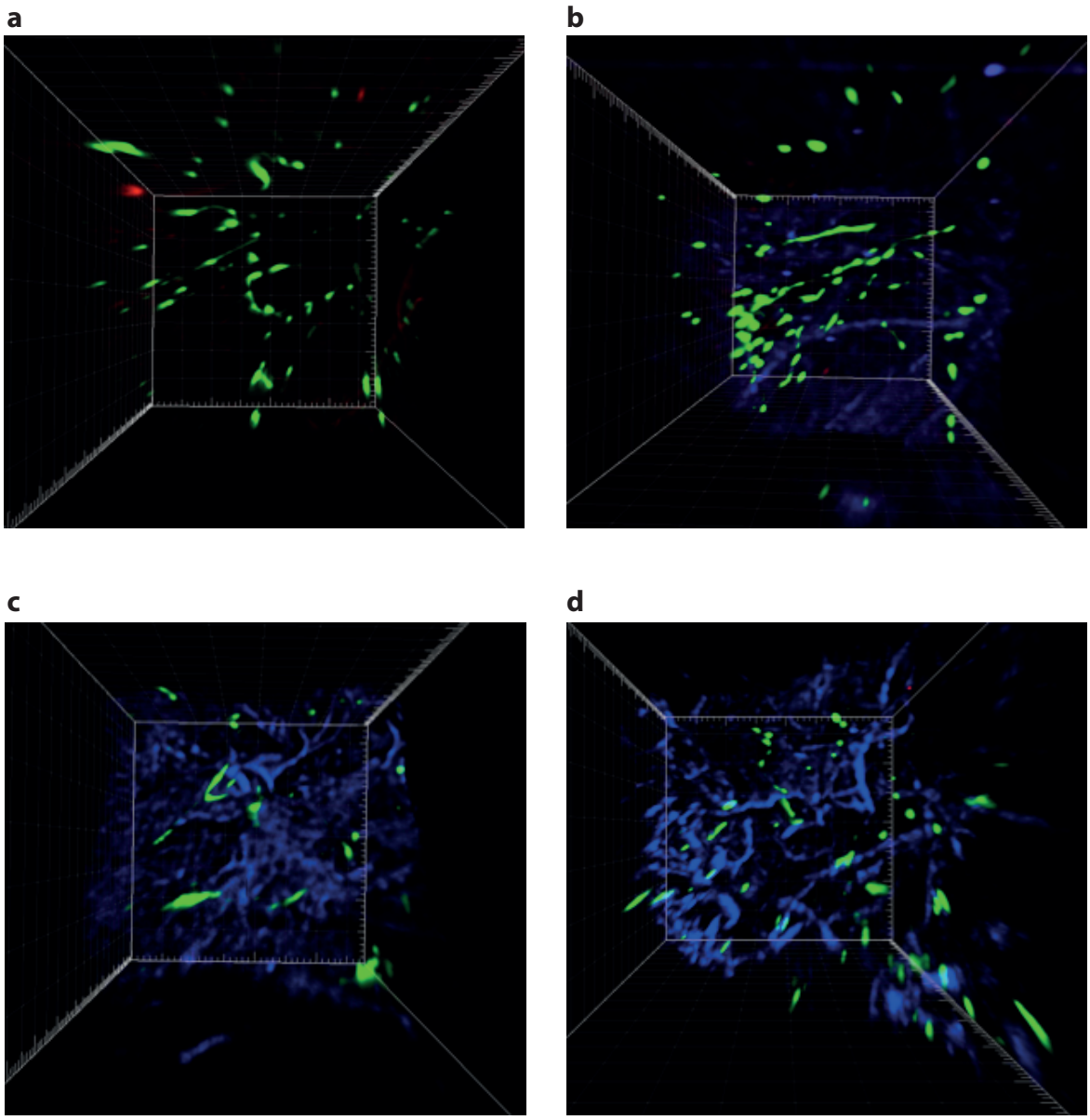


Figure 5.13 Multiphoton microscopy confirmed the presence of viable hMSCs throughout the LBL collagen/CS scaffolds Representative images obtained from (a) LBL collagen/CS/BMP-2, (b) LBL collagen, (c) LBL collagen/CS/HA 30 wt%, (d) LBL collagen/CS/HA 50 wt%. All images were obtained with a modified BioRad Radiance 2100 MP Multiphoton Microscope (Zeiss, Germany). hMSCS, human mesenchymal stem cells; LBL, layer-by-layer; CS, chondroitin sulphate; HA, hydroxyapatite.

FIGURE 5.14

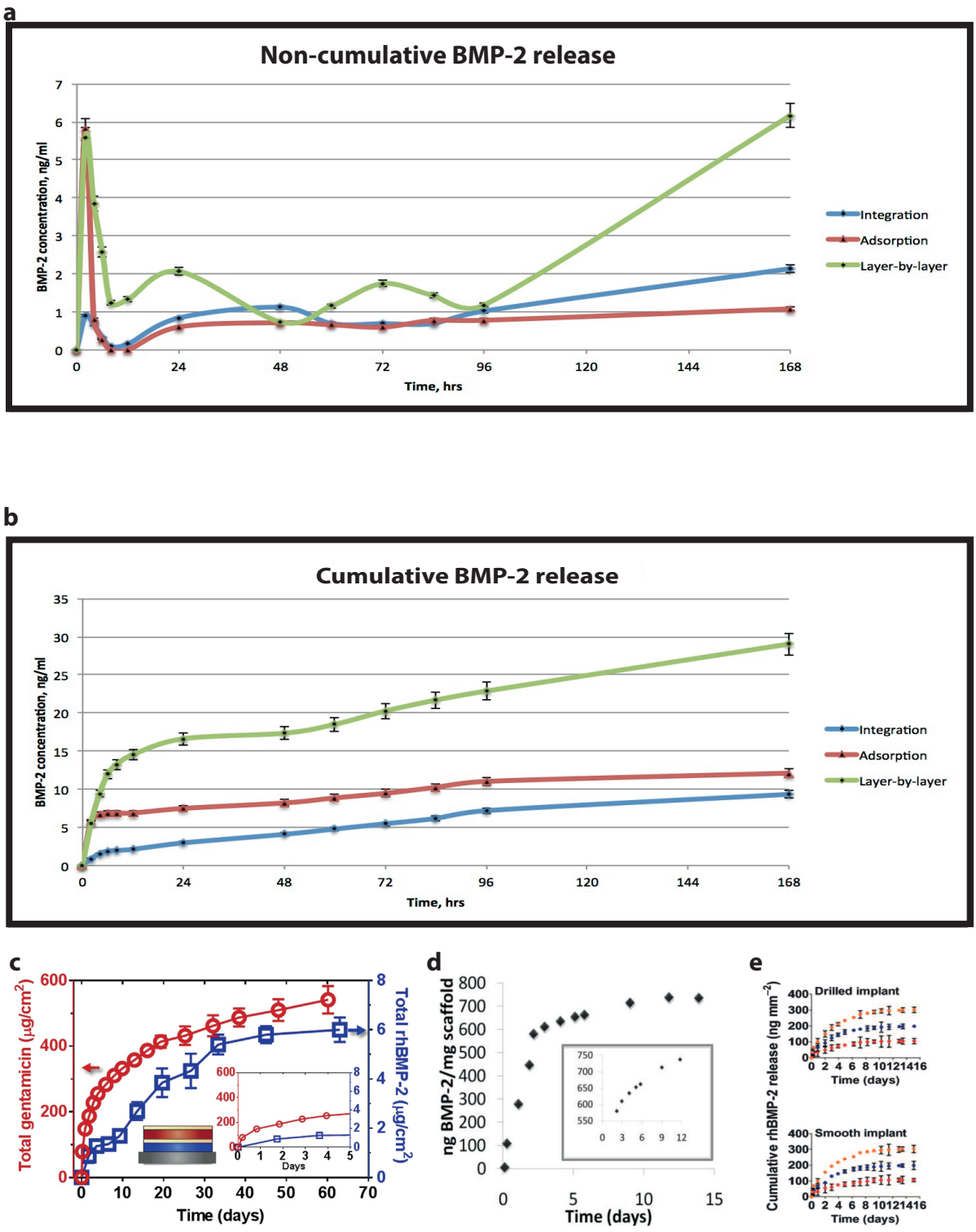


Figure 5.14 BMP-2 is released from LBL scaffolds in a phasic pattern (a) Non-cumulative release profile of BMP-2 from BMP-2-containing scaffolds (integrated, adsorbed and LBL fabrication methods) from 0 to 168 h. (b) Cumulative release profile of BMP-2 from BMP-2-containing scaffolds (integrated, adsorbed and LBL fabrication methods) from 0 to 168 h. BMP-2 concentration measured using ELISA assay (Sigma-Aldrich). Error bars, standard deviation. Examples of data from published studies of BMP-2 release from LBL scaffolds: (c) Min et al, 2014, (d) MacDonald et al, 2011, (e) Shah et al, 2013.

5.7 Discussion and Conclusions

Using a layer-by-layer approach, a collagen/CS/HA scaffold has been fabricated and characterised.

EDX was employed to assess the presence of CS. Indeed, CS was present on the surface of and within the scaffold. After testing a range of pH values of the CS solution, it was found that the maximal uptake of CS was at pH 7.4 and 10.0. In order for the material to be physiologically compatible, it was decided to proceed with the fabrication of scaffolds using pH 7.4 CS solution.

Subsequently, these LBL collagen/CS/±HA scaffolds were tested using FTIR analysis, which further confirmed the presence of carbon-oxygen-sulphur bonds and carbon-sulphur double bonds. All the scaffolds had peaks at 845 cm^{-1} and 1230-1250 cm^{-1}, which represent the C-O-S and C=O bonds, respectively (Tamaddon et al. 2013; Tian et al. 2012; Amrutkar & Gattani 2009).

It has been reported that when CS solution is added to a collagen scaffold, peaks between wavenumbers 800 and 1600 are observed when a 4 cm^{-1} absorbance mode setting is used (Tamaddon et al. 2013; Tian et al. 2012; Amrutkar & Gattani 2009; Rodrigues, Salgado, Sahu, Garcia, Fernandes & Monteiro 2013a).

Additional peaks of interest (as shown in **Figure 5.4**) represent known bonds in collagen and HA. Amide I (1658 cm^{-1}) and II (1550 cm^{-1}) are related to C=O, C-N and N-H bonds, which are contained within collagen (Tamaddon et al. 2013; Belbachir et al. 2009; D.-A. Wang et al. 2007) and OH (3569 cm^{-1}) and PO_4^{3-} (1056 cm^{-1}) are contained within HA (Tian et al. 2012; Rehman & Bonfield 1997; Rodrigues, Salgado, Sahu, Garcia, Fernandes & Monteiro 2013a).

However, it must be noted that it is quite difficult to differentiate between collagen and CS peaks as they fall within the same wavenumber range and there

is significant overlap between the peaks (Tamaddon et al. 2013). Completing a second derivative spectroscopy analysis is one way that might help to better identify the specific bonds.

DSC was undertaken to determine the thermal stability of the scaffolds and therefore to assess their suitability *in vivo* at 37^0C. The integrated scaffolds, used as a comparison for the LBL scaffolds, each showed a denaturation temperature (Td) of approximately 65^0C, consistent with previously published results (van Susante JLC et al. 2001; Pieper et al. 2002). The presence of HA at varying weight percent did not significantly alter the Td of the scaffolds. However, when the scaffolds were fabricated using LBL methodology, the Td was significantly higher for all scaffolds (up to 125^0C).

It has been proven that cross-linking agents 1-ethyl-3- (dimethyl-aminopropyl)carbodiimide (EDC) or N-hydroxysuccinimide (NHS), when combined with collagen, can increase the Td of a collagen scaffold in the presence of either CS or HA (van Susante JLC et al. 2001; Pieper et al. 2002; S. Teixeira et al. 2010). However, a literature search yielded no results to prove that any cross-linking occurs when collagen is combined with CS and HA. Yet, based on these results and the fact that CS has sticky, gel-like properties, it is hypothesized that the CS does help to strengthen the bonds within the collagen scaffold. Examining the width of the peak leading to denaturation between collagen samples with CS integrated and LBL further supports this hypothesis. When a small amount of CS was integrated into the scaffold, a larger amount of energy was required for denaturation, but it occurred over a much narrower temperature range. The width of the peak is proportional to the thermal stability of the material where a broader shape corresponds to increased stability

(Gelinsky et al. 2008). The LBL collagen/CS scaffolds had a much broader DSC peak and hence represent a more thermally stable material. The LBL scaffolds should degrade over a longer period of time *in vivo*, resulting in a longer sustained release of the drugs and better support for cell growth.

SEM was used to analyse the pore structure in all scaffolds. Pore size and connectivity are essential for cell growth to allow for proper proliferation, migration and diffusion of nutrients and wastes (Freyman et al. n.d.; Tamaddon et al. 2013; Croll et al. 2006; Singh et al. 2009). It has been reported that *in vivo* bone growth requires pore widths greater than 100 μm for MSCs proliferation (Singh et al. 2009; Freyman et al. n.d.). A highly connected, 3-dimensional porous structure was present in all the LBL scaffolds, with average pore width greater than 170 μm for all scaffold types, therefore showing that these scaffolds have the capability to support proliferation of MSCs. Using MPM, the scaffolds were shown to support the proliferation of hMSCs and viable hMSCs were evident throughout the scaffold, not only at the surface.

Previous studies have demonstrated the release profile of BMP-2 from a range of LBL scaffolds (**Figures 5.14c-d**). For example, BMP-2 was released from a chitosan/clay/BMP-2 LBL scaffold in a burst release profile (**Figure 5.14c**) (Min, Braatz & Hammond 2014a). A similar burst release profile was obtained from polycaprolactone/β-TCP/BMP-2 LBL scaffolds (Macdonald et al. 2011) and also from PEEK/titanium/HA/chitosan/BMP-2 LBL scaffolds (Shah et al. 2013) (**Figures 5.14d and e**, respectively).

The results presented here in this thesis demonstrated an initial burst release of BMP-2, followed by sustained and phasic release, therefore showing these LBL collagen/CS scaffolds can deliver BMP-2s in a sustained fashion.

A biomimetic scaffold has been created using a layer-by-layer approach, which has potential for orthopaedic application.

Chapter 6 Discussion

The ideal scaffold for bone regeneration should fulfil the components of the 'diamond concept', comprising of growth factors, scaffold, hMSCs and, critically, the appropriate mechanical environment (Giannoudis et al. 2007). The scaffold is the key determinant of bone healing and an ideal scaffold should have predictable biodegradability, biocompatibility, low immunogenicity, enhancement of cellular attachment, affinity to bone, controlled growth factor release, lack toxicity, stability and cost-effectiveness.

In summary, this work has detailed the fabrication and characterisation of a novel collagen/HA/CS scaffold, including its osteogenic capability and its use as a delivery system for BMP-2. The scaffold was tailored such that each component allowed maximal osteoninductive capability. Atelocollagen can support bone regeneration, as shown in a study of bone formation and histological changes in rat calvarial defects following atelocollagen implantation (Kagawa et al. 2012). After 1 week, osteogenic cells showed RUNX2 positivity, by 3 weeks most of the atelocollagen had been replaced by new bone with resorption cavities and by 4 weeks, the new bone also contained haematopoietic marrow.

Other previously reported uses of atelocollagen in bone tissue engineering include as a composite scaffold with hydroxyapatite-PLGA (leading to increased osteoblast attachment and proliferation (Takechi et al. 2012). Atelocollagen/HA scaffolds have been used to support the growth of osteoblasts *in vitro* (G. L. Jones et al. 2010).

The glycosaminoglycan CS was added to the scaffold to further mimic the ECM of bone. The combination of afibrillar Type II atelocollagen with CS has previously

been reported, with an observed improvement in compressive strength and an increase in circularity of pores (Tamaddon et al. 2013). However, no studies have reported the use of any atelocollagen/CS scaffolds in combination with cell culture.

It is widely believed that atelocollagen, through telopeptide removal, has a minimal level of immunogenicity compared to fibrillar collagen (Iwasa et al. 2003; Sakai et al. 2003; Uchio et al. 2000). However, the antigenic determinants of collagen are helical (antibody recognition of the 3-d triple helix), central (recognition of the amino acid sequence, but not 3-d conformation, within the triple helical portion) and terminal (recognition of the nonhelical terminal telopeptides). To date, only one study has reported the human antigenic response to exogenous collagen, and this was pepsin-solubilized (telopeptide-deficient) bovine collagen (Ellingsworth et al. 1986); no such studies of the terminal antigenic sites has been reported, therefore the immunogenicity of bovine atelocollagen in humans is unknown.

The principal component of human bone is HA and nanoHA has been shown to have superior biophysical properties, therefore nanoHA was added to the scaffolds in this study at a range of weight percentages. NanoHA has been studied in combination with collagen as a cryogel (Rodrigues, Salgado, Sahu, Garcia, Fernandes & Monteiro 2013b) and is also known to be osteoconductive (X. Zhang et al. 2014). However, nanoHA alone would not be a suitable scaffold due to its low mechanical strength.

The novel combination of self-organising fibrillar atelocollagen with CS and nanoHA in this work has led to the fabrication of a range of porous 3-dimensional biomimetic scaffolds containing the key components of bone. The self-organising ability of the collagen facilitates the integration of the other components in such a way that they are interwoven throughout the fibrils, which is a unique feature of this model. The interconnected pore structure supports and indeed promotes the growth and proliferation of human MSCs.

The physical properties of the scaffolds have been detailed in this work and compare well to previously published results, where available. For example, the denaturation temperature (Td) of the scaffolds increased with crosslinking, as shown by others (Ciardelli et al. 2010; Tampieri et al. 2003). However, I did not find an increase in Td with increasing HA content as shown by Ciardelli et al, 2010 (56-75^{0}C). The same study was unable to determine the Td for samples with more than 50 wt% HA 'because of the low amount of collagen leading to decreased intensity of denaturation thermal events'. It would not be expected for HA to change the Td of a collagen-based scaffold given that the melting temperature of HA is approximately 1100^{0}C, therefore it is likely any increase in Td observed with increasing HA content in the published study was an inaccurate result.

Whilst all the scaffolds tested in this work were stable at physiological body temperature, crosslinked scaffolds exhibited the highest Td (74.1^{0}C). Although far above normal body temperature, the higher the denaturation temperature,

the longer the degradation time for the scaffold. Rapid degradation at the site of bone healing is a frequent limitation of previously published scaffolds, particularly when the scaffold is acting as a carrier for growth factors such as BMPs (He et al. 2014). In spinal fusion surgery, bone formation should begin to be observed by 6 weeks, so a slower-degrading scaffold is preferred. In order to decrease the rate of degradation and therefore sustain bone healing, crosslinking agents have been studied. These agents promote the formation of covalent or ionic bonds between molecules and can be broadly divided into chemical and enzymatic agents: chemical agents include dimethyl suberimidate, bissulfosuccinimidyl suberate (BS3), glutaraldehyde and formaldehyde (which all induce nucleophilic attack of the amino group of lysine and subsequent covalent bonding), and the zero-length carbodimiide crosslinker 1-Ethyl-3-[3-dimethylaminopropyl]carbodiimide hydrochloride (EDC) (which couples carboxyl groups to lysine residues or other primary amines). Enzymatic agents include tyrosinases and transglutaminases (two main forms: tissue, which is calcium-dependent, and microbial). mTG has been studied as a crosslinking agent for elastin-like polypeptide and poly(ethylene glycol) hydrogels in cartilage repair (McHale et al. 2005; M. E. R. Jones & Messersmith 2007) and for hydrogels used as an alternative to fibrin sealant, where it was shown to improve the shear adhesive strength (Hu & Messersmith 2005). Scaffolds of fibrillar collagen (not atelocollagen) combined with micro-HA were crosslinked with mTG and an increase in thermal stability was observed (Ciardelli et al. 2010). Although SEM is a well-established technique, it has not previously been widely used to demonstrate the characteristic d-banding pattern of collagen. SEM is an extremely sensitive technique and can be used to analysed small amount of

material with a high degree of accuracy. The only published report of it having been used to present collagen fibrils was in 2008 in a fossilized specimen (Lingham-Soliar & Wesley-Smith 2008).

Mechanical testing of the scaffolds showed the Young's modulus of mineralised collagen was close to that of cancellous bone. Previous reports of compressive strength vary greatly, with vertebral bone ranging from 1 to 175 MPa (Lindahl 1976; Mosekilde et al. 1987) and tibial bone ranging from 3 to 2000 MPa (Lindahl 1976; Ding et al. 1997). The Young's moduli for the mineralised scaffolds fabricated here are within this range and demonstrate that the strength of the scaffolds is increased by the addition of HA.

The scaffolds were combined with hMSCs in an attempt to increase the osteoinductive capability of the scaffolds. As hMSCs are present in human bone marrow and are self-renewing with the ability to differentiate into bone-forming osteoblasts, they were selected as the cell line of choice. In addition, bone marrow-derived hMSCs have previously been used in spinal fusion surgery with good effect, producing fusion rates similar to iliac crest bone graft and supporting their application in clinical practice (P. Zhang et al. 2008; Neen et al. 2006).

hMSCs expressed significantly higher levels of genes associated with bone formation when grown in collagen/HA scaffolds compared to 2-D culture and collagen-only scaffolds. Of note, BMP-2 was expressed at very high levels in hMSCs grown in mineralised collagen scaffolds (over 300-fold increase

compared to BMP-2 levels in hMSCs grown in collagen-only scaffolds and 2-D culture), and previously published work suggests that direction of hMSCs towards an osteogenic lineage might be due to the increased stiffness of collagen/HA/CS scaffolds (Murphy et al. 2012; YuKan Liu et al. 2009). Such elevated levels of BMP-2 transcript could, depending on the post-transcriptional modifications and stability of the translated protein, correspond to a significantly increased level of BMP-2 protein, but it was not possible to test this here. Attempts were made to harvest cell lysates for protein extraction and quantification, but low cell numbers precluded accurate assessment. Few studies have published the results of protein levels from hMSCs cultured in 3-d scaffolds and it is likely that improved techniques of harvesting cells from these scaffolds will facilitate enhanced assessment of proteins (Shim et al. 2014).

The addition of hMSCs to collagen/30 wt% HA scaffolds led to an increase in mineralisation as evidenced by micro CT analysis. The variable results from micro CT could represent inaccuracies with seeding densities, as no adjustments can be made in the analysis for different cell numbers in each scaffold. As expected, the scaffolds with 75 wt% HA showed the highest bone mineral density, although no significant difference was observed between those scaffolds seeded with and without cells. Longer incubation times of cells on the scaffolds (for example, more than two weeks) could provide clearer results. Micro CT has been used previously to assess bone mineral density *in vitro* of scaffolds and one study showed that despite early induction of gene expression, long-term mineralization, shown by micro CT, occurred in PLGA scaffolds after eight weeks (Kruger et al. 2011). Similarly, another study of collagen mineralisation with

culture of preosteoblasts showed effects after seven weeks, suggesting a much longer time scale is needed than that used in this work (Pedraza et al. 2010). Further evidence for mineralisation of scaffolds by hMSCs is provided by an increase in compressive strength observed in collagen/β-TCP scaffolds (Arahira & Todo 2014).

Recombinant BMP-2 was chosen as a growth factor to combine with the scaffold due to its osteoinductive ability and the fact that it is already approved for clinical use in orthopaedic surgery. An *E. coli* expression system was used and, until recently, this had not been used in humans. However, a recent study demonstrated its clinical safety and therefore it could have potential in future orthopaedic applications (M.-S. Kim et al. 2014).

The release of BMP-2 from collagen/CS scaffolds fabricated using adsorption, integration and layer-by-layer (LBL) was studied for 7 days. In principal, any other BMPs (or combinations of) could be combined with this collagen-based scaffold in the same way. LBL scaffolds released the largest amount of BMP-2 (approximately double that released from the other scaffolds at the same timepoints) and in a sustained release profile. The non-cumulative release profiles showed a phasic release of BMP-2 from the LBL scaffolds that could represent degradation of a layer(s) of scaffold followed by release of BMP-2, in a cyclical fashion. However, previous studies of LBL BMP-2-scaffolds have shown burst release profiles and the reason for this observed difference is unclear, as the same fabrication method has essentially been employed although subtle differences in solution concentrations and number of cycles could contribute to

differences in BMP-2 release (Shah et al. 2013; Macdonald et al. 2011; Min, Braatz & Hammond 2014b).

To date, the only published studies of atelocollagen/BMP-2 scaffold are integrated scaffolds for tissue-engineering with no study of release profile (E. C. Ko et al. 2012; Takeuchi et al. 2009). In this study, a novel BMP-2-containing scaffold has been fabricated and the release profile has been characterised, showing potential for clinical use as a sustained delivery carrier.
Characterisation showed a significantly higher denaturation temperature of LBL scaffolds compared to other scaffolds, further supporting its use as a delivery system *in vivo*.

In summary, using a novel self-organising collagen scaffold combined with nano-hydroxyapatite and chondroitin sulphate and by employing the latest materials techniques, I have studied the osteogenic capability of a biomimetic graft for use in spinal fusion surgery. The mineralised collagen scaffold has compressive strength comparable to human cancellous bone and can support the proliferation of viable human mesenchymal stem cells. This porous scaffold can be combined with human mesenchymal stem cells to further promote bone growth, as evidenced by an upregulation in the levels of bone-forming genes and mineralisation of the scaffold. This scaffold can act as a carrier system for BMP-2, with wider application for other growth factors or drugs, providing sustained release when fabricated as a layer-by-layer scaffold.
An alternative bone substitute for use in spinal surgery has been designed and characterised, with exciting potential for use *in vivo*.

Chapter 7 Conclusions and Future Work

This study has detailed the fabrication and characterisation of novel collagen biomimetic scaffolds for potential use in spinal fusion surgery. This chapter details the areas in which further work is required and outlines the limitations of this study.

The majority of material characterisation and cell study has been performed with collagen/HA/CS scaffolds. BMP-2 was added to collagen/CS scaffolds in order to study its release profile. However, it has not been possible to study the osteogenic effect of BMP-2 with hMSCs and future work would combine the collagen/CS/HA scaffolds with BMP-2 and study the growth of hMSCs and osteogenic effects. This work should also include a comparison of LBL and integration methods of BMP-2 incorporation on the osteogenic effects of the scaffolds with hMSC culture.

Crosslinking was studied in order to fabricate a non-toxic scaffold with optimal degradation properties. However, the degree of crosslinking was not measured in this study and the observed increase in denaturation temperature was attributed to crosslinking without precise knowledge of the amount of crosslinking. Future work could include a quantitative assessment of crosslinking using such methods as amine group quantification that would confirm the presence of crosslinking (Bubnis & Ofner 1992; Orban et al. 2004).

This study did not address the effect of crosslinking on osteogenic capability of the scaffold in detail, other than to compare crosslinked collagen with collagen and gene expression levels. Future work could study the effects of crosslinked collagen on gene expression in mineralised scaffolds seeded with MSCs.

hMSCs were chosen as the cell line for culturing on the scaffolds, but due to time and financial limitations, comparisons with other cell lines (for example, osteoblasts) were not possible. Future work could compare osteoblasts to MSCs in order to quantify the degree of osteogenic differentiation of MSCs on the scaffold.

This study did not address the question of how to harvest hMSCs from patients undergoing spinal surgery. Various sources of hMSCs exist, including bone marrow and peripheral blood. Certainly peripheral blood and stromal vascular fractions are gaining increasing interest as sources of hMSCs, particularly due to the low morbidity of harvesting and as extraction techniques are improved and developed (N. L. Anderson & N. G. Anderson 2002; Astori et al. 2007). Further optimisation of the harvesting of MSCs could potentially improve spinal fusion rates and should be studied both *in vitro* and *in vivo*.

The purpose of the scaffold described herein is to improve spinal fusion rates and therefore a significant limitation of this work is the lack of *in vivo* experimental data. Such work has large financial and time implications and it was not possible to undertake these experiments, but it would be extremely interesting and informative to collect data from *in vivo* studies in the future. Fortunately, all the components described in this study have previously been used in clinical studies; therefore it would be theoretically possible to plan a clinical trial, pending pre-clinical data.

Whilst BMP-2 release was analysed, this was only performed over a one-week period. Ideally, at least six weeks should be included, to allow for degradation of the scaffold over time. A longer study time was not possible in this work due to the financial limitations of the BMP-2 ELISA kits, but it is important to know how the release profile changes over longer time periods, given that the scaffold would be used to promote spinal fusion over a period of at least six weeks. This work has demonstrated a sustained release of BMP-2 over time and this scaffold could therefore be used as a carrier system for other growth factors and/or drugs. Future work could also study how the protein level of BMP-2 changes with growth of MSCs on mineralised scaffolds. If the observed increase in transcript levels was mirrored at protein level, it might not be necessary to combine the scaffold with additional recombinant BMP-2.

The principles involved in this fabrication process have wider application, where the *in vitro* study of biological disease states has critical dependency on context. For example, the ECM of many cancers has been shown to be of huge importance in cancer cell behaviour and therefore the oncologists and oncological surgeons have been involved in collaborative work in designing tissue-specific models of diseases. Specifically, the human urinary bladder is comprised of four main layers and these can be recreated in a scaffold model, selecting the critical components of each layer. Together with urological surgeons, I have created an *in vitro* model of muscle-invasive bladder cancer, which has huge potential to serve as a more accurate model of the clinical disease state in the laboratory, and, using which, new treatments can be both identified and tested.

Study objective	*Findings from this thesis*	*Outstanding questions*
1. To fabricate and characterise a mineralised collagen scaffold containing glycosaminoglycans	• Novel self-organising collagen/chondroitin sulphate/nano-hydroxyapatite scaffold was fabricated • This scaffold showed interconnected porous structure with fibril formation • Mineralised collagen scaffolds showed compressive strength comparable to human cancellous bone • Mineralised scaffolds suitable for *in vivo* use based on thermal analysis	• Does transglutaminase lead to crosslinking that can be quantitatively assessed? • Does this scaffold have biocompatibility *in vivo*?
2. To test the ability of the mineralised scaffold to promote bone growth *in vitro*	• Mineralised collagen scaffolds supported the growth of viable hMSCs • Mineralised scaffold showed osteogenic capability with upregulation of key bone-forming genes • Mineralised scaffold seeded with MSCs were suggestive of an increase in bone formation with micro CT	• What is the optimal method of harvesting hMSCs from patients? • How do transcript levels of osteogenic genes correlate with protein levels? • Is micro CT an accurate measure of bone formation *in vitro*? • Do MSCs promote bone formation in mineralised scaffolds *in vivo*?
3. To fabricate a fibrillar collagen scaffold containing the growth factor BMP-2 and study its release profile	• Collagen scaffold was combined with BMP-2 using three methods: integration, adsorption and layer-by-layer • BMP-2 release from LBL scaffolds was sustained and phasic • LBL scaffolds displayed maintained porous structure and significantly higher denaturation temperature	• What is the long-term release profile of BMP-2 from these scaffolds? • How does the presence of BMP-2 affect osteogenesis of hMSCs? • What is the effect of BMP-2-containing scaffolds *in vivo*? • Can the collagen scaffold act as a carrier system for other growth factors or drugs?

Table 7.1
Summary of thesis findings

Chapter 8 References

Adams, M.A. & Dolan, P., 2012. Intervertebral disc degeneration: evidence for two distinct phenotypes. *Journal of Anatomy*, 221(6), pp.497-506.

Adams, M.A. & Roughley, P.J., 2006. What is intervertebral disc degeneration, and what causes it? *Spine*, 31(18), pp.2151–2161.

Aebi, M., 2005. The adult scoliosis. *European Spine Journal*, 14(10), pp.925–948.

Alanay, A. et al., 2008. The adjunctive effect of a binding peptide on bone morphogenetic protein enhanced bone healing in a rodent model of spinal fusion. *Spine*, 33(16), pp.1709–1713.

Albee, F.H., 2007. Transplantation of a portion of the tibia into the spine for Pott's disease: a preliminary report 1911. *Clinical Orthopaedics and Related Research*, 460, pp.14–16.

Albert, T.J. et al., 1995. Health Outcome Assessment Before and After Adult Deformity Surgery - a Prospective-Study. *Spine*, 20(18), pp.2002–2004.

Amrutkar, J.R. & Gattani, S.G., 2009. Chitosan-chondroitin sulfate based matrix tablets for colon specific delivery of indomethacin. *AAPS PharmSciTech*, 10(2), pp.670–677.

An, H.S. et al., 1995. Comparison between allograft plus demineralized bone matrix versus autograft in anterior cervical fusion. A prospective multicenter study. *Spine*, 20(20), pp.2211-2216.

Anasetti, F. et al., 2010. Spine stability after implantation of an interspinous device: an in vitro and finite element biomechanical study. *Journal of Neurosurgery: Spine*, 13(5), pp.568–575.

Andersen, T.T. et al., 2001. Smoking as a predictor of negative outcome in lumbar spinal fusion. *Spine*, 26(23), pp.2623–2628.

Anderson, N.L. & Anderson, N.G., 2002. The human plasma proteome: history, character, and diagnostic prospects. *Molecular & cellular proteomics : MCP*, 1(11), pp.845–867.

Andersson, G., 1999. Epidemiological features of chronic low-back pain. *The Lancet*, 354(9178), pp.581-585.

Aono, A. et al., 1995. Potent ectopic bone-inducing activity of bone morphogenetic protein-4/7 heterodimer. *Biochemical and Biophysical Research Communications*, 210(3), pp.670-677.

Apkarian, A.V. et al., 2004. Chronic back pain is associated with decreased prefrontal and thalamic gray matter density. *The Journal of Neuroscience*, 24(46), pp.10410-10415.

Arahira, T. & Todo, M., 2014. Effects of Proliferation and Differentiation of Mesenchymal Stem Cells on Compressive Mechanical Behavior of

Collagen/beta-TCP Composite Scaffold. *Journal of the Mechanical Behavior of Biomedical Materials*, 39, pp.218–230.

Arce, C.A. & Dohrmann, G.J., 1985. Herniated thoracic disks. *Neurologic clinics*, 3(2), pp.383–392.

Arosarena, O.A. & Collins, W.L., 2005. Bone regeneration in the rat mandible with bone morphogenetic protein-2: a comparison of two carriers. *Otolaryngology -- Head and Neck Surgery*, 132(4), pp.592–597.

Arya, N. et al., 2012. Recapitulating tumour microenvironment in chitosan-gelatin three-dimensional scaffolds: an improved in vitro tumour model. *Journal of the Royal Society, Interface / the Royal Society*, 9(77), pp.3288–3302.

Astori, G. et al., 2007. "In vitro" and multicolor phenotypic characterization of cell subpopulations identified in fresh human adipose tissue stromal vascular fraction and in the derived mesenchymal stem cells. *Journal of translational medicine*, 5, p.55.

Autefage, H. et al., 2009. Adsorption and release of BMP-2 on nanocrystalline apatite-coated and uncoated hydroxyapatite/β-tricalcium phosphate porous ceramics. *Journal of Biomedical Materials Research Part B: Applied Biomaterials*, 91B(2), pp.706–715.

Bauer, F.C. & Urist, M.R., 1981. Human osteosarcoma-derived soluble bone morphogenetic protein. *Clinical Orthopaedics and Related Research*, (154), pp.291–295.

Bear, R.S., 1952. The structure of collagen fibrils. *Advances in protein chemistry*, 7, pp.69–160.

Beebe, F.A., Barkin, R.L. & Barkin, S., 2005. A clinical and pharmacologic review of skeletal muscle relaxants for musculoskeletal conditions. *American Journal of Therapeutics*, 12(2), pp.151–171.

Belbachir, K. et al., 2009. Collagen types analysis and differentiation by FTIR spectroscopy. *Analytical and bioanalytical chemistry*, 395(3), pp.829–837.

Bessa, P.C., Casal, M. & Reis, R.L., 2008a. Bone morphogenetic proteins in tissue engineering: the road from the laboratory to the clinic, part I (basic concepts). *Journal of tissue engineering and regenerative medicine*, 2(1), pp.1–13.

Bessa, P.C., Pedro, A.J., et al., 2008b. Osteoinduction in human fat-derived stem cells by recombinant human bone morphogenetic protein-2 produced in Escherichia coli. *Biotechnology Letters*, 30(1), pp.15–21.

Bessey, O.A., Lowry, O.H. & Brock, M.J., 1946. A method for the rapid determination of alkaline phosphates with five cubic millimeters of serum. *J Biol Chem*, 164, pp.321–329.

Bhattarai N., Gunn, J. & Zhang M., 2010. Chitosan-based hydrogels for controlled, localized drug delivery. *Adv Drug Deliv Rev.*, 62(1), pp.83–99.

Bhattarai, N., Li Z., Edmondson, D. & Zhang, M., 2006. Alginate-Based Nanofibrous Scaffolds: Structural, Mechanical, and Biological Properties. *Advanced Materials*, 18(11), pp.1463–1467.

Birmingham, E.E. et al., 2012. Osteogenic differentiation of mesenchymal stem cells is regulated by osteocyte and osteoblast cells in a simplified bone niche. *European Cells and Materials*, 23, pp.13–27.

Boden, S.D. et al., 1990. Abnormal magnetic-resonance scans of the lumbar spine in asymptomatic subjects. A prospective investigation. *Journal of Bone and Joint Surgery (American)*, 72(3), pp.403–408.

Boden, S.D. et al., 1998. Lumbar spine fusion by local gene therapy with a cDNA encoding a novel osteoinductive protein (LMP-1). *Spine*, 23(23), pp.2486–2492.

Boden, S.D. et al., 2000. The use of rhBMP-2 in interbody fusion cages - Definitive evidence of osteoinduction in humans: A preliminary report. *Spine*, 25(3), pp.376–381.

Boden, S.D. et al., 2002. Use of recombinant human bone morphogenetic protein-2 to achieve posterolateral lumbar spine fusion in humans - A prospective, randomized clinical pilot trial - 2002 Volvo Award in clinical studies. *Spine*, 27(23), pp.2662–2673.

Bonewald, L.F., 1999. Establishment and characterization of an osteocyte-like cell line, MLO-Y4. *Journal of bone and mineral metabolism*, 17(1), pp.61–65.

Boos, N. et al., 2002. Classification of age-related changes in lumbar intervertebral discs: 2002 Volvo Award in basic science. *Spine*, 27(23), pp.2631–2644.

Boyan, B.D. et al., 1992. Initial effects of partially purified bone morphogenetic protein on the expression of glycosaminoglycan, collagen, and alkaline phosphatase in nonunion cell cultures. *Clinical Orthopaedics and Related Research*, (278), pp.286–304.

Boyle, W.J., Simonet, W.S. & Lacey, D.L., 2003. Osteoclast differentiation and activation. *Nature*, 423(6937), pp.337–342.

Braccini, A. et al., 2005. Three-dimensional perfusion culture of human bone marrow cells and generation of osteoinductive grafts. *Stem cells*, 23(8), pp.1066–1072.

Bradford, D.S., Tay, B.K. & Hu, S.S., 1999. Adult scoliosis: surgical indications, operative management, complications, and outcomes. *Spine*, 24(24), pp.2617–2629.

Bresalier, R.S. et al., 2005. Cardiovascular events associated with rofecoxib in a colorectal adenoma chemoprevention trial. *New England Journal of Medicine*, 352(11), pp.1092–1102.

Bridwell, K.H. et al., 2009. Does treatment (nonoperative and operative) improve the two-year quality of life in patients with adult symptomatic lumbar scoliosis: a prospective multicenter evidence-based medicine study. *Spine*, 34(20), pp.2171–2178.

Browder, D.A. et al., 2007. Effectiveness of an extension-oriented treatment approach in a subgroup of subjects with low back pain: a randomized clinical trial. *Physical Therapy*, 87(12), pp.1608–1609.

Brown, M.A. et al., 2005. Crystal structure of BMP-9 and functional interactions with pro-region and receptors. *Journal of Biological Chemistry*, 280(26), pp.251118-25118.

Brox, J.I. et al., 2010. Four-year follow-up of surgical versus non-surgical therapy for chronic low back pain. *Annals of the Rheumatic Diseases*, 69(9), pp.1643–1648.

Brox, J.I. et al., 2006. Lumbar instrumented fusion compared with cognitive intervention and exercises in patients with chronic back pain after previous surgery for disc herniation: a prospective randomized controlled study. *Pain*, 122(1-2), pp.145-155.

Brox, J.I. et al., 2003. Randomized clinical trial of lumbar instrumented fusion and cognitive intervention and exercises in patients with chronic low back pain and disc degeneration. *Spine*, 28(17), pp.1913–1921.

Bubnis, W.A. & Ofner, C.M.3., 1992. The determination of epsilon-amino groups in soluble and poorly soluble proteinaceous materials by a spectrophotometric method using trinitrobenzenesulfonic acid. *Analytical biochemistry*, 207(1), pp.129–133.

Buckalew, N. et al., 2008. Chronic pain is associated with brain volume loss in older adults: preliminary evidence. *Pain medicine (Malden, Mass.)*, 9(2), pp.240–248.

Burger, E.H., Klein-Nulend, J. & Smit, T.H., 2003. Strain-derived canalicular fluid flow regulates osteoclast activity in a remodelling osteon—a proposal. *Journal of Biomechanics*, 36(10), pp.1453-1459.

Burkus, J.K. et al., 2002. Anterior lumbar interbody fusion using rhBMP-2 with tapered interbody cages. *Journal of Spinal Disorders & Techniques*, 15(5), pp.337–349.

Burkus, J.K. et al., 2005. Use of rhBMP-2 in combination with structural cortical allografts: clinical and radiographic outcomes in anterior lumbar spinal surgery. *The Journal of Bone and Joint Surgery. American volume*, 87(6), pp.1205-1212.

Buttermann, G.R. et al., 1997. Revision of failed lumbar fusions: a comparison of anterior autograft and allograft. *Spine*, 22(23), pp.2748-2755.

Cahill, K.S. et al., 2009. Prevalence, complications, and hospital charges associated with use of bone-morphogenetic proteins in spinal fusion procedures. *JAMA*, 302(1), pp.58–66.

Campbell, J.J. et al., 2011. A Multifunctional 3D Co-Culture System for Studies of Mammary Tissue Morphogenesis and Stem Cell Biology. *PLoS ONE*, 6(9), p.e25661.

Caplan, A.I., 2005. Review: mesenchymal stem cells: cell-based reconstructive therapy in orthopedics. *Tissue Eng.*, 11(7-8), pp.1198–1211.

Carragee, E.J., Alamin, T.F. & Carragee, J.M., 2006. Low-pressure positive discography in subjects asymptomatic of significant low back pain illness. *Spine*, 31(5), pp.505–509.

Carreon, L.Y. et al., 2005. Platelet gel (AGF) fails to increase fusion rates in instrumented posterolateral fusions. *Spine*, 30(9), pp.E243–E246.

Carter, O.D. & Haynes, S.G., 1987. Prevalence rates for scoliosis in US adults: results from the first National Health and Nutrition Examination Survey. *International journal of epidemiology*, 16(4), 537-544.

Celeste, A.J. et al., 1990. Identification of transforming growth factor beta family members present in bone-inductive protein purified from bovine bone. *Proc Natl Acad Sci U S A*, 87(24), pp.9843–9847.

Chang, C. et al., 2001. Twisted gastrulation can function as a BMP antagonist. *Nature*, 410(6827), pp.483-487.

Chang, V., Gonzalez, P. & Akuthota, V., 2008. Evidence-informed management of chronic low back pain with adjunctive analgesics. *Spine Journal: Official Journal of the North American Spine Society*, 8(1), pp.21–27.

Charosky, S. et al., 2012. Complications and risk factors of primary adult scoliosis surgery: a multicenter study of 306 patients. *Spine*, 37(8), pp.693–700.

Chen, F.-M. et al., 2009. In vitro cellular responses to scaffolds containing two microencapulated growth factors. *Biomaterials*, 30(28), pp.5215–5224.

Chen, W.J. et al., 2005. The fusion rate of calcium sulfate with local autograft bone compared with autologous iliac bone graft for instrumented short-segment spinal fusion. *Spine*, 30(20), pp.2293-2297.

Chen, Y.G. et al., 1998. Determinants of specificity in TGF-beta signal transduction. *Genes Dev*, 12(14), pp.2144–2152.

Chen, Z. et al., 2012. Recombinant human bone morphogenetic protein-2 versus autogenous iliac crest bone graft for lumbar fusion: a meta-analysis of ten

randomized controlled trials. *Archives of Orthopaedic & Trauma Surgery*, 132(12), pp.1725–1740.

Chien, C.S. et al., 2012. Incorporation of exudates of human platelet-rich fibrin gel in biodegradable fibrin scaffolds for tissue engineering of cartilage. *Journal of Biomedical Materials Research. Part B, Applied Biomaterials*, 100(4), pp.948–955.

Childs, J.D. et al., 2004. A clinical prediction rule to identify patients with low back pain most likely to benefit from spinal manipulation: A validation study. *Annals of Internal Medicine*, 141(12), pp.920–928.

Cho, S.K.S. et al., 2012. Major complications in revision adult deformity surgery: risk factors and clinical outcomes with 2- to 7-year follow-up. *Spine*, 37(6), pp.489–500.

Choi, Y. et al., 2007. A bridging demineralized bone implant facilitates posterolateral lumbar fusion in New Zealand white rabbits. *Spine*, 32(1), pp.36–41.

Choong, C.S. et al., 2006. Co-culture of bone marrow fibroblasts and endothelial cells on modified polycaprolactone substrates for enhanced potentials in bone tissue engineering. *Tissue Engineering*, 12(9), pp.2521–2531.

Choong, C. et al., 2012. Optimization of poly(ε-caprolactone) surface properties for apatite formation and improved osteogenic stimulation. *Journal of biomedical materials research. Part A*, 100A(2), pp.353–361.

Chou, R. & Huffman, L.H., 2007. Nonpharmacologic therapies for acute and chronic low back pain: A review of the evidence for an American pain Society/American college of physicians clinical practice guideline. *Annals of Internal Medicine*, 147(7), pp.492–504.

Chou, R. et al., 2009. Interventional Therapies, Surgery, and Interdisciplinary Rehabilitation for Low Back Pain An Evidence-Based Clinical Practice Guideline From the American Pain Society. *Spine*, 34(10), pp.1066–1077.

Chou, R. et al., 2007. Medications for acute and chronic low back pain: a review of the evidence for an American Pain Society/American College of Physicians clinical practice guideline. *Annals of Internal Medicine*, 147(7), pp.505–514.

Chvapil, M., 1977. Collagen sponge: theory and practice of medical applications. *Journal of Biomedical Materials Research Part B: Applied Biomaterials*, 11(5), pp.721–741.

Clark, S.L. & Hammond, P.T., 2000. The Role of Secondary Interactions in Selective Electrostatic Multilayer Deposition. *Langmuir*, 16(26), pp.10206–10214.

Clarke, B., 2008. Normal bone anatomy and physiology. *Clinical journal of the American Society of Nephrology*, 3 Suppl 3, pp.S131–9.

Cohen, D.B. et al., 2000. Pseudarthrosis repair: Autogenous iliac crest versus femoral ring allograft. *Clinical Orthopaedics and Related Research*, (371), pp.46–55.

Colom, A. et al., 2013. Oxygen diffusion and consumption in extracellular matrix gels: Implications for designing 3D cultures. *Journal of Biomedical Materials Research. Part A*, 102(8), pp.2776-2784.

Connolly, J.F., 1998. Clinical use of marrow osteoprogenitor cells to stimulate osteogenesis. *Clinical Orthopaedics and Related Research*, (355 Suppl), pp.S257–S266.

Cooper, R.G. et al., 1995. Herniated intervertebral disc-associated periradicular fibrosis and vascular abnormalities occur without inflammatory cell infiltration. *Spine*, 20(5), pp.591–598.

Costa, R.R. & Mano, J.F., 2014. Polyelectrolyte multilayered assemblies in biomedical technologies. *Chemical Society Reviews*, 43(10), pp.3453–3479.

Cox, G. et al., 2011. The use of the reamer-irrigator-aspirator to harvest mesenchymal stem cells. *Journal of Bone & Joint Surgery - British Volume*, 93(4), pp.517–524.

Croll, T.I. et al., 2006. A blank slate? Layer-by-layer deposition of hyaluronic acid and chitosan onto various surfaces. *Biomacromolecules*, 7(5), pp.1610–1622.

Crombez, G. et al., 1999. Pain-related fear is more disabling than pain itself: evidence on the role of pain-related fear in chronic back pain disability. *Pain*, 80(1-2), pp.329–339.

Cui, Q. et al., 2001. Comparison of lumbar spine fusion using mixed and cloned marrow cells. *Spine*, 26(21), pp.2305–2310.

Cui, Y. et al., 1998. BMP-4 is proteolytically activated by furin and/or PC6 during vertebrate embryonic development. *The EMBO journal*, 17(16), pp.4735-4743.

Dallari, D., Savarino, L. & Stagni, C., 2007. Enhanced tibial osteotomy healing with use of bone grafts supplemented with platelet gel or platelet gel and bone marrow stromal cells. *The Journal of Bone and Joint Surgery. American volume*, 89(11), pp.2413-2420.

Danneels, L.A. et al., 2001. Effects of three different training modalities on the cross sectional area of the lumbar multifidus muscle in patients with chronic low back pain. *British Journal of Sports Medicine*, 35(3), pp.186–191.

Davison, P.F. et al., 1967. Serologic Specificity of Tropocollagen Telopeptides. *Journal of Experimental Medicine*, 126(2), pp.331–346.

Dawson, E. et al., 2009. Recombinant human bone morphogenetic protein-2 on an absorbable collagen sponge with an osteoconductive bulking agent in

posterolateral arthrodesis with instrumentation. A prospective randomized trial. *The Journal of bone and joint surgery. American volume*, 91(7), pp.1604-1613.

Dawson, E.G., Lotysch, M. & Urist, M.R., 1981. Intertransverse process lumbar arthrodesis with autogenous bone graft. *Clinical Orthopaedics and Related Research*, (154), pp.90–96.

Decher, G. & Hong, J.D., 1991. Buildup of Ultrathin Multilayer Films by a Self-Assembly Process: II. Consecutive Adsorption of Anionic and Cationic Bipolar Amphiphiles and Polyelectrolytes on Charged Surfaces. *Berichte der Bunsengesellschaft für physikalische Chemie*, 95(11), pp.1430–1434.

Declercq, H.A. et al., 2013. The role of scaffold architecture and composition on the bone formation by adipose derived stem cells. *Tissue Engineering. Part A*, 20(1-2), pp.434-444.

DeForest, C.A. & Anseth, K.S., 2012. Photoreversible patterning of biomolecules within click-based hydrogels. *Angewandte Chemie (International ed. in English)*, 51(8), pp.1816–1819.

Deyo, R.A. & Weinstein, J.N., 2001. Low Back Pain. *New England Journal of Medicine*, 344(5), pp.363–370.

Dimar, J.R. et al., 2009. Clinical and radiographic analysis of an optimized rhBMP-2 formulation as an autograft replacement in posterolateral lumbar spine arthrodesis. *The Journal of Bone and Joint Surgery. American volume*, 91(6), pp.1377-1386.

Dimar, J.R. et al., 2006. Clinical outcomes and fusion success at 2 years of single-level instrumented posterolateral fusions with recombinant human bone morphogenetic protein-2/compression resistant matrix versus iliac crest bone graft. *Spine*, 31(22), pp.2534-2539.

Ding, M. et al., 1997. Age variations in the properties of human tibial trabecular bone. *Journal of Bone & Joint Surgery - British Volume*, 79(6), pp.995–1002.

Dobnig, H.H. & Turner, R.T.R., 1995. Evidence that intermittent treatment with parathyroid hormone increases bone formation in adult rats by activation of bone lining cells. *Endocrinology*, 136(8), pp.3632–3638.

Dominici, M. et al., 2006. Minimal criteria for defining multipotent mesenchymal stromal cells. The International Society for Cellular Therapy position statement. *Cytotherapy*, 8(4), pp.315–317.

Douglas, T. et al., 2006. Fibrillogenesis of collagen types I, II, and III with small leucine-rich proteoglycans decorin and biglycan. *Biomacromolecules*, 7(8), pp.2388–2393.

Ducy, P. et al., 1997. Osf2/Cbfa1: a transcriptional activator of osteoblast differentiation. *Cell*, 89(5), pp.747–754.

Ekman, P. et al., 2009. A prospective randomised study on the long-term effect of lumbar fusion on adjacent disc degeneration. *European Spine Journal*, 18(8), pp.1175–1186.

Ellingsworth, L.R. et al., 1986. The human immune response to reconstituted bovine collagen. *Journal of immunology (Baltimore, Md. : 1950)*, 136(3), pp.877–882.

Elsdale, T.A., Bard, J., 1972. Collagen substrata for studies on cell behaviour. *Journal of Cell Biology*, 54(3), pp.626–637.

Emery, S.E. et al., 1994. Robinson anterior cervical fusion comparison of the standard and modified techniques. *Spine*, 19(6), pp.660–663.

Epstein, J.A., Epstein, B.S. & Jones, M.D., 1979. Symptomatic lumbar scoliosis with degenerative changes in the elderly. *Spine*, 4(6), pp.542–547.

Epstein, N.E., 2006. A preliminary study of the efficacy of Beta Tricalcium Phosphate as a bone expander for instrumented posterolateral lumbar fusions. *Journal of Spinal Disorders & Techniques*, 19(6), pp.424–429.

Epstein, N.E., 2012. Iliac crest autograft versus alternative constructs for anterior cervical spine surgery: Pros, cons, and costs. *Surgical Neurology International*, 3(Suppl 3), pp.S143–56.

Fairbank, J. et al., 2005. Randomised controlled trial to compare surgical stabilisation of the lumbar spine with an intensive rehabilitation programme for patients with chronic low back pain: the MRC spine stabilisation trial. *British Medical Journal*, 330(7502), pp.1233.

Fairbank, J.C. & Pynsent, P.B., 2000. The Oswestry Disability Index. *Spine*, 25(22), pp.2940–2952.

Fei, Z. et al., 2008. Preparation and property of a novel bone graft composite consisting of rhBMP-2 loaded PLGA microspheres and calcium phosphate cement. *Journal of Materials Science. Materials in Medicine*, 19(3), pp.1109–1116.

Fierro, B. et al., 2010. Repetitive transcranial magnetic stimulation (rTMS) of the dorsolateral prefrontal cortex (DLPFC) during capsaicin-induced pain: modulatory effects on motor cortex excitability. *Experimental brain research*, 203(1), pp.31–38.

Fishbain, D., 2000. Evidence-based data on pain relief with antidepressants. *Annals of Medicine*, 32(5), pp.305–316.

Fisher, J.P. et al., 2004. Thermoreversible hydrogel scaffolds for articular cartilage engineering. *Journal of biomedical materials research. Part A*, 71(2), pp.268–274.

Flandin, F., Buffevant, C. & Herbage, D., 1984. A differential scanning calorimetry

analysis of the age-related changes in the thermal stability of rat skin collagen. *Biochimica et Biophysica Acta*, 791(2), pp.205-211.

Flynn, T. et al., 2002. A clinical prediction rule for classifying patients with low back pain who demonstrate short-term improvement with spinal manipulation. *Spine*, 27(24), pp.2835–2843.

Frame, J.W., Brady, C.L. & Browne, R.M., 1981. Augmentation of the edentulous mandible using bone and hydroxyapatite: a comparative study in dogs. *International Journal of Oral Surgery*, 10(Suppl 1), pp.88–92.

France, J.C., Yaszemski, M.J., Lauerman, W.C., Cain, J.E., et al., 1999. A randomized prospective study of posterolateral lumbar fusion. Outcomes with and without pedicle screw instrumentation. *Spine*, 24(6), pp.553–560.

Fraser, J.F. & Härtl, R., 2007. Anterior approaches to fusion of the cervical spine: a metaanalysis of fusion rates. *Journal of Neurosurgery: Spine*, 6(4), pp.298–303.

Freyman, T.M., Yannas, I.V. & Gibson, L.J., Cellular materials as porous scaffolds for tissue engineering. *Progress in Materials Science*, 46(3–4), pp.273–282.

Fritz, J.M., Whitman, J.M. & Childs, J.D., 2005. Lumbar spine segmental mobility assessment: an examination of validity for determining intervention strategies in patients with low back pain. *Archives of physical medicine and rehabilitation*, 86(9), pp.1745–1752.

Fritzell, P. et al., 2001. 2001 Volvo Award winner in clinical studies: Lumbar fusion versus nonsurgical treatment for chronic low back pain - A multicenter randomized controlled trial from the Swedish Lumbar Spine Study Group. *Spine*, 26(23), pp.2521–2532.

Fu, K.-M.G. et al., 2014. Patients with adult spinal deformity treated operatively report greater baseline pain and disability than patients treated nonoperatively; however, deformities differ between age groups. *Spine*, 39(17), pp.1401–1407.

Fu, R. et al., 2013. Effectiveness and harms of recombinant human bone morphogenetic protein-2 in spine fusion: a systematic review and meta-analysis. *Annals of Internal Medicine*, 158(12), pp.890–902.

Gale, M. et al., 1995. Sequential assembly of collagen revealed by atomic force microscopy. *Biophysical journal*, 68(5), pp.2124-2128.

García, A.J. & Reyes, C.D., 2005. Bio-adhesive surfaces to promote osteoblast differentiation and bone formation. *Journal of Dental Research*, 84(5), pp.407-413.

Gaur, T. et al., 2005. Canonical WNT signaling promotes osteogenesis by directly stimulating Runx2 gene expression. *Journal of Biological Chemistry*, 280(39), pp.33132–33140.

Gazzerro, E., Deregowski, V., et al., 2005a. Overexpression of twisted gastrulation inhibits bone morphogenetic protein action and prevents osteoblast cell differentiation in vitro. *Endocrinology*, 146(9), pp.3875–3882.

Gazzerro, E., Gangji, V. & Canalis, E., 1998. Bone morphogenetic proteins induce the expression of noggin, which limits their activity in cultured rat osteoblasts. *Journal of Clinical Investigation*, 102(12), pp.2106–2114.

Gazzerro, E., Pereira, R.C., et al., 2005b. Skeletal overexpression of gremlin impairs bone formation and causes osteopenia. *Endocrinology*, 146(2), pp.655–665.

Gazzerro, E.E. & Canalis, E.E., 2006. Bone morphogenetic proteins and their antagonists. *Reviews in Endocrine & Metabolic Disorders*, 7(1-2), pp.51–65.

Geiger, M., Li, R.H. & Friess, W., 2003. Collagen sponges for bone regeneration with rhBMP-2. *Advanced Drug Delivery Reviews*, 55(12), pp.1613–1629.

Gelinsky, M. et al., 2008. Porous three-dimensional scaffolds made of mineralised collagen: Preparation and properties of a biomimetic nanocomposite material for tissue engineering of bone. *Porous Inorganic Materials for Biomedical Applications*, 137(1), pp.84–96.

Giannotti, S. et al., 2013. Use of Autologous Human mesenchymal Stromal Cell/Fibrin Clot Constructs in Upper Limb Non-Unions: Long-Term Assessment. *PLoS ONE*, 8(8), p.e73893.

Giannoudis, P.V., Einhorn, T.A. & Marsh, D., 2007. Fracture healing: the diamond concept. *Injury*, 38 Suppl 4, pp.S3–S6.

Gibson, L.J., 2000. Mechanical behavior of metallic foams. *Annual Review of Materials Science*, 30(1), pp.191-227.

Giesecke, T. et al., 2004. Evidence of augmented central pain processing in idiopathic chronic low back pain. *Arthritis and Rheumatism*, 50(2), pp.613–623.

Girardi, F.P. & Cammisa, F.P.J., 2003. The effect of bone graft extenders to enhance the performance of iliac crest bone grafts in instrumented lumbar spine fusion. *Orthopedics*, 26(5 Suppl), pp.s545–8.

Glassman, S.D. et al., 2008. RhBMP-2 versus iliac crest bone graft for lumbar spine fusion: a randomized, controlled trial in patients over sixty years of age. *Spine*, 33(26), pp.2843-2849.

Glassman, S.D. et al., 2000. The effect of cigarette smoking and smoking cessation on spinal fusion. *Spine*, 25(20), pp.2608–2615.

Glassman, S.D. et al., 1998. The Effect of Postoperative Nonsteroidal Anti-inflammatory Drug Administration on Spinal Fusion. *Spine*, 23(7), p.834.

Gottfried, O.N. & Dailey, A.T., 2008. Mesenchymal stem cell and gene therapies for spinal fusion. *Neurosurgery*, 63(3), pp.380–382.

Goz, V. et al., 2013. Comparison of complications, costs, and length of stay of three different lumbar interbody fusion techniques: an analysis of the Nationwide Inpatient Sample database. *Spine Journal: Official Journal of the North American Spine Society*, pp.S1529-9430(13)01965-7

Griffith, D.L., Keck, P.C. & Sampath, T.K., 1996. Three-dimensional structure of recombinant human osteogenic protein 1: structural paradigm for the transforming growth factor beta superfamily. *Proceedings of the National Academy of Sciences of the U S A*, 93(2), pp.878-883.

Grubb, S.A. & Kelly, C.K., 2000. Cervical discography: clinical implications from 12 years of experience. *Spine*, 25(11), pp.1382–1389.

Gruskay, J.A. et al., 2014. Factors Affecting Length of Stay and Complications Following Elective Anterior Cervical Discectomy and Fusion: A Study of 2164 Patients From The American College of Surgeons National Surgical Quality Improvement Project Database (ACS NSQIP). *Journal of Spinal Disorders & Techniques*. Feb 12, Epub.

Gupta, M.C. et al., 2007. Efficacy of mesenchymal stem cell enriched grafts in an ovine posterolateral lumbar spine model. *Spine*, 32(7), pp.720–727.

Haid, R.W., Jr et al., 2004. Posterior lumbar interbody fusion using recombinant human bone morphogenetic protein type 2 with cylindrical interbody cages. *Spine Journal: Official Journal of the North American Spine Society*, 4(5), pp.527–538.

Haidar, Z.S., Hamdy, R.C. & Tabrizian, M., 2009a. Delivery of recombinant bone morphogenetic proteins for bone regeneration and repair. Part A: Current challenges in BMP delivery. *Biotechnology Letters*, 31(12), pp.1817–1824.

Haidar, Z.S., Hamdy, R.C. & Tabrizian, M., 2009b. Delivery of recombinant bone morphogenetic proteins for bone regeneration and repair. Part B: Delivery systems for BMPs in orthopaedic and craniofacial tissue engineering. *Biotechnology Letters*, 31(12), pp.1825–1835.

Hale, M.E. et al., 1999. Efficacy and safety of controlled-release versus immediate-release oxycodone: randomized, double-blind evaluation in patients with chronic back pain. *Clinical Journal of Pain*, 15(3), pp.179–183.

Halloran, D.M.O. et al., 2006. Characterization of a microbial transglutaminase cross-linked type II collagen scaffold. *Tissue Eng.*, 12(6), pp.1467–1474.

Han, X. et al., 2009. A meta-analysis of circumferential fusion versus instrumented posterolateral fusion in the lumbar spine. *Spine*, 34(17), pp.E618–25.

Harris, J.R., Soliakov, A. & Lewis, R.J., 2013. In vitro fibrillogenesis of collagen type

I in varying ionic and pH conditions. *Micron*, 49, pp.60–68.

Hartman, O. et al., 2009. Microfabricated electrospun collagen membranes for 3-D cancer models and drug screening applications. *Biomacromolecules*, 10(8), pp.2019–2032.

Hauge, E.M. et al., 2001. Cancellous bone remodeling occurs in specialized compartments lined by cells expressing osteoblastic markers. *Journal of Bone and Mineral Research*, 16(9), pp.1575–1582.

Hazama et al., 1995. Efficient Expression of a Heterodimer of Bone Morphogenetic Protein Subunits Using a Baculovirus Expression System. *Biochemical and Biophysical Research Communications*, 209(3), pp.8–8.

He, X. et al., 2014. Enhanced healing of rat calvarial defects with MSCs loaded on BMP-2 releasing chitosan/alginate/hydroxyapatite scaffolds. *PLoS ONE*, 9(8), pp.e104061–e104061.

Hee, H.T. et al., 2003. Do autologous growth factors enhance transforaminal lumbar interbody fusion? *European Spine Journal*, 12(4), pp.400–407.

Heiple, K.G., Chase, S.W. & Herndon, C.H., 1963. A comparative study of the healing process following different types of bone transplantation. *The Journal of Bone & Joint Surgery. American volume*, 45, pp.1593-1616.

Hendrich, C. et al., 2009. Safety of autologous bone marrow aspiration concentrate transplantation: initial experiences in 101 patients. *Orthopedic Reviews*, 1(2), pp.e32–e32.

Hernández-Díaz, S.S. & García-Rodríguez, L.A.L., 2001. Epidemiologic assessment of the safety of conventional nonsteroidal anti-inflammatory drugs. *The American Journal of Medicine*, 110 Suppl 3A, pp.20S–27S.

Hicks, G.E. et al., 2005. Preliminary development of a clinical prediction rule for determining which patients with low back pain will respond to a stabilization exercise program. *Archives of physical medicine and rehabilitation*, 86(9), pp.1753–1762.

Hollister, S.J., 2005. Porous scaffold design for tissue engineering. *Nature Materials*, 4(7), pp.518–524.

Hu, B.-H. & Messersmith, P.B., 2005. Enzymatically cross-linked hydrogels and their adhesive strength to biosurfaces. *Orthodontics & craniofacial research*, 8(3), pp.145–149.

Hwang, C.M. et al., 2008. Microfluidic chip-based fabrication of PLGA microfiber scaffolds for tissue engineering. *Langmuir*, 24(13), pp.6845–6851.

Iler, R.K., Multilayers of colloidal particles. *Journal of Colloid and Interface Science*, 21(6), pp.569–594.

Israel, D.I. et al., 1996. Heterodimeric bone morphogenetic proteins show enhanced activity in vitro and in vivo. *Growth factors (Chur, Switzerland)*, 13(3-4), pp.291–300.

Itoh, S. et al., 2004. Development of a hydroxyapatite/collagen nanocomposite as a medical device. *Cell Transplantation*, 13(4), pp.451–461.

Itoh, T.T. et al., 1998. Repair of ulnar segmental defect by recombinant human bone morphogenetic protein-2 in dogs. *Journal of Veterinary Medical Science*, 60(4), pp.451–458.

Iwasa, J. et al., 2003. Effects of cell density on proliferation and matrix synthesis of chondrocytes embedded in atelocollagen gel. *Artificial Organs*, 27(3), pp.249–255.

Jacobs, W.C.H., Vreeling, A. & de Kleuver, M., 2006. Fusion for low-grade adult isthmic spondylolisthesis: a systematic review of the literature. *European Spine Journal*, 15(4), pp.391–402.

Jaeger, A.A. et al., 2013. Microfabricated polymeric vessel mimetics for 3-D cancer cell culture. *Biomaterials*, 34(33), pp.8301–8313.

Janssen, M.E. et al., 2000. Biological cages. *European Spine Journal*, 9 Suppl 1, pp.S102–S109.

Jarcho, M., 1981. Calcium phosphate ceramics as hard tissue prosthetics. *Clinical Orthopaedics and Related Research*, (157), pp.259–278.

Jayakumar, R. et al., 2010. Novel chitin and chitosan nanofibers in biomedical applications. *Biotechnology Advances*, 28(1), pp.142–150.

Jäger, M. et al., 2011. Bridging the gap: bone marrow aspiration concentrate reduces autologous bone grafting in osseous defects. *Journal of Orthopaedic Research*, 29(2), pp.173–180.

Jeon, O. et al., 2007. Enhancement of ectopic bone formation by bone morphogenetic protein-2 released from a heparin-conjugated poly(L-lactic-co-glycolic acid) scaffold. *Biomaterials*, 28(17), pp.2763–2771.

Jones, C.F. & Grainger, D.W., 2009. In vitro assessments of nanomaterial toxicity. *Adv Drug Deliv Rev.*, 61(6), pp.438–456.

Jones, G.L. et al., 2010. Primary human osteoblast culture on 3D porous collagen-hydroxyapatite scaffolds. *Journal of biomedical materials research. Part A*, 94(4), pp.1244–1250.

Jones, M.E.R. & Messersmith, P.B., 2007. Facile coupling of synthetic peptides and peptide-polymer conjugates to cartilage via transglutaminase enzyme. *Biomaterials*, 28(35), pp.5215–5224.

Jorgenson, S.S. et al., 1994. A prospective analysis of autograft versus allograft in posterolateral lumbar fusion in the same patient. A minimum of 1-year follow-up in 144 patients. *Spine*, 19(18), pp.2048–2053.

Kagawa, R. et al., 2012. Chronological histological changes during bone regeneration on a non-crosslinked atelocollagen matrix. *Journal of bone and mineral metabolism*, 30(6), pp.638–650.

Kai, H. et al., 2009. Fabrication of a two-level tumor bone repair biomaterial based on a rapid prototyping technique. *Biofabrication*, 1(2), p.025003.

Kai, T., Shao-qing, G. & Geng-ting, D., 2003. In vivo evaluation of bone marrow stromal-derived osteoblasts-porous calcium phosphate ceramic composites as bone graft substitute for lumbar intervertebral spinal fusion. *Spine*, 28(15), pp.1653–1658.

Kaito, T. et al., 2005. Potentiation of the activity of bone morphogenetic protein-2 in bone regeneration by a PLA-PEG/hydroxyapatite composite. *Biomaterials*, 26(1), pp.73–79.

Kang, Q. et al., 2004. Characterization of the distinct orthotopic bone-forming activity of 14 BMPs using recombinant adenovirus-mediated gene delivery. *Gene Therapy*, 11(17), pp.1312–1320.

Karageorgiou, V. & Kaplan, D., 2005. Porosity of 3D biomaterial scaffolds and osteogenesis. *Biomaterials*, 26(27), pp.5474–5491.

Kavya, K.C. et al., 2012. Synthesis and characterization of chitosan/chondroitin sulfate/nano-SiO2 composite scaffold for bone tissue engineering. *Journal of Biomedical Nanotechnology*, 8(1), pp.149–160.

Kempen, D.H.R. et al., 2009. Effect of local sequential VEGF and BMP-2 delivery on ectopic and orthotopic bone regeneration. *Biomaterials*, 30(14), pp.2816–2825.

Kenley, R. et al., 1994. Osseous regeneration in the rat calvarium using novel delivery systems for recombinant human bone morphogenetic protein-2 (rhBMP-2). *Journal of Biomedical Materials Research*, 28(10), pp.1139-1147.

Khil, M.-S. et al., 2005. Novel fabricated matrix via electrospinning for tissue engineering. *Journal of Biomedical Materials Research Part B: Applied Biomaterials*, 72(1), pp.117–124.

Kikuchi, M. et al., 2001. Self-organization mechanism in a bone-like hydroxyapatite/collagen nanocomposite synthesized in vitro and its biological reaction in vivo. *Biomaterials*, 22(13), pp.1705–1711.

Kim, M.-S. et al., 2014. Prospective randomized, controlled trial of sinus grafting using Escherichia-coli-produced rhBMP-2 with a biphasic calcium phosphate

carrier compared to deproteinized bovine bone. *Clinical Oral Implants Research*, 00, pp.1-8, doi: 10.1111/clr.12471

Kim, S.-S., Gwak, S.-J. & Kim, B.-S., 2008. Orthotopic bone formation by implantation of apatite-coated poly(lactide-co-glycolide)/hydroxyapatite composite particulates and bone morphogenetic protein-2. *Journal of Biomedical Materials Research. Part A*, 87(1), pp.245–253.

Kirkaldy-Willis, W.H. & Farfan, H.F., 1982. Instability of the lumbar spine. *Clinical Orthopaedics and Related Research*, (165), pp.110–123.

Kirkbride, K.C. et al., 2008. Bone morphogenetic proteins signal through the transforming growth factor-beta type III receptor. *J Biol Chem*, 283(12), pp.7628–7637.

Kirker-Head, C.A., 2000. Potential applications and delivery strategies for bone morphogenetic proteins. *Advanced Drug Delivery Reviews*, 43(1), pp.65–92.

Kitoh, H. et al., 2007. Transplantation of culture expanded bone marrow cells and platelet rich plasma in distraction osteogenesis of the long bones. *Bone*, 40(2), pp.522-528.

Ko, E.C. et al., 2012. BMP-2 embedded atelocollagen scaffold for tissue-engineered cartilage cultured in the medium containing insulin and triiodothyronine--a new protocol for three-dimensional in vitro culture of human chondrocytes. *Tissue Engineering Part*

Ko, L., Ma, G.X. & Gao, H.L., 1990. Purification and chemical modification of porcine bone morphogenetic protein. *Clinical Orthopaedics and Related Research*, (256), pp.229–237.

Kobayashi, Y. et al., 2009. Augmented cerebral activation by lumbar mechanical stimulus in chronic low back pain patients: an FMRI study. *Spine*, 34(22), pp.2431–2436.

Kolf, C.M., Cho, E. & Tuan, R.S., 2007. Mesenchymal stromal cells. Biology of adult mesenchymal stem cells: regulation of niche, self-renewal and differentiation. *Arthritis research & therapy*, 9(1), pp.204–204.

Kozak, J.A., Heilman, A.E. & O'Brien, J.P., 1994. Anterior lumbar fusion options. Technique and graft materials. *Clinical Orthopaedics and Related Research*, (300), pp.45–51.

Kraiwattanapong, C. et al., 2005. Comparison of Healos/bone marrow to INFUSE(rhBMP-2/ACS) with a collagen-ceramic sponge bulking agent as graft substitutes for lumbar spine fusion. *Spine*, 30(9), pp.1001–1007.

Kruger, E.A. et al., 2011. In vitro mineralization of human mesenchymal stem cells on three-dimensional type I collagen versus PLGA scaffolds: a comparative analysis. *Plastic and reconstructi*

Krummenacher, P. et al., 2010. Prefrontal cortex modulates placebo analgesia. *Pain*, 148(3), pp.368–374.

Kumar, G. et al., 2011. The determination of stem cell fate by 3D scaffold structures through the control of cell shape. *Biomaterials*, 32(35), pp.9188–9196.

Kurz, L.T., Garfin, S.R. & Booth, R.E., 1989. Harvesting Autogenous Iliac Bone-Grafts - a Review of Complications and Techniques. *Spine*, 14(12), pp.1324–1331.

Kuwahara, K. et al., 2011. Enzymatic crosslinking and degradation of gelatin as a switch for bone morphogenetic protein-2 activity. *Tissue Eng Part A.*, 17(23-24), pp.2955–2964.

Lai, C.-F. & Cheng, S.-L., 2002. Signal transductions induced by bone morphogenetic protein-2 and transforming growth factor-beta in normal human osteoblastic cells. *Journal of Biological Chemistry*, 277(18), pp.15514–15522.

Lee, K.S. et al., 2000. Runx2 is a common target of transforming growth factor beta1 and bone morphogenetic protein 2, and cooperation between Runx2 and Smad5 induces osteoblast-specific gene expression in the pluripotent mesenchymal precursor cell line C2C12. *Molecular & Cellular Biology*, 20(23), pp.8783–8792.

Lepperdinger, G., 2011. Inflammation and mesenchymal stem cell aging. *Current Opinion in Immunology*, 23(4), pp.518–524.

Liang, D. et al., 2005. [In vitro osteogenesis of the compound of chitosan and recombinant human bone morphogenetic protein 2]. *Zhongguo Xiufu Chongjian Waike Zazhi/Chinese Journal of Reparative and Reconstructive Surgery*, 19(9), pp.721–724.

Lim, T.H. et al., 2001. Effect of endplate conditions and bone mineral density on the compressive strength of the graft-endplate interface in anterior cervical spine fusion. *Spine*, 26(8), pp.951–956.

Lindahl, O., 1976. Mechanical properties of dried defatted spongy bone. *Acta Orthopaedica Scandinavica*, 47(1), pp.11–19.

Lingham-Soliar, T. & Wesley-Smith, J., 2008. First investigation of the collagen D-band ultrastructure in fossilized vertebrate integument. *Proceedings. Biological sciences / The Royal Society*, 275(16

Little, S.C. & Mullins, M.C., 2009. Bone morphogenetic protein heterodimers assemble heteromeric type I receptor complexes to pattern the dorsoventral axis. *Nature Cell Biology*, 11(5), pp.637–643.

Liu, C.Z. et al., 2008. Novel 3D collagen scaffolds fabricated by indirect printing technique for tissue engineering. *Journal of Biomedical Materials Research.*

Part B, Applied Biomaterials, 85(2), pp.519–528.

Liu, Y., de Groot, K. & Hunziker, E.B., 2005. BMP-2 liberated from biomimetic implant coatings induces and sustains direct ossification in an ectopic rat model. *Bone*, 36(5), pp.745–757.

Liu, Y. et al., 2004. Bone morphogenetic protein 2 incorporated into biomimetic coatings retains its biological activity. *Tissue Engineering*, 10(1-2), pp.101–108.

Liu, Y. et al., 2009. In vitro effects of nanophase hydroxyapatite particles on proliferation and osteogenic differentiation of bone marrow-derived mesenchymal stem cells. *Journal of biomedical materials research. Part A*, 90(4), pp.1083–1091.

Loguidice, V.A. et al., 1988. Anterior lumbar interbody fusion. *Spine*, 13(3), pp.366–369.

Long, S. et al., 2006. Expression, purification, and renaturation of bone morphogenetic protein-2 from Escherichia coli. *Protein Expression and Purification*, 46(2), pp.374–378.

Lorenz, J., Minoshima, S. & Casey, K.L., 2003. Keeping pain out of mind: the role of the dorsolateral prefrontal cortex in pain modulation. *Brain : a journal of neurology*, 126(Pt 5), pp.1079–1091.

Lorenz, M. et al., 1991. A comparison of single-level fusions with and without hardware. *Spine*, 16(8 Suppl), pp.S455–S458.

Lou, T., Wang, X. & Song, G., 2013. Fabrication of nano-fibrous poly(l-lactic acid) scaffold reinforced by surface modified chitosan micro-fiber. *International Journal of Biological Macromolecules*, 61, pp.353–358.

Louis-Ugbo, J. et al., 2004. Evidence of osteoinduction by Grafton demineralized bone matrix in nonhuman primate spinal fusion. *Spine*, 29(4), pp.360–3Z1.

Love, J.G. & Schorn, V.G., 1965. Thoracic-disk protrusions. *Journal of the American Medical Association*, 191, pp.627–631.

Lowery, G.L., Kulkarni, S. & Pennisi, A.E., 1999. Use of autologous growth factors in lumbar spinal fusion. *Bone*, 25(2 Suppl), pp.47S–50S.

Lu, S.S. et al., 2007. The osteoinductive properties of Nell-1 in a rat spinal fusion model. *Spine Journal: Official Journal of the North American Spine Society*, 7(1), pp.50–60.

Luginbuehl, V. et al., 2004. Localized delivery of growth factors for bone repair. *European Journal of Pharmaceutics and Biopharmaceutics*, 58(2), pp.197–208.

Luoma, K. et al., 2000. Low back pain in relation to lumbar disc degeneration.

Spine, 25(4), pp.487–492.

Ma, C. & Wang, X.-F., 2008. In vitro assays for the extracellular matrix protein-regulated extravasation process. *CSH protocols*, 2008, p.pdb.prot5034.

Macdonald, M.L. et al., 2011. Tissue integration of growth factor-eluting layer-by-layer polyelectrolyte multilayer coated implants. *Biomaterials*, 32(5), pp.1446–1453.

Maniadakis, N. & Gray, A., 2000. The economic burden of back pain in the UK. *Pain*, 84(1), pp.95–103.

Martel-Estrada, S.A. et al., 2010. Synthesis and thermo-physical properties of chitosan/poly(dl-lactide-co-glycolide) composites prepared by thermally induced phase separation. *Carbohydrate Polymers*, 81(4), pp.775–783.

Martin, G.J. et al., 1999. New formulations of demineralized bone matrix as a more effective graft alternative in experimental posterolateral lumbar spine arthrodesis. *Spine*, 24(7), pp.637–645.

Martínez-Pérez, C.A. & Olivas-Armendariz, I., 2011. Scaffolds for tissue engineering via thermally induced phase separation. *Advances in Regenerative Medicine*, Dr Sabine Wislet-Gendebien (Ed.), ISBN: 978-953-307-732-1, InTech

Mata, A. et al., 2009. A three-dimensional scaffold with precise micro-architecture and surface micro-textures. *Biomaterials*, 30(27), pp.4610–4617.

Mayer, M. et al., 1996. Maxillary alveolar cleft repair in dogs using recombinant human bone morphogenetic protein-2 and a polymer carrier. *Plastic and reconstructive surgery*, 98(2), pp.247–259.

McFadden, T.M. et al., 2013. The delayed addition of human mesenchymal stem cells to pre-formed endothelial cell networks results in functional vascularization of a collagen-glycosaminoglycan scaffold in vivo. *Acta Biomaterialia*, 9(12), pp.9303–9316.

McGuire, R.A. & Amundson, G.M., 1993. The use of primary internal fixation in spondylolisthesis. *Spine*, 18(12), pp.1662–1672.

McHale, M.K., Setton, L.A. & Chilkoti, A., 2005. Synthesis and in vitro evaluation of enzymatically cross-linked elastin-like polypeptide gels for cartilaginous tissue repair. *Tissue Eng.*, 11(11-12), pp.1768–

McKay, W.F., Peckham, S.M. & Badura, J.M., 2007. A comprehensive clinical review of recombinant human bone morphogenetic protein-2 (INFUSE Bone Graft). *International Orthopaedics*, 31(6), pp.729–734.

McLain, R.F. et al., 2005. Aspiration of osteoprogenitor cells for augmenting spinal fusion: comparison of progenitor cell concentrations from the

vertebral body and iliac crest. *Journal of Bone and Joint Surgery (American)*, 87(12), pp.2655–2661.

Miles, C.A. & Ghelashvili, M., 1999. Polymer-in-a-Box Mechanism for the Thermal Stabilization of Collagen Molecules in Fibers. *Biophysical journal*, 76(6), pp.3243–3252.

Miller, L.D. et al., 1999. Investigation of the nanofibrillar morphology in silk fibers by small angle X-ray scattering and atomic force microscopy. *International Journal of Biological Macromolecules*, 24(2-3), pp.159–165.

Miller, J.A., Schmatz, C. & Schultz, A.B., 1988. Lumbar disc degeneration: correlation with age, sex, and spine level in 600 autopsy specimens. *Spine*, 13(2), pp.173–178.

Min, J., Braatz, R.D. & Hammond, P.T., 2014. Tunable staged release of therapeutics from layer-by-layer coatings with clay interlayer barrier. *Biomaterials*, 35(8), pp.2507–2517.

Minamide, A. et al., 2005. The use of cultured bone marrow cells in type I collagen gel and porous hydroxyapatite for posterolateral lumbar spine fusion. *Spine*, 30(10), pp.1134–1138.

Mirza, S.K. & Deyo, R.A., 2007. Systematic review of randomized trials comparing lumbar fusion surgery to nonoperative care for treatment of chronic back pain. *Spine*, 32(7), pp.816–823.

Miyazono, K., 1999. Signal transduction by bone morphogenetic protein receptors: functional roles of Smad proteins. *Bone*, 25(1), pp.91–93.

Mizutani, H. & Urist, M.R., 1982. The nature of bone morphogenetic protein (BMP) fractions derived from bovine bone matrix gelatin. *Clinical Orthopaedics and Related Research*, (171), pp.213–223.

Modic, M.T. et al., 1988. Degenerative disk disease: assessment of changes in vertebral body marrow with MR imaging. *Radiology*, 166(1 Pt 1), pp.193–199.

Moller, H. & Hedlund, R., 2000. Instrumented and noninstrumented posterolateral fusion in adult spondylolisthesis--a prospective randomized study: part 2. *Spine*, 25(13), pp.1716–1721.

Mont, M.A. et al., 2004. Use of bone morphogenetic proteins for musculoskeletal applications. An overview. *Journal of Bone and Joint Surgery (American)*, 86-A Suppl 2, pp.41–55.

Mouthuy, P.-A. et al., 2010. Physico-chemical characterization of functional electrospun scaffolds for bone and cartilage tissue engineering. *Proceedings of the Institution of Mechanical Engineers, Part H: Journal of Engineering in Medicine*, 224(12), pp.1401–1414.

Moutos, F.T.F., Freed, L.E.L. & Guilak, F.F., 2007. A biomimetic three-dimensional woven composite scaffold for functional tissue engineering of cartilage. *Nature Materials*, 6(2), pp.162–167.

Murphy, C.M.C. et al., 2012. Mesenchymal stem cell fate is regulated by the composition and mechanical properties of collagen-glycosaminoglycan scaffolds. *Journal of the Mechanical Behavior of Biomedical Materials*, 11, pp.53–62.

Muschler, G.F. & Midura, R.J., 2002. Connective tissue progenitors: Practical concepts for clinical applications. *Clinical Orthopaedics and Related Research*, (395), pp.66–80.

Nair, L.S. & Laurencin, C.T., 2007. Biodegradable polymers as biomaterials. *Progress in Polymer Science*, 32(8-9), pp.762–798.

Nakajima, T. et al., 2007. Evaluation of posterolateral spinal fusion using mesenchymal stem cells: differences with or without osteogenic differentiation. *Spine*, 32(22), pp.2432-2436.

Nakamura, A. et al., 2009. Osteocalcin secretion as an early marker of in vitro osteogenic differentiation of rat mesenchymal stem cells. *Tissue Engineering Part C: Methods*, 15(2), pp.169–180.

Nakamura, K.K. et al., 1999. p38 Mitogen-Activated Protein Kinase Functionally Contributes to Chondrogenesis Induced by Growth/Differentiation Factor-5 in ATDC5 Cells. *Experimental Cell Research*, 250(2), pp.13–13.

Nakashima, K. et al., 2002. The novel zinc finger-containing transcription factor osterix is required for osteoblast differentiation and bone formation. *Cell*, 108(1), pp.17–29.

Nakayama, G.R. et al., 1997. Assessment of the Alamar Blue assay for cellular growth and viability in vitro. *Journal of immunological methods*, 204(2), pp.205–208.

Neen, D. et al., 2006. Healos and bone marrow aspirate used for lumbar spine fusion: a case controlled study comparing healos with autograft. *Spine*, 31(18), pp.E636–40.

Newman, M.H. & Grinstead, G.L., 1992. Anterior lumbar interbody fusion for internal disc disruption. *Spine*, 17(7), pp.831–833.

Nguyen, P.K. et al., 2013. Clickable Poly(ethylene glycol)-Microsphere-Based Cell Scaffolds. *Macromolecular Chemistry & Physics*, 214(8), pp.948–956.

Nie, H. & Wang, C.-H., 2007. Fabrication and characterization of PLGA/HAp composite scaffolds for delivery of BMP-2 plasmid DNA. *Journal of Controlled Release*, 120(1-2), pp.11–11.

Niu, X. et al., 2009. Porous nano-HA/collagen/PLLA scaffold containing chitosan

microspheres for controlled delivery of synthetic peptide derived from BMP-2. *Journal of Controlled Release*, 134(2), pp.111–117.

Nohe, A. et al., 2002. The mode of bone morphogenetic protein (BMP) receptor oligomerization determines different BMP-2 signaling pathways. *Journal of Biological Chemistry*, 277(7), pp.5330–5338.

Norman, J.J. & Desai, T.A., 2006. Methods for Fabrication of Nanoscale Topography for Tissue Engineering Scaffolds. *Annals of Biomedical Engineering*, 34(1), pp.89–101.

Noshi, T. et al., 2001. Recombinant human bone morphogenetic protein-2 potentiates the in vivo osteogenic ability of marrow/hydroxyapatite composites. *Artificial Organs*, 25(3), pp.201–208.

Occhetta, P. et al., 2013. Fabrication of 3D cell-laden hydrogel microstructures through photo-mold patterning. *Biofabrication*, 5(3), p.035002.

Ochs, B.G. et al., 2008. Acetabular bone reconstruction in revision arthroplasty: a comparison of freeze-dried, irradiated and chemically-treated allograft vitalised with autologous marrow versus frozen non-irradiated allograft. *Journal of Bone & Joint Surgery - British Volume*, 90(9), pp.1164–1171.

Ohgushi, H., Goldberg, V.M. & Caplan, A.I., 1989. Heterotopic osteogenesis in porous ceramics induced by marrow cells. *Journal of Orthopaedic Research*, 7(4), pp.568–578.

Ohtori, S. et al., 2011. Surgical Versus Nonsurgical Treatment of Selected Patients With Discogenic Low Back Pain A Small-Sized Randomized Trial. *Spine*, 36(5), pp.347–354.

Oikarinen, J. & Korhonen, L.K., 1979. The bone inductive capacity of various bone transplanting materials used for treatment of experimental bone defects. *Clinical orthopaedics and related research*, (140), pp.208-215.

Okubo et al., 2000. Osteoinduction by recombinant human bone morphogenetic protein-2 at intramuscular, intermuscular, subcutaneous and intrafatty sites. *International Journal of Oral and Maxillofacial Surgery*, 29(1), pp.4–4.

Olivas-Armendariz, I. et al., 2009. Synthesis and Characterization of Porous Polyurethane-Chitosan Blends. *Cellular Polymers*, 28(3), pp.179–191.

Onichtchouk, D. et al., 1999. Silencing of TGF-beta signalling by the pseudoreceptor BAMBI. *Nature*, 401(6752), pp.480–485.

Orban, J.M. et al., 2004. Crosslinking of collagen gels by transglutaminase. *Journal of biomedical materials research. Part A*, 68(4)

Ottani, V. et al., 2002. Hierarchical structures in fibrillar collagens. *Micron*, 33(7-8), pp.587–596.

Ozkaynak, E. et al., 1992. Osteogenic protein-2. A new member of the transforming growth factor-beta superfamily expressed early in embryogenesis. *Journal of Biological Chemistry*, 267(35), pp.25220–25227.

Pagani, F., Francucci, C.M. & Moro, L., 2005. Markers of bone turnover: biochemical and clinical perspectives. *Journal of endocrinological investigation*, 28(10 Suppl), pp.8–13.

Parenteau-Bareil, R., Gauvin, R. & Berthod, F., 2010. Collagen-based biomaterials for tissue engineering applications. *Materials*, 3(3), pp.1863-1887.

Pariente, J. et al., 2005. Expectancy and belief modulate the neuronal substrates of pain treated by acupuncture. *NeuroImage*, 25(4), pp.1161–1167.

Park, D.-J. et al., 2005. Injectable bone using chitosan-alginate gel/mesenchymal stem cells/BMP-2 composites. *Journal of cranio-maxillo-facial surgery : official publication of the European Association for Cranio-Maxillo-Facial Surgery*, 33(1), pp.50–54.

Park, S.J. et al., 2013. Melt-spun shaped fibers with enhanced surface effects: Fiber fabrication, characterization and application to woven scaffolds. *Acta Biomaterialia*, 9(8), pp.7719–7726.

Pathi, S. et al., 1999. Interaction of Ihh and BMP/Noggin Signaling during Cartilage Differentiation. *Developmental Biology*, 209(2), pp.239–253.

Pecchi, E. et al., 2012. A potential role of chondroitin sulfate on bone in osteoarthritis: inhibition of prostaglandin E 2 and matrix metalloproteinases synthesis in interleukin-1β-stimulated osteoblasts. *Osteoarthritis and Cartilage*, 20(2), pp.127-135.

Pedraza, C.E. et al., 2010. An in vitro assessment of a cell-containing collagenous extracellular matrix-like scaffold for bone tissue engineering. *Tissue Eng Part A.*, 16(3), pp.781–793.

Pereira, R.C., Economides, A.N. & Canalis, E., 2000. Bone morphogenetic proteins induce gremlin, a protein that limits their activity in osteoblasts. *Endocrinology*, 141(12), pp.4558–4563.

Petrie Aronin, C.E. & Tuan, R.S., 2010. Therapeutic potential of the immunomodulatory activities of adult mesenchymal stem cells. *Birth defects research. Part C, Embryo today : reviews*, 90(1), pp.67–74.

Phillips, F.M. et al., 2013. Lumbar Spine Fusion for Chronic Low Back Pain Due to Degenerative Disc Disease A Systematic Review. *Spine*, 38(7), pp.E409–E422.

Piccolo, S. et al., 1996. Dorsoventral Patterning in Xenopus: Inhibition of Ventral Signals by Direct Binding of Chordin to BMP-4. *Cell*, 86(4), pp.589–598.

Pieper, J.S. et al., 2002. Crosslinked type II collagen matrices: preparation, characterization, and potential for cartilage engineering. *Biomaterials*,

23(15), pp.3183–3192.

Pirlo, R.K. et al., 2012. PLGA/hydrogel biopapers as a stackable substrate for printing HUVEC networks via BioLP. *Biotechnology and bioengineering*, 109(1), pp.262–273.

Pittenger, M.F. et al., 1999. Multilineage potential of adult human mesenchymal stem cells. *Science*, 284(5411), pp.143–147.

Plotkin, L.I., Manolagas, S.C. & Bellido, T., 2002. Transduction of cell survival signals by connexin-43 hemichannels. *Journal of Biological Chemistry*, 277(10), pp.8648–8657.

Polizzotti, B.D., Fairbanks, B.D. & Anseth, K.S., 2008. Three-dimensional biochemical patterning of click-based composite hydrogels via thiolene photopolymerization. *Biomacromolecules*, 9(4), pp.1084–1087.

Portenoy, R.K., 1996. Opioid therapy for chronic nonmalignant pain: a review of the critical issues. *Journal of Pain and Symptom Management*, 11(4), pp.203–217.

Poynton, A.R. & Lane, J.M., 2002. Safety profile for the clinical use of bone morphogenetic proteins in the spine. *Spine*, 27(16 Suppl 1), pp.S40–S48.

Prabaharan, M. & Mano, J.F., 2005. Chitosan-based particles as controlled drug delivery systems. *Drug Delivery*, 12(1), pp.41–57.

Pratap, J. et al., 2003. Cell growth regulatory role of Runx2 during proliferative expansion of preosteoblasts. *Cancer Research*, 63(17), pp.5357–5362.

Quarto, R. et al., 2001. Repair of large bone defects with the use of autologous bone marrow stromal cells. *New England Journal of Medicine*, 344(5), pp.385–386.

Rackwitz, B. et al., 2006. Segmental stabilizing exercises and low back pain. What is the evidence? A systematic review of randomized controlled trials. *Clinical Rehabilitation*, 20(7), pp.553–567.

Rajaee, S.S. et al., 2012. Spinal fusion in the United States: analysis of trends from 1998 to 2008. *Spine*, 37(1), pp.67–76.

Rajaee, S.S., Kanim, L.E.A. & Bae, H.W., 2014. National trends in revision spinal fusion in the USA: patient characteristics and complications. *Bone and Joint Journal*, 96B(6), pp.807–816.

Rao, P. & Knaus, E.E., 2008. Evolution of nonsteroidal anti-inflammatory drugs (NSAIDs): cyclooxygenase (COX) inhibition and beyond. *Journal of Pharmacy & Pharmaceutical Sciences*, 11(2), pp.81s-110s

Rawadi, G. et al., 2003. BMP-2 controls alkaline phosphatase expression and osteoblast mineralization by a Wnt autocrine loop. *Journal of Bone and*

Mineral Research, 18(10), pp.1842–1853.

Rehman, I. & Bonfield, W., 1997. Characterization of hydroxyapatite and carbonated apatite by photo acoustic FTIR spectroscopy. *Journal of Material Science & Material Medicine*, 8(1), pp.1–4.

Rich, A. & Crick, F., 1955. The structure of collagen. *Nature*, 176, pp.915-916.

Riekerink, M.B.O. et al., 2003. Gas plasma etching of PEO/PBT segmented block copolymer films. *Journal of biomedical materials research. Part A*, 65(4), pp.417–428.

Riew, K.D., Ecker, E. & Dettori, J.R., 2010. Anterior cervical discectomy and fusion for the management of axial neck pain in the absence of radiculopathy or myelopathy. *Evidence-based spine-care journal*, 1(3), pp.45–50.

Ripamonti, U., 1992. Calvarial regeneration in primates with autolyzed antigen-extracted allogeneic bone. *Clinical Orthopaedics and Related Research*, (282), pp.293–303.

Rodrigues, S.C. et al., 2013. Preparation and characterization of collagen-nanohydroxyapatite biocomposite scaffolds by cryogelation method for bone tissue engineering applications. *Journal of biomedical materials research. Part A*, 101(4), pp.1080–1094.

Roelofs, P.D. et al., 2008. Nonsteroidal anti-inflammatory drugs for low back pain: an updated Cochrane review. *Spine*, 33(16), pp.1766–1774.

Rohl, L. et al., 1991. Tensile and compressive properties of cancellous bone. *Journal of biomechanics*, 24(12), pp.1143–1149.

Rosen, V.V. et al., 1989. Purification and molecular cloning of a novel group of BMPs and localization of BMP mRNA in developing bone. *Connective Tissue Research*, 20(1-4), pp.313–319.

Rubin, A.L.A. et al., 1963. Tropocollagen: significance of protease-induced alterations. *Science*, 139(3549), pp.37–39.

Rubin, C.T. & Lanyon, L.E., 1987. Kappa Delta Award paper. Osteoregulatory nature of mechanical stimuli: function as a determinant for adaptive remodeling in bone. *Journal of Orthopaedic Research*, 5(2), pp.300–310.

Ruppert, R. & Hoffmann, E., 1996. Human Bone Morphogenetic Protein 2 Contains a Heparin-Binding Site which Modifies Its Biological Activity. *European Journal of Biochemistry*, 237(1), pp.295-302.

Sachlos, E. et al., 2008. The impact of critical point drying with liquid carbon dioxide on collagen-hydroxyapatite composite scaffolds. *Acta Biomaterialia*, 4(5), pp.1322–1331.

Sacks, S., 1965. Anterior interbody fusion of the lumbar spine. *Journal of Bone &*

Joint Surgery - British Volume, 47, pp.211–223.

Saito, A. et al., 2003. Activation of osteo-progenitor cells by a novel synthetic peptide derived from the bone morphogenetic protein-2 knuckle epitope. *Biochimica et Biophysica Acta (BBA) - Proteins and Proteomics*, 1651(1), pp.60–67.

Saito, N. et al., 2001. A biodegradable polymer as a cytokine delivery system for inducing bone formation. *Nature Biotechnology*, 19(4), pp.332–335.

Saito, N. et al., 1999. New synthetic absorbable polymers as BMP carriers: plastic properties of poly-D,L-lactic acid-polyethylene glycol block copolymers. *Journal of Biomedical Materials Research Part B: Applied Biomaterials*, 47(1), pp.104–110.

Sakai, D. et al., 2003. Transplantation of mesenchymal stem cells embedded in Atelocollagen gel to the intervertebral disc: a potential therapeutic model for disc degeneration. *Biomaterials*, 24(20), pp.35

Salerno, S.M., Browning, R. & Jackson, J.L., 2002. The effect of antidepressant treatment on chronic back pain: a meta-analysis. *Archives of Internal Medicine*, 162(1), pp.19–24.

Sampath, T.K. & Reddi, A.H., 1981. Dissociative extraction and reconstitution of extracellular matrix components involved in local bone differentiation. *Proceedings of the National Academy of Sciences U S A*, 78(12), pp.7599–7603.

Sampath, T.K. et al., 1992. Recombinant human osteogenic protein-1 (hOP-1) induces new bone formation in vivo with a specific activity comparable with natural bovine osteogenic protein and stimulates osteoblast proliferation and differentiation in vitro. *Journal of Biological Chemistry*, 267(28), pp.20352–20362.

Sandhu, H.S. et al., 1995. Evaluation of rhBMP-2 with an OPLA carrier in a canine posterolateral (transverse process) spinal fusion model. *Spine*, 20(24), pp.2669–2682.

Sansur, C.A. et al., 2010. Morbidity and mortality in the surgical treatment of 10,242 adults with spondylolisthesis. *Journal of Neurosurgery: Spine*, 13(5), pp.589–593.

Sassard, W.R. et al., 2000. Augmenting local bone with Grafton demineralized bone matrix for posterolateral lumbar spine fusion: Avoiding second site autologous bone harvest. *Orthopedics*, 23(10), pp.1059–1064.

Sawyer, A.A. et al., 2009. The stimulation of healing within a rat calvarial defect by mPCL-TCP/collagen scaffolds loaded with rhBMP-2. *Biomaterials*, 30(13), pp.2479–2488.

Scheufler, C., Sebald, W. & Hülsmeyer, M., 1999. Crystal structure of human bone morphogenetic protein-2 at 2.7 A resolution. *Journal of molecular biology*,

287(1), pp.103–115.

Schliephake, H. et al., 2007. In vitro characterization of a slow release system of polylactic acid and rhBMP2. *Journal of biomedical materials research. Part A*, 83(2), pp.455–462.

Schmid, U. et al., 2007. [A novel therapeutic approach to bone replacement: vitalisation of industrial processed allogenic bone graft with autologous bone marrow]. *Zeitschrift für Orthopädie und Unfallchirurgie*, 145(2), pp.221–229.

Schmidt-Wilcke, T. et al., 2006. Affective components and intensity of pain correlate with structural differences in gray matter in chronic back pain patients. *Pain*, 125(1-2), pp.89–97.

Schmitt, F.O. et al., The antigenicity of tropocollagen. *Proceedings of the National Academy of Sciences of the United States of America,* 51(3), pp.493-497.

Schmittgen, T.D. & Livak, K.J., 2008. Analyzing real-time PCR data by the comparative CT method. *Nature protocols*, 3(6), pp.1101-1108.

Schneider, C.A., Rasband, W.S. & Eliceiri, K.W., 2012. NIH Image to ImageJ: 25 years of image analysis. *Nature Methods*, 9(7), pp.671-675

Schubert, T. et al., 2013. Critical size bone defect reconstruction by an autologous 3D osteogenic-like tissue derived from differentiated adipose MSCs. *Biomaterials*, 34(18), pp.4428–4438.

Schwab, F.J. et al., 1995. Effects of spinal instrumentation on fusion of the lumbosacral spine. *Spine*, 20(18), pp.2023–2028.

Scott, I.C. et al., 2001. Homologues of Twisted gastrulation are extracellular cofactors in antagonism of BMP signalling. *Nature*, 410(6827), pp.475–478.

Shah, N.J. et al., 2013. Surface-mediated bone tissue morphogenesis from tunable nanolayered implant coatings. *Science translational medicine*, 5(191), p.191ra83.

Shamsul, B.S. et al., 2014. Posterolateral spinal fusion with ostegenesis induced BMSC seeded TCP/HA in a sheep model. *Tissue and Cell*, 46(2), pp.152–158.

Shim, J.B. et al., 2014. A study of a three-dimensional PLGA sponge containing natural polymers co-cultured with endothelial and mesenchymal stem cells as a tissue engineering scaffold. *Biomedical Materials*, 9(4), p.045015.

Shimasaki, S. et al., 2004. The bone morphogenetic protein system in mammalian reproduction. *Endocrine reviews*, 25(1), pp.72–101.

Sigurdsson, T.J. et al., 1995. Periodontal repair in dogs: recombinant human bone morphogenetic protein-2 significantly enhances periodontal regeneration. *Journal of Periodontology*, 66(2), pp.131–138.

Silcox, D.H., 1998. Laparoscopic bone dowel fusions of the lumbar spine. *Orthopedic Clinics of North America*, 29(4), pp.655–663.

Silver, I.A., Murrills, R.J. & Etherington, D.J., 1988. Microelectrode studies on the acid microenvironment beneath adherent macrophages and osteoclasts. *Experimental Cell Research*, 175(2), pp.266–276.

Silverstein, F.E. et al., 2000. Gastrointestinal toxicity with celecoxib vs nonsteroidal anti-inflammatory drugs for osteoarthritis and rheumatoid arthritis: the CLASS study: A randomized controlled trial. Celecoxib Long-term Arthritis Safety Study. *Journal of the American Medical Association*, 284(10), pp.1247–1255.

Simmons, C.A. et al., 2004. Dual growth factor delivery and controlled scaffold degradation enhance in vivo bone formation by transplanted bone marrow stromal cells. *Bone*, 35(2), pp.562–569.

Simmons, D.J., 1985. Fracture healing perspectives. *Clinical Orthopaedics and Related Research*, (200), pp.100-113.

Singh, R. et al., 2009. Characterization of the structure and permeability of titanium foams for spinal fusion devices. *Acta Biomaterialia*, 5(1), pp.477–487.

Smith, J.S. et al., 2009. Improvement of back pain with operative and nonoperative treatment in adults with scoliosis. *Neurosurgery*, 65(1), pp.86–84.

Smith, J.W., 1968. Molecular pattern in native collagen. *Nature*, 219(5150), pp.157-158.

Sokolsky-Papkov, M.M. et al., 2007. Polymer carriers for drug delivery in tissue engineering. *Advanced Drug Delivery Reviews*, 59(4-5), pp.20–20.

Stauffer, R.N. & Coventry, M.B., 1972. Posterolateral lumbar-spine fusion. Analysis of Mayo Clinic series. *Journal of Bone and Joint Surgery (American)*, 54(6), pp.1195–1204.

Steinert, A.F. et al., 2012. Concise review: The clinical application of mesenchymal stem cells for musculoskeletal regeneration: Current status and perspectives. *Stem Cells Translational Medicine*, 1(3), pp.237–247.

Steinert, A.F. et al., 2007. Major biological obstacles for persistent cell-based regeneration of articular cartilage. *Arthritis research & therapy*, 9(3), pp.213–213.

Stevens MM, G.J., 2005. Exploring and engineering the cell surface interface. *Science*, 310(10), pp.1135–1138.

Tagliazucchi, E. et al., 2010. Brain resting state is disrupted in chronic back pain patients. *Neuroscience letters*, 485(1), pp.26–31.

Taillard, W.F., 1976. Etiology of Spondylolisthesis. *Clinical Orthopaedics and Related Research*, (117), pp.30–39.

Takechi, M. et al., 2012. 3-dimensional composite scaffolds consisting of apatite-PLGA-atelocollagen for bone tissue engineering. *Dental materials journal*, 31(3), pp.465–471.

Takeuchi, A. et al., 2009. Recombinant human bone morphogenetic protein-2/atelocollagen composite as a new material for ossicular reconstruction. *Journal of biomedical materials research. Part A*, 89(1), pp.36–45.

Tamaddon, M. et al., 2013. Characterisation of freeze-dried type II collagen and chondroitin sulfate scaffolds. *Journal of Material Science & Material Medicine*, 24(5), pp.1153–1165.

Tampieri, A. et al., 2003. Biologically inspired synthesis of bone-like composite: self-assembled collagen fibers/hydroxyapatite nanocrystals. *Journal of biomedical materials research. Part A*, 67(2), pp.618–625.

Tazaki, J. et al., 2009. BMP-2 release and dose-response studies in hydroxyapatite and beta-tricalcium phosphate. *Bio-Medical Materials and Engineering*, 19(2-3), pp.141–146.

Teitelbaum, S.L. & Ross, F.P., 2003. Genetic regulation of osteoclast development and function. *Nature reviews. Genetics*, 4(8), pp.638–649.

Teixeira, L.S.M. et al., 2012. Enzyme-catalyzed crosslinkable hydrogels: emerging strategies for tissue engineering. *Biomaterials*, 33(5), pp.1281–1290.

Teixeira, S. et al., 2010. Heparinized hydroxyapatite/collagen three-dimensional scaffolds for tissue engineering. *Journal of Material Science & Material Medicine*, 21(8), pp.2385–2392.

Thalgott, J.S. et al., 1999. Anterior interbody fusion of the cervical spine with coralline hydroxyapatite. *Spine*, 24(13), pp.1295–1299.

Thalgott, J.S., Giuffre, J.M., et al., 2002a. Anterior lumbar interbody fusion with titanium mesh cages, coralline hydroxyapatite, and demineralized bone matrix as part of a circumferential fusion. *Spine Journal: Official Journal of the North American Spine Society*, 2(1), pp.63–69.

Thalgott, J.S., Klezl, Z., et al., 2002b. Anterior lumbar interbody fusion with processed sea coral (coralline hydroxyapatite) as part of a circumferential fusion. *Spine*, 27(24), pp.E518–525.

Thomsen, K.K. et al., 1997. 1997 Volvo Award winner in clinical studies. The effect of pedicle screw instrumentation on functional outcome and fusion rates in posterolateral lumbar spinal fusion: a prospective, randomized clinical study. *Spine*, 22(24), pp.2813–2822.

Tian, H. et al., 2012. Interaction study in homogeneous collagen/chondroitin

sulfate blends by two-dimensional infrared spectroscopy. *Carbohydrate Polymers*, 89(2), pp.542–550.

Tortora, G.J., 2004. *Principles of Human Anatomy, Tenth Edition, Wiley International Edition*, John Wiley & Sons.

Tribus, C.B., 2003. Degenerative lumbar scoliosis: evaluation and management. *Journal of the American Academy of Orthopaedic Surgeons*, 11(3), pp.174–183.

Uchio, Y. et al., 2000. Human chondrocyte proliferation and matrix synthesis cultured in Atelocollagen gel. *Journal of Biomedical Materials Research Part B: Applied Biomaterials*, 50(2), pp.138–143.

Ulrich, T.A. et al., 2010. Probing cellular mechanobiology in three-dimensional culture with collagen-agarose matrices. *Biomaterials*, 31(7), pp.1875–1884.

Uludag, H.H. et al., 1999. rhBMP-collagen sponges as osteoinductive devices: effects of in vitro sponge characteristics and protein pI on in vivo rhBMP pharmacokinetics. *Annals of the New York Academy of Sciences*, 875, pp.369–378.

Unger, R.E. et al., 2004. Growth of human cells on a non-woven silk fibroin net: a potential for use in tissue engineering. *Biomaterials*, 25(6), pp.1069–1075.

Urist, M.R., 1965. Bone: formation by autoinduction. *Science*, 150(3698), pp.893–899.

Urist, M.R., Mikulski, A. & Lietze, A., 1979. Solubilized and insolubilized bone morphogenetic protein. *Proceedings of the National Academy of Sciences of the U S A*, 76(4), pp.1828–1832.

Vaccaro, A.R., Martyak, G.G. & Madigan, L., 2001. Adult isthmic spondylolisthesis. *Orthopedics*, 24(12), pp.1172–1177.

Vallejo, L.F. et al., 2002. Renaturation and purification of bone morphogenetic protein-2 produced as inclusion bodies in high-cell-density cultures of recombinant Escherichia coli. *Journal of Biotechnology*, 94(2), pp.185-194.

van Dam, B.E., 1988. Nonoperative treatment of adult scoliosis. *Orthopedic Clinics of North America*, 19(2), pp.347–351.

van Susante, J.L.C. et al., 2001. Linkage of chondroitin-sulfate to type I collagen scaffolds stimulates the bioactivity of seeded chondrocytes in vitro. *Biomaterials*, 22(17), pp.2359–2369.

Vater, C.A., Harris, E.D. & Siegel, R.C., 1979. Native cross-links in collagen fibrils induce resistance to human synovial collagenase. *Biochem J*, 181(3), pp.639-645.

Wager, T.D. et al., 2004. Placebo-induced changes in FMRI in the anticipation and

experience of pain. *Science*, 303(5661), pp.1162–1167.

Waldman, H.J., 1994. Centrally acting skeletal muscle relaxants and associated drugs. *Journal of Pain and Symptom Management*, 9(7), pp.434–441.

Wang, L. et al., 2003. Evaluation of sodium alginate for bone marrow cell tissue engineering. *Biomaterials*, 24(20), pp.3475–3481.

Wang, C.-K. et al., 2009. Controlled-release of rhBMP-2 carriers in the regeneration of osteonecrotic bone. *Biomaterials*, 30(25), pp.4178–4186.

Wang, D.-A. et al., 2007. Multifunctional chondroitin sulphate for cartilage tissue-biomaterial integration. *Nature Materials*, 6(5), pp.385–392.

Wang, E.A. et al., 1990. Recombinant human bone morphogenetic protein induces bone formation. *Proceedings of the National Academy of Sciences of the U S A*, 87(6), pp.2220–2224.

Wang, T. et al., 2005. Evaluation of autologous bone marrow mesenchymal stem cell-calcium phosphate ceramic composite for lumbar fusion in rhesus monkey interbody fusion model. *Tissue engineering*, 11(7-8), pp.1159-1167.

Wang, W.W. et al., 2000. Ski represses bone morphogenic protein signaling in Xenopus and mammalian cells. *Proceedings of the National Academy of Sciences of the U S A*, 97(26), pp.14394–14399.

Warnke, P.H. et al., 2004. Growth and transplantation of a custom vascularised bone graft in a man. *The Lancet*, 364(9436), pp.766–770.

Wei, G. et al., 2007. The enhancement of osteogenesis by nano-fibrous scaffolds incorporating rhBMP-7 nanospheres. *Biomaterials*, 28(12), pp.2087–2096.

Wendt, D., Marsano, A. & Jakob, M., 2003. Oscillating perfusion of cell suspensions through three-dimensional scaffolds enhances cell seeding efficiency and uniformity. *Biotechnology and Bioengineering*, 84(2), pp.205-214.

Whyte, M.P., 1994. Hypophosphatasia and the role of alkaline phosphatase in skeletal mineralization. *Endocrine reviews*, 15(4), pp.439–461.

Wiech, K. et al., 2006. Anterolateral prefrontal cortex mediates the analgesic effect of expected and perceived control over pain. *The Journal of neuroscience : the official journal of the Society for Neuroscience*, 26(44), pp.11501–11509.

Wiltse, L.L., Newman, P.H. & Macnab, I., 1976. Classification of spondylolisis and spondylolisthesis. *Clinical Orthopaedics and Related Research*, (117), pp.23–29.

Winet, H. & Hollinger, J.O., 1993. Incorporation of polylactide-polyglycolide in a cortical defect: neoosteogenesis in a bone chamber. *Journal of Biomedical*

Materials Research Part B: Applied Biomaterials, 27(5), pp.667–676.

Wood, G.W. et al., 1995. The effect of pedicle screw/plate fixation on lumbar/lumbosacral autogenous bone graft fusions in patients with degenerative disc disease. *Spine*, 20(7), pp.819–830.

Wozney, J.M. et al., 1988. Novel regulators of bone formation: molecular clones and activities. *Science*, 242(4885), pp.1528–1534.

Xiao, Y.T., Xiang, L.X. & Shao, J.Z., 2007. Bone morphogenetic protein. *Biochemical and biophysical research communications*, 362(3), pp.550-553.

Xie, J., Li, X. & Xia, Y., 2008. Putting Electrospun Nanofibers to Work for Biomedical Research. *Macromolecular Rapid Communications*, 29(22), pp.1775–1792.

Xie, Y. et al., 2002. Nanoscale modifications of PET polymer surfaces via oxygen-plasma discharge yield minimal changes in attachment and growth of mammalian epithelial and mesenchymal cells in vitro. *Journal of Biomedical Materials Research Part B: Applied Biomaterials*, 61(2), pp.234–245.

Xu, J. et al., 2009. Sustained and localized in vitro release of BMP-2/7, RANKL, and tetracycline from FlexBone, an elastomeric osteoconductive bone substitute. *Journal of Orthopaedic Research*, 27(10), pp.1306–1311.

Yadla, S. et al., 2010. Adult scoliosis surgery outcomes: a systematic review. *Neurosurgical Focus*, 28(3), pp.E3–E3.

Yahyouche, A. et al., 2013. Improved angiogenic cell penetration in vitro and in vivo in collagen scaffolds with internal channels. *Journal of Materials Science: Materials in Medicine*, 24(6), pp.1571–1580.

Yanagita, M., 2005. BMP antagonists: their roles in development and involvement in pathophysiology. *Cytokine & Growth Factor Reviews*, 16(3), pp.309–317.

Yee, A.J.M. et al., 2003. Augmentation of rabbit posterolateral spondylodesis using a novel demineralized bone matrix-hyaluronan putty. *Spine*, 28(21), pp.2435–2440.

Yeung, T. et al., 2005. Effects of substrate stiffness on cell morphology, cytoskeletal structure, and adhesion. *Cell Motility and the Cytoskeleton*, 60(1), pp.24–34.

Yilgor, P. et al., 2009. Incorporation of a sequential BMP-2/BMP-7 delivery system into chitosan-based scaffolds for bone tissue engineering. *Biomaterials*, 30(21), pp.3551–3559.

Yoneda, M. et al., 2005. Repair of an intercalated long bone defect with a synthetic biodegradable bone-inducing implant. *Biomaterials*, 26(25), pp.5145–5152.

Yoshida, Y. et al., 2000. Negative regulation of BMP/Smad signaling by Tob in osteoblasts. *Cell*, 103(7), pp.1085-1097.

Yuan, H. et al., 2001. Use of an osteoinductive biomaterial as a bone morphogenetic protein carrier. *Journal of Materials Science: Materials in Medicine*, 12(9), pp.761–766.

Zellin, G. & Linde, A., 1997. Importance of delivery systems for growth-stimulatory factors in combination with osteopromotive membranes. An experimental study using rhBMP-2 in rat mandibular defects. *Journal of Biomedical Materials Research Part B: Applied Biomaterials*, 35(2), pp.181–190.

Zhang, D. et al., 2002. A role for the BMP antagonist chordin in endochondral ossification. *Journal of Bone and Mineral Research*, 17(2), pp.293–300.

Zhang, P. et al., 2008. Clinical study of lumbar fusion by hybrid construct of stem cells technique and biodegradable material. *Zhonghua wai ke za zhi [Chinese journal of surgery]*, 46(7), pp.493–496.

Zhang, S., Doschak, M.R. & Uludağ, H., 2009. Pharmacokinetics and bone formation by BMP-2 entrapped in polyethylenimine-coated albumin nanoparticles. *Biomaterials*, 30(28), pp.5143–5155.

Zhang, X. et al., 2014. Polymer-ceramic spiral structured scaffolds for bone tissue engineering: effect of hydroxyapatite composition on human fetal osteoblasts. *PLoS ONE*, 9(1), p.e85871.

Zhang, Y. et al., 2001. Regulation of Smad degradation and activity by Smurf2, an E3 ubiquitin ligase. *Proceedings of the National Academy of Sciences of the U S A*, 98(3), pp.974–979.

Zhao, Y. et al., 2010. The osteogenic effect of bone morphogenetic protein-2 on the collagen scaffold conjugated with antibodies. *Journal of Controlled Release*, 141(1), pp.30–37.

Zhu, H. et al., 1999. A SMAD ubiquitin ligase targets the BMP pathway and affects embryonic pattern formation. *Nature*, 400(6745), pp.687–693.

Zhu, W. et al., 2006. Noggin regulation of bone morphogenetic protein (BMP) 2/7 heterodimer activity in vitro. *Bone*, 39(1), pp.61–71.

Zimmerman, L.B., De Jesús-Escobar, J.M. & Harland, R.M., 1996. The Spemann Organizer Signal noggin Binds and Inactivates Bone Morphogenetic Protein 4. *Cell*, 86(4), pp.599–606.

Zvaifler, N.J. et al., 2000. Mesenchymal precursor cells in the blood of normal individuals. *Arthritis Research*, 2(6), pp.477–488.

Appendices

i. Primers

Primer sequences used for real time quantitative reverse transcriptase PCR (RT PCR).

Primer Name	Sequence
ALP f	ACCACCACGAGAGTGAACCA
ALP r	CGTTGTCTGAGTACCAGTCCC
BGLAP (Osteocalcin) f	TCACACTCCTCGCCCTATT
BGLAP (Osteocalcin) r	TGAAAGCCGATGTGGTCAG
BMP-2 f	GGGTGGAATGACTGGATTGT
BMP-2 r	GTCAAGGTACAGCATCGAGATAG
GAPDH f	ACAGTCAGCCGCATCTTCTT
GAPDH r	AATGAAGGGGTCATTGATGG
RUNX2 f	CACTATCCAGCCACCTTTACTT
RUNX2 r	AGCGTCAACACCATCATTCT
SP7 (Osterix) f	CCTCTGCGGGACTCAACAAC
SP7 (Osterix) r	AGCCCATTAGTGCTTGTAAAGG
TGFβ1 f	GTGGAAACCCACAACGAAATC
TGFβ1 r	GTGTCCAGGCTCCAAATGTA
TBP f	GAATATAATCCCAAGCGGTTTG
TBP r	ACTTCACATCACAGCTCCCC
βACTIN f	GTTTGAGACCTTCAACACCC
βACTIN r	ATGTCACGCACGATTTCCC
UBC f	ATTTGGGTCGCGGTTCTTG
UBC r	TGCCTTGACATTCTCGATGGT